COLLAGEN- AND FIBRONECTIN-MIMETIC INTEGRIN-SPECIFIC SURFACES THAT PROMOTE OSSEOINTEGRATION

A Dissertation
Presented to
The Academic Faculty

by

Catherine Diane Reyes

In Partial Fulfillment
of the Requirements for the Degree
Doctor of Philosophy in the
School of Mechanical Engineering

Georgia Institute of Technology
August 2006

MIXED COLLAGEN- AND FIBRONECTIN-MIMETIC INTEGRIN-SPECIFIC SURFACES THAT PROMOTE OSSEOINTEGRATION

Approved by:

Dr. Andres J. Garcia, Advisor
School of Mechanical Engineering
Georgia Institute of Technology

Dr. Ravi Bellamkonda
Department of Biomedical Engineering
Georgia Institute of Technology

Dr. Barbara D. Boyan
Department of Biomedical Engineering
Georgia Institute of Technology

Dr. Elliot L. Chaikof
Department of Surgery
Emory University

Dr. David M. Collard
School of Chemistry & Biochemistry
Georgia Institute of Technology

Dr. Robert E. Guldberg
School of Mechanical Engineering
Georgia Institute of Technology

Date Approved: July 5, 2006

To Mom and Dad, whose gifts are immeasurable
&
To Charlie, who always believes in me

ACKNOWLEDGEMENTS

The most unexpected lesson that I've learned as a graduate student is that, in the right hands, science is a wildly creative process. And Georgia Tech has been a wonderfully creative place for me to ask and answer and learn about myself. The past six years have been an unforgettable adventure, and I have been inspired and nourished by so many people along the way. To them, I owe my sincerest gratitude; this thesis was made possible by their guidance, support, friendship, laughter, and constant encouragement.

Above all, I offer my heartfelt thanks to my advisor, Andrés García. He single-handedly convinced me to come to Georgia Tech six years ago, and I have never regretted that decision. Working with him has been a privilege and a pleasure. He has given me a tremendous amount of freedom to develop my project, sprinkled with just the right bits of guidance and advice, and topped off with a huge dollop of humor and camaraderie. I appreciate his trust in me and his constant support of my ideas and goals. Thank you, Andrés, for your guidance and your friendship. And thank you for the cannolis… and don't forget that life is too short to skip dessert. Muchas gracias, boss!

My fellow García labmates have made grad school a fun and meaningful experience. Thanks to Ben Keselowsky for taking me under his wing in the lab, despite my annoying tendency to ask questions as though he wasn't going to explain them later. He was my partner and inspiration for many adventures in science-jargon poetry, fun-time buffers, clam digging, and philosophical musings. Thank you, Ben, for always understanding and for being the best of friends. And now that my thesis is complete, we shall ascend together, my friend!

I have to thank Ben Byers for all those lab lessons and for taking a break from the science every once in a while to get downright silly. I will never hear a Nelly song without picturing an Indiana boy rapping and shaking his thang. Thanks for all those late night chats in lab (back when I actually worked long hours) and impromptu trips to Lil'Dinos.

Thanks to Nate Gallant for always goofing off with me, sharing in my lab notebook inadequacies, and reading my mind with uncanny accuracy and empathy. I'm grateful for the countless laughs, good times, witty remarks, and celebratory libations. He is also, without a doubt, the best listener I know. Thanks, Nate, for always caring, listening, and saying what's on your mind.

Kristin Michael started this journey with me, and I will always be grateful for her friendship. Together we have learned, grown, gotten stuck and unstuck, despaired, persevered, partied, shopped, and commiserated. Kristin is a courageous person with unique and remarkable qualities. Thank you for always being honest about yourself, passionate about life, and thoughtful of others. And thanks for all those birthday cakes, champagne toasts, and other little things that you do to make us all feel like a family.

Thank you, Jeff Capadona, for making sure I know where all the electrons go in an EDC/NHS reaction, for sharing you precious thiols even though I had no idea what I was doing, for forcing me to learn all the words to entirely too many country songs, and for introducing me to the unbearably exquisite experience of fajitas from Pappasito's – a love affair from which I may never recover.

Thanks to Lindsay Bryant for taking care of the lab and saving us from ourselves. Linz is truly a breath of fresh air, and I am so grateful for all our lunch dates and

afternoon chats. She saved me from life-threatening peril on a black diamond slope and taught me to say "y'all" like a Southerner. Now I know what color wedding invitations *should* be and what my official monogram is *supposed* to look like (something involving the letters C, R, and G). Thanks for your sweetness and smile and honesty. I love a Linz!

Jenn Phillips is a wonderful, one-of-a-kind friend and I am grateful for her support and encouragement. You can't help but get caught up in her enthusiasm, humor, exuberance, and contagious laughter. Thank you, Jenn, for introducing me to designer jeans, booty dancing, and feather boas.

Tim Petrie is indeed fantastic – a fantastic labmate, a fantastic beach-goer, a fantastic Starbucks enthusiast, a fantastic shopping buddy, and a fantastic friend. Little bits of Tim are hidden all over this thesis, including his masterful fragment manufacturing, generous e-beam coating, expert SPR spectroscoping, and all-star adventures in surgery (despite all that pesky blood). Thank you, Tim, for being generous, thoughtful, and all-around California cool.

Kellie Burns is my partner is caffeine addiction, walking avoidance, Chow Baby enthusiasm, and impulse buying. Thank you, Kellie, for taking care of me in the PRL, gassing my rats, introducing me to bomb-ass wings, doubling my shoe collection, and showing me that it really *is* better in Atlanta. You're an awesome friend and I've had fun hangin' with you every day. I'm going to miss our trips to bookstore every afternoon. See you in San Diego, Kel-Dog!

My gratitude and appreciation also goes out to Sean, Amanda, Abbey, and Dave for keeping the García traditions alive. The lab is in good hands.

There is never a dull moment in Wing 2D, and I thank everyone in the Boyan, Levenston, and Guldberg labs for making it a fun place to come to work every day. In particular, I would like to thank Blaise Porter for being Blaise – a guy who is fun and loveable and zesty, with an enviable vocabulary and a recipe for seven-layer bars that truly touches my soul. Thank you, Blaisey, for noticing when I got a haircut, appreciating my extremely overpriced jeans, exchanging witty repartee, discussing Aveda hair products, having tons of fun in seersucker at my wedding, teaching Srin and me how to wow kids with viscoelasticity, and being a great friend. I will never forget the Days of Blaise!

Thanks to Chris Gemmiti for appreciating my photo geekiness, getting me drunk with some kind of Italian raspberry-flavored goodness, reminiscing about Boston with me (mmmm Bluebeery), and letting us party in Jonesboro. I love it when the Goose is loose! I always have fun chatting with Chris and Amy, and I can't wait to watch little Nolan grow up.

All kinds of thanks and shout-outs and mad loves go to The Corner (aka The Procrastination Corner, aka The PC, aka The Noisiest People in the Lair). We've had so much fun and so many laughs and so many priceless moments over the years and even did a little bit of work along the way. I will miss you guys so much and work will never be the same.

Craig Duvall - ever since we embarked on Western blotting adventures together, I've had tons of fun hanging out with you, sharing Maker's Mark, cool ranch Doritos, Willy's burritos, and tons of laughs. You're awesome! For you, I would actually go to Kentucky.

Very special thanks and hugs go to Angela Lin. I don't think, in the six years that I've known Angela, I have adequately expressed how much I adore, admire, and respect her. She is a genuinely cool person, with a wonderful sense of self. I have never heard a single negative thing said about her (except that she's got some pesky ACLs) and that's because she never fails to be kind, fair, thoughtful, generous, and compassionate. All that and the girl can shotgun a beer with the best of them. What's not to love! Thanks, Jeela, for being my Asian lab twin and an awesome friend.

Srin Nagaraja is so much more than just my "brown friend" (or "world-class athlete"… I forget which…). First off, we rocked viscoelasticity. In fact, we totally rocked outreach, in general. I mean, educational outreach will never be reached-out that much again. Which is to say, we make a great team – Srin and I. And that is because he is truly a kindred spirit. He understands what a "Moms" is, why its important to do the right thing, why Bad Boys is the best movie ever, and why I can't resist buying socks from strangers. I will always think of him when I break out the Catholic-do-good card. Thanks, Srin, for all that four-tw…I mean, good conversation, crazy laughs, serious talks, long walks in the hallway, and nee-crop-see on my desk. You're good people. The very best. I am so grateful for your friendship, Srin. Call me.

Thanks to all the IBB faculty and staff who have helped me along the way. In particular, I would like to thank Sally Gerrish for all of her help, support, and encouragement and especially for putting up with Srin and me, with our egos, crazy ideas, and silly conversations.

Finally I must acknowledge the love and constant support of my family throughout the years. Dad, I am so grateful for your encouragement, support, and

excitement about everything that I do. I love all of our long talks and story exchanges and chats on the phone every week. Your advice and opinions mean the whole world to me. Mom, words can not express how thankful I am for everything that you've done for me in the past twenty-eight years. Everything that I am is because of you. I will always be amazed by what an incredible woman, mother, and friend you are. Thank you.

Jon, you're a wonderful, creative, unique, and genuinely good person with great taste in everything and mad grillin' skillz. One of my biggest regrets in going away to college is that we don't get to hang out as much. I am so proud of you and so glad that you're my brother.

Thanks also to Jane, Pete (X), Matt, and Amy Gersbach. You have been so supportive and have truly made me feel like a part of the family. I am so glad I'm a Gersbach!

Most importantly, I have to thank my husband, Charlie. Working together has been so much fun, and I feel extremely lucky to have shared this experience with him. I admire his creativity, integrity, courage, humor, dedication, and brilliant, wacky ideas so much more than I am usually willing to admit. He has made my life rich and meaningful in so many new and wonderful ways. Thank you, Charlie, for believing in me and encouraging me and supporting all my silly moods and interests and goals. You make me a better me and that is the very best gift.

This thesis is brought to you by the number 102,205, the letters GFOGER, the color "puke" green, the word "serendipity", unabashed quirkiness, wild compassion, and the spirit of succulent living.

TABLE OF CONTENTS

LIST OF TABLES

LIST OF FIGURES

LIST OF SYMBOLS AND ABBREVIATIONS

ALP	Alkaline Phosphatase
APC	Allophycocyanin
ANOVA	Analysis of Variance
BCA	Bicinchoninic acid
BIC	Bone-Implant Contact
BMP	Bone Morphogenetic Protein
BMSC	Bone Marrow Stromal Cells
BrdU	Bromodeoxyuridine
BSA	Bovine Serum Albumin
BSP	Bone Sialoprotein
c.p.	Commercially Pure
COL	Collagen
DTT	Dithiothreitol
ECF	Enzyme Catazlyed Fluorescence
ECM	Extracellular Matrix
EDC	1-Ethyl-3-(3-Dimethyllaminopropyl)Carbodiimide
EDTA	Ethylenediaminetetraacetic Acid
EG	Ethylene Glycol
ELISA	Enzyme-Linked Immunosorbent Assay
ERK	Extracellular Signal-Related Kinase
FAK	Focal Adhesion Kinase
FBS	Fetal Bovine Serum
FGF-2	Fibroblast Growth Factor-2

FITC	Fluorescein Isothiocyanate
FNIII7-10	Fibronectin Fragment, 7^{th}-10^{th} type III repeat units
FN	Fibronectin
HA	Hydroxyapatite
LTI	Low Temperature Isotropic
MAPK	Mitogen Activated Protein Kinase
NHS	N-hydroxysuccinimide
OCN	Osteocalcin
PAGE	Polyacrylamide Gel Electrophoresis
PBS	Phosphate Buffered Saline
PEO	poly(ethylene oxide)
PMSF	Phenylmethylsulfonyl
qRT-PCR	Quantitative Reverse Transcription Polymerase Chain Reaction
SAM	Self-Assembled Monolayer
SDS	Sodium Dodecylsulfate
SEM	Standard Error of the Mean
TAN	Ti-6Al-7Nb
TAV	Ti-6Al-4V
TBS	Tris-Buffered Saline
TCP	Tricalcium Phosphate
TFA	Trifluoroacetic Acid
TGF-β	Transforming Growth Factor-β

SUMMARY

Cell adhesion to the extracellular matrix through cell-surface integrin receptors is essential to development, wound healing, and tissue remodeling and therefore represents a central theme in the design of bioactive surfaces that successfully interface with the body. This is especially significant in the areas of integrative implant coatings and tissue engineering, since adhesion triggers signals that regulate cell cycle progression and differentiation in multiple cellular systems.

This research project focuses on establishing a molecular strategy for engineering biomimetic surfaces that promote bone formation and osseointegration. The *objective* is to engineer bioactive hybrid surfaces that support osteoblastic differentiation and promote osseointegration by targeting specific integrin receptors that are critical to osteoblast function. The *central hypothesis* of this project is that the controlled presentation of type I collagen and fibronectin binding domains onto well-defined substrates will result in integrin-specific bioadhesive surfaces that support osteoblastic differentiation, matrix mineralization, and osseointegration.

We tested this central hypothesis by designing and characterizing a collagen-mimetic peptide that specifically targets the $\alpha_2\beta_1$ integrin by incorporating the necessary primary, secondary, and tertiary conformations. The integrin $\alpha_2\beta_1$ recognizes the glycine-phenylalanine-hydroxyproline-glycine-glutamate-arginine (GFOGER) motif in residues 502-507 of the α1[I] chain of type I collagen. Integrin recognition is entirely dependent on the triple-helical conformation of the ligand similar to that of native collagen. Our first study focuses on engineering $\alpha_2\beta_1$-specific bioadhesive surfaces by

immobilizing our triple-helical collagen-mimetic peptide incorporating the GFOGER binding sequence onto model non-adhesive substrates. Circular dichroism spectroscopy verified that this peptide adopts a stable triple-helical conformation in solution. Passively adsorbed GFOGER-peptide exhibited dose-dependent HT1080 cell adhesion and spreading comparable to that observed on type I collagen. Subsequent antibody blocking conditions verified the involvement of integrin $\alpha_2\beta_1$ in these adhesion events. Focal adhesion formation was observed by immunofluorescent staining for $\alpha_2\beta_1$ and vinculin on MC3T3-E1 cells. Model functionalized surfaces were then engineered using three complementary peptide tethering schemes. These peptide-functionalized substrates supported $\alpha_2\beta_1$-mediated cell adhesion and focal adhesion assembly. Our results demonstrate that this peptide is active in an immobilized conformation and may be applied as a surface modification agent to promote $\alpha_2\beta_1$–specific cell adhesion.

Several studies indicate that the $\alpha_2\beta_1$ integrin interaction with type I collagen is a crucial signal for the induction of osteoblastic differentiation and matrix mineralization. Our next study demonstrates that the $\alpha_2\beta_1$ integrin-specific GFOGER-peptide triggers the activation of focal adhesion kinase (FAK) and alkaline phosphatase in MC3T3-E1 murine immature osteoblast-like cells - two proteins that have been implicated in the osteoblastic differentiation pathway. These GFOGER-peptide surfaces also support the expression of multiple osteoblast-specific genes, including osteocalcin and bone sialoprotein, and induce calcification and matrix mineralization in a manner similar to type I collagen, suggesting that this triple-helical peptide represents a promising surface modification strategy for the design of collagen-mimetic bioadhesive surfaces that support osteoblastic differentiation and bone formation.

Implant osseointegration, defined as close bone apposition and functional fixation, is a prerequisite for clinical success in orthopaedic and dental applications, many of which are restricted by implant loosening.(Pilliar, 2005)(Anderson, 2001) Our strategy to improve osseointegration of titanium implants focuses on presenting the GFOGER collagen-mimetic peptide that triggers $\alpha_2\beta_1$ cellular integrin receptor binding, which is crucial for bone mineral deposition. Titanium surfaces presenting integrin-specific GFOGER-peptide trigger osteoblastic differentiation in primary rat bone marrow stromal cells, including bone-specific gene expression, alkaline phosphatase activity, and mineral deposition, leading enhanced osteoblastic function compared to unmodified orthopaedic-grade titanium. Furthermore, this integrin-targeted surface coating significantly improved peri-implant bone regeneration and mechanical osseointegration compared to untreated titanium in a rat tibia cortical bone implant model. Faster integration of these GFOGER coated implants would result in sooner and more reliable loading in a clinical setting, improving device function and patient outcomes. This study establishes a simple, single-step biologically active implant coating that enhances bone repair and titanium implant integration for clinical orthopaedic and dental applications.

The objective of our next study was to engineer bioactive hybrid surfaces that control cell function by mimicking integrin-ECM interactions. We target two specific integrins essential to differentiation in several cell systems – the type I collagen (COL-I) receptor $\alpha_2\beta_1$ and the fibronectin (FN) receptor $\alpha_5\beta_1$ – by tethering varying densities of a collagen-mimetic peptide and a recombinant fragment of FN onto non-adhesive supports.

The wide range of controlled mixed ligand densities generated by this process demonstrates the feasibility of generating integrin-specific hybrid surfaces. Results

indicate increased cell adhesion and synergistic activation of FAK, which underscore the advantage of specifically targeting more than one integrin implicated in a particular signaling pathway and downstream cellular effect. Proliferation rate results confirm that the enhanced signaling effects of mixed ligand surfaces translate to downstream cellular responses. This study suggests that, instead of focusing on a single integrin-ligand interaction, in some cases it may be advantageous to consider the interplay of multiple integrins implicated in a desired cell response and their combined effect on downstream cellular signals.

Extracellular matrix proteins are also attractive biomimetic targets for functionalizing orthopaedic implant surfaces in order to promote healing, bone formation, and implant fixation. Again, we target two specific integrins essential to differentiation in osteoblast cells – the type I collagen (COL-I) receptor $\alpha_2\beta_1$ and the fibronectin (FN) receptor $\alpha_5\beta_1$ – using the GFOGER triple helical peptide and the recombinant FNIII7-10 fibronectin fragment. This final study compares the osseointegrative potential of these single-component integrin-specific peptides to a mixed surface treatment presenting both peptides. We also examine the efficacy of the biomimetic integrin-targeted peptides compared to their native matrix proteins as implant coating treatments.

The *in vivo* results indicate that either of the integrin-targeted peptide treatments is sufficient to improve bone formation and implant mechanical integration compared to unmodified titanium. These biomimetic peptides also show improved osseointegration over the native matrix proteins, fibronectin and type I collagen. However, the combination treatment of both biomimetic peptides did not confer any osseointegrative advantage over the single-component coatings.

This thesis proposes a specific biomolecular strategy to engineer implant surfaces that enhance bone formation and osseointegration. We designed and evaluated a collagen mimetic peptide as an $\alpha_2\beta_1$ integrin-specific surface modification agent for biomaterials, implant surface treatments, and tissue engineering scaffolds. This peptide was verified in the osteoblast cell model, but may be applied to several other cell systems that express $\alpha_2\beta_1$, including platelets, epithelial cells, fibroblasts, chondrocytes, endothelial cells, and lymphocytes. We also established the extent to which the presentation of multiple integrin-binding ligands synergize to enhance intracellular signaling. This allows for the rational engineering of optimal biospecific surfaces for implant coatings and tissue engineering scaffolds. Finally, by analyzing the osseointegrative properties of these bioinspired materials, we have established the potential of this biomimetic ligand approach as a beneficial surface treatment for orthopaedic implants. As a whole, this project has established a targeted biomolecular surface engineering strategy for designing and optimizing biologically active implant coatings and grafting substrates that enhance implant bone repair.

CHAPTER 1

SPECIFIC AIMS

Implant integration is critical to numerous orthopaedic replacement applications, many of which are limited by implant loosening and wear, especially in younger patients. Current implant surface technologies focus on porous coatings for bone ingrowth and bone-bonding ceramic coatings to promote integration with the surrounding bone and provide mechanical friction. However, these approaches are restricted by inadequate cell-surface interactions leading to slow rates of osseointegration and poor mechanical integrity. Therefore, developing biologically active osseous implant coatings should address the inadequate bone cell-material interactions that currently hinder existing technologies.

Cell adhesion to the extracellular matrix through cell-surface integrin receptors is essential to development, wound healing, and tissue remodeling and therefore represents a central theme in the design of bioactive surfaces that successfully interface with the body. This is especially significant in the areas of integrative implant coatings and tissue engineering, since adhesion triggers signals that regulate cell cycle progression and differentiation in multiple cellular systems.

This research project focuses on establishing a molecular strategy for engineering biomimetic surfaces that promote bone formation and osseointegration. **The *objective* is to engineer bioactive hybrid surfaces that support osteoblastic differentiation and promote osseointegration by targeting specific integrin receptors that are critical to osteoblast function. The *central hypothesis* of this project is that the controlled**

presentation of mixed type I collagen and fibronectin binding domains onto well-defined substrates will result in integrin-specific bioadhesive surfaces that support osteoblastic differentiation, matrix mineralization, and osseointegration. Binding of specific integrins to the extracellular matrix proteins fibronectin and type I collagen has been shown to induce differentiation and bone matrix mineralization in several osteoblastic cell models.

Aim 1: Engineer $\alpha_2\beta_1$ integrin-specific surfaces that support cell adhesion and direct osteoblastic differentiation in vitro.

The *working hypothesis* is that a type I collagen-mimetic synthetic peptide of minimal recognition sequence can be grafted to a stable, non-adhesive substrate to produce biologically active, chemically well-defined surfaces that support $\alpha_2\beta_1$-specific cell adhesion and direct osteoblastic differentiation. A triple-helical collagen mimetic peptide will be designed to incorporate the central $\alpha_2\beta_1$-binding domain from type I collagen. Its bioadhesive activity will be characterized using several surface modification techniques, including passive adsorption, specific noncovalent surface interaction, and covalent immobilization.

Aim 2: Identify optimal surface densities of mixed fibronectin- and type I collagen-mimetic ligands that promote osteoblastic differentiation and matrix mineralization.

The *working hypothesis* is that controlled presentation of mixed fibronectin- and type I collagen-mimetic ligands will support immature osteoblast cell adhesion, osteoblastic differentiation, and mineralization more effectively than single ligand or non-functionalized surfaces. Model integrin-specific surfaces, such as mixed biotinylated

ligands on avidin substrates, will be used to screen a wide range of mixed surface formulations and identify optimal ligand densities for biomimetic implant coatings.

Aim 3: Evaluate the ability of integrin-specific biomimetic surfaces to improve osseointegration.

The *working hypothesis* is that biomimetic surfaces presenting mixed fibronectin and type I collagen ligands will exhibit enhanced osseointegrative properties compared with single ligand or unmodified implant surfaces. Titanium implants will be functionalized with single and mixed biomimetic ligands. Osseointegration will be evaluated in a rat tibia cortical bone model using quantitative histomorphometry and pull-out mechanical testing.

Project Significance

Orthopedic disorders, including non-union fractures and bone loss associated with trauma, joint replacements, and tumors, have a tremendous socioeconomic impact in the U.S. in terms of personal and occupational disability and related health care costs. For example, over 713,000 joint arthoplasties, primarily hip and knee procedures in arthritic patients, at a cost of approximately $15 billion were performed in 2000.(American Academy of Orthopaedic Surgeons, 2000) One of the most compelling factors that restrict current joint replacement applications is insufficient implant integration into the surrounding bone, resulting in implant loosening. This often leads to patient discomfort, pain and ultimately revision surgery. More importantly, the lifetime of these implants must increase as the number of younger patients needing joint replacements continues to steadily increase.(Arthritis Foundation and CDC, 1999) Considerable efforts have focused on implant surface technologies that promote early integration into the

surrounding bone, particularly porous coatings for bone ingrowth and bone-bonding ceramic coatings.(Bauer and Schils, 1999b) However, slow osseointegration and biological activity, particularly in terms of bone cell-materials interactions, severely hinder these current approaches.(Ducheyne and Cuckler, 1992) With this project, we have established a specific biomolecular strategy to overcome these inadequate osteogenic cell-material interactions associated with current implant coatings. **The research is *significant* because it seeks to engineer biospecific surfaces targeting particular integrin receptors associated with cellular responses that are critical to osseointegration and bone repair.** Numerous bioadhesive surfaces have been designed to incorporate short cell binding sequences such as the fibronectin triplet RGD, which binds a variety of cell surface receptors. However this project is fundamentally different in that its objective is to target two specific integrin receptors essential to osteoblast differentiation – the type I collagen receptor $\alpha_2\beta_1$ and the fibronectin receptor $\alpha_5\beta_1$ – by presenting peptides with specific secondary conformations and binding site orientations. **This integrin-targeted biomolecular approach provides a versatile and robust strategy for developing bioactive surfaces that support osteoblastic differentiation and enhance bone repair.** Due to the fundamental character of the receptor-ligand principles addressed in this research project, these general engineering strategies can be applied to a variety of other cell systems in the body and may well contribute to the genesis of research projects that address medical concerns in areas other than orthopedic bioengineering.

CHAPTER 2

LITERATURE REVIEW

Bone Anatomy and Function

Bone tissue serves three primary functions in the human body (Yaszemski et al., 1996b). First, bone is the central calcium reservoir for the body, exchanging this mineral with the extracellular fluids to maintain tightly regulated ion homeostasis. Second, the marrow cavities within bone supply hematopoietic and mesenchymal stem cells and infection-fighting white blood cells. Finally, the third function of bone is its mechanical role as the structural support for the body and its vital organs and tissues as well as the skeletal anchor points for muscles, tendons, and ligaments that generate force and provide locomotion. It is mainly this mechanical function of bone that drives the development of bone regeneration, transplantation, and fixation strategies in a wide variety of clinical settings. The restoration of compromised mechanical integrity is a central requirement in a patient's skeletal rehabilitation (Puleo and Nanci, 1999;Yaszemski, Payne, Hayes, Langer, and Mikos, 1996b).

There are three groups of bones – short, flat, and long (Stewart, 1997). Short bones, such as the tarsals, carpals, and vertebral bodies, have approximately the same dimensions in all directions. Flat and long bones have one dimension that longer or shorter than the other two. Long bones, such as femur and tibia, form extended cylinders with a flared structure at either end (epiphysis and metaphysis), flanking a thick-walled central region (diaphysis) (Yaszemski et al., 1996a).

Morphologically, the mature human skeleton consists of trabecular (cancellous) bone and cortical (compact) bone, each of which is defined by the spatial orientation of the mineral and by its characteristic locations in the body (Marks and Hermey, 1996;Yaszemski, Payne, Hayes, Langer, and Mikos, 1996a;Buckwalter et al., 1995a). Cortical bone is denser than trabecular bone and consists of concentric lamellae of densely packed collagen fibrils. This type of bone comprises the outer cylindrical shell of the long bones and the outer surfaces of the short and flat bones and generally provides the mechanical and protective functions of the bone tissue (Marks and Hermey, 1996). Trabecular bone has a loosely organized, porous structure, resembling open-celled foam and comprised of rods and plates. It occurs near the ends of the long bones, the interior of short bones, and between the outer surfaces of flat bones (Yaszemski, Payne, Hayes, Langer, and Mikos, 1996a) and represents the primary site of bone's metabolic functions (Marks and Hermey, 1996).

Bone Cell Types and Functions

The cells within bone tissue have the unique capacity to heal fractures and defects without the formation of a fibrous scar tissue. The four main cell types are osteoblasts, osteocytes, and bone-lining cells that originate from the mesenchymal stem-cell line and osteoclasts that originate from the hematopoietic stem-cell line (Marks and Hermey, 1996).

Osteoblasts are the differentiated cells responsible for the deposition and mineralization of the bone matrix at the tissue surface (Aubin and Liu, 1996). The cytoplasmic processes of osteoblasts extend through the osteoid matrix to come into contact with osteocytes within the mineralized matrix (Buckwalter, Glimcher, Cooper,

and Recker, 1995a). These specialized cell contacts may help to coordinate the activities of these two types of cells. Systemic hormones, such as parathyroid hormone, and local cytokines also stimulate these osteoblasts to release mediators that activate osteoclasts in order to regulate skeletal homeostasis (Athanasou, 1996;Buckwalter, Glimcher, Cooper, and Recker, 1995a). Active osteoblasts may follow one of three fates. They may remain on the surface of the bone, decrease their synthetic activity, and assume the flatter form of bone-lining cells; they may surround themselves with matrix and become osteocytes; or they may disappear from the site of bone formation (Buckwalter, Glimcher, Cooper, and Recker, 1995a).

Bone-lining cells, sometimes referred to as resting osteoblasts or surface osteocytes, sit directly on resting bone surfaces and have a flattened morphology (Marks and Hermey, 1996;Buckwalter, Glimcher, Cooper, and Recker, 1995a). In the presence of parathyroid hormone, these cells contract and secrete enzymes that remove the thin layer of osteoid that covers the mineralized matrix, permitting osteoclasts to attach to the surface begin resorption of bone (Buckwalter, Glimcher, Cooper, and Recker, 1995a). Through these and other actions, bone-lining cells may have a role in attracting osteoclasts to specific sites and in stimulating them to resorb bone.

Comprising more than 90 percent of the bone cells in the human skeleton, osteocytes are mature osteoblasts that have become embedded in bone matrix and are responsible for tissue maintenance (Buckwalter, Glimcher, Cooper, and Recker, 1995a). Each osteocyte occupies a single lacunae within the matrix and extends long, branching cytoplasmic processes through the canaliculi to contact processes of adjacent cells (Marks and Hermey, 1996;Buckwalter, Glimcher, Cooper, and Recker, 1995a). These

connections allow communication with neighboring osteocytes, the internal and external surfaces of the bone, and with blood vessels and also allow the bone cell network to sense deformation of the bone matrix and streaming potentials.

Osteoclasts are large multi-nucleated cells that resorb bone through mineral dissolution and enzymatic digestion of the organic matrix (Marks and Hermey, 1996;Athanasou, 1996;Buckwalter, Glimcher, Cooper, and Recker, 1995a). They are characterized by plentiful mitochondria, which fill much of their cytoplasm to supply the energy that is required to resorb bone, and by the complex folding of their cytoplasmic membranes at the sites of bone matrix resorption. Within these ruffled borders, membrane-bound proton pumps transport protons into the sealed space at the interface of the bone, decreasing the pH from approximately 7 to approximately 4. This acidic pH solubilizes the bone mineral. To degrade the remaining organic matrix, the osteoclasts secrete acid proteases.

Bone Matrix

Bone is a composite material consisting of an organic and an inorganic component (Buckwalter, Glimcher, Cooper, and Recker, 1995a). The inorganic component contributes approximately 65 percent of the wet weight of the bone. The organic component usually contributes approximately 20 percent of the wet weight, and water contributes approximately 10 percent. The organic component, primarily collagen, gives bone its form and tensile strength, while the inorganic, or mineral, component primarily resists compression.

The organic matrix is composed mainly of collagens, particularly type I collagen. The remaining 10 percent of the organic matrix consists of non-collagenous

glycoproteins and bone-specific proteoglycans that may influence the organization of the matrix, the mineralization of the bone, and the behavior of the bone cells. These proteins include osteocalcin, osteonectin, bone sialoprotein, bone phosphoproteins, and small proteoglycans.

The inorganic mineral phase of bone serves as an ion reservoir. Approximately 99 percent of the body's calcium, approximately 85 percent of phosphorus, and between 40 and 60 percent of sodium and magnesium are associated with the bone mineral crystals, which are the major source of these ions to and from the extracellular fluid (Buckwalter, Glimcher, Cooper, and Recker, 1995a). The calcium-phosphate crystals (hydroxyapatite with both carbonate and acid phosphate substitutions) of the mineral phase also give bone much of its stiffness and strength.

Bone Formation, Remodeling, and Healing

Bone formation can be first recognized when undifferentiated mesenchymal cells or preosteoblasts develop into osteoblasts and begin to secrete a specialized extracellular matrix (Buckwalter et al., 1995b). As this matrix mineralizes, the osteoblasts that are surrounded by the resultant mineral become osteocytes. Osteoclasts are then mobilized to begin the remodeling process that converts immature woven bone into mature, structurally sound lamellar bone.

This process of bone formation may occur within cartilage (enchondral ossification), within an organic matrix membrane (intramembranous ossification), or by deposition of new bone on existing bone (appositional bone formation) (Buckwalter, Glimcher, Cooper, and Recker, 1995b).

Endochondral ossification is responsible for the formation of embryonic long bones and weight-bearing bones, such as vertebrae, and occurs via a preexisting cartilaginous template (Buckwalter, Glimcher, Cooper, and Recker, 1995b). After the formation of hyaline or hyaline-like cartilage, the chondrocytes become hypertrophic and initiate calcification of the template. These cells then become apoptotic triggering vascular buds to invade the cartilage and incomings cells to resorb portions of the cartilage, creating marrow cavities. Osteoprogenitor cells invade the region and differentiate into osteoblasts, which form bone matrix on the mineralized cartilage. Osteoclasts then resorb the calcified cartilage and immature bone, and osteoblasts replace the mixture of calcified cartilage and immature bone with mature lamellar bone.

Intramembranous ossification leads to the development of flat bones, such as the skull, and occurs without the presence of a cartilaginous intermediate (Buckwalter, Glimcher, Cooper, and Recker, 1995b). Instead this process is triggered by the aggregation of undifferentiated mesenchymal cells into layers or membranes. These cells synthesize a loose organic matrix that often contains blood vessels, fibroblasts, and osteoprogenitor cells. The osteoprogenitor cells differentiate into osteoblasts and initiate the assembly of osteoid (uncalcified bone matrix). Trabecular bone and vascular structures then begin to form within this tissue. As the trabecular bone fragments thicken they begin to fuse into continuous plates, and the irregular woven bone is replaced with structured lamellar bone.

Appositional bone formation occurs during periosteal enlargement of bones and during bone-modeling and remodeling (Buckwalter, Glimcher, Cooper, and Recker, 1995b). Unlike endochondral or intramembranous ossification, appositional formation

begins with the alignment of osteoblasts on an existing bone surface. These cells then synthesize osteoid, often in successive layers that form bone lamellae.

After the initial ossification of the embryonic skeleton, osteoclasts and osteoblasts begin modeling and remodeling each bone (Marks and Hermey, 1996;Buckwalter, Glimcher, Cooper, and Recker, 1995b). Bone remodeling is a highly coordinated balance between osteoclast resorption and osteoblast production, through a sequence of events that include osteoclast activation, resorption of bone, osteoblast activation, and formation of new bone at the site of resorption.

Bone modeling and remodeling can also be associated with bone implants, as more types of implants are developed and the use of these devices increases. The stabilization of fracture-fixation devices, implants designed to correct skeletal deformity, and joint replacements to the underlying bone structure necessarily alters the loading pattern of the skeleton. For instance, a stiff plate rigidly fixed to bone tends to unload the bone, leading to increased porosity of the cortex (Buckwalter, Glimcher, Cooper, and Recker, 1995b). Adaptive modeling or remodeling also occurs in response to other types of implants, including joint replacements (Vasu et al., 1986).

A fracture to the bone disrupts skeletal continuity, mechanical function, and blood supply. This triggers the process of fracture healing, which via distinct biological stages (Yaszemski, Payne, Hayes, Langer, and Mikos, 1996a). The biological stages are inflammation, repair, and remodeling by which the defect heals through endochondral ossification. The first event after trauma is the development of a haematoma and fibrin clot due to damaged blood vessels. The clotting and inflammatory cascades proceed, with aggregated platelets releasing vasoactive mediators and growth factors. Acute

inflammatory cells (polymorphonuclear leukocytes, macrophages) arrive at the site and remove the necrotic tissue.

The repair phase is marked by osteoblasts and osteoprogenitor cells infiltrating the defect site from the blood stream and marrow tissues (Yaszemski, Payne, Hayes, Langer, and Mikos, 1996a). These cells secrete organic matrix which ossifies to form new woven bone. This new material, consisting of osteoblasts, cartilaginous matrix, and woven bone, forms the fracture callous.

The third and longest biological stage in fracture healing is remodeling. In this phase, the woven bone goes through several steps of resorption and deposition to form organized lamellar bone, in which the mineral and organic phases are optimally aligned to resist local stresses (Yaszemski, Payne, Hayes, Langer, and Mikos, 1996a).

Bone-Anchored Implants

Over 700,000 joint arthroplasties and between 100,000 and 300,000 dental implant surgeries are performed each year in the United States to replace or regenerate function to damaged and diseased tissues at a cost of over $15 billion (Puleo and Nanci, 1999),(American Academy of Orthopaedic Surgeons,) Today many of these titanium implant-based surgeries and joint replacements are relatively successful, with restored function lasting over ten years in some cases. However, implant loosening still remains one of the most compelling complications of all major joint arthroplasty and bone fixation surgeries, due to poorly optimized anchorage of the implant to the bone tissue (Puleo and Nanci, 1999). This often leads to patient discomfort, pain, and ultimately revision surgery, resulting in a significant socioeconomic impact in the U.S., in terms of both personal disability and health care costs. More importantly, the lifetime of these

implants must increase as the number of younger patients needing joint replacements continues to steadily increase (Arthritis Foundation and CDC, 1999). In this clinical climate, advances in bone in-growth and osseointegration, by optimizing the bone-implant interface, should improve the long term results of these procedures.

Osseointegration

The goal of current orthopedic implantology is the design of devices that induce controlled, guided, and rapid healing and osseointegration. Osseointegration is defined as the direct anchorage of an implant to bone through the formation of bony tissue around the implant without the growth of a fibrous capsule at the bone-implant interface (Branemark, 1996).

R. Branemark and R. Skalak have proposed a complete definition of osseointegration as the sum of definitions from various viewpoints as reproduced below (Branemark, 1996).

1. *From the viewpoint of the patient:*

   An implant fixture is osseointegrated if it provides a stable and apparently immobile support of a prosthesis under functional loads, without pain, inflammation, or loosening over the lifetime of the patient.

2. *From the viewpoint of macro- and microscopic biology and medicine:*

   Osseointegration of a fixture in bone is defined as the close apposition of new and reformed bone in congruency with the fixture, including surface irregularities, so that at light microscopic level there is no interpositioned connective or fibrous tissue and that a direct structural and functional connection is established, capable

of carrying normal physiological loads without excessive deformation and without initiating rejecting mechanisms.

3. *From a macroscopic, biomechanical point of view:*

   A fixture is osseointegrated if there is no progressive relative motion between the fixture and the surrounding living bone and marrow under functional levels and types of loading for the entire life of the patient and exhibits deformations of the same order of magnitude as when the same loads are applied directly to the bone.

4. *From a microscopic biophysical point of view:*

   Osseointegration implies that at light microscopic and electron microscopic levels, the identifiable components of tissue within a thin zone of a fixture surface are identified as normal bone and marrow constituents which continuously grade into a normal bone structure surrounding the fixture and that mineralized tissue is found to be in contact with the fixture surface over most of the surface within nanometers so that no functionally significant intervening material exists at the interface.

These outcomes allow for faster patient recuperation and stable fixation between the bone and the implant that would permit early or immediate loading of the device (Puleo and Nanci, 1999). This has great potential in terms of decreased patient morbidity, improved patient psychology, and decreased healthcare costs. Achieving these goals, however, requires an intimate understanding of the tissue healing events involves in a rigid orthopedic biomaterial implantation.

Host Response and Healing at the Bone-Implant Interface

The tissue response to implants surgically anchored in bone involves a cascade of cell and matrix events that ideally result in the intimate apposition of bone to the biomaterial (i.e. osseointegration). Development of this interface is complex, involving numerous factors primarily at the bone-implant junction. These disparate factors include implant material, shape, topography, and surface chemistry as well as mechanical loading, surgical technique, and patient bone quality (Puleo and Nanci, 1999;Boyan et al., 1996;Kieswetter et al., 1996;Schwartz and Boyan, 1994).

The surgical trauma associated with bone implantation is similar to that of a bone fracture previously described. After implantation, a hematoma is formed, which initiates the clotting cascade. Bone debris produced during drilling and implant fixation is deposited around the implantation site (Branemark, 1996), which will eventually be cleared by macrophages and multinucleated foreign body giant cells and/or covered by new bone (Sennerby et al., 1993). Approximately three days after implantation of titanium implants, mesenchymal cells migrate from the bone marrow into the defect site and osteoblasts begin producing osteoid at the endosteal surface of the cortex (Sennerby, Thomsen, and Ericson, 1993). Woven bone formation begins to occur after three to five days both at the implant, at the endosteal surface, and in the intermedullary canal (Branemark, 1996). Thus bone formation occurs in two directions; healing bone approaches the biomaterial, and bone extends from the implant toward the healing bone (Puleo and Nanci, 1999). In fact, fluorochrome labeling indicates that the bone extending away from the implant forms about 30 percent faster than the bone moving toward the implant (Puleo and Nanci, 1999). This initial woven bone is gradually remodeled into

more mature compact lamellar bone, which is evident after three to four weeks (Branemark, 1996;Murai et al., 1996;Schwartz and Boyan, 1994). Mature bone morphology is event at four to six weeks (Branemark, 1996;Murai, Takeshita, Ayukawa, Kiyoshima, Suetsugu, and Tanaka, 1996). In most cases, around the seventh day, multinuclear foreign body giant cells are in direct contact with the implant and form a near continuous layer along the material surface (Sennerby, Thomsen, and Ericson, 1993). The number of these giant cells decreases with both time and increased bone-implant contact.

During this time, unfavorable conditions, such as excessive interfacial micromotion, will disrupt the newly forming tissue, leading to the formation of a fibrous capsule and poor osseointegration (Joos et al., 2006;Puleo and Nanci, 1999). It is possible that the relative motion between the bone and the implant surface damages the initial fibrin network and vasculature that form during the early bone healing process. Thus the events are shifted from a normal healing process to repair by scar tissue (Joos, Wiesmann, Szuwart, and Meyer, 2006;Puleo and Nanci, 1999).

This cascade of healing events around bone-anchored implants is similar to the sequence of fracture healing, but is modulated by the host response induced by implant shape, material, and surface properties (Joos, Wiesmann, Szuwart, and Meyer, 2006;Branemark, 1996). The process is also dependent on the quality of the tissue, with increased healing capacity for growing skeletal tissue and decreased healing capacity in older individuals (Joos, Wiesmann, Szuwart, and Meyer, 2006;Murai, Takeshita, Ayukawa, Kiyoshima, Suetsugu, and Tanaka, 1996;Roberts et al., 1984). Variability in the host physiology is also a critical factor in the healing response, which is influenced by

nutrition, hormonal status, pharmaceutical history, immunology, or the presence of disease or infection (Schwartz and Boyan, 1994). Finally the mechanical and physical stresses that are translated to the implant or the healing tissue can have a significant impact on the healing process as well as the remodeling and maturation of the initial osseous template (Schwartz and Boyan, 1994).

Material Response at the Bone-Implant Interface

The first event that occurs upon implantation of metals, as with all biomaterials, is the adsorption of proteins from blood and tissue fluids at the wound site and later from cellular activity in the periprosthetic region (Puleo and Nanci, 1999;Horbett, 1996;Horbett and Brash, 1987). Once on the surface, these proteins can desorb, denature, or remain on the device to mediate tissue-biomaterial interactions by interacting with cell membrane receptors, such as integrins. Other organic and inorganic moieties may also coat the device surface, including lipids, and ions (Kieswetter, Schwartz, Dean, and Boyan, 1996). The catalogue of adsorbed proteins and other components initially present on an implant surface is highly dependent on surface characteristics, such as surface composition, roughness, topography, and surface energy, which collectively dictate the biological response to an implanted device (Kieswetter, Schwartz, Dean, and Boyan, 1996).

In addition to protein adsorption, significant changes also occur in the materials surface. While most implant biomaterials are chosen for their stable oxide layers, these metals may still undergo electrochemical changes in a physiological environment that increase the thickness of the oxide film (Puleo and Nanci, 1999). Several studies have demonstrated that oxide films on pure titanium implants may grow as much a three times

thicker in human tissue (Puleo and Nanci, 1999). These events may also result in the release of metal ions into the tissue that accumulate locally and, in some cases, spread systemically (Puleo and Nanci, 1999).

Implant Material Selection

The vast majority of orthopedic implant materials are metals, metallic alloys, or metal composites, due to their bone-compatible biomaterial properties, such as tensile strength, stiffness, fracture toughness, and fatigue resistance (Muller et al., 2005b;Boyan, Hummert, Dean, and Schwartz, 1996). Stainless steels are often used for fracture fixation devices, such as bone plates and screws and spinal rods, because of favorable mechanical properties and cost effectiveness compared to other metallic implant materials (Muller, Abke, Schnell, Macionczyk, Gbureck, Mehrl, Ruszczak, Kujat, Englert, Nerlich, and Angele, 2005b;Disegi and Eschbach, 2000). Stainless steel bone screws are also desirable because, unlike titanium, the stainless steel allows the surgeon to feel the onset of plastic deformation and thus avoid overtorquing the device (Disegi and Eschbach, 2000). However, although stainless steel implants provide better biomechanical properties than cobalt or titanium alloys, their reduced corrosion resistance and biocompatibility limit their clinical applications (Muller, Abke, Schnell, Macionczyk, Gbureck, Mehrl, Ruszczak, Kujat, Englert, Nerlich, and Angele, 2005b).

Cobalt alloys (e.g. CoCrW, CoCrMo, etc.) are often chosen for implant materials because they are non-magnetic and wear, corrosion, and heat-resistant, exhibiting high strength even at elevated temperatures (Marti, 2000). They are mainly used in orthopedic prostheses for the knee, hip, and shoulder, which are long-term implants that must meet extremely stringent requirements for biocompatibility and corrosion resistance.

However, these alloys are extremely difficult to fabricate and are limited to joint replacement devices in which their favorable material properties compensate for more demanding and costly manufacturing (Marti, 2000). In other orthopedic applications, such as fracture fixation, the particular advantages of cobalt alloys are less effective in comparison with stainless steel and titanium.

Commercially pure titanium has been the most extensively used metal for osseointegrated implants, particularly in the fields of osteosynthesis, oral implantology, and in certain joint prosthetics (Pohler, 2000;Branemark, 1996). In the presence of oxygen, an oxide layer is rapidly formed on the titanium surface, consisting mainly of TiO_2. This passive oxide film adheres closely to the bulk metal and is very dense, rendering titanium one of the most highly corrosion-resistant metals in existence, even in the demanding physiological environment. The oxide layer forms near instantaneously after mechanical destruction and therefore no corrosion attach is evident under fretting conditions, such are relative motion between titanium screw heads and plate holes (Pohler, 2000).

Titanium oxide also has a high dielectric constant, resulting in stronger van der Waals bonds on titanium oxide relative to other oxides (Branemark, 1996). This may contribute to titanium's excellent biocompatibility as evidenced by very favorable tissue responses and the absence of allergic reactions (Pohler, 2000). Titanium is also well-known for its impressive osseointegrative properties. In orthopedic applications, bone cells and mineralized bone matrix are closely associated with titanium surfaces without interposition of other tissues (Pohler, 2000), making titanium the gold-standard for bulk orthopedic implant materials.

Titanium also exhibits a lower elastic modulus and greater flexibility than other orthopedic biomaterials (other than polymers). In fact, the elastic deformation of titanium implants is much closer to that of bone, reducing local stress concentrations and avoiding the stress shielding phenomena common to stiffer metals that result in bone resorption (Pohler, 2000). Titanium's mechanical properties may also be modified within a certain range by choosing different titanium grades (different trace element profiles) and by work hardening.

For applications in which greater strength is required, there are several suitable titanium alloys with improved strength and correspondingly more difficult manufacturing and processing procedures (Disegi, 2000). The most commonly used titanium implant alloys in orthopedic applications are Ti-6Al-7Nb (TAN) and Ti-6Al-4V (TAV). These applications include fracture fixation devices such as cannulated bone screws, intramedullary nails, spinal clamps, and stabilization plates.

Implant Surface Technologies

A wide variety of approaches are currently being used in the ongoing effort to obtain an optimal bone-implant interface. Because biological tissues mainly interact with the outermost atomic layers of an implant, many of these efforts focus on methods to modify existing biomaterial surfaces to achieve the desired biological response. Surface modification approaches fall into three categories - physicochemical, morphological, or biochemical (Puleo and Nanci, 1999).

Physicochemical Methods

Physicochemical characteristics, such as surface energy, surface charge, and surface composition, have been altered in order to improve the relative strength with

which certain serum constituents interact with the surface. This initial interaction between the host environment and the biomaterial can have significant downstream effects on cellular attachment and ultimately tissue response. Tailoring the surface chemistry of an implant material to elicit favorable protein adsorption, cell adhesion, and matrix production has emerged as a powerful tool for improving bone cell differentiation and osseointegration (Keselowsky et al., 2005a;Boyan, Hummert, Dean, and Schwartz, 1996;Schwartz and Boyan, 1994). Our lab has demonstrated that integrin binding specificity for adsorbed fibronectin protein regulates the differential effects of biomaterial surface chemistry on osteoblast differentiation and mineralization (Keselowsky, Collard, and Garcia, 2005a).

Given the role of electrostatic interactions in many biological events, presenting charged surfaces has been proposed as a method to optimize tissue integration (Schwartz and Boyan, 1994). Likewise, increased surface energy has also been shown to improve osteoblast differentiation on modified titanium surfaces (Zhao et al., 2005). Glow discharge has also been used to alter charge density and increase surface energy in order to increase tissue adhesion to implant surfaces (Puleo and Nanci, 1999).

Similarly, hydroxyapatite coatings have been investigated due to their chemical resemblance to native bone mineral and their ability to support rapid bone formation (Puleo and Nanci, 1999;Schwartz and Boyan, 1994). It is hypothesized that this surface many present a favorable surface energy for binding serum proteins and growth factors that support bone growth (Schwartz and Boyan, 1994).

Morphological Methods

Modifications of surface roughness and topography have also been used to improve cell and tissue responses to implants. Macro-porous coatings have been investigated based on the hypothesis that bone ingrowth would increase the stability and fixation of implants due to mechanical interlocking (Puleo and Nanci, 1999). In general, the short- and intermediate-term clinical results have been satisfactory. Based on retrieved porous components of joint replacements, implants are well-fixed, bone ingrowth is consistent, and osseointegration is enhanced, particularly in areas of rigid fixation and intimate apposition (Galante and Jacobs, 1992). However, a number of issues have emerged that may jeopardize the long-term success of porous-coated devices. These include femoral component subsidence, porous-surface delamination, endosteal bone loss, and proximal femoral atrophy (Galante and Jacobs, 1992). Retrieval data also demonstrates that only a relatively small percentage of the available pore volume is filled with bone mineral (Puleo and Nanci, 1999).

While porous coatings exploit mechanical interlocking phenomena to improve implant stability, several *in vivo* and *in vitro* studies have focused on generating surfaces with rough microtopographies to improve osteoblast differentiation and bone formation (Lossdorfer et al., 2004;Boyan et al., 2003;Li et al., 2002;Martin et al., 1995;Groessner-Schreiber and Tuan, 1992;Buser et al., 1991;Roberts, Smith, Zilberman, Mozsary, and Smith, 1984). *In vivo* studies have demonstrated that rougher surfaces promote higher levels of bone formation and apposition compared to smoother surfaces (Buser, Schenk, Steinemann, Fiorellini, Fox, and Stich, 1991) and exhibit increased removal torque (Li, Ferguson, Beutler, Cochran, Sittig, Hirt, and Buser, 2002). *In vitro* studies reveal that microrough implant surface topographies improve the phenotypic expression of

osteoblast-like cells (Martin, Schwartz, Hummert, Schraub, Simpson, Lankford, Jr., Dean, Cochran, and Boyan, 1995;Groessner-Schreiber and Tuan, 1992), promote the formation of an osteogenic microenvironment (Boyan, Lossdorfer, Wang, Zhao, Lohmann, Cochran, and Schwartz, 2003), and reduce osteoclast formation and activity (Lossdorfer, Schwartz, Wang, Lohmann, Turner, Wieland, Cochran, and Boyan, 2004). These results have lead to the development of several methods to produce rougher implant surfaces, including plasma-spraying, acid etching, and sandblasting as well as sintered-bead and metal fiber surfaces. These surface roughness approaches not only improve mechanical interlocking and stability and enhance surface area for greater binding of attachment proteins and growth facts, but they also alter phenotypic expression in osteoblast (Schwartz and Boyan, 1994). However, while these approaches are generally successful, they can be restricted by slow rates of osseointegration and poor mechanical anchorage in challenging clinical cases, such as those associated with large bone loss and poor bone quality (Bauer and Schils, 1999a).

Biochemical Methods

Significant advances in understanding the role of biomolecules in regulating cell adhesion, differentiation, and tissue remodeling have led to the investigation of biochemical methods of surface modification. These involve immobilizing proteins, peptides, enzymes, or growth factors onto biomaterial surfaces to induce specific cell and tissue responses. The goal, in this case, is to control the tissue-implant integration with bioactive molecules delivered directly to the interface.

Since the extracellular matrix controls both cell adhesion and function, recent biomimetic strategies have focused on the immobilization of matrix components,

including native structural proteins, (Bernhardt et al., 2005;Becker et al., 2002) peptide sequences, (Bernhardt, van den, Bierbaum, Beutner, Scharnweber, Jansen, Beckmann, and Worch, 2005;Elmengaard et al., 2005a;Elmengaard et al., 2005b;Alsberg et al., 2002b;Ferris et al., 1999b) or synthetic derivatives based on matrix molecules (Lutolf and Hubbell, 2005). The most common peptide-based strategy involves the surface deposition of peptides containing the Arg-Gly-Asp (RGD) sequence, which mediates cell attachment to several matrix proteins, including fibronectin, vitronectin, osteopontin, and bone sialoprotein. However, these bio-inspired strategies have yielded marginal increases in implant integration and mechanical fixation. Because RGD is recognized by a large number of integrins in numerous cell types, this approach lacks specificity for particular targeted integrin signaling and results in non-discriminatory attachment of cells to the RGD-coated surfaces. Therefore, engineering peptides that specifically target integrin signaling cascades implicated in specific tissue responses, for example osteogenesis, would allow the optimization of surface coatings for enhanced integration and performance.

Some groups are addressing this problem by using longer peptide derivatives or proteins that are more specifically associated with the bone environment, such as bone sialoprotein (Rezania et al., 1997), type I collagen (Muller, Abke, Schnell, Macionczyk, Gbureck, Mehrl, Ruszczak, Kujat, Englert, Nerlich, and Angele, 2005b;Becker, Geissler, Hempel, Bierbaum, Scharnweber, Worch, and Wenzel, 2002;Geissler et al., 2000), or heparin-binding domains (Rezania and Healy, 1999;Dee et al., 1998).

While cell adhesion molecules may improve initial bone-implant interactions and cell phenotype, growth factors have also been applied to implant surfaces in order to

improve bone formation. For example, FGF-2 improves proliferation and TGF-β1 enhances collagen synthesis (Puleo and Nanci, 1999). Recently, bone morphogenetic proteins (BMPs) have proven effective in inducing osteogenesis in a wide variety of applications. Several studies focus on combining immobilized peptides or matrix coatings BMPs to improve mineralization (Dee et al., 1996;Rutherford et al., 1992). It is evident that biomimetic peptide and growth factor approaches have great potential for improving the rate and quality of new bone formation at an implant interface, although optimal delivery methods still remain elusive.

Delivery of Biomolecules to the Tissue-Implant Interface

Several factors must be considered in choosing a delivery method for these biomolecules. The biomolecule must be present at the implantation site at or above some threshold concentration, and it must remain for a long enough period of time in order to initiate favorable cellular events (Puleo and Nanci, 1999). To control levels of exposure and concentration, retention and/or release of biomolecules can be modified using methods such as adsorption, covalent immobilization, and release from coatings (Puleo and Nanci, 1999).

The simplest way to delivery biomolecules to the tissue-implant interface is to adsorb from a protein solution prior to implantation. Studies have shown that simple adsorption of TGF-b onto porous coatings can enhance bone ingrowth (Sumner et al., 1995). Similar approaches demonstrated that adsorbed alkaline phosphatase adsorbed on plasma-sprayed titanium improved periprosthetic bone formation (Piattelli et al., 1996). Clearly a major disadvantage with adsorption method is that it allows very little control over the delivery, including retention, release, and orientation of the biomolecules.

Certain biomolecules with stringent exposure, concentration, or conformation requirements may not be compatible with an adsorption delivery method. However, positive responses to adsorbed surfaces have been observed and the simplicity of this approach is particularly attractive for clinical applications.

Covalent tethering of biomolecules to implant surfaces is an alternative to passive adsorption for delivery to the tissue-implant interface. However, in this case, the protein will not be released from the surface, which may be a disadvantage for certain growth factor approaches. Also, for orthopedic and dental applications, metals are particularly deficient in functional groups necessary for immobilizing chemical species, with only oxide layers presenting anchoring sites. For example, silanes have been covalently immobilized to implant materials through surface hydroxyl groups present on the passivating oxide film (Nanci et al., 1998;Puleo, 1997;Puleo, 1995). Plasma treatments and self-assembled monolayers (SAMs) have been used to circumvent the lack of functional group diversity on implant metals. Plasma treatments can increase the number of available hydroxyl groups as well as deposit reactive amino and carboxyl groups, offering versatility for protein tethering (Puleo and Nanci, 1999) Studies have demonstrated that these plasma-deposited films are stable and effective for biomolecule immobilization (Morra and Cassinelli, 1997). Similarly, stable SAMs can be formed by depositing alkanethiols with different terminal functional groups on gold substrates (Tanahashi and Matsuda, 1997;Mrksich et al., 1996). However, deposition of gold and/or assembly of SAMs on the imperfect surfaces of polycrystalline implant metals have not been adequately explored.

Coatings that are impregnated with biomolecules are also being used to delivery biomolecules to the tissue-implant interface. This approach is advantageous because it addresses the issues of exposure time and concentration in a more controlled manner. Coating materials for this application have included ethylene vinyl acetate (EVAc) (Walsh et al., 1995), poly(lactide-co-glycolide) (PLGA) (Agrawal et al., 1997), and collagen (Puleo, 1999).

Experimental Models of Osseointegration

Several experimental models have been proposed for the mechanical evaluation of implant osseointegration. These can be divided into four categories (Branemark, 1996):

1. *Push- or pull-out test of transcortically placed implants* (**Table 2.1**)

   Transcortical implantations represent the simplest *in vivo* model in terms of surgical procedure and mechanical evaluation. Due to their simplicity, these methods are used extensively in testing orthopaedic biomaterials.

2. *Push- or pull-out test of intramedullary placed implants* (**Table 2.2**)

   Intramedullary implantations are clinically relevant models for joint replacement applications such as the total hip replacement. These models are also used for investigating the influence of cyclic loading.

3. *Removal torque of rotationally symmetrical implants* (**Table 2.3**)

   Removal torque is often used to evaluate materials for fixation devices, such as bone screws, and relies on rotational symmetry of cylindrical, often threaded, implants.

4. *Misc. tests, including fracture mechanics*

Push-out, pull-out, and torsion tests are essentially structural evaluations and only provide an apparent bond strength, obtained by dividing the load at failure by the interfacial area or area of bone apposition (if available). More recently, a fracture mechanics approach was proposed to evaluate the interfacial strength in terms of fracture toughness (Wang et al., 1996). This method measures the energy required to extend an interfacial crack and measures interfacial bonding strength in terms of an intrinsic fracture property.

Several studies indicate that there is little value in comparing absolute results from different test setups, especially the push- or pull-out tests (Wang, Subramanian, Dhanda, and Agrawal, 1996;Shirazi-Adl et al., 1994;Dhert et al., 1992;Harrigan et al., 1990). In particular, differences in species, implantation site (e.g. cortex, trabecular bone, intramedullar), surgical technique (e.g. drilling/cooling methods, mode of insertion), loading conditions, and evaluation procedures all have profound effects on the removal load or shear stress measured in *in vivo* osseointegration models. Specimen size and geometry are also important factors in interfacial strength testing (Wang, Subramanian, Dhanda, and Agrawal, 1996).

Table 2.1. Push- or pull-out tests of transcortically placed implants*

(? = conditions not clearly stated)

Reference	Species	Healing Time	Testing	Anatomical location	Implant Material	Surface	Shear stress (Mpa)
Anderson et al (1984)(Anderson et al., 1984)66	Dog	6 months	Fresh ?	Femur	Ti, carbon-coated Ti, pyrolytic carbon	Porous	1.9 - 27.1
Bobyn et al (1980)(Bobyn et al., 1980)67	Dog	4, 8, 12 weeks	Within 3 hours	Femur	Cobalt alloy, powder coated	Porous	3.5 – 17.2
Boone et al (1989)(Boone et al., 1989)68	Rabbit	0, 4, 12 weeks	?	Femur	Polyurethane, thermoplastic elastomer, HA	Porous	0.048 – 8.19
Branemark et al (1995)(Branemark et al., 1998)69	Dog	14 – 18 weeks	Fresh	Tibia	Ti	-	78.64 – 124.44
Branemark et al (1997)(Branemark et al., 1997)70	Rat	0, 2, 4, 8, 16 weeks	Fresh	Tibia	Ti	-	11 - 16
Cook et al (1985)(Cook et al., 1985)71	Dog	12 weeks	Fresh	Femur	Co-Cr-Mo	Porous	13.3 – 22.6
Dhert et al (1991)(Dhert et al., 1991)72	Goat	12, 25 weeks	Within 24 hours	Femur, humerus	Ti-6Al-4V, HA fluoroapatite, Mg-Whitlockite	Grit-blasted	3.3 – 17.3
Elmengaard et al (2005)(Elmengaard, Bechtold, and Soballe, 2005a)45	Dog	4 weels	Stored at -20°C	Tibia	Ti-6Al-4V	Rough, RGD	3.23 – 4.47
Ferris et al (1999)(Ferris, Moodie, Dimond, Gioranni, Ehrlich, and Valentini, 1999b)43	Rat	2, 4 weeks	Fresh	Femur	Ti	Gold, RGD	0.13 - 0.18
Klein et al (1991)(Klein et al., 1991)73	Dog	3 months	Within 1 hour	Femur	Ti-6Al-4V, HA, TCP	Rough	9.7 - 34.3
Lee et al (2001)(Lee et al., 2001)74	Dog	3, 12 weeks	Fresh	Femur	Ti-6Al-4V	HA, TCP	7.04 - 13.13
Lee et al (2004)(Lee et al., 2004)75	Dog	6, 12 weeks	Fresh	Femur	Ti-6Al-4V	HA, ZrO2	4.39 - 14.31
Muller et al (2005)(Muller et al., 2005a)76	Rabbit	12 weeks	Within 4-8 hours	Femur	Ti-6Al-4V	Open pores	3.95 - 20.49
Thomas et al (1985)(Thomas et al., 1985)77	Dog	12 - 24 weks	Within 24 hours	Femur	LTI pyrolytic carbon	Varying	1.34 - 3.40

* modified from Branemark,R. A biomechanical study of osseointegration: In-vivo measurements in rat, rabbit, dog, and man. 1-89. 1996. Goteborg University. Thesis/Dissertation.

Table 2.2. Push- or pull-out tests of intramedullary placed implants

(? = conditions not clearly stated)

Reference	Species	Healing Time	Testing	Anatomical location	Implant Material	Surface	Shear stress (Mpa)
Clemow et al (1988)(Clemow et al., 1981)	Rabbit	3, 12 weeks	?	Femur	Ti-6Al-4V	Porous	3.53 - 8.64
de Groot et al (1987)(de et al., 1987)	Dog	6 weeks, 3, 6, 12 months	?	Femur	Ti-6Al-4V	HA	0.6 - 62
Ducheyne et al (1977)(Ducheyne et al., 1977)	Dog	8 weeks	Frozen at -32°C	Femur	Stainless Steel	Porous	0.2 - 6.2
Feighan et al (1995)(Feighan et al., 1995)	Rabbit	12 weeks	Within 24 hours	Femur	Ti-6Al-4V	Polished blasted	0.5 - 3.5
Heck et al (1986)(Heck et al., 1986)	Dog	12 weeks	Frozen	Femur, tibia	Ti-6Al-4V sintered with cp Ti	Porous	0.44 - 4.01
Oonishi et al (1989)(Oonishi et al., 1989)	Goat	2, 4, 12 weeks	?	Tibia	Ti-6Al-4V	HA	0.53 - 25.5
O'Toole et al (2004)(O'Toole et al., 2004)	Rat	10, 20, 30 days	Fresh	Femur	Ti	Etched, BSP coated	-
Rivero et al (1988)(Rivero et al., 1988)	Dog	1, 2, 3, 6 weeks	Frozen	Humerus	cp Ti	Porous Fiber	0.75 - 2.75
Wong et al (1995)(Wong et al., 1995)	Pigs	12 weeks	Fresh	Femur, tibia	cp Ti, TAN, TAV, HA	Fine, rough, blasted, etched	-

* modified from Branemark,R. A biomechanical study of osseointegration: In-vivo measurements in rat, rabbit, dog, and man. 1-89. 1996. Goteborg University. Thesis/Dissertation.

Table 2.3. Removal torque tests on rotationally symmetrical implants
(? = conditions not clearly stated)

Reference	Species	Healing Time	Testing	Anatomical location	Implant Material	Surface	Shear stress (Mpa)
Branemark et al (1995) (Branemark, Ohrnell, Skalak, Carlsson, and Branemark, 1998)	Dog	14 - 18 weeks	Fresh	Tibia	Ti	-	3.3 - 6.5
Branemark et al (1997) (Branemark, Ohrnell, Nilsson, and Thomsen, 1997)	Rat	0, 2, 4, 8, 16 weeks	Fresh	Tibia	Ti	-	1.9 - 4.3
Gotfredsen et al (1992)(Gotfredsen et al., 1992)	Dog	12 weeks	In vivo	Tibia	cp Ti	TiO2-blasted	1.13 - 6.6
Hahn and Palich (1970)(Hahn and Palich, 1970)	Sheep	14, 26, 45 weeks	?	Femur	cp Ti	Plasma coating	0.103 - 17.24
Ivanoff et al (1996)(Ivanoff et al., 1996)	Rabbit	6, 12 weeks	In vivo	Tibia	cp Ti	Machined	7.9 - 11.3

* modified from Branemark,R. A biomechanical study of osseointegration: In-vivo measurements in rat, rabbit, dog, and man. 1-89. 1996. Goteborg University. Thesis/Dissertation.

Cell Adhesion and Osteoblast Differentiation

Cell adhesion to extracellular matrix (ECM) proteins controls complex biological processes such as development, wound healing, immune response, and tissue function through specific and dynamic regulation of cell behavior (Hynes, 2002). Cell attachment to the ECM is primarily mediated by integrins, a widely expressed family of heterodimeric cell surface adhesion receptors consisting of non-covalently associated α and β subunits (Hynes, 2002). In addition to anchoring cells and providing tissue

structure, integrins transmit intracellular signals that direct cell migration, proliferation, cell cycle progression, and differentiation (Nobes and Hall, 1999;Leng et al., 1999;Sechler and Schwarzbauer, 1998;Zhu et al., 1996;Clark and Brugge, 1995;Roskelley et al., 1994). Integrins thus function as the principal mediators of the molecular dialogue between a cell and its ECM environment.

The interactions of osteoblasts with their surrounding ECM are essential for skeletal development and homeostasis and the maintenance of the mature osteoblastic phenotype (Xiao et al., 2002;Suzawa et al., 2002;Ikeuchi et al., 2002;Mizuno and Kuboki, 2001;Regazzoni et al., 2001;Tamura et al., 2001b;Mizuno et al., 2000;Xiao et al., 2000a;Jikko et al., 1999;Takeuchi et al., 1997b;Lynch et al., 1995). During the early stages of differentiation, osteoblasts synthesize an ECM consisting primarily of type I collagen. As matrix deposition progresses, the osteoblastic differentiation pathway is characterized by the activation of transcriptional pathways leading to the temporal expression of multiple proteins, including alkaline phosphatase, osteocalcin, and bone sialoprotein (Aubin and Liu, 1996;Stein et al., 1996). The distinctive feature of the mature osteoblastic phenotype is their ability to induce the mineralization of the ECM (Aubin and Liu, 1996).

Integrins are the central transducers of ECM signals that regulate this process of osteoblast commitment and differentiation. The integrins $\alpha_1\beta_1$ and $\alpha_2\beta_1$ are the major collagen-binding integrins, with $\alpha_1\beta_1$ having a higher affinity for the basement membrane type IV collagen and $\alpha_2\beta_1$ having a higher affinity for the fibrillar type I collagen, the major protein constituent of bone (Tulla et al., 2001;Kapyla et al., 2000;Nykvist et al., 2000). In fact, the $\alpha_2\beta_1$ integrin is highly expressed on osteoblast-like cells and is one of

the predominant adhesion receptors used by osteoblast-like cells to adhere to the collagen matrix (Gronthos et al., 1997). Several studies indicate that the $\alpha_2\beta_1$ integrin interaction with type I collagen is a crucial signal for the induction of osteoblastic differentiation and matrix mineralization (Suzawa, Tamura, Fukumoto, Miyazono, Fujita, Kato, and Takeuchi, 2002;Mizuno and Kuboki, 2001;Mizuno, Fujisawa, and Kuboki, 2000;Jikko, Harris, Chen, Mendrick, and Damsky, 1999;Xiao et al., 1998;Takeuchi et al., 1997a). For example, $\alpha_2\beta_1$-mediated osteoblast adhesion to type I collagen activates Runx2/Cbfa1, a transcription factor that controls osteoblast differentiation and matrix mineralization (Xiao, Wang, Benson, Karsenty, and Franceschi, 1998;Takeuchi, Suzawa, Kikuchi, Nishida, Fujita, and Matsumoto, 1997a). Furthermore, the collagen-$\alpha_2\beta_1$ integrin interaction has been shown to induce the osteoblastic phenotype in multipotent bone marrow cells (Mizuno and Kuboki, 2001;Mizuno, Fujisawa, and Kuboki, 2000). Integrin $\alpha_2\beta_1$-mediated attachment to type I collagen stimulates the tyrosine phosphorylation of focal adhesion kinase (FAK) and subsequently the activation of extracellular signal-related kinase (ERK), a mitogen-activated protein kinase (MAPK) that has been implicated in the control of osteoblast-specific gene expression and matrix mineralization (Suzawa, Tamura, Fukumoto, Miyazono, Fujita, Kato, and Takeuchi, 2002;Tamura, Takeuchi, Suzawa, Fukumoto, Kato, Miyazono, and Fujita, 2001b;Xiao et al., 2000b;Takeuchi, Suzawa, Kikuchi, Nishida, Fujita, and Matsumoto, 1997b). Disrupting the $\alpha_2\beta_1$ integrin interaction with type I collagen using function-blocking antibodies blocks the expression of osteoblast-specific genes, such as osteocalcin, and inhibits calcification and formation of a mineralized matrix (Mizuno, Fujisawa, and

Kuboki, 2000;Jikko, Harris, Chen, Mendrick, and Damsky, 1999;Xiao, Wang, Benson, Karsenty, and Franceschi, 1998).

Osteoblasts and osteoprogenitor cells also express $\alpha_5\beta_1$, the principal fibronectin receptor (Gronthos, Stewart, Graves, Hay, and Simmons, 1997). Adhesive interactions involving $\alpha_5\beta_1$ and fibronectin have also been identified as central to osteoblastic functions. For example, using blocking antibodies in primary osteoblast cultures, Damsky and colleagues demonstrated that $\alpha_5\beta_1$ integrin binding to fibronectin is essential to osteoblast survival, proliferation, osteoblast-specific gene expression, and matrix mineralization (Globus et al., 1998;Moursi et al., 1997a;Moursi et al., 1996).

$\alpha_2\beta_1$ Integrin and Type I Collagen Peptides

The collagens constitute a family of abundant ECM molecules that contribute significantly to the integrity and mechanical properties of tissues such as bone, skin, cartilage, and tendon (Prockop and Kivirikko, 1995). These structural proteins also play a fundamental role in promoting cell adhesion and mediating intracellular signals critical to tissue function (Heino, 2000;McCarthy et al., 1996). Integrin-type collagen receptors, such as $\alpha_1\beta_1$, $\alpha_2\beta_1$, $\alpha_3\beta_1$, $\alpha_{10}\beta_1$, and $\alpha_{11}\beta_1$, mediate cell adhesion to various collagen types and activate cytoplasmic signal transduction pathways (Broberg et al., 2001;McCarthy, Vachhani, and Iida, 1996). In particular, integrin $\alpha_2\beta_1$, the primary receptor for type I collagen, is abundantly expressed on platelets, epithelial cells, fibroblasts, osteoblasts, chondrocytes, endothelial cells, and lymphocytes (Heino, 2000).

Collagen tertiary structure consists of three left-handed polyproline-like chains supercoiled in a right-handed helix about a common axis, yielding a characteristic triple helical coiled-coil (Lehninger et al., 1993). The primary sequence of these polypeptide

units often consists of the repeating trimer $(Gly\text{-}X\text{-}Y)_n$. The strict sequence constraint of glycine at every third position is required for close packing at the interface of the three strands. The X and Y positions of the repeat units are frequently occupied by proline and 4-hydroxyproline, respectively. These two imino acids further stabilize the triple helical structure by imparting a high degree of steric restriction on the local twisting of polypeptide chains. The repeating 4-hydroxyproline non-standard imino acid also enables intramolecular hydrogen bonding.

Using cyanogen bromide-derived collagen fragments and overlapping collagen model peptides, recent studies have proposed the hexapeptide sequence GFOGER from residues 502-507 of the α_1(I) chain of type I collagen as a major binding locus for the $\alpha_2\beta_1$ integrin (Knight et al., 2000;Knight et al., 1998;Morton et al., 1994). These studies correlate with recent protein-mapping data that identifies the GFOGER sequence as residing in a major integrin-binding region of human type I collagen (Di Lullo et al., 2002). This hexapeptide sequence fully supported $\alpha_2\beta_1$-dependent cell adhesion and exhibited divalent cation-dependent binding to isolated $\alpha_2\beta_1$ and recombinant α_2 I-domain (Onley et al., 2000;Knight, Morton, Peachey, Tuckwell, Farndale, and Barnes, 2000). In addition, recognition of this sequence is entirely dependent upon the presence of a triple helical conformation, underscoring the crucial role of collagen's tertiary structure in $\alpha_2\beta_1$ integrin binding (Knight, Morton, Peachey, Tuckwell, Farndale, and Barnes, 2000;Messent et al., 1998;Morton et al., 1997;Morton, Peachey, Zijenah, Goodall, Humphries, and Barnes, 1994). Recently, a triple helical model peptide containing the GFOGER adhesion motif was co-crystallized with the α_2 I-domain,

verifying its association with the integrin's metal ion-dependent adhesion site (MIDAS) (Emsley et al., 2000).

Engineering Bioadhesive Surfaces

Incorporating discrete cell adhesion motifs, such as the GFOGER hexapeptide, into bioactive materials and surfaces offers a robust strategy to enhance cell-material interactions and encourage biospecific cell adhesion (Hubbell, 1999). Numerous cell adhesive surfaces have been designed to incorporate the RGD tripeptide sequence found in a wide variety of ECM proteins and recognized by a number of integrins, including $\alpha_v\beta_3$, and $\alpha_{IIb}\beta_3$ (Ruoslahti, 1996). Several critical factors limit the potential of this approach for bone repair. First, the biological activity of short linear adhesive peptides is significantly lower than that of the native protein, due to conformation-dependent effects and the absence of additional functional domains (Akiyama et al., 1995;Aota et al., 1994a). More significantly, RGD peptides are limited by a lack of specificity for particular integrins and thus allow minimal control over cellular responses. RGD also does not bind $\alpha_5\beta_1$, a crucial receptor in osteoblast function. $\alpha_5\beta_1$-binding requires both the PHSRN sequence in the 9th type III repeat and the RGD motif in the 10th type III repeat of fibronectin (Aota, Nomizu, and Yamada, 1994a). Due to the acute sensitivity of $\alpha_5\beta_1$ to small perturbations in the orientation of these domains, the development of proper structural orientation using synthetic peptides remains a challenge. Finally, osteogenic cells require signals from non RGD-binding integrins, particularly $\alpha_2\beta_1$, for osteoblastic differentiation and matrix mineralization. This study addresses these critical limitations by engineering surfaces that *specifically* target $\alpha_2\beta_1$ and $\alpha_5\beta_1$, using collagen-

and fibronectin-mimetic ligands with optimal secondary conformations and binding site orientations.

CHAPTER 3

ENGINEERING INTEGRIN-SPECIFIC ADHESIVE SURFACES WITH A TRIPLE-HELICAL COLLAGEN-MIMETIC PEPTIDE*

Summary

Integrin-mediated cell adhesion to extracellular matrix proteins anchors cells and triggers signals that direct cell function. The integrin $\alpha_2\beta_1$ recognizes the glycine-phenylalanine-hydroxyproline-glycine-glutamate-arginine (GFOGER) motif in residues 502-507 of the α1[I] chain of type I collagen. Integrin recognition is entirely dependent on the triple-helical conformation of the ligand similar to that of native collagen. This study focuses on engineering $\alpha_2\beta_1$-specific bioadhesive surfaces by immobilizing a triple-helical collagen-mimetic peptide incorporating the GFOGER binding sequence onto model non-adhesive substrates. Circular dichroism spectroscopy verified that this peptide adopts a stable triple-helical conformation in solution. Passively adsorbed GFOGER-peptide exhibited dose-dependent HT1080 cell adhesion and spreading comparable to that observed on type I collagen. Subsequent antibody blocking conditions verified the involvement of integrin $\alpha_2\beta_1$ in these adhesion events. Focal adhesion formation was observed by immunofluorescent staining for $\alpha_2\beta_1$ and vinculin on MC3T3-E1 cells. Model functionalized surfaces were then engineered using three complementary peptide tethering schemes. These peptide-functionalized substrates

*Modified from Reyes,C.D. & Garcia,A.J. Engineering integrin-specific surfaces with a triple-helical collagen- mimetic peptide. *J. Biomed. Mater. Res.* **65A**, 511-523 (2003).

supported $\alpha_2\beta_1$-mediated cell adhesion and focal adhesion assembly. Our results suggest that this peptide is active in an immobilized conformation and may be applied as a surface modification agent to promote $\alpha_2\beta_1$–specific cell adhesion. Engineering surfaces that specifically target certain integrin-ligand interactions and signaling cascades provides a biomolecular strategy for optimizing cellular responses in biomaterials and tissue engineering applications.

Introduction

Incorporating discrete cell adhesion motifs, such as the GFOGER hexapeptide, into bioactive materials and surfaces offers a robust strategy to enhance cell-material interactions and encourage biospecific cell adhesion (Hubbell, 1999). Numerous cell adhesive surfaces have been designed to incorporate the RGD tripeptide sequence found in a wide variety of ECM proteins and recognized by a number of integrins, including $\alpha_5\beta_1$, $\alpha_v\beta_3$, and $\alpha_{IIb}\beta_3$ (Ruoslahti, 1996). Such surfaces are often limited by a lack of specificity for particular integrins and thus allow minimal control over cellular responses. The presentation of short sequences, such as RGD, may also result in the loss of full biological activity due to the absence of additional functional domains present in the native, three-dimensional structure of the ECM molecule (Danen et al., 1995;Aota, Nomizu, and Yamada, 1994a). The goal of this study is to engineer stable bioadhesive surfaces that specifically target the $\alpha_2\beta_1$ integrin, allowing us to directly control intracellular signaling and, ultimately, cell function. We designed a stable triple-helical, collagen-mimetic peptide that contains the GFOGER adhesion motif from type I collagen. This peptide specifically targets the $\alpha_2\beta_1$ integrin receptor, and its cell adhesion activity is comparable to that of type I collagen. We also demonstrate that the peptide is

active for three complementary immobilization schemes suggesting that this triple-helical peptide represents a robust and versatile approach to the design of collagen-mimetic bioadhesive surfaces that specifically target the $\alpha_2\beta_1$ integrin. Controlling specific integrin binding through this biomolecular strategy may provide a versatile approach to optimize cell function for applications such as biomaterials and tissue engineering scaffold design.

Materials and Methods

Cells and Reagents

HT1080 human fibrosarcoma cells (CCL-121, American Type Culture Collection, Manassas, VA) were grown in Dulbecco's Modified Eagle medium containing 10% fetal bovine serum and 1% penicillin-streptomycin. MC3T3-E1 murine immature osteoblast-like cells (RIKEN Cell Bank, Tokyo, Japan) were cultured in α-Modified Eagle Medium supplemented with 10% fetal bovine serum and 1% penicillin-streptomycin. Both cell types were subcultured every two days using standard techniques.

Goat anti-biotin antibody was obtained from Pierce (Rockford, IL). Rabbit anti-integrin β_1 polyclonal antibody (AB1952) and adhesion-blocking mouse anti-human integrin alpha 2 monoclonal antibody (MAB1950Z) were purchased from Chemicon (Temecula, CA). Alkaline phosphatase-conjugated donkey anti-goat IgG and anti-rabbit IgG were obtained from Jackson ImmunoResearch Laboratories (West Grove, PA). Alkaline phosphatase-conjugated monoclonal mouse anti-biotin IgG was ordered from Sigma (St. Louis, MO). Mouse monoclonal anti-vinculin IgG was obtained from Upstate Biotechnology (Lake Placid, NY). AlexaFluor 488 goat anti-rabbit and anti-mouse IgG

conjugates, rhodamine-phalloidin, and calcein-AM were purchased from Molecular Probes (Eugene, OR). Bovine type I collagen (Vitrogen-100) was purchased from Cohesion (Palo Alto, CA). All cross-linking and biotinylation reagents were obtained from Pierce. Fetal bovine serum was purchased from Hyclone (Logan, UT). Additional cell culture reagents were obtained from Invitrogen (Carlsbad, CA). All other reagents were purchased from Sigma.

Peptide Synthesis

The peptide GGYGGGPC$(GPP)_5$GFOGER$(GPP)_5$GPC [O=hydroxyproline] was designed by C. D. Reyes and synthesized by the Emory University Microchemical Facility at the Winship Cancer Institute, Atlanta, GA. The synthesis was performed on an Applied Biosystem 430A peptide synthesizer by stepwise solid-phase procedures on a *t*-Boc-L-Gly-PAM resin. The *t*-Boc group was used for amino terminus protection. The peptides were cleaved from the resin using hydrogen fluoride and redissolved in 0.1% trifluoroacetic acid (TFA). The purity of the peptide was greater than 99% by analytical reverse-phase HPLC on an Applied Biosystems 130A microbore HPLC and mass spectrometry on a Bruker Model Protein-TOF MALDI mass spectrometer. Peptide was supplied in the purified form as a TFA salt and reconstituted at a stock concentration of 10 mg/ml in 0.1% TFA. In some experiments, the peptide was diluted to 10 μg/ml in 0.1%TFA for cross-linking to create a multimer as previously described(Morton et al., 1995). The heterobifunctional cross-linking reagent, 3-(2-pyridyldithio)propionic acid N-hydroxysuccinimide ester (SPDP), was added to the peptide solution at a 1mM concentration. The cross-linking reaction proceeded for 1 hour at room temperature.

Circular Dichroism

Circular dichroism (CD) spectra and melting curves were recorded on a Jasco Model J-810 spectropolarimeter (Jasco, Easton, MD). Peptide samples were prepared at a concentration of 0.33 mg/ml in Dulbecco's phosphate buffered saline (DPBS). Type I collagen samples were prepared at a concentration of 0.37 mg/ml in DPBS. A quartz cuvette with a path length of 1 mm was filled with 200 µl of sample, and the temperature in the cuvette was controlled with a Peltier thermoelectric temperature controller. For continuous wavelength scans, the data pitch was 0.1 nm and the scan speed was 100 nm/min. Data were recorded at 25 ºC. For equilibrium melting transitions, the temperature in the cell was increased at a rate of 2 ºC/min and equilibrated for 1 min at each temperature before collecting a data point. Data were recorded at a constant wavelength of 225 nm.

Peptide Biotinylation

For surface density measurements and immobilization, the peptide was biotinylated using a biotin-LC-PEO-amine reagent. The terminal primary amine of this molecule selectively labels the terminal carboxyl group of the peptide. The peptide and the biotin reagent were dissolved in 0.1 M N-morpholinoethane sulfonic acid (MES) buffer, pH 5.5. A water soluble diimide, 1-ethyl-3-(3-dimethylaminopropyl)carbodiimide hydrochloride (EDC), was added to the solution at 100 mg/ml to form an *O*-acylisourea intermediate on the peptide carboxyl which in turn reacts with amine of the biotin reagent. The reaction was incubated for 2 hours at room temperature on a vortexer. The sample was then dialyzed in DPBS without Ca^{2+}/Mg^{2+} to remove any unreacted biotinylation reagent and EDC by-products from biotinylated peptide. The final concentration of biotinylated peptide was determined by monitoring the 280 nm

absorbance on a Shimadzu UV-1601 UV-visible spectrophotometer (Shimadzu, Columbia, MD).

Biotinylated Peptide Immobilization

Tissue culture-treated polystyrene surfaces were incubated with goat anti-biotin antibody (1:50,000 dilution) or avidin (NeutrAvidin, 100 μg/ml, Pierce) for 1 hour at room temperature. After washing, the surface was blocked with 1% heat denatured bovine serum albumin (BSA) for 1 hour to prevent non-specific protein adsorption. Varying concentrations of biotinylated peptide were then introduced to the surfaces for 1 hour at room temperature, followed by blocking in 1% heat denatured BSA for 1 hour.

Covalent Peptide Immobilization

Tissue culture treated polystyrene surfaces were preadsorbed with 1% heat denatured BSA for 1 hour at room temperature. The cross-linking agents *N*-hydroxysulfosuccinimide (sulfo-NHS, 5 mM) and 1-ethyl-3-(3-dimethylaminopropyl)carbodiimide (EDC, 2 mM) were dissolved in an activation buffer (0.1 M MES, 0.5 M NaCl, pH 6.0) and added to each BSA-coated surface for 15 minutes at room temperature. Unreacted EDC was quenched with 20 mM 2-mercaptoethanol in activation buffer. Following aspiration, peptide was introduced to the activated surfaces in varying concentrations for 2 hours at room temperature. Unreacted sulfo-NHS was quenched with 20 mM glycine. The surfaces were then blocked in 1% heat denatured BSA for 1 hour.

Surface Density Measurements

Biotinylated peptide was adsorbed or immobilized onto a 96-well plate as previously described and blocked with blocking buffer (5% horse serum in DPBS) for 1 hour. The surfaces were then incubated in goat anti-biotin antibodies (1:50,000 dilution) for 1 hour at 37°C. After washing, wells were incubated in alkaline phosphatase-conjugated donkey anti-goat IgG (1:4000 dilution) for 1 hour at 37°C. Substrate (4-methyl-umbelliferyl-phosphate, 60 μg/ml) was then added for 1 hour at 37°C. Reaction product fluorescence was measured in a microwell plate reader (360-nm excitation, 465-nm emission). Because BSA contains IgG that reacts with anti-goat IgG, the covalently immobilized peptide surfaces were probed with an alkaline phosphatase-conjugated mouse anti-biotin antibody (1:10,000 dilution). All experiments were performed in triplicate.

Cell Adhesion Assay

Cell adhesion to modified surfaces was measured using a centrifugation assay that applies controlled detachment forces. Tissue culture polystyrene 96-well plates were coated with peptide or cross-linked peptide diluted in 0.1% TFA or DPBS for 1 hour at room temperature or treated with the immobilization scheme described above. Additional control wells were coated with type I collagen in deionized water. All wells were then blocked in 1% heat denatured BSA for 1 hour to prevent non-specific protein adsorption.

Near-confluent HT1080 cells were loaded with 2 μg/ml calcein-AM (Molecular Probes), a membrane permeable green-fluorescent dye, detached using trypsin + EDTA, and resuspended serum-free in PBS + 2 mM dextrose. Cells were seeded onto the substrates (10,000 cells/well) and allowed to attach for 1 hour at room temperature. For

blocking experiments, cells were incubated in the presence of 1 μg/ml anti-human α_2 antibody. Each well was then aspirated and refilled with PBS-dextrose for an initial fluorescence reading to determine the density of cells prior to detachment. The plate was covered with sealing tape and centrifuged upside-down at the specified speed for 5 minutes on a Beckman Allegra 6 centrifuge (GH 6.8 rotor) to detach the cells. Again the wells were aspirated and refilled with PBS-dextrose for a post-spin fluorescence reading to determine the number of adherent cells. Fluorescence data was obtained from a Perkin Elmer HTS 7000 Plus Bio Assay microwell plate reader (485 nm excitation, 535 nm emission). The post-spin fluorescence data was normalized by the pre-spin data and plotted against ligand concentration to obtain adhesion profiles (fraction of adherent cells vs. coating concentration). Adhesion profiles were fitted to the following 4-parameter sigmoidal curve to obtain estimates for the 50% detachment points (C_{50}) using SigmaPlot 2001 software (SPSS Science, Chicago, IL):

$$f = f_o + \frac{f_{sat}}{1 + e^{-(\frac{c - c_{50}}{b})}}$$

The parameters f_{sat} and b represent the maximum adhesive fraction and the slope of the curve at the inflection point, respectively. The parameter C_{50} represents the concentration of protein/peptide required for 50% maximal adhesion and was used as a measure of adhesion strength to compare different surfaces. All experiments were performed in triplicate.

Immunofluorescent Staining for Focal Adhesions

Substrates were prepared as described above and MC3T3-E1 cells were seeded at a density of 225 cells/mm^2 in 0.1% serum for 6 hours. Cells were then permeabilized in

ice-cold buffer (50 mM NaCl, 150 mM sucrose, 3 mM $MgCl_2$, 50 mM Tris, pH 6.8) supplemented with 0.5% Triton X-100 and protease inhibitors (20 μg/ml aprotinin, 1 μg/ml leupeptin, 2 mM phenylmethylsulfonyl fluoride) for 5 minutes to remove membranes and soluble non-cytoskeletal cytoplasmic components. Detergent extracted cells were fixed in cold formaldehyde (3.7% in DPBS) for 5 minutes, blocked in blocking buffer (5% fetal bovine serum in DPBS) for 1 hour, and incubated with primary antibodies (anti-β_1, anti-vinculin; 1:500 dilution) diluted in blocking buffer for 60 minutes at room temperature. Primary antibodies were visualized using AlexaFluor 488-conjugated secondary antibodies (anti-rabbit IgG, anti-mouse IgG; 1:200 dilution) incubated for 1 hour and F-actin was simultaneously stained with rhodamine-phalloidin (1:200) diluted in DPBS. Images were captured using a Nikon Eclipse E400 fluorescence microscope with a 60x objective and ImagePro Plus image acquisition software.

Statistics

Results were analyzed by one-way ANOVA using SYSTAT 8.0 (SPSS). If treatment level differences were determined to be significant, pair-wise comparisons were performed with a Tukey post-hoc test. A 95% confidence level was significant.

Results

The collagen-mimetic peptide used in these experiments has the following primary sequence: $GGYGGGPC(GPP)_5GFOGER(GPP)_5GPC$. The GPP triplets on either side of the GFOGER recognition site provide cooperative clusters that promote the formation of a stable right-handed triple helical structure at room temperature (Knight, Morton, Peachey, Tuckwell, Farndale, and Barnes, 2000;Nagarajan et al., 1998;Fields

and Prockop, 1996). This triple-helical conformation is essential for integrin recognition and $\alpha_2\beta_1$-mediated cell adhesion(Messent, Tuckwell, Knauper, Humphries, Murphy, and Gavrilovic, 1998;Morton, Peachey, Knight, Farndale, and Barnes, 1997;Morton, Peachey, Zijenah, Goodall, Humphries, and Barnes, 1994). The GPC triplets allow peptide polymerization, which is necessary to evaluate the effects of collagen's quaternary structure on $\alpha_2\beta_1$-mediated cell adhesion. The tyrosine residue allows for future radiolabeling experiments.

Circular Dichroism Spectroscopy

CD spectroscopy was used to verify that the collagen-mimetic peptide adopts a triple helical conformation in solution. The CD spectrum of the peptide exhibited the spectral features characteristic of a triple helix, including a small positive peak near 225 nm, a crossover around 215 nm, and a large negative trough near 197 nm (**Fig. 3.1.a**) (Goodman et al., 1998;Fields and Prockop, 1996). In addition, the peptide exhibited the same general spectral characteristics as a control sample of type I collagen, demonstrating that the peptide adopts a stable collagen-like triple helix in solution (Fig. **3.1.b**). The thermal transition curve of the peptide (**Fig. 3.2.a**), obtained by monitoring the change in molar ellipticity at 225 nm, indicates a triple-helix ↔ random coil transition similar to that observed for type I collagen (**Fig. 3.2.b**). The midpoint of the peptide's folding transition (T_m) differs significantly from collagen's T_m, which is to be expected given the considerable difference in size between the peptide and the full collagen protein. This size difference may also explain the broadness of the peptide's melting curve relative to the sharp, cooperative folding transition observed for type I collagen. These differences aside, the negative $[\theta]_{225}$ at high temperatures indicates a

(a)

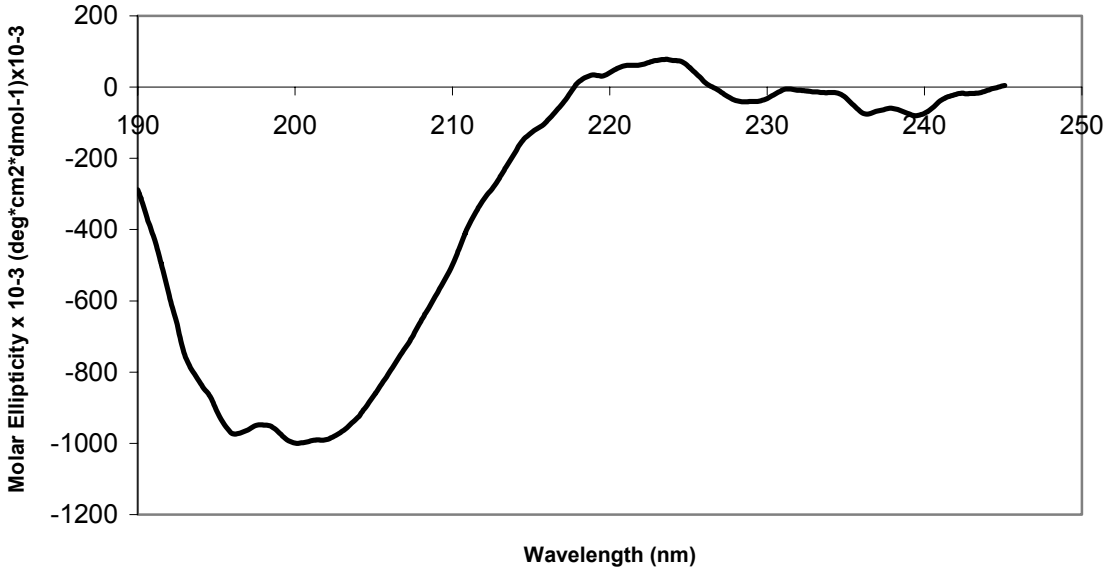

(b)

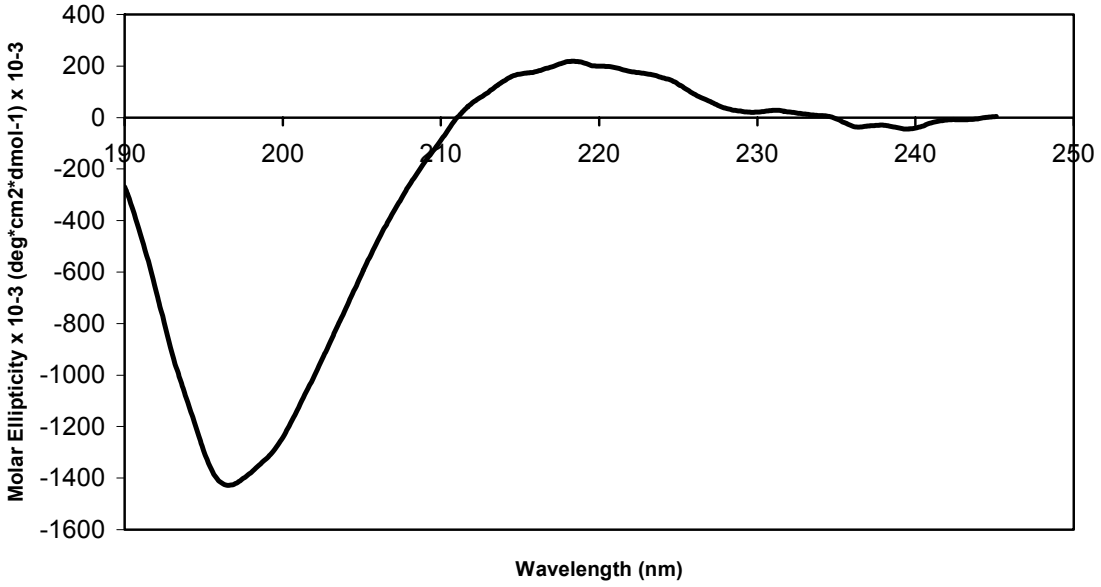

Figure 3.1. CD spectra of **(a)** GFOGER-peptide, 0.33 mg/ml, and **(b)** type I collagen, 0.37 mg/ml in DPBS at 25ºC.

(a)

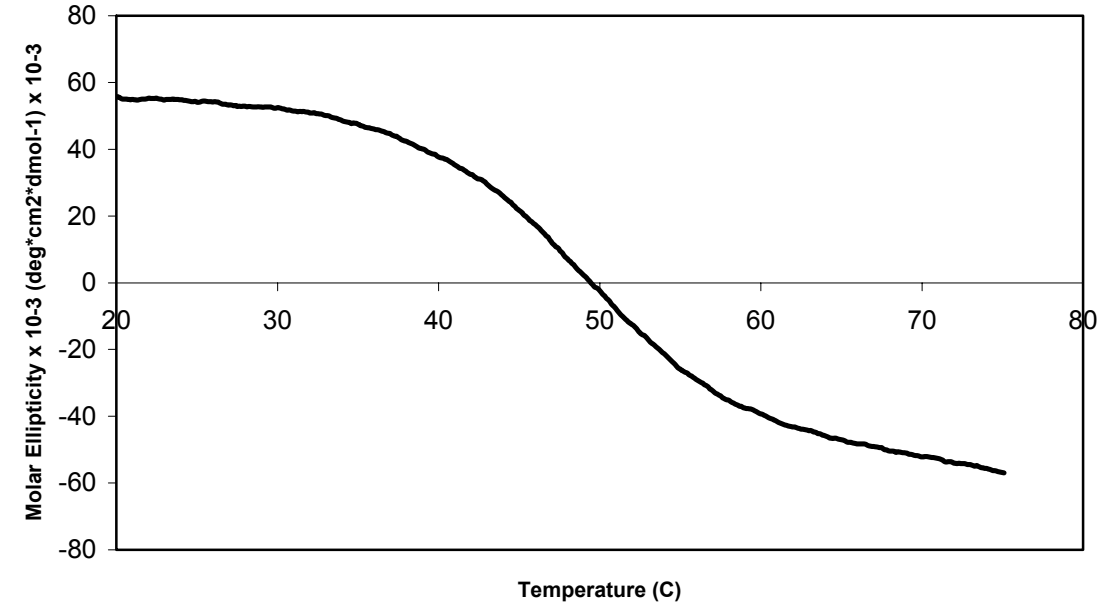

(b)

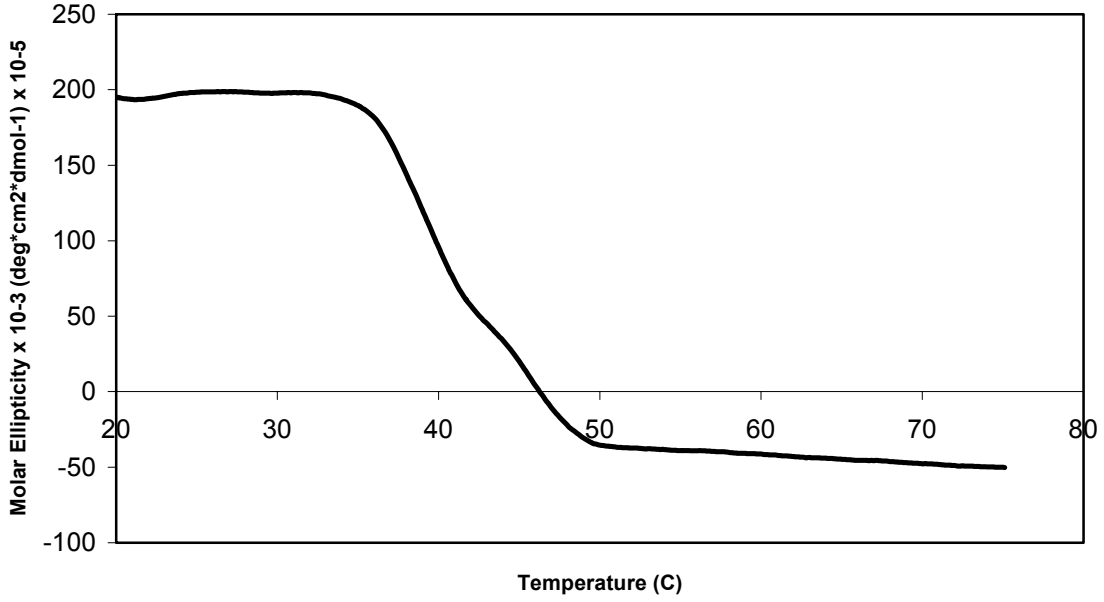

Figure 3.2. Thermal transition curves for (a) GFOGER-peptide, 0.33 mg/ml, and (b) type I collagen, 0.37 mg/ml in DPBS at 225 nm.

melted or denatured triple helix with little or no residual structure for both the peptide and the control collagen sample. These results demonstrate that the collagen-mimetic peptide has a stable triple helical structure at physiological temperature.

Peptide Activity

We initially examined the activity of the peptide passively adsorbed onto tissue-culture treated polystyrene at varying concentrations. An HT1080 human fibrosarcoma cell model was chosen because these cells adhere to type I collagen by a single mechanism involving the integrin $\alpha_2\beta_1$ (Messent, Tuckwell, Knauper, Humphries, Murphy, and Gavrilovic, 1998;Ruggiero et al., 1996;Tuckwell et al., 1995;Weston et al., 1994;Grenz et al., 1993;Cardarelli et al., 1992). Cell adhesion was examined using a centrifugation assay in which the cells are seeded for 1 hour under serum-free conditions and then the substrate is centrifuged at 12g for 5 minutes to detach the cells. As shown in **Fig. 3.3**, cells adhered to the adsorbed peptide in a density-dependent manner. This adhesion was statistically comparable to that observed on the control type I collagen surfaces. In addition, incubating cells on the adsorbed peptide surfaces with an anti-α_2 antibody completely blocked all adhesion above background indicating that the cell adhesion activity of this peptide is specific for the $\alpha_2\beta_1$ integrin.

Peptide Quaternary Structure

Recent literature has shown that collagen's quaternary structure (polymerized fibrils) as well as its tertiary triple helix is essential for platelet aggregation and implies that it may also be necessary for cell adhesion (Morton, Hargreaves, Farndale, Young, and Barnes, 1995)

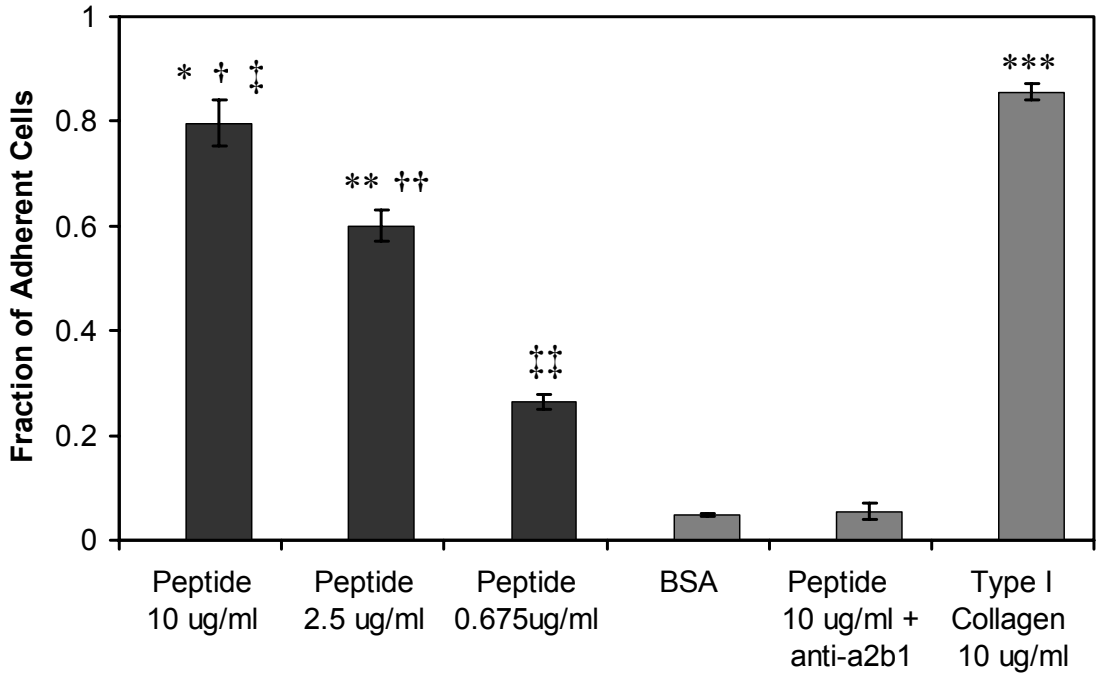

Figure 3.3. Dose-dependent HT1080 cell adhesion to adsorbed peptide and adsorbed type I collagen (1 hour cell adhesion, centrifugation at 12g for 5 min). Anti- α_2 antibody blocking demonstrates specificity for the $\alpha_2\beta_1$ integrin. (mean ± standard error; three separate experiments in triplicate) ANOVA: $p<0.00000001$; Pairwise comparisons: *peptide 10 μg/ml > peptide 2.5 μg/ml ($p<0.04$); †peptide 10 μg/ml > peptide 0.675 μg/ml ($p<0.00002$); ‡peptide 10 μg/ml > BSA ($p<0.000007$); **peptide 2.5 μg/ml > peptide 0.675 μg/ml ($p<0.001$); ††peptide 2.5 μg/ml > BSA ($p< 0.00002$); ‡‡peptide 0.675 μg/ml >

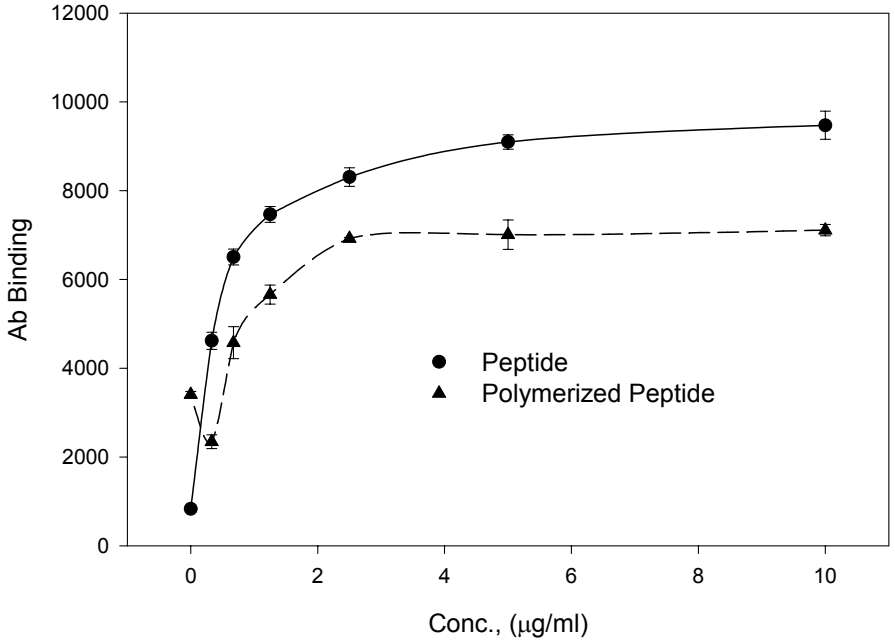

Figure 3.4. ELISA results for adsorbed peptide and polymerized peptide (1 hour adsorption). (mean ± standard error; two separate experiments in triplicate)

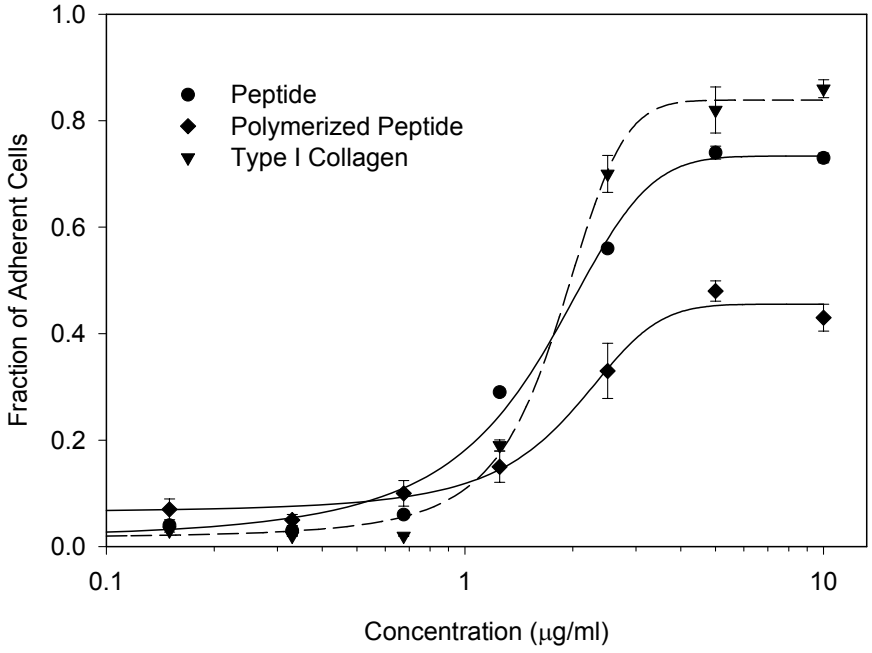

Figure 3.5. HT1080 cell adhesion to adsorbed peptide, adsorbed polymerized peptide, and adsorbed type I collagen (1 hour cell adhesion, centrifugation at 12g for 5 min). (mean ± standard error; three separate experiments in triplicate)

. To further examine this issue, the GFOGER peptides were cross-linked to produce a polymeric or fibrillar network using SPDP, a heterobifunctional cross-linker that tethers a primary amine to the thiol in cysteine. MALDI-TOF mass spectrometry verified that, prior to the addition of SPDP, the GFOGER peptide exists as a monomer in aqueous solution and does not undergo any appreciable disulfide bond formation (data not shown).

To detect the peptide via a standard enzyme-linked immunosorbant assay (ELISA), the carboxyl terminus of the peptide was biotinylated using a polyethylene oxide (PEO) linker arm attached to a biotin group. Surfaces were then probed with an anti-biotin antibody and amplified with a labeled secondary. The results in **Fig. 3.4** verified that the relative peptide surface density can be controlled by varying the concentration of either the polymerized peptide or the peptide monomer in solution. The difference between the two curves may be due to differences in the peptide adsorption profiles but may also be attributed to antibody accessibility. These ELISA results demonstrate concentration-mediated control over the relative surface density of both the polymerized peptide and peptide monomer on the adsorbed surfaces.

To investigate the importance of collagen's quaternary structure in $\alpha_2\beta_1$ integrin binding events, a centrifugation cell adhesion assay was used to compare the activity of the polymerized peptide to the peptide monomer. Cells exhibited concentration-dependent adhesion profiles for both peptide systems, although adhesion to the polymerized peptide was significantly lower than adhesion to the peptide monomer surfaces and nearly half that of type I collagen (**Fig. 3.5**). These differences most likely arise from differences in adsorbed density or recognition site accessibility. Nevertheless,

this data demonstrates that collagen's quaternary structure is not necessary for $\alpha_2\beta_1$-mediated cell adhesion.

Effects of Adsorption Buffer on Peptide Activity

An acidic buffer is preferable for peptide reconstitution and stabilization; however dilution in a buffer with a pH closer to neutral would optimize crosslinking and immobilization conditions, yielding greater reaction efficiency than an acidic environment. Therefore ELISA and cell adhesion assays were used to evaluate the activity of the peptide diluted in two different buffers – 0.1% trifluoroacetic acid (TFA) in H_2O and Dulbecco's phosphate buffered saline (DPBS, pH 7.4) – to rule out loss of activity due to partial unfolding of the triple helix or to clumping and precipitation of the peptide. ELISA results (**Fig. 3.6**) verify the concentration-dependent adsorption of the peptide under the two solvent conditions. Similarly, the adhesion profiles shown in **Fig. 3.7** reveal an increase in cell adhesion with increasing peptide concentration, demonstrating that either solvent is conducive to the concentration-dependent cell adhesion activity of the peptide. All subsequent experiments were performed in DPBS for convenience and reagent compatibility.

Surface Immobilization Schemes

We next designed three complementary schemes for tethering this peptide to a model surface to assess its activity in an immobilized conformation and ultimately its potential as a surface modification agent for biomaterials and tissue engineering applications (**Fig. 3.8**). The first two immobilization schemes involve biotinylating the carboxyl terminus of the peptide using a PEO linker arm attached to a biotin group. The biotinylated peptide was then introduced to surfaces treated with either adsorbed avidin

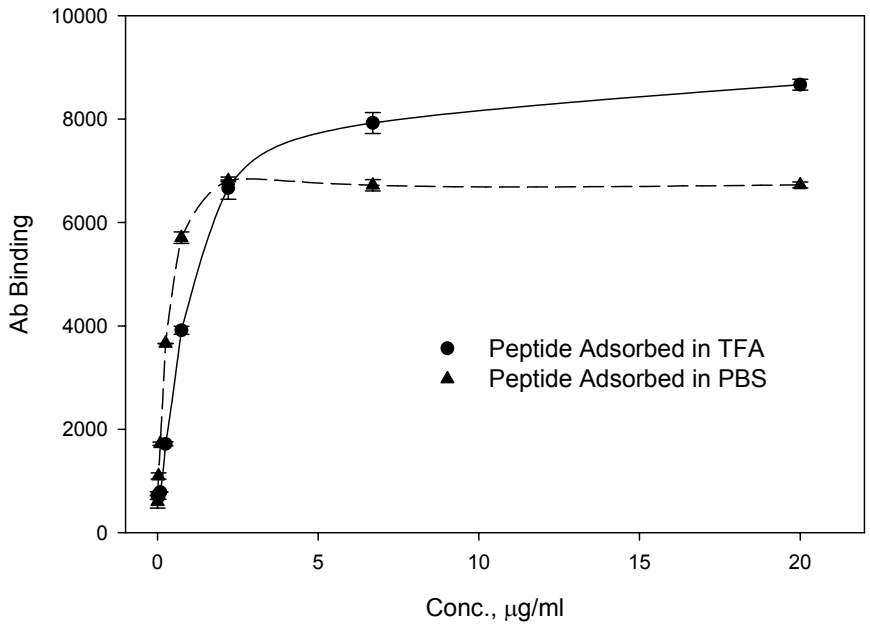

Figure 3.6. ELISA results for peptide adsorbed in trifluoroacetic acid (TFA) and peptide adsorbed in phosphate buffered saline (PBS). (mean ± standard error; two separate experiments in triplicate)

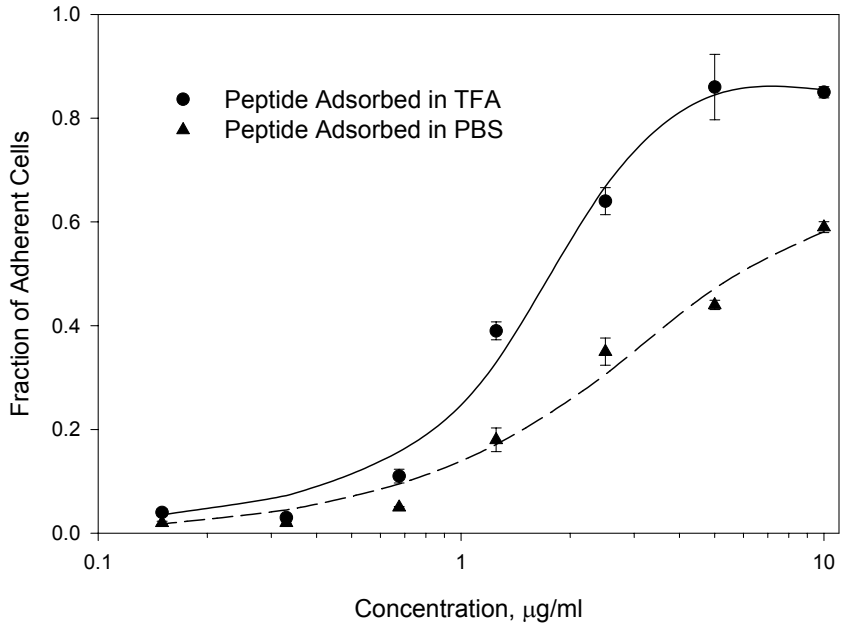

Figure 3.7. HT1080 cell adhesion to peptide adsorbed in trifluoroacetic acid (TFA) and peptide adsorbed in phosphate buffered saline (PBS) (1 hour cell adhesion, centrifugation at 12g for 5 min). (mean ± standard error; three separate experiments in triplicate)

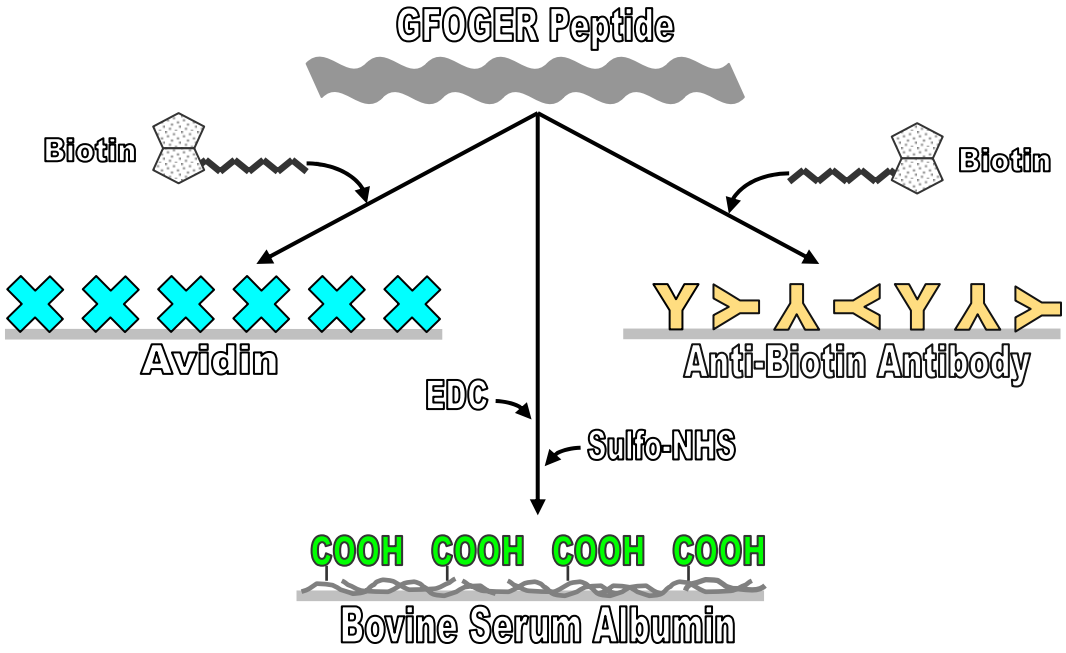

Figure 3.8. Three complementary schemes for tethering the GFOGER peptide to a surface. The first two immobilization schemes involve biotinylating the peptide and introducing it to surfaces treated with either adsorbed avidin or adsorbed anti-biotin antibody. The third scheme involves covalently cross-linking the peptide to passively adsorbed bovine serum albumin using the cross-linking agents EDC ands sulfo-NHS.

or adsorbed anti-biotin antibody. The third scheme involved covalently crosslinking the peptide to passively adsorbed bovine serum albumin using the crosslinking agents EDC ands sulfo-NHS. The BSA provided a non-fouling, non-adhesive background surface with carboxylate anchoring groups for the peptide.

1. Antibody-Mediated Surface Immobilization

To immobilize the peptide to an underlying surface, the carboxyl terminus of the peptide was biotinylated using a polyethylene oxide (PEO) linker arm attached to a biotin group, as previously described. The biotinylated peptide was then introduced to surfaces treated with adsorbed anti-biotin antibody to exploit the specificity and integrity of antibody-antigen associations. **Fig. 3.9** shows that the biotinylated peptide promotes concentration-dependent cell adhesion on anti-biotin coated surfaces. Although this adhesion is slightly lower than that observed on control type I collagen and adsorbed peptide surfaces, results demonstrate peptide activity in this immobilized conformation.

2. Avidin Surface Immobilization

To complement the antibody surface immobilization results, the biotinylated peptide was also introduced to surfaces treated with adsorbed NeutrAvidin™ biotin-binding protein, a commercially available deglycosylated avidin derivative with exceptionally low nonspecific binding properties. The avidin-biotin interaction was chosen to demonstrate peptide immobilization because it represents the strongest known noncovalent biological recognition between protein and ligand ($K_a=10^{15}$ M^{-1}). In addition, the bond formation between biotin and avidin occurs very rapidly. Once formed, it is unaffected by most extremes of pH, organic solvents, and other denaturing conditions and thus, for the purposes of these experiments, can be considered non-

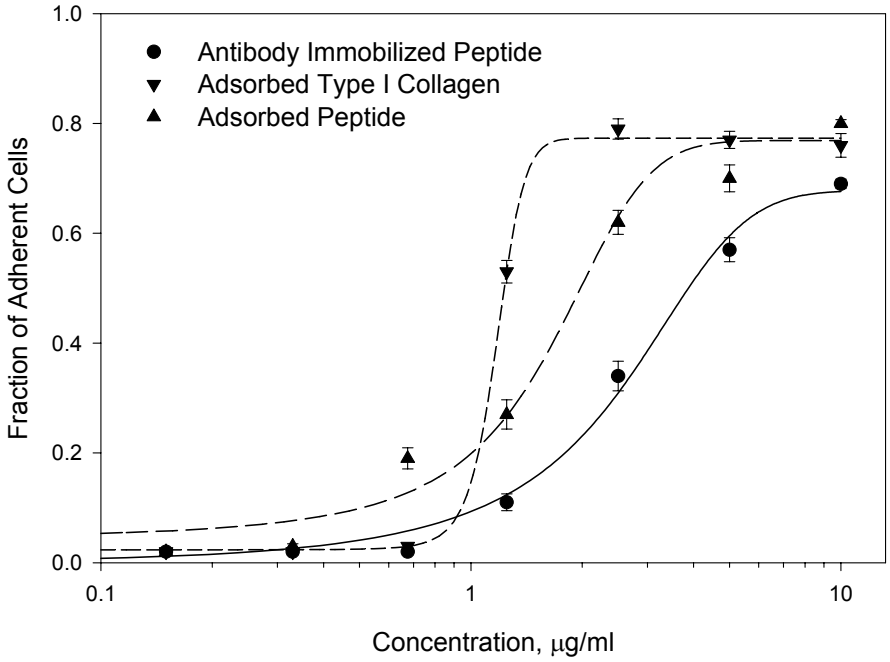

Figure 3.9. HT1080 cell adhesion to antibody immobilized peptide, adsorbed peptide, and adsorbed type I collagen (1 hour cell adhesion, centrifugation at 12g for 5 min). (mean ± standard error; three separate experiments in triplicate)

reversible. Cell adhesion results showed that the biotinylated peptide also promotes concentration-dependent cell adhesion on the avidin-coated surfaces (**Fig. 3.10**). This adhesion was comparable, although slightly lower, than that observed on control type I collagen and adsorbed peptide surfaces. To demonstrate that this cell adhesion activity is a consequence of the peptide immobilization treatment and not a result of non-specific peptide adsorption, the experiment was repeated with non-biotinylated peptide. As shown in **Fig. 3.10**, eliminating the peptide immobilization potential completely eliminated all cell adhesion, indicating that the previously observed peptide activity was a direct result of this particular immobilization treatment. In addition, incubating cells on the avidin-immobilized peptide surfaces with an anti-α_2 antibody completely blocked all adhesion above background demonstrating that the cell adhesion activity of the immobilized peptide is specific for the $\alpha_2\beta_1$ integrin.

3. Covalent Surface Immobilization

Covalent surface modification remains the most promising technique for immobilizing bioactive ligands such as the GFOGER-peptide. The third immobilization scheme evaluated in this study involved covalently tethering the peptide to passively adsorbed bovine serum albumin (BSA) using a sequential coupling reaction with the cross-linking agents EDC and sulfo-NHS (Grabarek and Gergely, 1990;Staros et al., 1986). The EDC reacts with carboxyl groups on the BSA surface to form an intermediate that is unstable in aqueous solutions unless stabilized by sulfo-NHS. This sulfo-NHS reaction results in an amine reactive NHS ester that subsequently couples with the GFOGER peptide, immobilizing it to the underlying BSA layer. The BSA provides a non-fouling, non-adhesive background surface with carboxylate anchoring groups for the

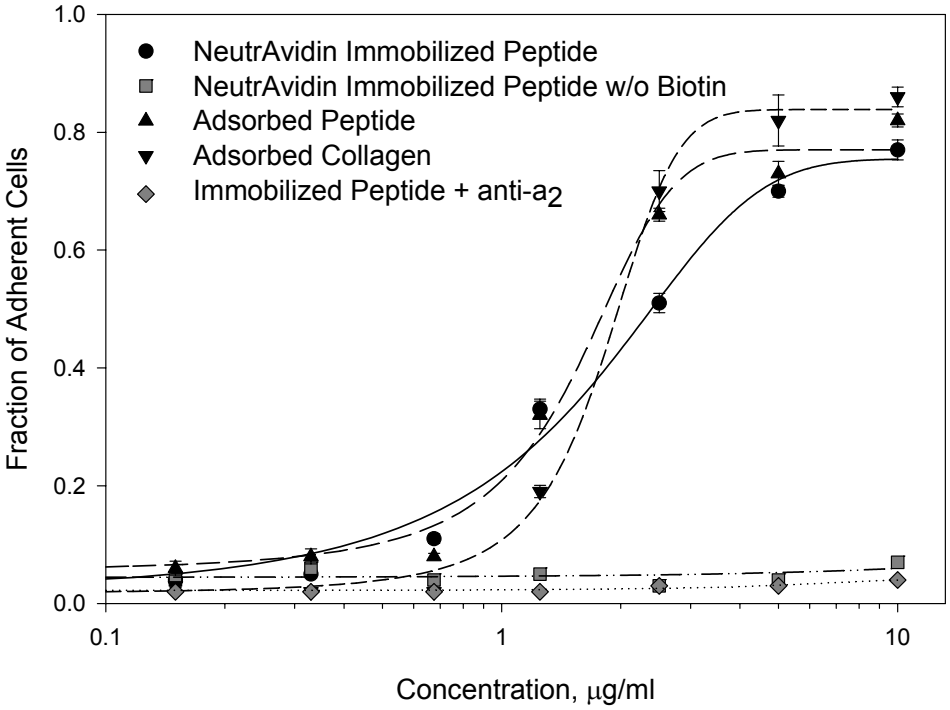

Figure 3.10. HT1080 cell adhesion to NeutrAvidin immobilized peptide. The two positive controls are adsorbed peptide and adsorbed type I collagen. The negative control is a surface treated non-biotinylated peptide. Anti- α_2 antibody blocking demonstrates specificity for the $\alpha_2\beta_1$ integrin. (1 hour cell adhesion, centrifugation at 12g for 5 min). (mean ± standard error; three separate experiments in triplicate) ANOVA of C_{50} values: $p<0.0000001$; NeutrAvidin > antibody blocking ($p<0.000008$); NeutrAvidin > NeutrAvidin w/o biotin ($p<0.000008$); adsorbed peptide > NeutrAvidin ($p<0.001$); adsorbed collagen > NeutrAvidin ($p<0.00002$).

peptide. A centrifugation cell adhesion assay was used to assess the activity of this covalently immobilized peptide layer. The two positive controls were adsorbed peptide and adsorbed type I collagen. The negative control treatment was a surface treated with BSA and peptide as in the standard covalent immobilization scheme, except that both cross-linkers were omitted. **Fig. 3.11** demonstrates that cell adhesion to the immobilized peptide was nearly five fold that of the negative control treatment and the adhesion profile was similar to that of adsorbed peptide and collagen, although somewhat reduced. This reduction in cell adhesion on the immobilized peptide surface could be due to differences in peptide density based on the efficiency of the crosslinking reaction. To assess possible differences in peptide surface density, an ELISA assay was performed on surfaces treated with the covalently immobilization scheme. The results in **Fig. 3.12** reveal a 6-fold lower density of peptide on these surfaces compared with adsorbed peptide. Given that the cell adhesion to the covalently immobilized peptide was only about half of the adhesion observed on the adsorbed peptide surfaces, these ELISA results suggest that the peptide is nearly three times more active in the immobilized conformation compared with passive absorption. In addition, incubating cells on the covalently immobilized peptide surfaces with an anti-α_2 antibody completely blocked all adhesion above background demonstrating that this cell adhesion activity is specific for the $\alpha_2\beta_1$ integrin (**Fig. 3.11**).

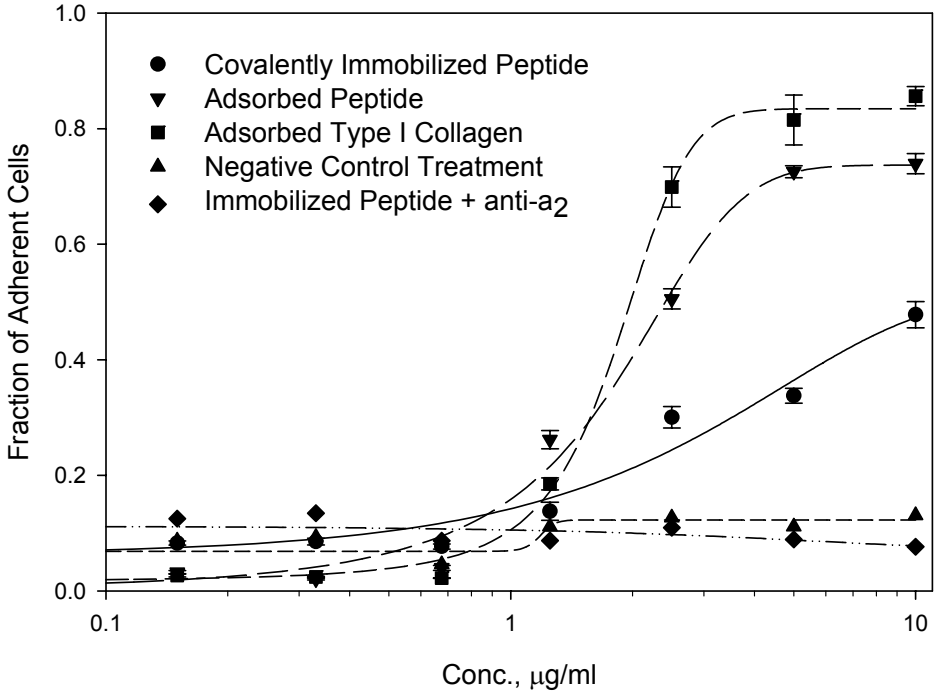

Figure 3.11. HT1080 cell adhesion to covalently immobilized peptide. The two positive controls are adsorbed peptide and adsorbed type I collagen. The negative control treatment is a surface treated without the addition of cross-linking agents. Anti-α_2 antibody blocking demonstrates specificity for the $\alpha_2\beta_1$ integrin. (1 hour cell adhesion, centrifugation at 12g for 5 min). (mean ± standard error; three separate experiments in triplicate) ANOVA of C_{50} values: $p<0.003$; covalently immobilized peptide > negative control ($p<0.02$); covalently immobilized peptide > antibody blocking ($p<0.02$); adsorbed peptide > covalently immobilized peptide ($p<0.004$).

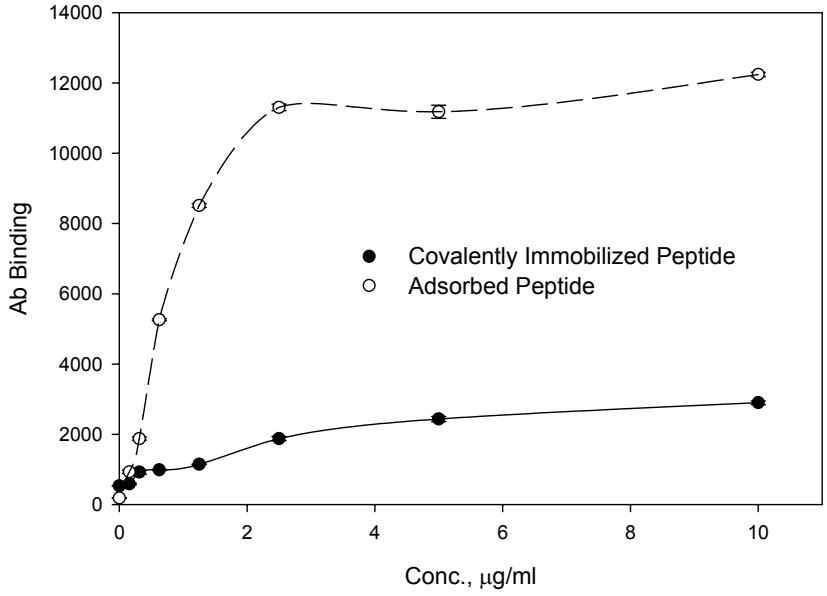

Figure 3.12. ELISA results for covalently immobilized peptide and adsorbed peptide. (mean ± standard error; two separate experiments in triplicate)

Immunofluorescent Staining for Focal Adhesions

MC3T3-E1 murine immature osteoblast-like cells were seeded onto covalently immobilized peptide surfaces, adsorbed peptide surfaces, and control type I collagen surfaces for 6 hours in 0.1% serum to promote the formation of mature integrin-mediated focal adhesions. The cells were then extracted, fixed, and stained for $\alpha_2\beta_1$ integrin subunits and vinculin, an intracellular structural protein that localizes to focal adhesion plaques. These cells were selected because they assemble robust integrin-containing focal adhesion plaques characterized by clustered integrin components and intracellular structural and signaling proteins attached to the actin cytoskeleton (Stephansson et al., 2002;Tamura et al., 2001a). These cells also exhibited collagen-like adhesion profiles on GFOGER-peptide surfaces comparable to those reported for HT1080 cells (unpublished observations), and thus represent a particularly relevant model for focal adhesion formation on these surfaces. In addition, MC3T3-E1 cells express osteoblast-specific proteins and produce mineralized nodules during in vitro maturation, and therefore will be examined in future studies as a model for osteoblast differentiation on GFOGER-peptide modified surfaces (Choi et al., 1996;Sudo et al., 1983).

Fig. 3.13 demonstrates that MC3T3-E1 cells assemble vinculin- and β_1 subunit-containing focal adhesions on the adsorbed and immobilized GFOGER-peptide surfaces. The co-localization of vinculin and β_1 integrin subunit on the periphery of the cells suggests that both peptide surfaces promote the formation of mature integrin-mediated focal adhesions. In addition, these adhesions plaques localize to the periphery of the cells in a pattern similar to that observed on control type I collagen, verifying the collagen-mimetic nature of the GFOGER-peptide surfaces.

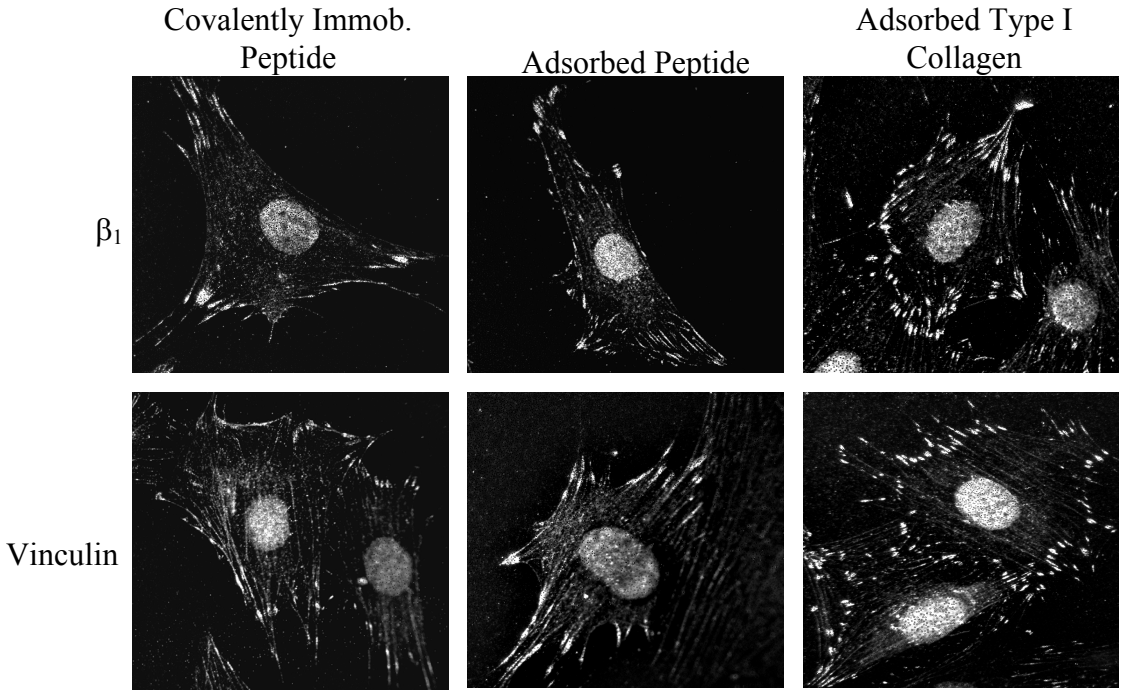

Figure 3.13. Immunofluorescent images demonstrating co-localization of β_1 integrin subunit and vinculin focal adhesion protein on the periphery of MC3T3-E1 cells seeded for 6 hours in 0.1% serum on covalently immobilized peptide, adsorbed peptide, and adsorbed type I collagen surfaces.

Discussion

Bioactive surfaces that provide specific signals to cells through well-characterized integrin-ligand interactions may lead to controlled cellular responses and improved tissue formation in tissue engineering and wound healing applications. Previous studies have incorporated the minimal cell recognition sequence RGD found in a wide variety of ECM proteins and implicated in a number of ligand-receptor interactions, (Ruoslahti, 1996). While its ability to bind a wide variety of cells makes it an exceptionally useful sequence for promoting general cell adhesion, the RGD tripeptide exhibits limited specificity for specific integrins and thus allows minimal control over cellular responses. The presentation of short sequences, such as RGD, may also result in the loss of full biological activity due to the absence of additional functional domains present in the native, three-dimensional structure of the ECM molecule (Danen, Aota, van Kraats, Yamada, Ruiter, and van Muijen, 1995;Aota, Nomizu, and Yamada, 1994a). This work fundamentally differs from such studies in that its objective is to engineer surfaces that mimic the tertiary or three-dimensional structure as well as primary structure of collagen and thus exhibit specificity for the particular integrin receptor, $\alpha_2\beta_1$. In order to engineer an integrin-specific bioadhesive surface, we have designed a triple helical collagen-mimetic peptide that incorporates the hexapeptide sequence GFOGER from residues 502-507 of the α_1(I) chain of type I collagen, a major binding site for the $\alpha_2\beta_1$ integrin. CD spectroscopy verified that this peptide adopts a stable triple helical conformation and that its triple helix is similar to that observed in native type I collagen. Passively adsorbed GFOGER-peptide actively promoted HT1080 concentration-dependent cell adhesion and spreading comparable to that observed on type I collagen. The involvement of integrin

$\alpha_2\beta_1$ in these adhesion events was verified with antibody blocking conditions, fulfilling our requirement of integrin-specific peptide activity.

Recent literature has shown that collagen's quaternary or polymeric structure as well as its tertiary triple helix is essential for platelet aggregation and activation (Morton, Peachey, Knight, Farndale, and Barnes, 1997;Morton, Hargreaves, Farndale, Young, and Barnes, 1995). Although this particular platelet reactivity response was shown to be an $\alpha_2\beta_1$-independent event, platelet adhesion to collagen also involves $\alpha_2\beta_1$-mediated mechanisms (Morton, Peachey, Zijenah, Goodall, Humphries, and Barnes, 1994). Therefore, we sought to determine whether collagen's quaternary structure was essential not only for conformation-dependent processes such as platelet aggregation but also for specific integrin recognition events. Cell adhesion to polymerized GFOGER-peptide was significantly lower than adhesion to the uncross-linked peptide surfaces and nearly half that of type I collagen. This reduction in functional recognition may be due to differences in adsorbed peptide density or to changes in binding site accessibility or conformation. Regardless, we can conclude that collagen's quaternary structure does not promote nor enhance $\alpha_2\beta_1$-mediated recognition and is not essential for integrin-specific cell adhesion.

Next we designed three complementary schemes for tethering this GFOGER-peptide to a surface in order to assess its activity in an immobilized conformation and ultimately its potential as a surface modification agent for biomaterials and tissue engineering applications (**Fig. 3.8**). The first two immobilization schemes involve biotinylating the carboxyl terminus of the peptide using a PEO linker arm attached to a biotin group. The biotinylated peptide was then introduced to surfaces treated with either

adsorbed avidin or adsorbed anti-biotin antibody, both of which resist non-specific protein adsorption. The third scheme involved covalently crosslinking the peptide to passively adsorbed bovine serum albumin using the crosslinking agents EDC ands sulfo-NHS. The BSA provided a non-fouling, non-adhesive background surface with carboxylate anchoring groups for the peptide. Cell adhesion results demonstrated that the peptide was active for all three immobilization schemes and will promote $\alpha_2\beta_1$-mediated adhesion when covalently tethered to a substrate, as indicated by antibody blocking conditions. Combined with ELISA data, these results also suggest that the peptide exhibits nearly three-fold higher adhesion activity in the immobilized conformation than passively adsorbed onto the surface. Because the peptide can only be covalently crosslinked to the substratum through the primary amine terminal group, all of the peptides on the surface should be in a single orientation with the GFOGER cell recognition site in a highly accessible environment. In contrast, when the peptide is passively adsorbed, it can adopt a range of orientations, some of which may not be favorable for binding site recognition and cell adhesion, thus explaining the lower activity observed on the adsorbed peptide surfaces.

Immunofluorescent staining of MC3T3-E1 osteoblast-like cells revealed the assembly of focal adhesion plaques containing both the β_1 integrin subunit and vinculin structural protein on the peptide surfaces in a pattern similar to that observed on type I collagen, further verifying the collagen-mimetic nature of the GFOGER-peptide. In addition, since focal adhesions represent junctions of integrin-mediated intracellular signaling, these images suggest that the GFOGER-peptide not only promotes adhesion

comparable to type I collagen but may also mimic the post-adhesion signaling characteristics of collagen surfaces, allowing specific control of cell function.

Conclusion

We have engineered a collagen-mimetic, triple helical peptide and verified its activity using several surface modification techniques, including passive adsorption, specific noncovalent surface interaction, and covalent immobilization, demonstrating that this triple helical peptide represents a robust and versatile approach to the design of bioadhesive surfaces that specifically target the $\alpha_2\beta_1$ integrin. Surface immobilization remains the most promising method for incorporating the GFOGER peptide into applications that benefit from enhanced control over cell function due to higher adhesion activity and greater surface stability.

In terms of a viable surface modification scheme, these studies reveal that this adhesion-promoting synthetic peptide of minimal recognition sequence and specific tertiary conformation can be covalently grafted to a stable, non-adhesive substrate to produce biologically active, chemically well-defined surfaces that support $\alpha_2\beta_1$-specific cell adhesion. Controlling integrin binding through covalent surface modification in turn allows us to optimize cell function for applications such as biomaterials processing and tissue engineering scaffold design. In addition, these surfaces may be useful in the study of fundamental $\alpha_2\beta_1$-mediated adhesion events in various cell models and biotechnological applications.

CHAPTER 4

$\alpha_2\beta_1$ INTEGRIN-SPECIFIC COLLAGEN MIMETIC SURFACES THAT SUPPORT OSTEOBLASTIC DIFFERENTIATION

Summary

The interactions of osteoblasts with their surrounding ECM are essential for skeletal development, homeostasis, and maintenance of the mature osteoblastic phenotype. Integrins are the principal transducers of ECM signals that regulate this process of osteoblast commitment and differentiation. Several studies indicate that the $\alpha_2\beta_1$ integrin interaction with type I collagen is a crucial signal for the induction of osteoblastic differentiation and matrix mineralization. The integrin $\alpha_2\beta_1$ recognizes the Gly-Phe-Hyp-Gly-Glu-Arg (GFOGER) motif in residues 502-507 of the α1[I] chain of type I collagen. This study demonstrates that an $\alpha_2\beta_1$ integrin-specific GFOGER-peptide triggers the activation of focal adhesion kinase (FAK) and alkaline phosphatase in MC3T3-E1 murine immature osteoblast-like cells - two proteins that have been implicated in the osteoblastic differentiation pathway. These GFOGER-peptide surfaces also support the expression of multiple osteoblast-specific genes, including osteocalcin and bone sialoprotein, and induce calcification and matrix mineralization in a manner similar to type I collagen, suggesting that this triple-helical peptide represents a

*Modified from Reyes,C.D. & Garcia,A.J. Alpha2beta1 integrin-specific collagen-mimetic surfaces supporting osteoblastic differentiation. *J. Biomed. Mater. Res. A* **69**, 591-600 (2004).

promising surface modification strategy for the design of collagen-mimetic bioadhesive surfaces that support osteoblastic differentiation.

Introduction

The interactions of osteoblasts with their surrounding ECM are essential for skeletal development and homeostasis and the maintenance of the mature osteoblastic phenotype (Xiao, Gopalakrishnan, Jiang, Reith, Benson, and Franceschi, 2002;Suzawa, Tamura, Fukumoto, Miyazono, Fujita, Kato, and Takeuchi, 2002;Ikeuchi, Dohi, Horiuchi, Ohgushi, Noshi, Yoshikawa, Yamamoto, and Sugimura, 2002;Mizuno and Kuboki, 2001;Regazzoni, Winterhalter, and Rohrer, 2001;Tamura, Takeuchi, Suzawa, Fukumoto, Kato, Miyazono, and Fujita, 2001b;Mizuno, Fujisawa, and Kuboki, 2000;Xiao, Jiang, Thomas, Benson, Guan, Karsenty, and Franceschi, 2000a;Jikko, Harris, Chen, Mendrick, and Damsky, 1999;Takeuchi, Suzawa, Kikuchi, Nishida, Fujita, and Matsumoto, 1997b;Lynch, Stein, Stein, and Lian, 1995). During the early stages of differentiation, osteoblasts synthesize an ECM consisting primarily of type I collagen. As matrix deposition progresses, the osteoblastic differentiation pathway is characterized by the activation of transcriptional pathways leading to the temporal expression of multiple proteins, including alkaline phosphatase, osteocalcin, and bone sialoprotein (Aubin and Liu, 1996;Stein, Lian, Stein, van Wijnen, Frenkel, and Montecino, 1996). The distinctive feature of the mature osteoblastic phenotype is their ability to induce the mineralization of the ECM (Aubin and Liu, 1996).

Integrins are the central transducers of ECM signals that regulate this process of osteoblast commitment and differentiation. The integrins $\alpha_1\beta_1$ and $\alpha_2\beta_1$ are the major collagen-binding integrins, with $\alpha_1\beta_1$ having a higher affinity for the basement membrane

type IV collagen and $\alpha_2\beta_1$ having a higher affinity for the fibrillar type I collagen, the major protein constituent of bone (Tulla, Pentikainen, Viitasalo, Kapyla, Impola, Nykvist, Nissinen, Johnson, and Heino, 2001;Kapyla, Ivaska, Riikonen, Nykvist, Pentikainen, Johnson, and Heino, 2000;Nykvist, Tu, Ivaska, Kapyla, Pihlajaniemi, and Heino, 2000). In fact, the $\alpha_2\beta_1$ integrin is highly expressed on osteoblast-like cells and is one of the predominant adhesion receptors used by osteoblast-like cells to adhere to the collagen matrix (Gronthos, Stewart, Graves, Hay, and Simmons, 1997). Several studies indicate that the $\alpha_2\beta_1$ integrin interaction with type I collagen is a crucial signal for the induction of osteoblastic differentiation and matrix mineralization (Suzawa, Tamura, Fukumoto, Miyazono, Fujita, Kato, and Takeuchi, 2002;Mizuno and Kuboki, 2001;Mizuno, Fujisawa, and Kuboki, 2000;Jikko, Harris, Chen, Mendrick, and Damsky, 1999;Xiao, Wang, Benson, Karsenty, and Franceschi, 1998;Takeuchi, Suzawa, Kikuchi, Nishida, Fujita, and Matsumoto, 1997a). For example, $\alpha_2\beta_1$-mediated osteoblast adhesion to type I collagen activates Runx2/Cbfa1, a transcription factor that controls osteoblast differentiation and matrix mineralization (Xiao, Wang, Benson, Karsenty, and Franceschi, 1998;Takeuchi, Suzawa, Kikuchi, Nishida, Fujita, and Matsumoto, 1997a). Furthermore, the collagen-$\alpha_2\beta_1$ integrin interaction has been shown to induce the osteoblastic phenotype in multipotent bone marrow cells (Mizuno and Kuboki, 2001;Mizuno, Fujisawa, and Kuboki, 2000). Integrin $\alpha_2\beta_1$-mediated attachment to type I collagen stimulates the tyrosine phosphorylation of focal adhesion kinase (FAK) and subsequently the activation of extracellular signal-related kinase (ERK), a mitogen-activated protein kinase (MAPK) that has been implicated in the control of osteoblast-specific gene expression and matrix mineralization (Suzawa, Tamura, Fukumoto,

Miyazono, Fujita, Kato, and Takeuchi, 2002;Tamura, Takeuchi, Suzawa, Fukumoto, Kato, Miyazono, and Fujita, 2001b;Xiao, Jiang, Thomas, Benson, Guan, Karsenty, and Franceschi, 2000b;Takeuchi, Suzawa, Kikuchi, Nishida, Fujita, and Matsumoto, 1997b). Disrupting the $\alpha_2\beta_1$ integrin interaction with type I collagen using function-blocking antibodies blocks the expression of osteoblast-specific genes, such as osteocalcin, and inhibits calcification and formation of a mineralized matrix (Mizuno, Fujisawa, and Kuboki, 2000;Jikko, Harris, Chen, Mendrick, and Damsky, 1999;Xiao, Wang, Benson, Karsenty, and Franceschi, 1998).

Incorporating discrete cell adhesion motifs, such as the collagen mimetic GFOGER hexapeptide, into bioactive materials and surfaces offers a promising strategy to enhance cell-material interactions and encourage biospecific cell adhesion and differentiation (Hubbell, 1999). We have previously demonstrated our ability to engineer stable bioadhesive surfaces that specifically target the $\alpha_2\beta_1$ integrin by adsorbing or immobilizing a stable triple-helical, collagen-mimetic peptide that contains the GFOGER adhesion motif from type I collagen (Reyes and Garcia, 2003b). This peptide specifically targets the $\alpha_2\beta_1$ integrin receptor, and its cell adhesion activity is comparable to that of type I collagen (Reyes and Garcia, 2003b). In the present study, we demonstrate that this $\alpha_2\beta_1$ integrin-specific GFOGER-peptide triggers the activation of FAK and alkaline phosphatase in MC3T3-E1 murine immature osteoblast-like cells. These surfaces also support the expression of multiple osteoblast-specific genes and the mineralization of the ECM in a manner similar to type I collagen, suggesting that this triple-helical peptide represents a robust approach to the design of collagen-mimetic bioadhesive surfaces that specifically target the $\alpha_2\beta_1$ integrin. Controlling specific integrin binding through this

biomolecular surface modification strategy may allow the optimization of cell function, in particular osteoblastic differentiation, for applications such as orthopedic biomaterials and bone tissue engineering scaffold design.

Materials and Methods

Cells and Reagents

MC3T3-E1 murine immature osteoblast-like cells (RBD1126) were purchased from the Riken Cell Bank (Hirosawa, Japan). Bovine type I collagen (Vitrogen-100) was purchased from Cohesion (Palo Alto, CA). Rabbit polyclonal anti-FAK antibody was obtained from Upstate Biotechnology (Lake Placid, NY). Rabbit polyclonal anti-FAK [pY397], anti-FAK [pY576], and anti-FAK [pY861] phospho-specific antibodies were purchased from BioSource International, Inc. (Camarillo, CA). Biotin-conjugated donkey anti-rabbit IgG was obtained from Jackson Immunoresearch (West Grove, PA). Alkaline phosphates-conjugated anti-biotin (clone BN-43) mouse IgG was purchased from Sigma Chemical Co. (St. Louis, MO). The micro BCA protein assay reagent kit was purchased from Pierce (Rockford, IL). ECF susbtrate for Western blotting was acquired from Amersham Pharmacia Biotech Inc (Piscataway, NJ). Purified calf intestinal alkaline phosphatase enzyme and 4-methyl-umbelliferyl-phosphate substrate were obtained from Sigma Chemical Co. RNA isolation and DNA purification reagents were acquired from Qiagen (Valencia, CA). Molecular biology reagents for reverse transcription polymerase chain reaction (RT-PCR) were purchased from Invitrogen (Carlsbad, CA), reagents for real-time PCR were obtained from Applied Biosystems (Foster City, CA), and PCR oligonucleotides were acquired from Integrated DNA Technologies (Coralville, IA). Fetal bovine serum was purchased from Hyclone (Logan,

UT). Additional cell culture reagents and Western blotting supplies were obtained from Invitrogen. All other chemical reagents were purchased from Sigma Chemical Co.

Cell Culture

MC3T3-E1 cells were cultured in α-minimum essential medium (α-MEM) supplemented with 10% fetal bovine serum and 1% penicillin-streptomycin. Cells were subcultured every two days using standard techniques. For alkaline phosphatase activity, gene expression, and matrix mineralization studies, cells were seeded onto the various surfaces at a density of 10,000 cells/cm^2 using 6-well tissue culture plates. After 24 h, the culture media was supplemented with 50 μg/ml L-ascorbic acid and 3 mM sodium β-glycerophosphate to support osteoblastic differentiation and mineralization. Media was replaced every 48 h.

Peptide and type I collagen surface preparation

The peptide GGYGGGPC(GPP)$_5$GFOGER(GPP)$_5$GPC [O=hydroxyproline] was synthesized by the Emory University Microchemical Facility at the Winship Cancer Institute (Atlanta, GA), as previously described (Reyes and Garcia, 2003b). Peptide was supplied in the purified form as a trifluoroacetic acid (TFA) salt and reconstituted at a stock concentration of 10 mg/ml in 0.1% TFA. Type I collagen was supplied as a 3.0 mg/ml protein solution in 0.012N HCl. In all experiments, the peptide and type I collagen were diluted to 10 μg/ml in Dulbecco's phosphate-buffered saline (DPBS). These solutions were then incubated on tissue culture-treated polystyrene surfaces for 1 h at 22ºC, followed by blocking in 1% heat-denatured BSA for 1 h.

Western blotting analysis of FAK activation

MC3T3-E1 cells were seeded onto the various surfaces at a density of 30,000 cells/cm^2 for 60 min, serum free at 37ºC. FAK activation was analyzed as previously described.(Garcia and Boettiger, 1999) Adherent cells were washed once in DPBS and lysed in cold radioimmunoprecipitation assay (RIPA) buffer (1% Triton X-100, 1% sodium deoxycholate, 0.1% SDS, 150 mM NaCl, 150 mM Tris-HCl pH 7.2, 350 μg/ml phenylmethylsulfonyl fluoride (PMSF), 10 μg/ml leupeptin, 10 μg/ml aprotinin, and 1 mM sodium orthovanadate) for 20 min on ice. The lysates were pipetted up and down ~25 times to shear the DNA and then clarified by centrifugation at 10,000g for 10 min. Protein concentration was then determined using a Pierce Micro BCA protein assay kit. Equal amounts of protein were boiled in Laemmli sample buffer (2% SDS, 10% glycerol, 100 mM DTT, 60 mM Tris-HCl pH 6.8, and 0.001% bromophenol blue) for 10 min and separated on a 7% SDS-polyacrylamide gel electrophoresis (SDS-PAGE) gel. Proteins were transferred electrophoretically onto nitrocellulose membranes and blocked with Blotto (5% non-fat dry milk, 0.02% sodium azide, 0.2% Tween 20 in PBS w/o Ca^{2+}/Mg^{2+}) overnight at 4ºC. Membranes were then incubated with primary antibody – anti-FAK (1 μg/ml), anti-FAK pY397 (0.35 μg/ml), anti-FAK pY576 (0.5 μg/ml), or anti FAK pY861 (1 μg/ml) – in Blotto for 1 h at room temperature under gentle rocking. Membranes were washed in TBS-Tween (20 mM Tris HCl pH 7.6, 137 mM NaCl, 0.1% Tween 20) for 30 min and incubated in secondary antibody (biotin-conjugated anti-rabbit IgG, 1:20,000 dilution in Blotto) for 1 h at room temperature under gentle rocking. Membranes were washed again in TBS-Tween for 30 min and incubated in a tertiary or detection antibody (alkaline phosphatase-conjugated anti-biotin IgG, 1:10,000 dilution in

Blotto) for 1 h at room temperature under gentle rocking. After antibody incubation, membranes were washed in TBS-Tween for 30 min and immunoreactivity was detected using ECF fluorescent substrate. Bands were visualized using a Fuji Image Analyzer and further quantified using Adobe Photoshop software. FAK phosphorylation levels were normalized to the amount of total FAK in each experimental run. Multiple experimental runs were pooled for statistical purposes by normalizing to a control sample of lysate from cells seeded onto tissue culture-treated polystyrene.

Osteblast-specific gene expression

Osteoblast-specific gene expression was analyzed by real time reverse-transcriptase polymerase chain reaction (real time RT-PCR).(Byers et al., 2002a) Total RNA was isolated at 3 and 7 days after initial cell seeding using the Qiagen RNeasy RNA isolation kit. During RNA isolation and purification, samples were treated with DNaseI (27 Kunitz units/sample) for 15 min at room temperature to eliminate any genomic DNA contamination. The concentration of purified RNA was quantified using a UV spectrophotometer (Shimadzu, Columbia, MD) and 1 μg of total RNA was used to synthesize cDNA templates by oligo(dT) priming using the Superscript First-Strand cDNA Synthesis System.

Real-time RT-PCR was performed with the ABI Prism 7700 Sequence Detection System (Applied Biosystems; 40 cycles; melting for 15 s at 95ºC; annealing and extending for 60 s at 60ºC) using Sybr green DNA intercalating dye. Gene transcript concentration in the sample cDNA template solutions was quantified by preparing a functional range of dilutions from an absolute standard for each gene. Linear standard curves were then generated by plotting the log of the known concentration versus the C_T

value (the cycle number at which the fluorescence reached a pre-determined threshold level). Real-time RT-PCR oligonucleotide primers (**Table 4.1**) were designed using Primer Express software (Applied Biosystems).

Alkaline phosphatase biochemical activity

Alkaline phosphatase (ALP) activity was quantified at 7 days after initial cell seeding using a modification of the Sodek and Berkman method.(Stephansson, Byers, and Garcia, 2002;Sodek and Berkman, 1987) Briefly, cells were rinsed with DPBS and scraped in cold 50 mM Tris-HCl. After sonication and centrifugation, the total protein concentration was quantified using a Pierce Micro BCA protein assay kit. Equal amounts of protein (2.5 μg) were added to 60 μg/ml 4-methyl-umbelliferyl-phosphate fluorescent substrate in diethanolamine buffer (pH 9.5). After a 60 min incubation at 37ºC, the fluorescence was read at an excitation of 360 nm and an emission of 465 nm on an HTS 7000 Plus BioAssay Reader (Perkin Elmer). Enzymatic activity was standardized using purified calf intestinal alkaline phosphatase at known dilutions and normalized to the amount of total protein.

Von Kossa staining for mineralized matrix

Mineralized phosphate deposits were visualized by von Kossa staining.(Byers et al., 2002b) After 12 days, cultures were fixed in 70% ethanol for at least 30 min. Plates were exposed to uniform light for 30 min in the presence of 5% $AgNO_3$ to stain phosphate deposits in the matrix. The stain was then fixed in 5% Na_2SO_3 for 2 min. Cultures were subsequently rinsed with deionized H_2O and dried at 37ºC for 30 min. Mineralized surface area was quantified by averaging 16 representative 1.8x images

Table 4.1. Real-Time PCR Oligonucleotides for Murine Genes

Gene	*Forward Primer*	*Reverse Primer*	*Size (bp)*
ALP 6671532*	mAP-551.F RT 5'-GGG ACT GGT ACT CGG ATA ACG A-3'	mAP-621.R RT 5'-CTG ATA TGC GAT GTC CTT GCA-3'	71
OCN X04142	mOCN-126.F RT 5'-CGG CCC TGA GTC TGA CAA A-3'	mOCN-193.R RT 5'-GCC GGA GTC TGT TCA CTA CCT T-3'	68
BSP L20232	mBSP-219.F RT 5'-TCC TCC TCT GAA ACG GTT TCC-3'	mBSP-291.F RT 5'-GGA ACT ATC GCC GTC TCC ATT-3'	73

ALP, alkaline phosphatase; OCN, osteocalin; BSP, bone sialoprotein

* GenBank accession number

using an automated microscope stage and Image Pro image analysis software (Media Cybernetics, Silver Springs, MD).

Statistics

Data are reported as mean ± standard error. Results were analyzed by one-way ANOVA using SYSTAT 8.0 (SPSS). If treatment level differences were determined to be significant, pair-wise comparisons were performed using a Tukey post-hoc test. A 95% confidence level was considered significant. To make the variance independent of the mean, analyses of PCR data were performed after logarithmic transformation.

Results

The collagen-mimetic peptide used in these experiments has the following primary sequence: GGYGGGPC$(GPP)_5$GFOGER$(GPP)_5$GPC (Reyes and Garcia, 2003b). The GPP triplets on either side of the GFOGER recognition site provide cooperative clusters that promote the formation of a stable right-handed triple helical structure at room temperature (Knight, Morton, Peachey, Tuckwell, Farndale, and Barnes, 2000;Nagarajan, Kamitori, and Okuyama, 1998;Fields and Prockop, 1996). This triple-helical conformation is essential for integrin recognition and $\alpha_2\beta_1$-mediated cell adhesion (Messent, Tuckwell, Knauper, Humphries, Murphy, and Gavrilovic, 1998;Morton, Peachey, Knight, Farndale, and Barnes, 1997;Morton, Peachey, Zijenah, Goodall, Humphries, and Barnes, 1994). In order to evaluate its effectiveness as a collagen-mimetic surface modification agent, we passively adsorbed the GFOGER-peptide onto tissue culture polystyrene surfaces and compared its biological activity with adsorbed type I collagen and untreated polystyrene.

MC3T3-E1 murine immature osteoblast-like cells were used in all experiments. No gross differences in cell proliferation were observed among substrates, and cultures reached confluence at approximately 2 days.

Focal Adhesion Kinase (FAK) Activation

We previously demonstrated that GFOGER-peptide surfaces promote the formation of $\alpha_2\beta_1$ integrin-mediated focal adhesions that are similar to those assembled on type I collagen (Reyes and Garcia, 2003b). Since focal adhesions represent junctions of integrin-mediated intracellular signaling, these results suggest that our peptide not only promotes adhesion comparable to type I collagen but may also mimic the post-adhesion signaling events characteristic of collagen surfaces, allowing us to specifically control cell function - in particular, osteoblastic differentiation. Therefore, we examined whether these collagen-mimetic peptide surfaces trigger the activation of focal adhesion kinase (FAK), an intracellular signaling molecule implicated in integrin-mediated signal transduction and downstream osteoblastic differntiation pathways (Tamura, Takeuchi, Suzawa, Fukumoto, Kato, Miyazono, and Fujita, 2001b;Xiao, Jiang, Thomas, Benson, Guan, Karsenty, and Franceschi, 2000b;Takeuchi, Suzawa, Kikuchi, Nishida, Fujita, and Matsumoto, 1997b).

Using standard Western blotting techniques, we probed the phosphorylation of three different tyrosine (Y) sites on FAK – Y397, the autophosphorylation site of FAK, binds the Src family SH2 and the p85 subunit of PI3-kinase; Y861 is the major Src phosphorylation site; Y576 is located in the catalytic portion of FAK and when phosporylated results in maximal FAK kinase activity (Reust et al., 2000). Western blotting revealed comparable levels of signal activation on peptide and type I collagen

surfaces for all three tyrosine sites on FAK (**Fig. 4.1**). These activation levels were significantly greater than negative control cells kept in suspension. **Fig. 4.1** shows that phosphorylation levels of Y397 were statistically higher on GFOGER-peptide surfaces compared with type I collagen. This effect may be explained by possible differences in the surface density of GFOGER binding sites or by confounding effects of other cell binding sites present on the native collagen molecule.

Osteoblast-Specific Gene Expression

To investigate the osteoblastic differentiation potential of these collagen-mimetic surfaces, we used real-time RT-PCR to probe osteoblast-specific gene expression in 3 and 7 day cultures of MC3T3-E1 cells supplemented with ascorbic acid and Na-β-glycerophosphate. Expression levels of Runx2/Cbfa1, a transcription factor essential for bone formation and osteoblastic differentiation, were statistically equivalent on GFOGER-peptide and type I collagen surfaces and elevated compared to polystyrene (**Fig. 4.2.a**).

Additional osteoblast-specific genes were investigated, including osteocalcin (OCN), bone sialoprotein (BSP), and alkaline phosphatase (ALP). For all three of these bone-specific markers, RT-PCR revealed equivalent levels of gene expression on GFOGER-peptide and type I collagen surfaces (**Fig. 4.2.b**). Transcript levels were significantly greater than reference surfaces, including untreated polystyrene, shown in **Fig. 4.2.b**. In addition, these expression levels increased by day 7, indicating sustained up-regulation of osteoblast-specific gene expression on the integrin-specific GFOGER-peptide surfaces.

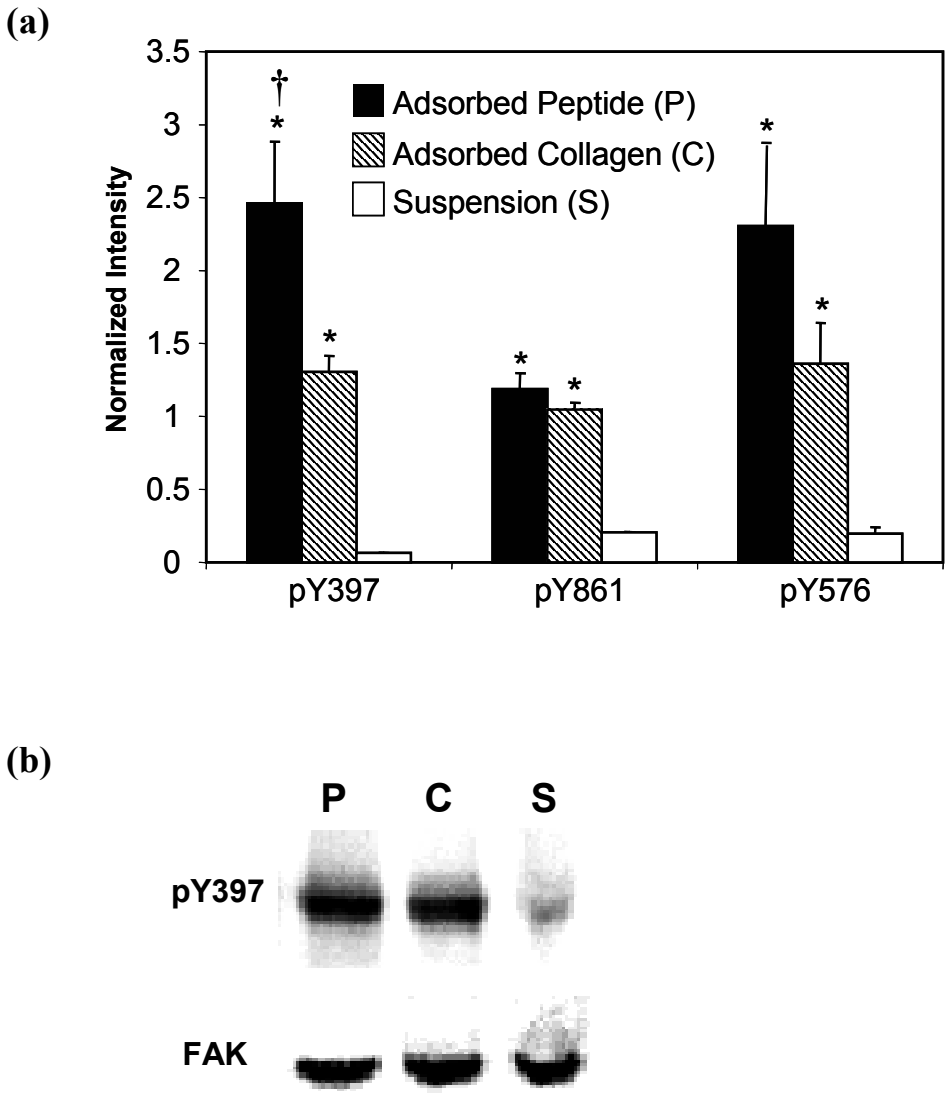

Figure 4.1. **(a)** Western blotting results measuring site-specific tyrosine phosphorylation of focal adhesion kinase (FAK) in MC3T3-E1 cells seeded onto adsorbed peptide or adsorbed type I collagen compared with cells kept in suspension (1 hour serum-free cell adhesion or suspension). Three tyrosine sites on FAK are shown. **(b)** Representative Western blot for phosphorylated tyrosine-397 on FAK. pY397 ANOVA: $p<0.002$; *peptide or collagen > suspension ($p<0.001$), †peptide > collagen ($p<0.03$). pY861 ANOVA: $p<0.00003$; *peptide = collagen > suspension ($p<0.00008$). pY576 ANOVA: $p<0.03$; *peptide = collagen > suspension ($p<0.03$). (mean ± standard error; three separate experiments in duplicate)

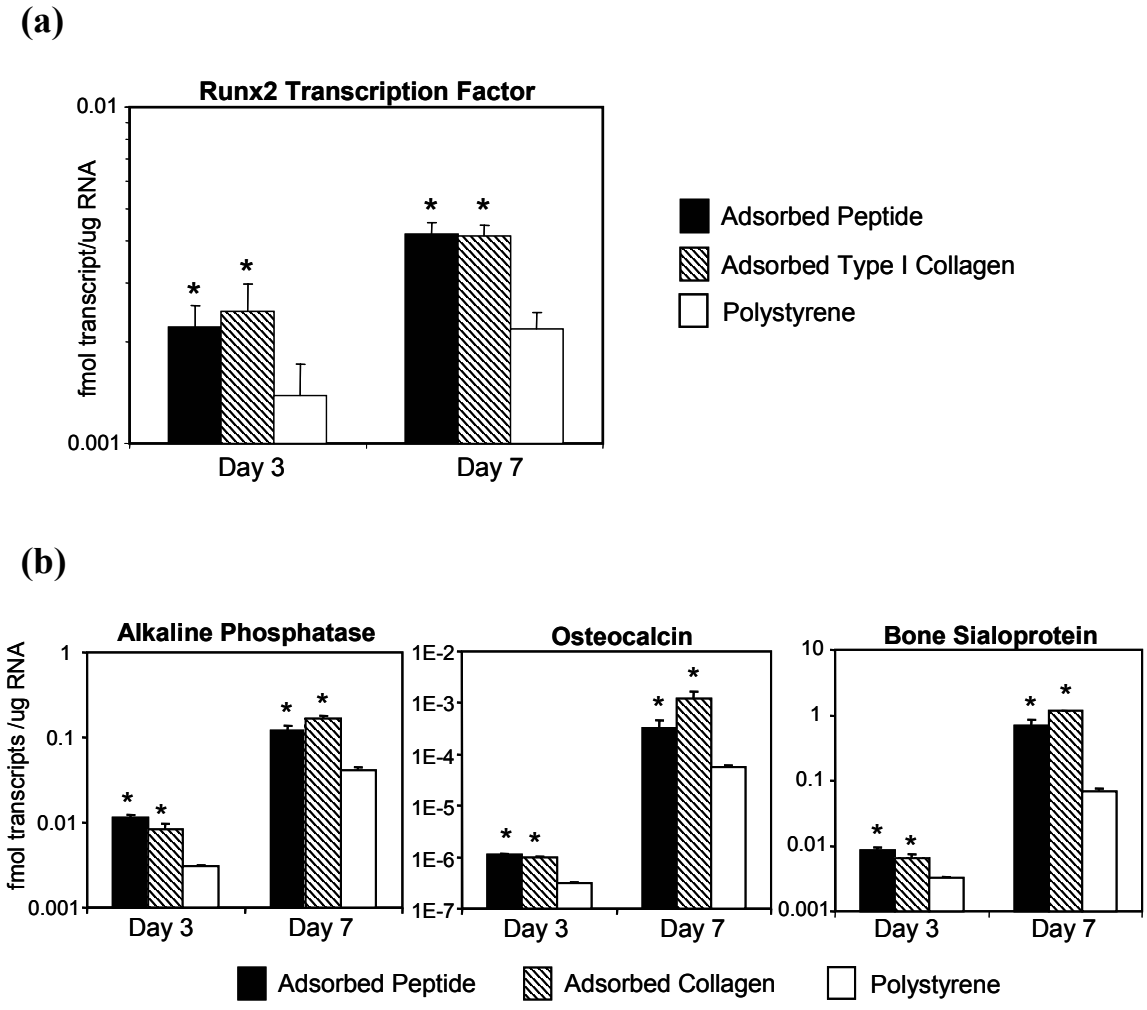

Figure 4.2. Osteoblast-specific gene expression measured by real-time RT-PCR for **(a)** Runx2 transcription factor and **(b)** alkaline phosphatase (ALP), osteocalcin (OCN), and bone sialoprotein (BSP) in MC3T3-E1 cells seeded for 3 or 7 days on adsorbed peptide, adsorbed type I collagen, or polystyrene. Runx2 ANOVA: $p<0.04$; *day 3 peptide = collagen > polystyrene ($p<0.05$), *day 7 peptide = collagen > polystyrene ($p<0.0008$). ALP ANOVA: $p<0.0006$; *day 3 peptide = collagen > polystyrene ($p<0.001$), *day 7 peptide = collagen > polystyrene ($p<0.003$). OCN ANOVA: $p<0.0003$; *day 3 peptide = collagen > polystyrene ($p<0.00002$), *day 7 peptide = collagen > polystyrene

Alkaline Phosphatase Biochemical Activity

An alkaline phosphatase biochemical assay revealed similar levels of activation on GFOGER-peptide and type I collagen surfaces after 7 days (**Fig. 4.3**). These levels were significantly greater than activity on several reference surfaces, including tissue culture plastic (data not shown) and polystyrene (**Fig. 4.3)**.

Matrix Mineralization

Matrix mineralization was examined in MC3T3-E1 cultures after 12 days. A von Kossa stain for phosphate deposits revealed that the percentage of mineralized area on the GFOGER-peptide surfaces was statistically equivalent to that of type I collagen (**Fig. 4.4**). Both were significantly greater than the mineralized area of several reference surfaces, including tissue culture plastic and untreated polystyrene (**Fig. 4.4)**. This mineralization data reveals that the collagen-mimetic peptide is capable of promoting matrix mineralization in osteoblast cultures, demonstrating the effects of controlled $\alpha_2\beta_1$ integrin binding on cell function - in this case, osteoblastic differentiation.

Discussion

Regulating cell behavior at a biomaterial interface requires strict control over the material's surface properties and an ability to assign the material a defined biological activity similar to that of the native ECM. Targeting a specific integrin-ligand interaction allows directed control over subsequent signaling pathways and cell functions without the confounding effects of additional binding sites present on the whole ECM molecule. We have previously designed a triple-helical collagen-mimetic peptide that preferentially targets the $\alpha_2\beta_1$ integrin and promotes integrin-mediated cell adhesion and focal adhesion

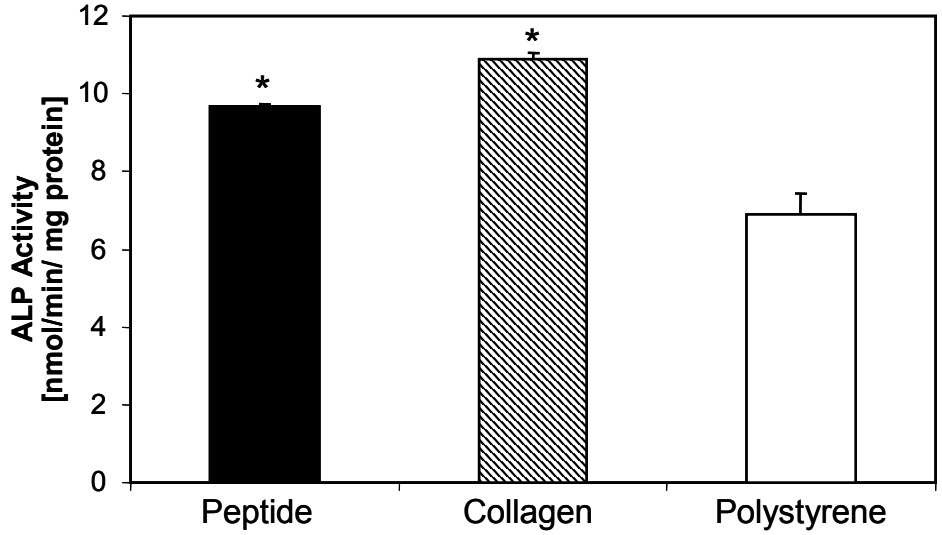

Figure 4.3. Alkaline phosphatase (ALP) biochemical activity from MC3T3-E1 cells seeded on adsorbed peptide, adsorbed type I collagen, or polystyrene for 7 days. ANOVA: $p<0.000002$; *peptide = collagen > polystyrene ($p<0.002$). (mean ± standard error; three separate experiments in triplicate)

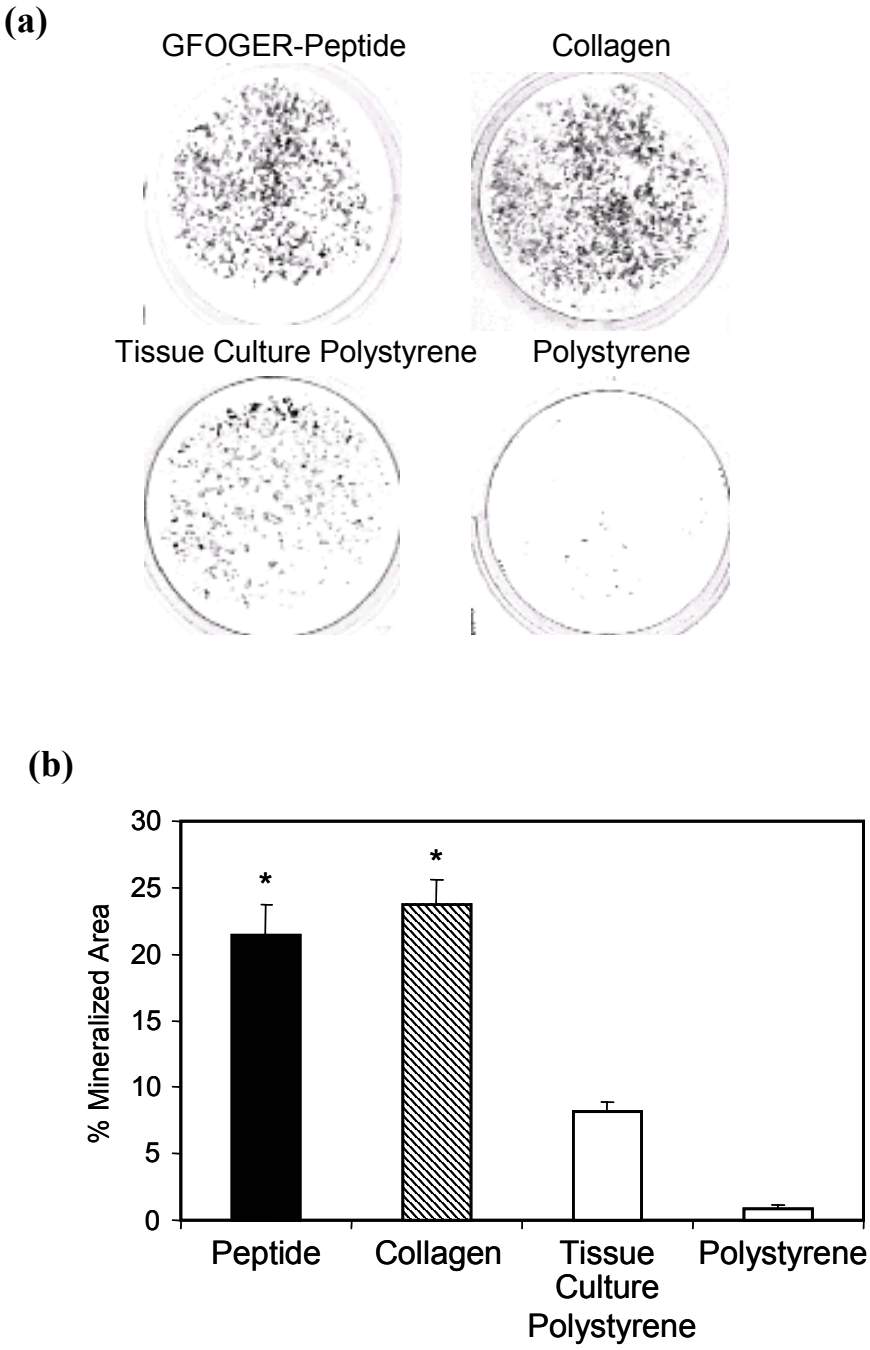

Figure 4.4. Matrix mineralization of MC3T3-E1 cells seeded on adsorbed peptide, adsorbed type I collage, tissue culture plastic, and polystyrene for 12 days. **(a)** von Kossa staining of mineralized matrix. **(b)** Quantification of mineralized area. ANOVA: $p<0.00002$; *peptide = collagen > tissue culture = polystyrene ($p<0.001$).

formation. (Reyes and Garcia, 2003b) The present study explores whether this integrin-specific peptide is capable of promoting similar signaling events and differentiation responses as native type I collagen in the osteoblast cell model.

One of the initial events triggered by the binding of the $\alpha_2\beta_1$ integrin to type I collagen is the association of the integrin's cytosolic domain with focal adhesion kinase (FAK), followed by phosphorylation at multiple sites to achieve full FAK activation. Phosphorylation of FAK's Y397 forms a binding site for Src-family kinases whereas Y861 is the major Src phosphorylation site (Reust, Roy, Ergang, Mernaugh, and Hanks, 2000;Calalb et al., 1996). In addition, the phosphorylation of Y576 in the kinase activation loop enhances FAK kinase activity (Reust, Roy, Ergang, Mernaugh, and Hanks, 2000;Calalb, Zhang, Polte, and Hanks, 1996). In all cases, specific activation of various tyrosine sites on FAK trigger signaling pathways that in turn affect cell functions such as differentiation. Several studies prove that the signaling pathway from the $\alpha_2\beta_1$ integrin to ERK/MAPK (extracellular signal-related kinase/mitogen-actived protein kinase) via FAK is required for osteoblastic differentiation (Lai et al., 2001;Tamura, Takeuchi, Suzawa, Fukumoto, Kato, Miyazono, and Fujita, 2001b;Takeuchi, Suzawa, Kikuchi, Nishida, Fujita, and Matsumoto, 1997b). In order to demonstrate the collagen-mimetic nature of the GFOGER-peptide, we compared its ability to trigger FAK phosphorylation with that of native type I collagen surfaces. A Western blot for specific tyrosine phosphorylation sites on FAK revealed similar levels of activation for cells plated on either GFOGER-peptide or type I collagen surfaces. These results indicate that the peptide triggers similar signaling pathways to type I collagen surfaces and may

promote the same phenotypic responses as the native molecule, including osteoblastic differentiation.

However, the β_1 integrin-FAK cascade is an initial signal transduction pathway that is widely activated among mesenchymal cells and therefore is not necessarily a specific indicator of osteoblastic differentiation (Guan, 1997). To verify that these peptide-induced signaling pathways result in the progression of the osteoblast phenotype, we examined the expression of Runx2/Cbfa1, a transcriptional activator that is essential for osteoblastic differentiation and bone formation. Runx2 DNA binding sequences have been discovered in the promoters of several osteoblast-specific genes, including osteocalcin (Ducy and Karsenty, 1995) and bone sialoprotein (Benson et al., 1999). Exogenous expression of Runx2 in nonosteoblastic cells induces expression of these genes (Byers et al., 2002c). The Runx2 transcription factor has been investigated as a central link between cell surface integrin activation by matrix proteins and subsequent osteoblast-specific gene expression (Xiao, Jiang, Thomas, Benson, Guan, Karsenty, and Franceschi, 2000b;Xiao, Wang, Benson, Karsenty, and Franceschi, 1998;Takeuchi, Suzawa, Kikuchi, Nishida, Fujita, and Matsumoto, 1997a). An increase in the expression of the type II isoform of this factor occurs in primary rat osteoblasts and murine MC3T3-E1 cells during progressive development of the osteoblast phenotype (Banerjee et al., 2001b). This developmental increase in Runx2 mRNA is paralleled by similar increases in Runx2 protein and osteoblast-specific DNA binding activity (Banerjee et al., 2001a). Real time RT-PCR results demonstrated the upregulation of this key osteoblast-specific transcription factor on both type I collagen and GFOGER-peptide surfaces,

demonstrating the ability of this collagen-mimetic peptide to trigger the transcriptional machinery necessary for osteoblastic differentiation.

To determine whether this pattern of increased Runx2 gene expression parallels similar increases in the expression of other osteoblast-specific genes, the transcript levels of osteocalcin, bone sialoprotein, and alkaline phosphatase were also examined. Alkaline phosphatase, the enzyme that initiates phosphate precipitation, is an early indicator of osteoblastic differentiation (Aubin and Liu, 1996). Osteocalcin is an ECM protein often used as a marker of the mature osteoblastic phenotype (Weinreb et al., 1990). Bone sialoprotein has been shown to enhance in vitro hydroxyapatite nucleation and thus plays a critical role in initiating bone mineralization (Hunter et al., 1996). Real time RT-PCR results demonstrated the sustained upregulation of these three genes on GFOGER-peptide surfaces after 3 and 7 days in culture. Gene expression patterns matched those observed on type I collagen surfaces, further verifying the collagen-mimetic nature of this peptide and its potential to trigger similar differentiation signals as type I collagen.

Osteoblastic differentiation is also characterized by the activation of multiple proteins including alkaline phosphatase. The alkaline phosphatase enzyme is often used as a marker for increased osteoblastic metabolic activity and an early indicator of osteoblastic differentiation (Aubin and Liu, 1996). An alkaline phosphatase biochemical assay revealed equivalent levels of activation on GFOGER-peptide and type I collagen surfaces after 7 days. Since alkaline phosphatase is the enzyme responsible for hydrolyzing phosphate esters and precipitating bone mineral (Aubin and Liu, 1996), these results suggest that this collagen-mimetic peptide might also be capable of promoting bone matrix mineralization in a manner similar to that of type I collagen.

In vitro mineralization was examined as an endpoint indicator of osteoblastic phenotype and the ultimate assessment of this collagen-mimetic biomolecular strategy. Several studies have demonstrated the critical role of type I collagen in mediating the signaling cascade for expression of a mature osteoblastic phenotype and subsequent in vitro matrix mineralization (Mizuno and Kuboki, 2001;Mizuno, Fujisawa, and Kuboki, 2000;Jikko, Harris, Chen, Mendrick, and Damsky, 1999;Xiao, Wang, Benson, Karsenty, and Franceschi, 1998;Lynch, Stein, Stein, and Lian, 1995). Under the appropriate conditions, immature osteoblast-like MC3T3-E1 cells endogenously express all factors necessary for in vitro mineralization. An enhanced capacity for mineralization was observed for cells cultured on type I collagen compared with reference surfaces. This enhanced mineralization was comparable to results from cells cultured on collagen-mimetic GFOGER-peptide. This capacity for mineralization on the GFOGER peptide-coated surfaces is in accordance with the previously observed up-regulation in osteoblast-specific gene expression and protein activity. These results verify the collagen-mimetic nature of the GFOGER-peptide and demonstrate the effects of controlled $\alpha_2\beta_1$ integrin-binding on cell function, in this case osteoblastic differentiation.

Conclusion

In conclusion, we have designed a triple-helical collagen-mimetic peptide that specifically targets the $\alpha_2\beta_1$ integrin receptor and promotes density dependent cell adhesion (Reyes and Garcia, 2003b), focal adhesion formation (Reyes and Garcia, 2003b), and FAK phosphorylation. These collagen-mimetic surfaces also support equivalent levels of osteoblastic gene expression, alkaline phosphatase activity, and matrix mineralization as native type I collagen. Designing biomaterials surfaces and

tissue engineering scaffolds using whole ECM molecules, such as type I collagen, is often limited by a lack of specificity for particular integrins and thus exhibit minimal control over cellular responses. In addition, native ECM proteins often have binding sites for other ligands, such as fibronectin or von Willebrand factor. Such ligands trigger separate signaling cascades that may ultimately confound phenotypic responses and interfere with controlled cell function. The GFOGER-peptide targets a specific integrin-ligand interaction that has been shown to be crucial in the development and maintenance of the osteoblast phenotype, as well as the mineralization of the extracellular matrix. As such, this peptide represents a robust and versatile approach to the design of collagen-mimetic bioadhesive surfaces that specifically target the $\alpha_2\beta_1$ integrin. We have previously demonstrated that this adhesion-promoting synthetic peptide of minimal recognition sequence and specific tertiary conformation can be covalently grafted to a stable, non-adhesive substrate to produce biologically active, chemically well-defined surfaces that support $\alpha_2\beta_1$-specific cell adhesion (Reyes and Garcia, 2003b). Controlling integrin binding through bioactive surface modification in turn allows control over cell function and possibly enhancement of tissue formation in tissue engineering, biomaterials, and wound healing devices. In particular, we have demonstrated the efficacy of this biomolecular strategy in the area of osteoblastic differentation and matrix mineralization for applications such as bone tissue engineering and osseointegration.

CHAPTER 5

COLLAGEN-MIMETIC PEPTIDE SURFACE COATING ENHANCES BONE FORMATION AND OSSEOINTEGRATION OF ORTHOPAEDIC IMPLANTS

Summary

Implant osseointegration, defined as close bone apposition and functional fixation, is a prerequisite for clinical success in orthopaedic and dental applications, many of which are restricted by implant loosening (Pilliar, 2005;Anderson, 2001). Surface modification approaches have had limited success in promoting integration. Our strategy to improve osseointegration of titanium implants focuses on presenting the GFOGER collagen-mimetic peptide that triggers $\alpha_2\beta_1$ cellular integrin receptor binding, which is crucial for bone mineral deposition. Titanium surfaces presenting integrin-specific GFOGER peptide trigger osteoblastic differentiation in primary rat bone marrow stromal cells, including bone-specific gene expression, alkaline phosphatase activity, and mineral deposition, leading enhanced osteoblastic function compared to unmodified orthopaedic-grade titanium. Furthermore, this integrin-targeted surface coating significantly improved peri-implant bone regeneration and mechanical osseointegration compared to untreated titanium in a rat tibia cortical bone implant model. Our study establishes a simple, single-step biologically active implant coating that enhances bone repair and implant integration for clinical orthopaedic and dental applications.

Introduction

Upon implantation, synthetic materials elicit an inflammatory response that results in a foreign body reaction and fibrous encapsulation.(Anderson, 2001) The foreign body reaction severely limits device integration and *in vivo* performance of numerous biomedical devices, including chemical biosensors, electrical leads/electrodes, therapeutic delivery systems, and orthopaedic and cardiovascular prostheses. Extensive efforts have concentrated on surface treatments and coatings to improve host tissue-implant integration. For instance, current orthopaedic and dental implant surface technologies focus on rough/porous coatings for bone ingrowth and bone-bonding ceramic coatings to promote integration with the surrounding bone and provide mechanical fixation (Bauer and Schils, 1999b)(Ducheyne and Qiu, 1999).

However, while these approaches are generally successful, they can be restricted by slow rates of osseointegration and poor mechanical anchorage in challenging clinical cases, such as those associated with large bone loss and poor bone quality (Ducheyne and Qiu, 1999). Since the extracellular matrix controls both cell adhesion and function, recent biomimetic strategies have focused on the immobilization of matrix components, including native structural proteins (Bernhardt, van den, Bierbaum, Beutner, Scharnweber, Jansen, Beckmann, and Worch, 2005;Becker, Geissler, Hempel, Bierbaum, Scharnweber, Worch, and Wenzel, 2002), peptide sequences (Bernhardt, van den, Bierbaum, Beutner, Scharnweber, Jansen, Beckmann, and Worch, 2005;Elmengaard, Bechtold, and Soballe, 2005a;Elmengaard, Bechtold, and Soballe, 2005b;Alsberg, Anderson, Albeiruti, Rowley, and Mooney, 2002b;Ferris, Moodie, Dimond, Gioranni, Ehrlich, and Valentini, 1999b), or synthetic derivatives based on matrix molecules

(Lutolf and Hubbell, 2005). The most common peptide-based strategy involves the surface deposition of peptides containing the Arg-Gly-Asp (RGD) sequence, which mediates cell attachment to several matrix proteins, including fibronectin, vitronectin, osteopontin, and bone sialoprotein. However, these bio-inspired strategies have yielded marginal increases in implant integration and mechanical fixation (Schliephake et al., 2002;Ferris, Moodie, Dimond, Gioranni, Ehrlich, and Valentini, 1999b). Because RGD is recognized by a large number of integrins in numerous cell types, this approach lacks specificity for particular targeted integrin signaling events and results in non-discriminatory attachment of cells to the RGD-coated surfaces. Therefore, engineering peptides that specifically target integrin signaling cascades implicated in specific tissue responses, for example osteogenesis, would allow the optimization of surface coatings for enhanced integration and performance.

The $\alpha_2\beta_1$ integrin is highly expressed on osteoblasts and is one of the predominant adhesion receptors for type I collagen (Gronthos, Stewart, Graves, Hay, and Simmons, 1997). $\alpha_2\beta_1$ integrin-type I collagen interactions provide crucial signals for the induction of osteoblastic differentiation and matrix mineralization (Suzawa, Tamura, Fukumoto, Miyazono, Fujita, Kato, and Takeuchi, 2002;Mizuno and Kuboki, 2001;Mizuno, Fujisawa, and Kuboki, 2000;Jikko, Harris, Chen, Mendrick, and Damsky, 1999;Xiao, Wang, Benson, Karsenty, and Franceschi, 1998;Takeuchi, Suzawa, Kikuchi, Nishida, Fujita, and Matsumoto, 1997a;Lynch, Stein, Stein, and Lian, 1995). For example, $\alpha_2\beta_1$-mediated osteoblast adhesion to type I collagen activates Runx2/Cbfa1 (Xiao, Wang, Benson, Karsenty, and Franceschi, 1998;Takeuchi, Suzawa, Kikuchi, Nishida, Fujita, and Matsumoto, 1997a), a transcription factor that regulates osteogenesis. Furthermore, the

collagen-$\alpha_2\beta_1$ integrin interaction induces osteoblastic differentiation in multipotent bone marrow stromal cells (Mizuno and Kuboki, 2001;Mizuno, Fujisawa, and Kuboki, 2000). We designed a stable triple-helical, collagen-mimetic peptide that contains the GFOGER adhesion motif from type I collagen that is recognized by the $\alpha_2\beta_1$ integrin (Reyes and Garcia, 2003b). This collagen-mimetic peptide specifically targets the $\alpha_2\beta_1$ integrin receptor and promotes density-dependent cell adhesion (Reyes and Garcia, 2003b), focal adhesion kinase signaling (Reyes and Garcia, 2004), and osteoblastic differentiation (Reyes and Garcia, 2004) in the MC3T3-E1 immature osteoblast cell line. We hypothesized that coating titanium implants with this peptide enhances peri-implant bone formation and mechanical osseointegration, thus providing a simple, clinically relevant strategy for improving orthopaedic implant integration.

Materials and Methods

Cell isolation and culture

Primary bone marrow stromal cells were harvested from the femora of young adult male Wistar rats in accordance with an IACUC-approved protocol (Maniatopoulos et al., 1988). After excision, hindleg femora and tibiae were cleared of soft tissue and processed through three consecutive 15 min rinses in growth medium (α-minimal essential medium supplemented with 10% fetal bovine serum, 1% penicillin–streptomycin, and 0.3 μg/ml amphotericin B). The ends of the long bones were then removed and the marrow space was flushed with culture medium (3-5 ml), using a syringe with an 18-gauge needle. Marrow isolates were pooled, centrifuged, resuspended in growth medium, and seeded for adhesion-dependent selection on tissue culture

polystyrene dishes. Non-adherent hematopoietic cells were removed during subsequent medium exchanges, which occurred every other day. Cells were subcultured every two days according to standard techniques. For *in vitro* osteogenic assays, cells were seeded at 10,000 cells/cm^2 in growth medium. After 24 h, cultures were maintained in osteogenic medium consisting of growth medium supplemented with 50 μg/ml L-ascorbic acid and 3 mM sodium β-glycerophosphate.

In vitro GFOGER peptide surface preparation

The peptide GGYGGGPC(GPP)$_5$GFOGER(GPP)$_5$GPC [O=hydroxyproline] was synthesized by the Emory University Microchemical Facility at the Winship Cancer Institute (Atlanta, GA).(Reyes and Garcia, 2003b) Peptide was supplied in the purified form as a trifluoroacetic acid (TFA) salt and reconstituted at a stock concentration of 10 mg/ml in 0.1% TFA. For the *in vitro assays*, glass chamber slides (16-well Lab-Tek Chamber Slides, Nalge Nunc) or tissue culture-treated polystyrene dishes were coated with 300 Å of pure titanium using an electron beam evaporator at a chamber base pressure between 1-2 x 10^{-6} torr with a deposition rate of 1.5 Å/second. The GFOGER peptide was diluted to 20 μg/ml in Dulbecco's phosphate-buffered saline (PBS) and incubated on the titanium surfaces for 1 h at 22ºC in preparation for all assays.

Cell adhesion assay

Cell adhesion to functionalized and untreated titanium surfaces was measured using a centrifugation assay that applies controlled detachment forces (Reyes and Garcia, 2003a;Reyes and Garcia, 2003b). Titanium-coated glass chamber slide wells were reassembled using a silicone-based adhesive and coated with 20 μg/ml GFOGER peptide

as described above or 20 μg/ml GRGDSPC peptide (BACHEM). Control titanium slides were coated with 10% FBS (to model serum protein adsorption) or blocking buffer (5% non-fat dry milk in PBS to produce a non adhesive support). Stromal cells were loaded with 2 μg/ml calcein-AM (Molecular Probes), a membrane permeable green-fluorescent dye, detached using trypsin + EDTA, and resuspended serum-free in PBS with 2 mM dextrose. Cells were seeded onto the substrates (10,000 cells/well) and allowed to attach for 1 h at 37ºC. For blocking experiments, cells were incubated in the presence of 20 μg/ml anti-rat α_2 antibody (hamster anti-rat CD49b monoclonal antibody, clone Ha1/29, BD Pharmingen) or 20 μg/ml anti-rat α_v antibody (mouse anti-rat integrin α_v chain monoclonal antibody, clone 21, BD Pharmingen). Isotype control antibodies had no effect on cell adhesion (data no shown). Initial fluorescence intensity was measured to quantify the number of adherent cells prior to application of centrifugal force. After filling the wells with PBS/dextrose and sealing with transparent adhesive tape, substrates were inverted and spun at a fixed speed in a centrifuge (Beckman Allegra 6, GH 3.8 rotor) to apply a centrifugal force corresponding to 12*g*. After centrifugation, media was exchanged and fluorescence intensity was read to measure remaining adherent cells. For each well, adherent cell fraction was calculated as the ratio of post-spin to pre-spin fluorescence readings.

Osteoblast-specific gene expression

Gene expression was analyzed by qRT-PCR.(Byers et al., 2002d) Total RNA was isolated at 7 days after initial cell seeding using the Qiagen RNeasy RNA isolation kit. During RNA isolation and purification, samples were treated with DNaseI (27 Kunitz units/sample) for 15 min at room temperature to eliminate any genomic DNA

contamination. The concentration of purified RNA was quantified using a NanoDrop (NanoDrop Technologies) and 1 μg of total RNA was used to synthesize cDNA templates by oligo(dT) priming using the Superscript First-Strand cDNA Synthesis System.

qRT-PCR was performed with the ABI Prism 7700 Sequence Detection System (Applied Biosystems; 40 cycles; melting for 15 s at 95ºC; annealing and extending for 60 s at 60ºC) using SYBR Green DNA intercalating dye. Gene transcript concentration in the sample cDNA template solutions was quantified by preparing a functional range of dilutions from an absolute standard for each gene. Linear standard curves were then generated by plotting the log of the known concentration versus the C_T value (the cycle number at which the fluorescence reached a threshold level). Oligonucleotide primers (**Table 5.1**) were designed using Primer Express software (Applied Biosystems).

Table 5.1. Real-Time PCR Oligonucleotides for Rat Genes

Gene/Gen Bank Accession Number	*Forward Primer*	*Reverse Primer*
Runx 2 / NM009820	5'-GGCCTTCAAGGTTGTAGCCC-3'	5'-CCCGGCCATGACGGTA-3'
OCN / X04141	5'-ACGAGCTAGCGGACCACATT-3'	5'-CCCTAAACGGTGGTGCCATA-3'
BSP / J04215	5'-TGACGCTGGAAAGTTGGAGTT-3'	5'-GCCTTGCCCTCTGCATGTC-3'

Alkaline phosphatase biochemical activity and calcium incorporation assays

ALP activity was quantified at 7 days after cell seeding using a modification of the Sodek and Berkman method (Stephansson, Byers, and Garcia, 2002;Sodek and Berkman, 1987). Briefly, cells were rinsed with PBS and scraped in cold 50 mM Tris-HCl. After sonication and centrifugation, the total protein concentration was quantified using a Pierce Micro BCA protein assay kit. Equal amounts of protein (2.5 μg) were

added to 60 μg/ml 4-methyl-umbelliferyl-phosphate fluorescent substrate in diethanolamine buffer (pH 9.5). After a 60 min incubation at 37ºC, the fluorescence was read at an excitation of 360 nm and an emission of 465 nm on an HTS 7000 Plus BioAssay Reader (Perkin Elmer). Enzymatic activity was standardized using purified calf intestinal alkaline phosphatase at known dilutions and normalized to the amount of total protein.

Calcium content was determined by dissolving mineralized deposits with 1 N acetic acid overnight. Appropriately diluted sample (25 μl) was added to 300 μl of arsenazo III-containing Calcium Reagent (Diagnostic Services Ltd). The absorbance of the resulting samples was measured at 650 nm and compared to a linear standard curve of $CaCl_2$ in 1 N acetic acid.

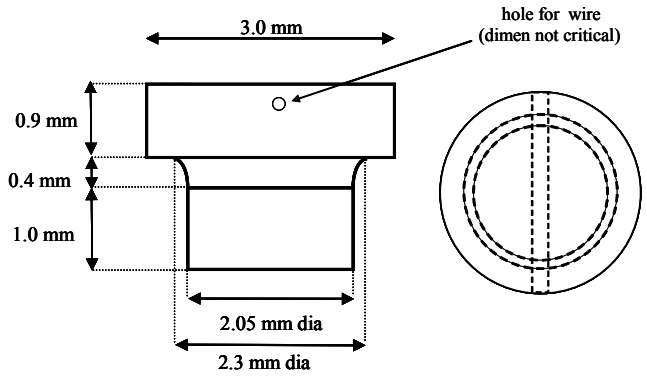

Figure 5.1. Diagram of cylindrical titanium implant rod with tapered stop collar and transverse hole for pull-out mechanical testing. The metal is ASTM F67 Grade 4 commercially pure titanium.

Tibial implantation procedure

Commercially pure titanium implants (**Fig. 5.1**) were sonicated in de-ionized water for 20 min to remove surface debris. Implants were then dipped in 4% HF for 30 sec to remove the existing oxide layer and then incubated in 35% HNO_3 for 30 min at 50 ºC to regenerate a new oxide coating. Samples were transferred to 1.8 N NaOH for 1 min to terminate the oxidation reaction. Implants were then rinsed and boiled in de-ionized water for 1 h. To create the bioactive coating, the implants were incubated in 20 μg/ml GFOGER peptide solution for 1 h. Control titanium rods were incubated in PBS.

Implantations were conducted in accordance with an IACUC-approved protocol (Branemark, Ohrnell, Nilsson, and Thomsen, 1997). Both hind legs of anesthetized, mature Sprague-Dawley male rats (250-350 g) were shaved and scrubbed with alcohol. The medial aspect of the proximal tibial metaphysis was exposed through an antero-medial skin incision, leaving the medial collateral ligament intact. Using a saline-cooled drill at ~2 rotations per minute (to avoid thermal trauma), two defects were created in each tibia. Sterile implant rods were press fit into the defects. Periosteum was mobilized and sutured over the implantation site, and the skin was closed with wound clips. Subjects were euthanized after 4 weeks and proximal tibiae were fixed in neutral buffered formalin for histology or recovered without fixation and maintained in PBS-moistened gauze for immediate mechanical testing.

Based on power calculations and previous reports in the literature (Branemark, Ohrnell, Nilsson, and Thomsen, 1997), we estimated that a minimum of eight implants per experimental group are required to detect differences of 10% in mechanical testing and a minimum of four implants per experimental group are required for

histomorphometry for a total of 11 implants per experimental group. In this model, each animal receives four implants, two per experimental condition. Each tibia contained one implant from each of the two conditions, in alternating positions. We used a total of eight animals with 16 implants per condition – seven for histology and nine for mechanical testing. One additional animal with two implants per condition was included as an extra in the event of tibia breakage during harvest or during the apparatus set-up for mechanical testing.

Histology and histomorphometry analyses and mechanical testing

Excised tibiae were fixed in 10% neutral buffered formalin for 1 week. Samples were then embedded, ground, and stained by Wasatch Histo Consultants, Inc. Briefly, the formalin-fixed tibiae were dehydrated in a graded series of alcohol incubations and then embedded in poly(methyl methacrylate). Ground sections of 50-80 μm were generated using the Exakt Grinding System. Two longitudinal ground sections were generated per tibia, each containing two titanium plugs inserted transverse to the tibia's long axis. Sections were then stained with Sanderson's Rapid Bone Stain™ and a van Gieson counter stain. Bone implant contact (BIC) was measured as the percentage of implant's circumference that was in direct contact with bone tissue (Adobe Photoshop CS imaging software).

Implant mechanical fixation to the bone was measured with a pull-out force test using a biomechanical testing apparatus (EnduraTEC Bose ELF 3200). Immediately after explantation, tibiae were cleaned of all soft tissue and prepared for mechanical testing. The ends of each excised tibia were secured in a custom designed holding apparatus with the exposed head of each implant facing in the direction of the pull motion

and centered along the axis of motion. A 0.014" diameter piano wire was threaded through the implant head and both wire ends attached firmly to an 11 lb. INTERFACE load cell. Samples were pre-loaded with 2 N to ensure proper and identical wire tautness among implants. Tests were performed at a constant force rate of 0.2 N/sec using WINTEST application software. The direction of the pull was parallel to the long axis of the implant. The pull-out force (N) was the maximum load achieved before failure and was determined from the recorded load vs. displacement data.

Statistics

Data are reported as mean ± standard error. Results were analyzed by one-way ANOVA using SYSTAT 8.0 (SPSS). If treatment level differences were determined to be significant, pair-wise comparisons were performed using a Tukey post-hoc test. A 95% confidence level was considered significant. All of the *in vitro* assays were performed as two separate experiments in triplicate. The quantitative histomorphometry consisted of a total sample size of seven implants per condition. The mechanical testing consisted of a total sample size of nine implants per condition.

Results

To reproduce titanium implant surfaces *in vitro*, polystyrene culture dishes were coated with a 300 Å titanium layer via electron beam evaporation. The GFOGER peptide was then passively adsorbed onto the titanium at a concentration of 20 μg/ml, creating the integrin-targeted bioactive coating.

Surface plasmon resonance spectroscopy revealed a final surface density of 123.2 ± 6.2 ng/cm^2. Primary rat bone marrow stromal cells were used to validate this surface treatment strategy *in vitro* due to their inherent osteogenic potential. A centrifugation cell

adhesion assay demonstrated greater stromal cell adhesion on the GFOGER-peptide surfaces compared to titanium surfaces pre-exposed to linear RGD peptide or serum (**Fig. 5.2**). In fact, cell adhesion to the RGD-treated surface was equivalent to background levels observed on titanium blocked with non-adhesive proteins, reflecting the inability of this short peptide to passively adsorb onto titanium. Importantly, a blocking anti-α_2 antibody completely eliminated cell adhesion to GFOGER-treated surfaces, verifying the peptide's specificity for the $\alpha_2\beta_1$ integrin. However, this $\alpha_2\beta_1$ antibody had no effect on adhesion to serum-exposed titanium, demonstrating that stromal cell adhesion to untreated titanium is not mediated by $\alpha_2\beta_1$ integrin. Since untreated titanium adsorbs abundant RGD-containing serum proteins, such as vitronectin, adhesion to these surfaces most likely involves the $\alpha_v\beta_3$ integrin, which recognizes RGD in a wide variety of proteins and synthetic peptides. Indeed, a function-perturbing anti-α_v antibody had no effect on adhesion to the GFOGER peptide but completely blocked adhesion above background on the serum-exposed titanium. These results clearly demonstrate that the bioactive GFOGER peptide specifically targets the $\alpha_2\beta_1$ integrin. These adhesion results also show that untreated titanium surfaces, which directly adsorb serum proteins, preferentially engage the $\alpha_v\beta_3$ integrin. Because GFOGER peptide-coated and control titanium surfaces each interact with unique integrins, these surfaces may recruit different cell populations at the implant site and/or have diverse effects on cellular maturation and bone formation *in vivo*.

To investigate the osteoblastic differentiation potential of these surfaces, we used quantitative RT-PCR (qRT-PCR) to probe osteoblast-specific gene expression in 7 day cultures of bone marrow stromal cells (**Fig. 5.3**). Expression levels of Runx2/Cbfa1, a

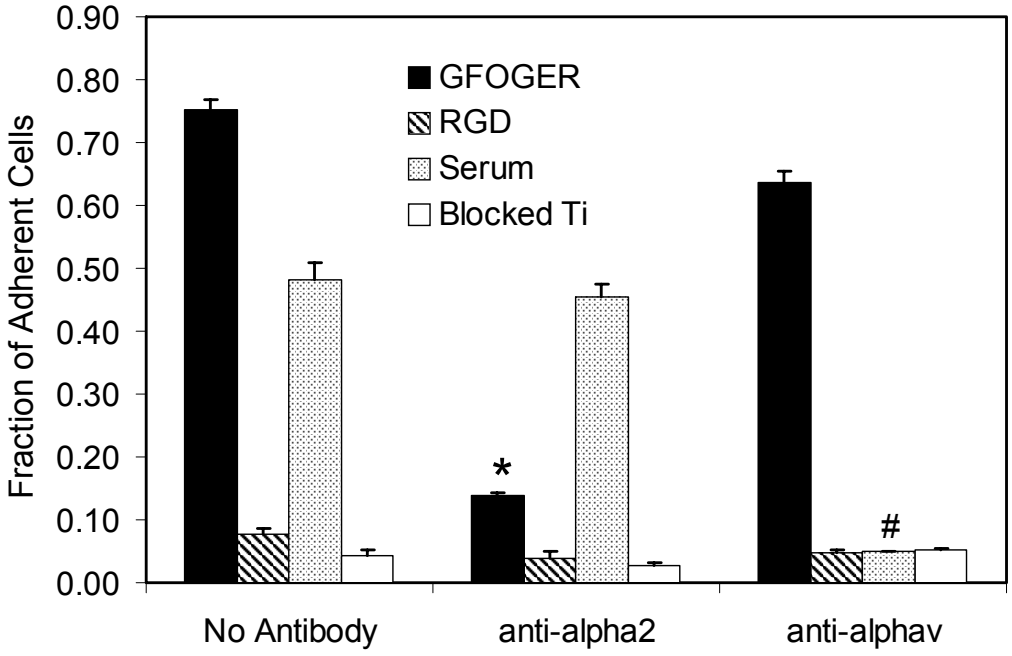

Figure 5.2. Cell adhesion is greater on adsorbed GFOGER surfaces than untreated titanium (Ti) and is specific for the $\alpha_2\beta_1$ integrin. Data represent 1 h serum-free bone marrow stromal cell adhesion and subsequent centrifugation at 12*g* for 5 min. Surfaces are adsorbed GFOGER peptide on Ti, adsorbed linear RGD peptide, adsorbed fetal bovine serum (10% in PBS), and non-adhesive blocked Ti. Cells were seeded without antibody or in the presence of either anti-α_2 or anti-α_v integrin blocking antibodies. ANOVA: $p<1E-9$; *GFOGER w/o Ab > GFOGER with anti-α_2 ($p<6E-6$); #serum w/o Ab > serum with anti-α_v ($p<6E-6$).

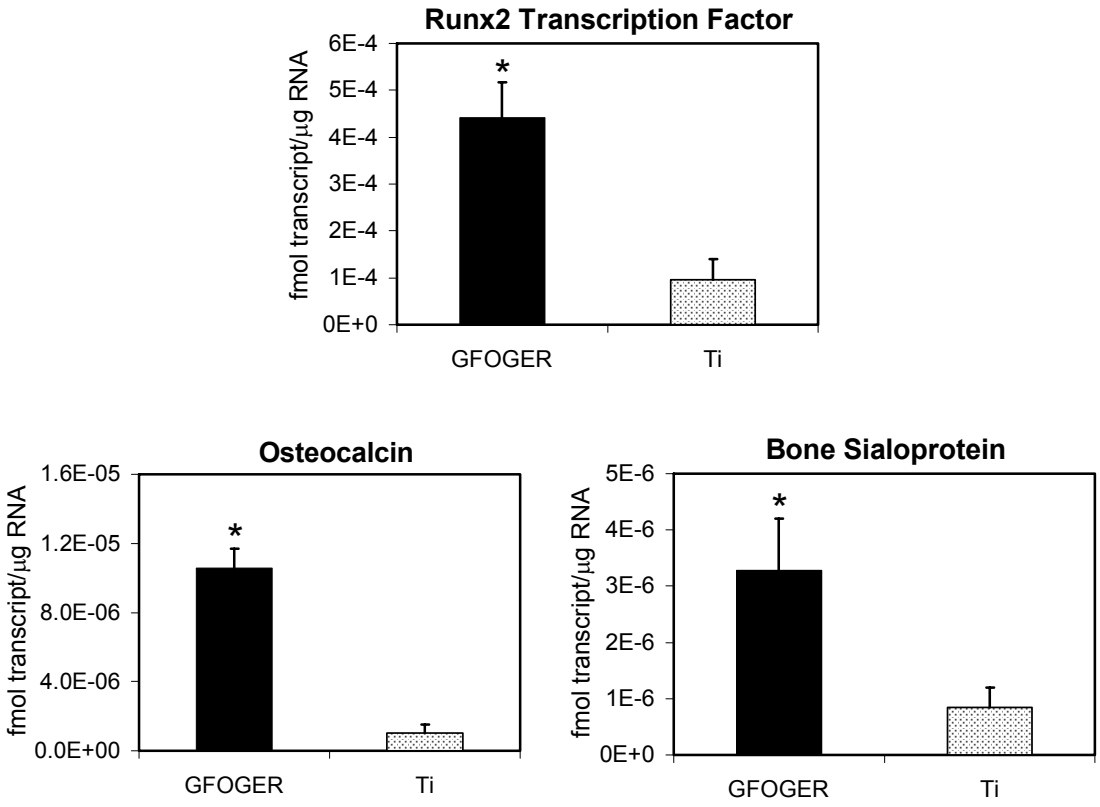

Figure 5.3. GFOGER surfaces enhance the expression of multiple osteoblast-specific genes. Data represent osteoblast-specific gene expression measured by qRT-PCR for Runx2 transcription factor, osteocalcin (OCN), and bone sialoprotein (BSP) in rat bone marrow stromal cells seeded for 7 days on GFOGER surfaces or untreated Ti. Runx2 ANOVA: *GFOGER > Ti ($p<0.02$); OCN ANOVA: *GFOGER > Ti ($p<0.002$); BSP ANOVA: *GFOGER > Ti ($p<0.05$).

transcription factor essential for bone formation and osteoblastic differentiation (Xiao, Jiang, Thomas, Benson, Guan, Karsenty, and Franceschi, 2000b;Xiao, Wang, Benson, Karsenty, and Franceschi, 1998;Takeuchi, Suzawa, Kikuchi, Nishida, Fujita, and Matsumoto, 1997a), were elevated on the GFOGER-treated surfaces compared to untreated titanium (**Fig. 5.3**). The upregulation of this key osteoblast-specific transcription factor demonstrates the ability of the bioactive GFOGER-peptide surface to trigger the transcriptional machinery necessary for osteoblastic differentiation. To determine whether this pattern of increased Runx2 gene expression parallels similar increases in the expression of other osteoblast-specific genes, the transcript levels of osteocalcin and bone sialoprotein were also examined. For both bone-specific markers, qRT-PCR revealed greater levels of gene expression on the GFOGER-peptide surfaces compared with untreated titanium (**Fig. 5.3**). These results indicate that the $\alpha_2\beta_1$ integrin-targeted peptide promotes the expression of multiple genes specifically associated with a mature osteoblastic phenotype.

Osteoblastic differentiation is also characterized by the activation of multiple proteins, including alkaline phosphatase (ALP). The ALP enzyme is often used as a marker for osteoblastic metabolic activity and an early indicator of osteoblastic differentiation.(Aubin and Liu, 1996) An ALP biochemical assay revealed elevated levels of activation on the GFOGER-peptide coating compared to untreated titanium (**Fig. 5.4.a**). Because ALP is the enzyme responsible for hydrolyzing phosphate esters and inducing bone mineralization (Aubin and Liu, 1996), these results suggest that this bioactive surface treatment may also be capable of promoting enhanced bone matrix mineralization.

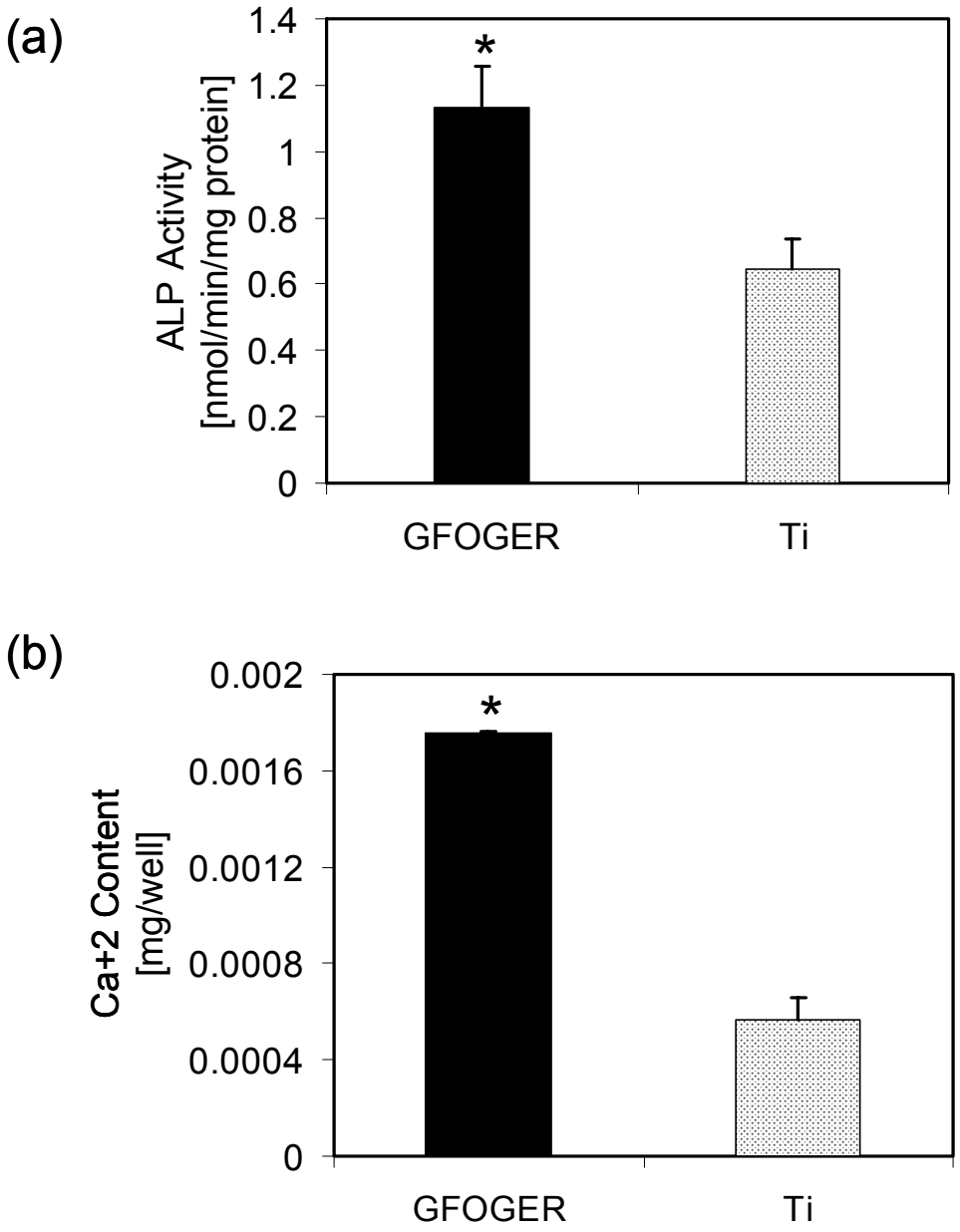

Figure 5.4. GFOGER surfaces enhance **(a)** alkaline phosphatase (ALP) activity and **(b)** matrix calcification in rat bone marrow stromal cultures compared to untreated titanium (Ti). ALP ANOVA: *GFOGER > Ti ($p<0.02$); Ca^{+2} ANOVA: *GFOGER > Ti ($p<2E-4$).

Matrix mineralization was examined as an *in vitro* end-point indicator of the osteoblastic phenotype in the bone marrow stromal cells. Calcium phosphate mineral deposition was examined after 14 days in culture using calcium content analysis. Cultures on GFOGER-treated surfaces displayed a three-fold enhancement in calcium-based mineral deposition compared to untreated titanium (**Fig. 5.4.b**). This enhanced capacity for mineralization on the peptide-treated surfaces is in excellent agreement with the observed up-regulation in osteoblast-specific gene expression and ALP activity. These results verify the advantageous effects of controlled $\alpha_2\beta_1$ integrin-binding on cell function, in this case osteoblastic differentiation and matrix mineralization.

To evaluate the performance of the bioactive GFOGER peptide treatment *in vivo*, we quantified osseointegration in a rat tibia cortical bone model using quantitative histomorphometry and pull-out mechanical testing.(Branemark, Ohrnell, Nilsson, and Thomsen, 1997) We designed a cylindrical titanium implant rod with a tapered stop collar (**Fig. 5.1**). The tapered head ensures that all implants are inserted into the bone at the same depth, guaranteeing uniform bone contact among treatments. Using a saline-cooled drill, two defects 2 mm in diameter were created in the medial aspect of the proximal tibial metaphysis. Implant rods consisting of GFOGER peptide functionalized or untreated (control) titanium were press fit into the cortical defects. After four weeks, the rat tibiae were harvested and evaluated for bone apposition by histological staining and mechanical integration by pull-out testing. Histological sections revealed substantial and contiguous bone mineral along the periphery of GFOGER-treated titanium implants (**Fig. 5.5.a**). Less mineral staining was visible on untreated titanium and the mineral deposits appear in isolated patches along the surface of the implants. Image

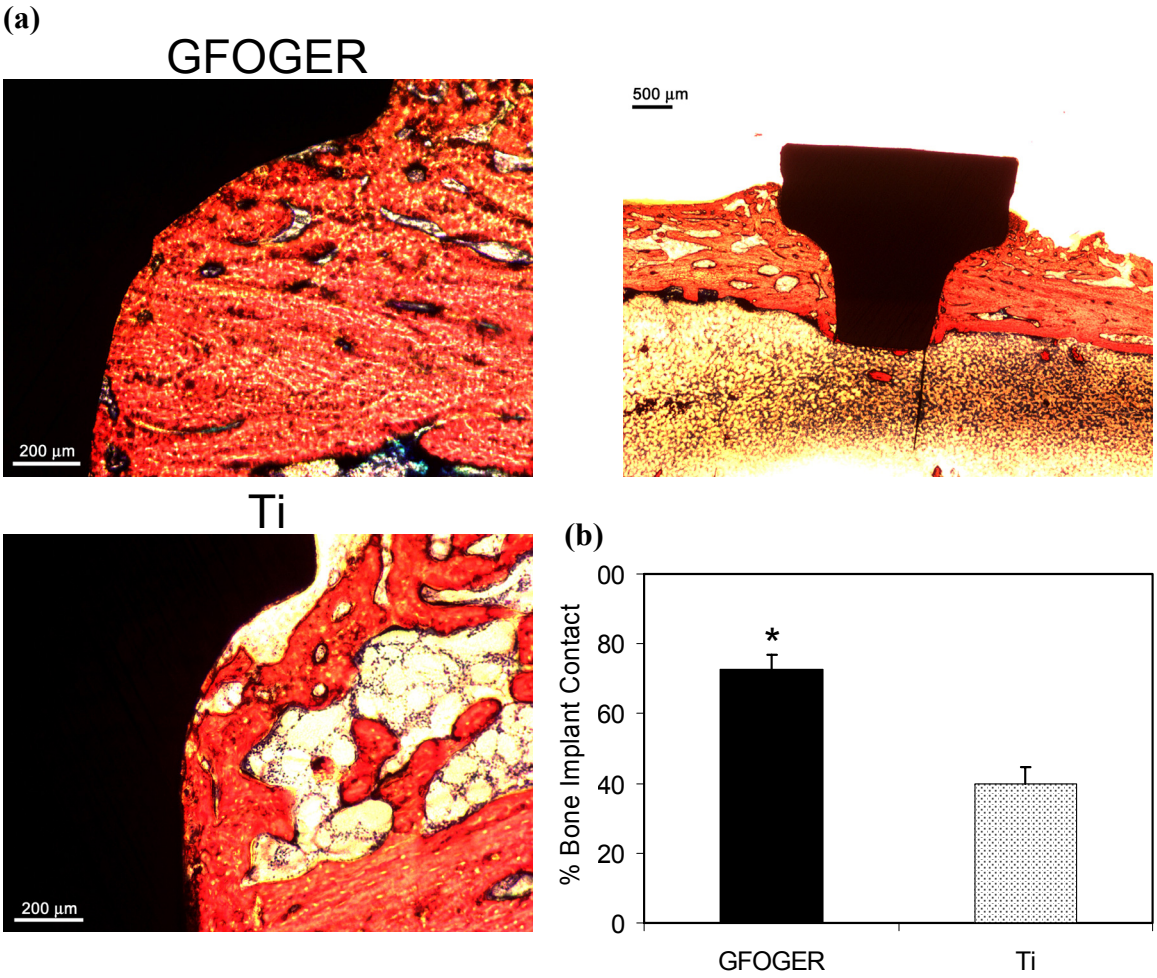

Figure 5.5. GFOGER surfaces improve peri-implant bone formation and mechanical osseointegration in an *in vivo* rat tibia cortical bone implantation model. **(a)** Representative micrographs show 50-80 µm longitudinal ground sections of rat tibia stained with Sanderson's Rapid Bone Stain™ and van Gieson counterstain. Cells stain dark to light blue, soft tissue elements stain blue-green, and bone matrix stains yellow orange to autumn orange. The top right micrograph is a GFOGER peptide-coated implant and shows an example of implant placement. **(b)** GFOGER surfaces exhibit greater amounts of newly formed bone at the implant surface compared with untreated Ti. Bone apposition is measured as the percentage of implant's circumference that is in direct contact with bone mineral in the histological sections. ANOVA: *GFOGER > Ti ($p<7E-4$).

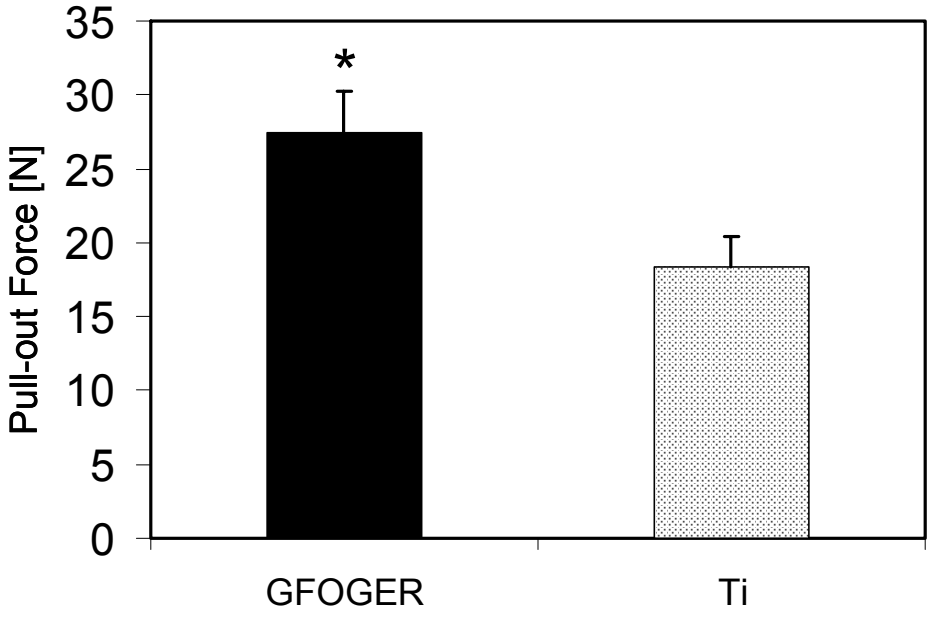

Figure 5.6. GFOGER surfaces demonstrate greater mechanical integration with the surrounding tissue compared with untreated Ti. Osseointegration is measured as the maximum force [N] necessary to dislodge the implant in a pull-out test. ANOVA: *GFOGER > Ti ($p<0.02$).

quantification to determine the percentage of the bone-implant apposition (bone implant contact, BIC) demonstrated a nearly two-fold enhancement in bone apposition on the GFOGER peptide-coated surfaces compared to untreated titanium (**Fig. 5.5b**). Pull-out mechanical testing indicated significantly higher mechanical fixation of the peptide-functionalized implants compared to untreated titanium (**Fig. 5.6**). These results demonstrate a greater quantity and continuity of peri-implant bone mineral on the integrin-targeted GFOGER peptide surfaces *in vivo* as well as enhanced mechanical integrity and osseointegration.

Discussion

This work proposes a specific biomolecular strategy to improve bone regeneration and osseointegration by exploiting the activity of type I collagen, the most abundant matrix component in bone. In particular, type I collagen modulates intracellular signal transduction by binding to the $\alpha_2\beta_1$ integrin, which enhances the expression of the osteoblastic phenotype (Suzawa, Tamura, Fukumoto, Miyazono, Fujita, Kato, and Takeuchi, 2002;Mizuno and Kuboki, 2001;Mizuno, Fujisawa, and Kuboki, 2000;Jikko, Harris, Chen, Mendrick, and Damsky, 1999;Xiao, Wang, Benson, Karsenty, and Franceschi, 1998;Takeuchi, Suzawa, Kikuchi, Nishida, Fujita, and Matsumoto, 1997a). It also exhibits low immunogenicity and high conformational stability, making it extremely suitable for implantation. However, designing surface treatments using whole matrix molecules, such as type I collagen, is often limited by a lack of specificity for particular integrins and thus exhibit minimal control over cellular responses. In addition, native matrix proteins often have binding sites for other ligands, such as fibronectin or von

Willebrand factor. Such ligands may trigger separate signaling cascades that may ultimately confound phenotypic responses and interfere with desired cell function.

The GFOGER peptide strategy described in this study targets the $\alpha_2\beta_1$ integrin-ligand interaction that is crucial for the development and maintenance of the osteoblast phenotype as well as the mineralization of the extracellular matrix. *In vitro* assays using bone marrow stromal cells verified that a GFOGER peptide coating enhances expression of multiple osteoblast-specific genes and alkaline phosphatase activity when compared to untreated titanium controls. This bioactive treatment also improved calcification of the extracellular matrix, demonstrating functional osteoblastic differentiation. Notably, the cortical bone implantation studies revealed greater bone tissue formation on the surface of GFOGER-treated titanium implants, in terms of both quantity and connectivity. Most significantly, we have shown that the GFOGER peptide coating improved the implant's mechanical fixation and functional osseointegration as determined by a quantitative pull-out test. Faster integration of these GFOGER coated implants would result in sooner and more reliable loading in a clinical setting, improving device function and patient outcomes.

Not only does this bioactive coating enhance bone formation and implant integration, but it is also created using a single-step procedure conducted under physiological conditions, thus eliminating the cytotoxicity and biocompatibility concerns associated with covalent immobilization methods. As such, this GFOGER peptide surface treatment represents a simple, clinically relevant approach to improving orthopaedic and dental titanium implant integration. Due to the fundamental character of receptor-ligand principles and the significance of cell-collagen interactions in multiple

tissues, this material coating strategy may also have the potential to improve implant integration in non-orthopaedic tissue systems.

CHAPTER 6

MIXED BIOMEMTIC INTEGRIN-SPECIFIC SURFACES SYNERGISTICALLY MODULATE SIGNAL TRANSDUCTION

Summary

Cell adhesion to the extracellular matrix (ECM) through cell-surface integrin receptors is essential to development, wound healing, and tissue remodeling, and therefore represents a central theme in the design of bioactive surfaces that successfully interface with the body. Extensive studies have focused on functionalizing surfaces with single integrin ligands, such as RGD, FN, or COL, in order to control both cell adhesion and differentiation. However, the native cellular environment is characterized by a variety of matrix proteins that target multiple integrins implicated in a downstream cellular response.

The objective of this study is to engineer bioactive hybrid surfaces that control cell function by mimicking integrin-ECM interactions. We target two specific integrins essential to differentiation in several cell systems – the type I collagen (COL-I) receptor $\alpha_2\beta_1$ and the fibronectin (FN) receptor $\alpha_5\beta_1$ – by tethering varying densities of a recombinant FN fragment and a collagen-mimetic peptide onto non-adhesive supports.

The wide range of controlled mixed ligand densities generated by this process demonstrates the feasibility of generating integrin-specific hybrid surfaces. Results indicate increased cell adhesion and synergistic activation of FAK, which underscore the

advantage of specifically targeting more than one integrin implicated in a particular signaling pathway and downstream cellular effect. Proliferation rate results confirm that the enhanced signaling effects of mixed ligand surfaces translate to downstream cellular responses. This study suggests that, instead of focusing on a single integrin-ligand interaction, in some cases it may be advantageous to consider the interplay of multiple integrins implicated in a desired cell response and their combined effect on downstream cellular signals.

Introduction

Extracellular matrices (ECMs) play critical roles in tissue morphogenesis, homeostasis, and repair by providing structural and signaling scaffolds that organize, coordinate, and regulate cellular activities (De Arcangelis and Georges-Labouesse, 2000a;Reichardt, 1999). Therefore, extracellular matrix proteins are attractive biomimetic targets for functionalizing synthetic materials in order to control cell functions and tissue structure and regeneration (Hubbell, 2004b). Extensive studies have focused on functionalizing surfaces with single integrin ligands, such as RGD, FN, or COL, in order to control both cell adhesion and differentiation.

In particular, biomimetic strategies presenting short bioadhesive oligopeptides, including the arginine-glycine-aspartic (RGD) motif present in numerous ECM components, to target integrin adhesion receptors have demonstrated *in vitro* control of cell adhesion and differentiation, and more importantly, enhancements in tissue healing responses in vivo, including bone formation and integration (Elmengaard et al., 2005c;Alsberg et al., 2002a;Eid et al., 2001;Ferris et al., 1999a), nerve regeneration (Yu and Bellamkonda, 2003;Schense et al., 2000), and corneal tissue repair (Li et al., 2003).

However, these bio-inspired strategies are limited by low activity of the oligopeptides compared to the native ligand due to the absence of complementary or modulatory domains (Garcia et al., 2002). For example, binding of integrin $\alpha_5\beta_1$ requires both the PHSRN sequence in the 9th type III repeat and RGD motif in the 10th type III repeat of fibronectin (FN) (Aota et al., 1994b), which synergistically bind to $\alpha_5\beta_1$ to provide stable adhesion (García et al., 2002;Redick et al., 2000). Moreover, linear RGD peptides exhibit limited specificity among particular integrin receptors (Hersel et al., 2003). This limitation is particularly important as recent evidence suggests that integrin binding specificity regulates cell proliferation and differentiation (Keselowsky et al., 2005b;Cheng et al., 2001;Moursi et al., 1997b). These single-component biomimetic strategies also ignore the complexity of the extracellular matrix and the involvement of more than one integrin signaling pathway in a particular downstream cellular response.

As an alternative strategy, we have focused on engineering high molecular weight ligands that recapitulate the primary, secondary, and tertiary structure of the native matrix protein in order to reconstitute full biological activity as well as integrin binding specificity. The recombinant fragment of FN encompasses both the PHSRN sequence in the 9th type III repeat and RGD motif in the 10th type III repeat of FN in their native structural orientations and is therefore specific for the $\alpha_5\beta_1$ integrin. The GFOGER peptide mimics the triple-helical structure of native type I collagen and targets the $\alpha_2\beta_1$ integrin.

The objective of this study is to engineer bioactive hybrid surfaces that control cell function by mimicking two separate integrin interactions, $\alpha_5\beta_1$ and $\alpha_2\beta_1$, using the FN- and collagen-mimetic ligands to mimic signals from native ECM. Both of these

integrin-ligand interactions have been implicated in several differentiation pathways, including osteoblastic differentiation. Our strategy uses mixed biotinylated ligands on avidin substrates, providing a simple and easily controlled approach to efficiently screen a large number of mixed surface compositions using short term assays. These surfaces were examined for cell adhesion, integrin binding, and integrin-mediated signaling responses.

Materials and Methods

Cells and Reagents

HT1080 human fibrosarcoma cells (CCL-121, American Type Culture Collection, Manassas, VA) were grown in Dulbecco's Modified Eagle medium containing 10% fetal bovine serum and 1% penicillin-streptomycin and subcultured every two days using standard techniques.

NHS-fluorescein, biotin-LC-PEO-amine reagent, and Slide-A-Lyzer Dialysis Cassettes (3,500 MWCO) were purchased from Pierce. Anti-FITC alkaline phosphatase conjugate (A5719) was purchased from Sigma. Anti-FN (HFN7.1) was obtained from the Developmental Studies Hybridoma Bank (Iowa City, IA). Rabbit polyclonal anti-FAK antibody was obtained from Upstate Biotechnology (Lake Placid, NY). Rabbit polyclonal anti-FAK [pY397], anti-FAK [pY576], and anti-FAK [pY861] phospho-specific antibodies were purchased from BioSource International, Inc. (Camarillo, CA). Biotin-conjugated donkey anti-rabbit IgG was obtained from Jackson Immunoresearch (West Grove, PA). Alkaline phosphates-conjugated anti-biotin (clone BN-43) mouse IgG was purchased from Sigma Chemical Co. (St. Louis, MO). The micro BCA protein assay reagent kit was purchased from Pierce (Rockford, IL). ECF susbtrate for spot blotting

was acquired from Amersham Pharmacia Biotech Inc (Piscataway, NJ). Purified calf intestinal alkaline phosphatase enzyme and 4-methyl-umbelliferyl-phosphate substrate were obtained from Sigma Chemical Co. DH5α and JM109 bacterial cells used for cloning and fragment production were obtained from Invitrogen and Promega (Madison, WI), respectively. The XA3 Pinpoint Vector biotinylation expression system was obtained from Promega. The APC BrdU Flow Kit was purchased from BD Biosciences (San Jose, CA). Fetal bovine serum was purchased from Hyclone (Logan, UT). Additional bacterial and mammalian cell culture reagents and spot blotting supplies were obtained from Invitrogen (Carlsbad, CA). All other chemical reagents were purchased from Sigma Chemical Co..

GFOGER Peptide Synthesis, Biotinylation and FITC Labeling

The peptide GGYGGGPC$(GPP)_5$GFOGER$(GPP)_5$GPC [O=hydroxyproline] was synthesized by the Emory University Microchemical Facility at the Winship Cancer Institute (Atlanta, GA), as previously described (Reyes and Garcia, 2003b). Peptide was supplied in the purified form as a trifluoroacetic acid (TFA) salt and reconstituted at a stock concentration of 10 mg/ml in 0.1% TFA. In all experiments, the GFOGER peptide was diluted to 10 μg/ml in Dulbecco's phosphate-buffered saline (DPBS).

For surface immobilization, the GFOGER peptide was biotinylated using a biotin-LC-PEO-amine reagent as previously described (Reyes and Garcia, 2002). The terminal primary amine of this molecule selectively labels the terminal carboxyl group of the GFOGER peptide.

For antibody detection, a subset of the biotinylated GFOGER peptide stock was labeled with fluorescein using an NHS-ester labeling reagent (NHS-fluorescein, Pierce)

targeting the terminal primary amine. For the coupling reaction, 0.5 mg of NHS-fluorescein was dissolved in 500 μl of DMSO to form a stock reagent solution. The stock reagent was slowly added to the GFOGER peptide stock solution (1 part NHS-fluorescein to 10 parts GFOGER peptide solution), while vortexing. The sample was then placed on ice for 2 h. Unreacted NHS-fluorescein was removed by overnight dialysis in PBS. The final concentration of fluorescein-labeled GFOGER peptide was determined by monitoring the 280 nm absorbance on a Shimadzu UV-1601 UV-visible spectrophotometer (Shimadzu, Columbia, MD).

Fibronectin Fragment (FNIII7-10) Expression and Purification

A monobiotinylated fibronectin fragment spanning the 7-10th type III repeats of FN, $FNIII_{7-10}$, was produced using standard recombinant DNA techniques. cDNA encoding for human $FNIII_{7-10}$ was ligated into the XA3 plasmid (Pinpoint System, Promega) and the resulting construct, which encodes for $FNIII_{7-10}$ with a biotin tagging sequence at the amine terminus, was amplified in DH5α cells and purified using Qiagen kits. DNA sequencing confirmed the ligated product.

JM109 bacterial cells were transformed with the $FNIII_{7-10}$-XA3 plasmid and streaked onto LB agar plates containing 100 μg/ml ampicillin and 2 μm d-biotin in 100 mM sodium phosphate buffer (pH 7.2) and incubated overnight. Colonies were isolated and dynamically cultured in 8 ml LB broth with 40 μg/ml ampicillin for 12 h at 37˚C. Next, 1.5 ml of concentrated bacterial small culture was added to 500 ml LB broth containing 100 μg/ml ampicillin and 2 μm d-biotin for 12-16 h. At 6 h, 100 μM isopropyl-β-d-thiogalactopyranoside (IPTG) was added to augment protein production. The cell broth was spun down at 8000*g* for 10 min at 4˚C, and the cell pellet was

resuspended at 10 ml/gram cell paste in cell lysis buffer (50 mM Tris-HCl pH 7.5, 50 mM NaCl, 5% glycerol). Lysozyme (1 mg/ml) was then added to the cell suspension and stirred at 4˚C for 20 min, and sodium deoxycholate (1 mg/ml) was added , stirring continuously for 5 min. Next, DNAase I was added at 40 μg/ml for an additional 10 min. The lysate was centrifuged at 10,000*g* for 20 min, and the protein supernatant recovered, filtered through a 0.45 μm sterile filter, and frozen at -80˚C.

Upon thawing, the solution was purified by affinity chromatography using a 5 ml column of Ultralink Immobilized Monomeric Avidin (Pierce) connected to a gradient pump, UV monitor, and fraction collector (BioRad, Hercules, CA). After sequential washes (10 min) of the column with regeneration, elution, and DPBS buffers, the protein solution was allowed to bind to the column for 1 h at a 0.4 ml/min flow rate. After washing for 15 min with DPBS, elution buffer (0.5 mg/ml d-biotin in DPBS) was flowed through at 1 ml/min and the fractions monitored for protein concentration. Each fraction containing substantial concentrations of protein was filtered using Millipore (Bedford, MA) 30 kDa Microcon centrifugal filter devices to remove d-biotin. Purified fractions was verified >98 % pure $FNIII_{7\text{-}10}$ by SDS-PAGE and Western blotting. Purified samples were flash frozen for storage at -80˚C.

Mixed Ligand Surface Preparation

Tissue culture treated polystyrene surfaces were incubated with avidin (NeutrAvidin, 100 μg/ml, Pierce) for 1 h at at 22ºC. The surface was then blocked with 1% heat denatured bovine serum albumin (BSA) for 1 h to prevent non-specific protein adsorption. After washing with DPBS, varying concentrations of FNII7-10 (0-5 μg/ml in PBS) were introduced to the avidin support layers for 1 h at 22ºC. Surfaces were washed

with DPBS and incubated with varying concentrations of GFOGER peptide (0-5 μg/ml in PBS) for 1 h at 22ºC.

Relative Surface Density Measurements

Mixed ligand surfaces were generated in a 96-well plate as previously described and blocked with 5% FBS in DPBS (blocking buffer) for 1 h. The surfaces were then incubated with an anti-FITC alkaline phosphatase conjugated antibody (1:1000 dilution in blocking buffer) for GFOGER peptide detection or a mouse anti-FN antibody (HFN7.1, 1:4000 dilution) for FNIII7-10 detection for 1 h at 37°C. After washing, the wells that were incubated with the mouse anti-FN antibody were then incubated with an anti-mouse alkaline phosphatase conjugated antibody (1:1000 dilution) for 1 h at 37°C. After rinsing all wells, substrate (4-methyl-umbelliferyl-phosphate, 60 μg/ml) was added for 1 h at 37°C. Reaction product fluorescence was measured in a microwell plate reader (360-nm excitation, 465-nm emission).

Centrifugation Cell Adhesion Assay

Mixed ligand surfaces were generated in a 96-well plate as previously described and blocked with 5% non-fat dry milk in PBS for 1 h to prevent non-specific protein adsorption and cell adhesion. Serum free cell adhesion to these surfaces was measured using a centrifugation assay as previously described (Reyes and Garcia, 2003a). Briefly, near-confluent HT1080 cells were loaded with 2 μg/ml calcein-AM and resuspended serum-free in PBS + 2 mM dextrose. Cells were seeded onto the substrates (10,000 cells/well) and allowed to attach for 1 h at 37°C. For blocking experiments, cells were incubated in suspension for 15 minutes in the presence of 20 μg/ml anti-human VLA-2

($\alpha_2\beta_1$) integrin monoclonal antibody (MAB1998Z) or anti-human CD49e (α_5) antibody and then seeded onto the mixed ligand surfaces for 1 hour at 37°C. The surfaces were then inverted and centrifuged at the specified speed for 5 min on a Beckman Allegra 6 centrifuge (GH 6.8 rotor) to detach the cells. The post-spin fluorescence data was normalized by the pre-spin data and plotted against ligand concentration to obtain adhesion profiles (fraction of adherent cells vs. coating concentration).

Immunofluorescent Staining for Focal Adhesions

Mixed ligand surfaces were prepared in 35 mm dishes as described above and blocked with 5% non-fat dry milk in PBS for 1 h to prevent non-specific protein adsorption and cell adhesion. HT1080 cells were seeded at a density of 225 cells/mm^2 in 10% serum for 6 h. Cells were then permeabilized in ice-cold buffer (50 mM NaCl, 150 mM sucrose, 3 mM $MgCl_2$, 50 mM Tris, pH 6.8) supplemented with 0.5% Triton X-100 and protease inhibitors (20 μg/ml aprotinin, 1 μg/ml leupeptin, 2 mM phenylmethylsulfonyl fluoride) for 5 min to remove membranes and soluble non-cytoskeletal cytoplasmic components. Detergent extracted cells were fixed in cold formaldehyde (3.7% in DPBS) for 5 min, blocked in blocking buffer (5% FBS in DPBS) for 1 h, and incubated with anti-vinculin (1:500 dilution in blocking buffer) 1 h at 37°C. Primary antibody were visualized using an AlexaFluor 488-conjugated secondary antibody (anti-mouse IgG; 1:200 dilution) with a 1 h incubation. Images were captured using a Nikon Eclipse E400 fluorescence microscope with a 100x objective and ImagePro Plus image acquisition software.

Immunoprecipitation and Western Blotting of Integrins

Mixed ligand surfaces were prepared in 60 mm dishes as described above and blocked with 5% non-fat dry milk in PBS for 1 h to prevent non-specific protein adsorption and cell adhesion. HT1080 cells were seeded at a density of 30,000 cells/cm^2 in 10% serum for 1 h. Cells were then lysed in 250 μl mild lysis buffer (1% NP-40, 0.15 N NaCl, 0.01 M sodium phosphate, pH 7.2, 2 mM EDTA, 50 mM sodium fluoride, 0.2 mM sodium orthovanadate, 100 U/ml aprotinin). Protein concentration was determined using a Pierce Micro BCA protein assay kit.

For the immunoprecipitation, volumes equivalent to 200 μg of sample protein were added to NET gel buffer (50mM tris HCl, pH7.5, 100 mM NaCl, 0.1% NP-40, 1 mM EDTA, pH 8.0, 0.25% gelatin, 0.02% NaN_3) for a total volume of 500 μl. To precipitate the α_2 integrin, 5 μl of rabbit anti-human integrin α_2 polyclonal antibody (AB1936, Chemicon) was added to each sample. These mixtures were then incubated overnight at 4ºC to encourage antibody binding.

Twelve hours later, 40 μl of protein A agarose beads (Immunopure, Pierce) was added to each sample and incubated for 3 hours with agitation. The beads were washed two times with NET gel buffer and one time with 0.1% NP-40 in 10 mM Tris. The beads were then boiled in Laemmli sample buffer (2% SDS, 10% glycerol, 100 mM DTT, 60 mM Tris-HCl pH 6.8, and 0.001% bromophenol blue) for 10 min and separated on a 7% SDS-polyacrylamide gel electrophoresis (SDS-PAGE) gel.

Proteins were transferred electrophoretically onto nitrocellulose membranes and blocked with Blotto (5% non-fat dry milk, 0.02% sodium azide, 0.2% Tween 20 in PBS w/o Ca^{2+}/Mg^{2+}) overnight at 4ºC. Membranes were then incubated with primary antibody – rabbit anti-integrin α_5 polyclonal antibody (1:1000 dilution, AB1928,

Chemicon) or rabbit anti-human integrin α_2 polyclonal antibody for verification of the IP (1:1000, AB1936, Chemicon) – in Blotto for 1 h at room temperature under gentle rocking. Membranes were washed in TBS-Tween (20 mM Tris HCl pH 7.6, 137 mM NaCl, 0.1% Tween 20) for 30 min and incubated in secondary antibody (biotin-conjugated anti-rabbit IgG, 1:20,000 dilution in Blotto) for 1 h at room temperature under gentle rocking. Membranes were washed again in TBS-Tween for 30 min and incubated in a tertiary or detection antibody (alkaline phosphatase-conjugated anti-biotin IgG, 1:10,000 dilution in Blotto) for 1 h at room temperature under gentle rocking. After antibody incubation, membranes were washed in TBS-Tween for 30 min and immunoreactivity was detected using ECF fluorescent substrate. Bands were visualized using a Fuji Image Analyzer.

BrdU Analysis of Cell Proliferation

Proliferation was measured using the APC bromodeoxyuridine (BrdU) flow kit from BD Biosciences according to the manufacturer's instruction manual. Mixed ligand surfaces were generated on 60 mm dishes and blocked with 5% non-fat dry milk in PBS for 1 hour to prevent non-specific protein adsorption and cell adhesion. HT1080 cells were seeded at a density of 5,000 cells/cm^2 in 10% serum for 24 h. Cells were then exposed to BrdU for 12 h to identify actively cycling populations. Cells were then fixed and permeabilized via the BrdU flow kit reagents. DNase was added to the samples to expose DNA epitopes. An APC-conjugated anti-BrdU antibody was used to stain for incorporated BrdU. Each sample was analyzed for APC-positive staining via flow cytometry.

Spot Blotting Analysis of Focal Adhesion Kinase Activation

Mixed ligand surfaces were generated in a 96-well plate as previously described and blocked with 5% non-fat dry milk in PBS for 1 hour to prevent non-specific protein adsorption and cell adhesion. HT1080 cells were incubated in serum-free suspension (DMEM + 5% BSA) for 40 minutes with mild shaking to reduce focal adhesion kinase (FAK) background activation. The cells were then seeded onto the surfaces (10,000 cells/well) and allowed to attach for 2 h at 37°C. For blocking experiments, cells were incubated in suspension for last 15 minutes in the presence of 20 μg/ml anti-human VLA-2 ($\alpha_2\beta_1$) integrin monoclonal antibody (MAB1998Z) or anti-human CD49e (α_5) antibody and then seeded onto the surfaces for 2 h at 37°C.

Adherent cells were washed once with DPBS and lysed with 110 μl cold radioimmunoprecipitation assay (RIPA) buffer (1% Triton X-100, 1% sodium deoxycholate, 0.1% SDS, 150 mM NaCl, 150 mM Tris-HCl pH 7.2, 350 μg/ml phenylmethylsulfonyl fluoride (PMSF), 10 μg/ml leupeptin, 10 μg/ml aprotinin, and 1 mM sodium orthovanadate) for 20 min on ice. Lysates were then split in half (to probe for total FAK and activated FAK) and added to the wells of a Minifold I Spot-Blot System (Schleicher & Schuell Bioscience) containing a 0.20 μm pore nitrocellulose membrane, prepared according to the instructions. The lysates were incubated for 30 min and then filtered through the membrane with a vacuum for 5 min. Membranes were blocked with blotto (5% non-fat dry milk, 0.02% sodium azide, 0.2% Tween 20 in PBS w/o Ca^{2+}/Mg^{2+}) overnight at 4ºC.

The membranes were then incubated with primary antibody – anti-FAK (1 μg/ml) or anti-FAK pY397 (0.35 μg/ml) – in blotto for 1 h at room temperature, rocking. Membranes were washed in TBS-Tween (20 mM Tris HCl pH 7.6, 137 mM NaCl, 0.1%

Tween 20) for 30 min and incubated in secondary antibody (biotin-conjugated anti-rabbit IgG, 1:20,000 dilution in blotto) for 1 h at room temperature, rocking. Membranes were washed again in TBS-Tween for 30 min and incubated in a tertiary or detection antibody (alkaline phosphatase-conjugated anti-biotin IgG, 1:10,000 dilution in blotto) for 1 h at room temperature, rocking. After antibody incubation, membranes were washed in TBS-Tween for 30 min and immunoreactivity was detected using an ECF fluorescent substrate. Bands were visualized using a Fuji Image Analyzer and further quantified and analyzed using Adobe Photoshop software. FAK phosphorylation levels were normalized to the amount of total FAK in each experimental run.

Statistics

All experiments were performed at least three times in triplicate unless otherwise noted. Data are reported as mean ± standard error. Results were analyzed by one-way ANOVA using SYSTAT 8.0 (SPSS). If treatment level differences were determined to be significant, pair-wise comparisons were performed using a Tukey post-hoc test. A 95% confidence level was considered significant.

Results and Discussion

Mixed Collagen- and Fibronectin-Mimetic Surfaces

The collagen-mimetic GFOGER peptide used in these experiments has the following primary sequence: GGYGGGPC$(GPP)_5$GFOGER$(GPP)_5$GPC. This synthetic peptide has been engineered to contain the hexapeptide sequence, GFOGER, from type I collagen that is recognized by the $\alpha_2\beta_1$ integrin. The GPP triplets on either side of the GFOGER recognition site provide cooperative clusters that promote the formation of a

stable right-handed triple helical structure at room temperature (Knight, Morton, Peachey, Tuckwell, Farndale, and Barnes, 2000;Nagarajan, Kamitori, and Okuyama, 1998;Fields and Prockop, 1996). This triple-helical conformation is essential for integrin recognition and $\alpha_2\beta_1$-mediated cell adhesion (Messent, Tuckwell, Knauper, Humphries, Murphy, and Gavrilovic, 1998;Morton, Peachey, Knight, Farndale, and Barnes, 1997;Morton, Peachey, Zijenah, Goodall, Humphries, and Barnes, 1994).

The fibronectin-mimetic ligand used in these experiments is FNIII7-10 (**Fig. 6.1**), a recombinant fragment of fibronectin (FN) that spans the 7-10th type III repeats of FN and contains the PHSRN and RGD adhesion motifs that cooperatively form the recognition site for the $\alpha_5\beta_1$ integrin(Garcia, Schwarzbauer, and Boettiger, 2002).

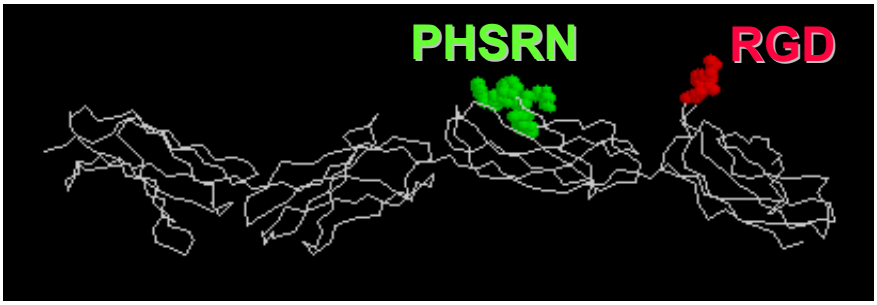

Figure 6.1. The fibronectin-mimetic ligand is FNIII7-10, a recombinant fragment of fibronectin (FN) that spans the 7-10th type III repeats of FN and contains the PHSRN and RGD adhesion motifs that cooperatively form the recognition site for the $\alpha_5\beta_1$ integrin

To create model mixed ligand surfaces, we exploited the high affinity and specificity of the biotin-avidin interaction. NeutrAvidin biotin-binding protein, a commercially available deglycosylated avidin derivative with exceptionally low

nonspecific binding properties, was passively adsorbed onto tissue culture treated polystyrene as a non-fouling support layer. To generate mixed ligand surfaces, the biotinylated ligands were added sequentially to the NeutrAvidin support layer. Based on the significant size differences between the FNIII7-10 fragment and the GFOGER-peptide, biotinylated fragment was introduced to the NeutrAvidin surface first for 1 hr. After rinsing, biotinylated GFOGER-peptide was added for an additional hour. Control experiments demonstrated that only biotinylated ligands were immobilized onto the NeutrAvidin surfaces (data not shown).

Relative Surface Density Measurements

An ELISA assay was used to determine the relative ligand densities present on the mixed surface formulations. For detection purposes, fluorescein was coupled to the terminal amine of the GFOGER peptide using NHS-fluorescein. The immobilized ligands were then be detected by ELISA using anti-FN or anti-fluorescein antibodies. **Fig. 6.2** shows the immobilized ligand densities for 4 FNIII7-10 coating concentrations (0, 0.2, 2.5, 5 μg/ml), each of which were incubated in 2-fold serial dilutions of GFOGER-peptide (from 0 to 5 μg/ml). As expected, the density of immobilized FNIII7-10 (**Fig. 6.2,** triangles, right axis) increases with increasing FNIII7-10 coating concentration and is insensitive to the coating concentration of GFOGER-peptide (horizontal axis). This effect is due to the fact that the FN fragment is allowed to tether before the GFOGER peptide is introduced. The density of tethered GFOGER-peptide (**Fig. 6.2,** circles, left axis) increases with peptide coating concentration and is modulated by the density of immobilized FN.

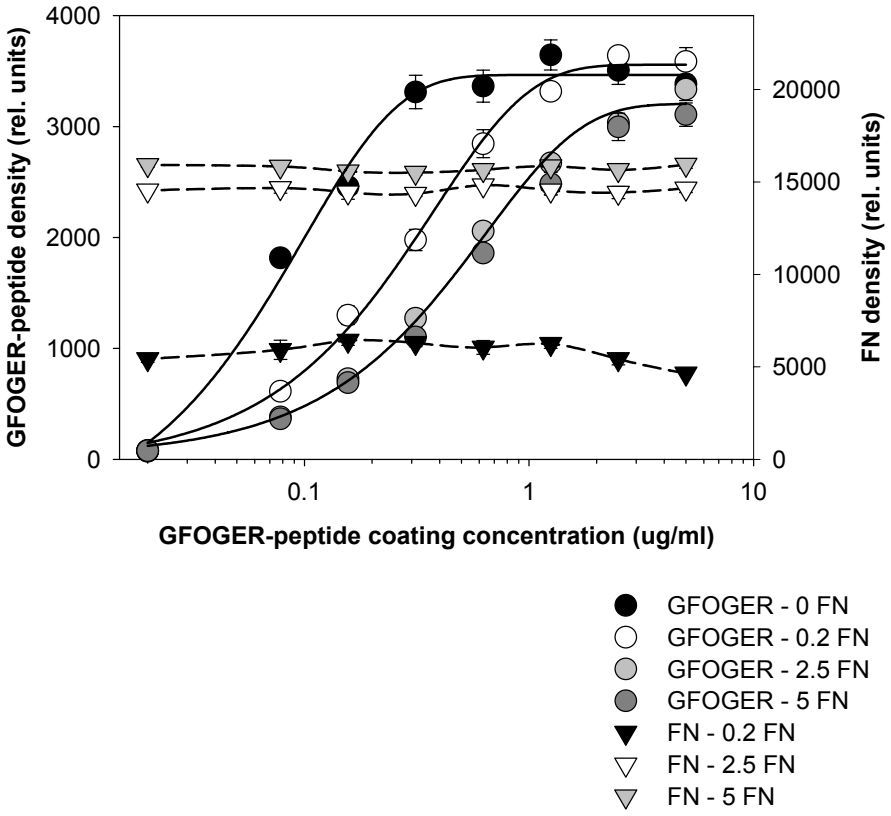

Figure 6.2. Mixed fibronectin- and collagen-mimetic surfaces. Varying concentrations of biotinylated FNIII7-10 and GFOGER-peptide (FITC labeled) were tethered to passively adsorbed NeutrAvidin. Relative surface density was quantified via ELISA using anti-FN antibody (Triangles, right axis) or anti-FITC antibody to detect the GFOGER-peptide (circles, left axis).

The leftmost GFOGER-peptide tethering profile represents a surface that contains no FN fragment. As the amount of FN fragment added to the surface increases, the fragment begins to occupy the surface anchoring sites first, leaving less available sites for GFOGER peptide tethering. This decrease in GFOGER immobilization with increasing amounts FNIII7-10 shifts the tethering profiles to the right, until the FN fragment is saturated on the surface. The wide range of controlled mixed ligand densities generated by this process demonstrates the feasibility of our proposed surface engineering strategy.

Cell Adhesion on the Mixed Ligand Surfaces

Cell adhesion on these mixed ligand surfaces was examined using a centrifugation assay in which HT1080 human fibrosarcoma cells were seeded for 1 h in serum-free conditions and then centrifuged to detach the cells. The resultant cell adhesion profiles (**Fig. 6.3**) correlated well with the relative ligand densities reflected in the ELISA data. The line graph shows that for high FNIII7-10 coating concentrations (**Fig. 6.3.a, circles**), adhesion is dominated by the FN fragment and the adhesion profiles are insensitive to changes in the GFOGER-peptide density, especially at low peptide densities. It is only when the amount of GFOGER peptide on the surface is nearly saturated that subsequent increases in adhesion are observed. As FNIII7-10 coating concentration decreases, adhesion drops at the lower peptide densities and the data begins to approach the more familiar profile of density-dependent increases in cell adhesion with increasing GFOGER peptide density (**Fig. 6.3.a, triangles, squares**). When the FN fragment is completely eliminated from the surface, the adhesion profile again shifts to the right demonstrating the reduced adhesive potential of the single-ligand functionalized surfaces compared with the mixed ligands (**Fig. 6.3.a, diamonds**).

(a)

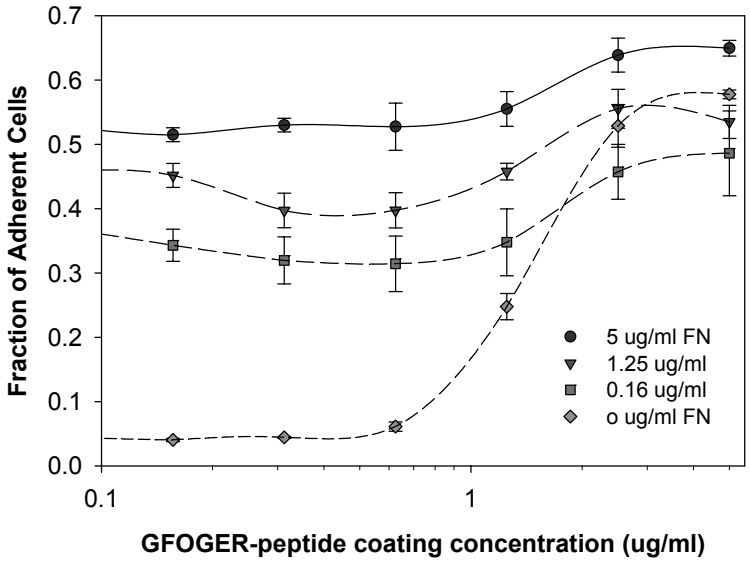

(b)

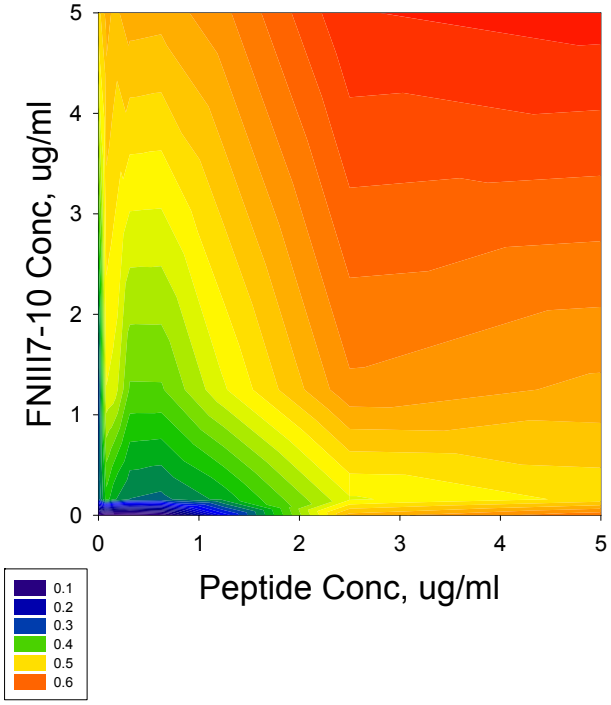

Figure 6.3. (a) HT1080 human fibrosarcoma cell adhesion on mixed ligand surfaces. (1 hour cell adhesion, 12g centrifugation for 5 min.) **(b)** Contour plot of cell adhesion on mixed ligand surfaces.

A contour plot of the cell adhesion data (**Fig. 6.3.b**), demonstrates the adhesive advantage of using saturating levels of both ligands, compared to the single ligand surfaces. Adhesion increases with increasing FNIII7-10 until the FN fragment is saturated on the surface. Adding GFOGER-peptide to this saturated level of FNIII7-10, further increases the surface's adhesive potential. Similarly, adhesion also increases with increasing GFOGER peptide. Adding FNIII7-10 to the surface first results in a decrease in cell adhesion, due to the fact that the FNIII7-10 is occupying anchoring sites that were previously available to the GFOGER peptide, reducing the amount of $\alpha_2\beta_1$ ligand on the surface. However, high densities of both ligands results in the highest observed levels of cell adhesion.

The relative contributions of the $\alpha_2\beta_1$ integrin and the $\alpha_5\beta_1$ integrin are demonstrated by blocking each integrin separately with a function blocking antibody. Blocking the $\alpha_2\beta_1$ integrin (**Fig. 6.4.a**) completely eliminates the effect of increasing GFOGER peptide density observed in **Fig. 6.3**. Adhesion increases with increasing FNIII7-10 density and remains insensitive to any changes in GFOGER peptide density. Conversely, blocking the $\alpha_5\beta_1$ integrin (**Fig. 6.4.b**) completely eliminates the effect of increasing FNIII7-10 density. Cell adhesion increases with increasing GFOGER peptide and the adhesion profiles are identical at two different levels of FNIII7-10 density (**Fig. 6.4.b, circles, triangles**). As expected, the blocking antibodies also eliminate any adhesive advantage conferred by high densities of both ligands compared to the single-ligand surfaces.

(a)

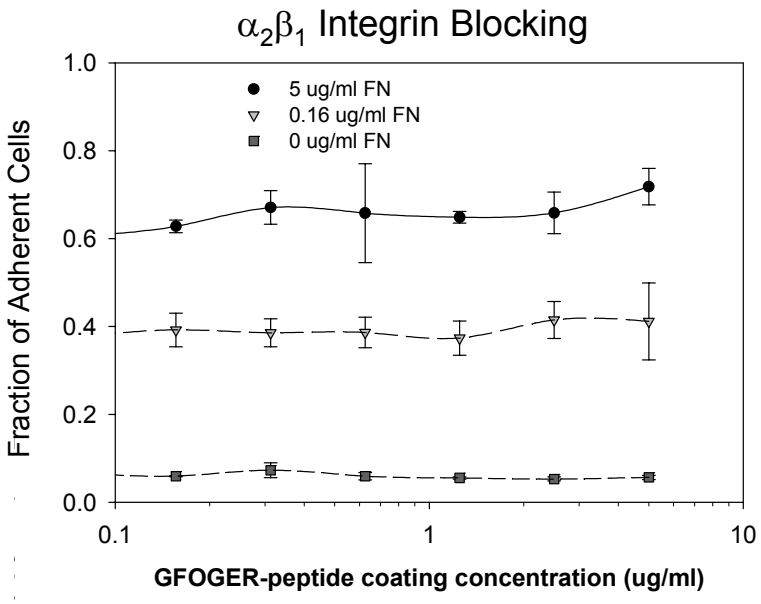

(b)

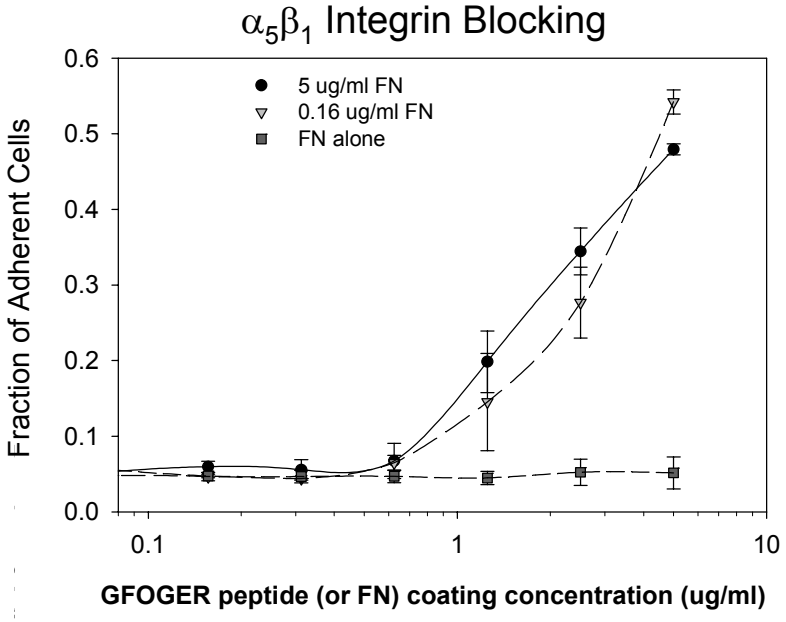

Figure 6.4. Effects of integrin blocking on cell adhesion. **(a)** Cell adhesion on mixed ligand surfaces in the presence of an $\alpha_2\beta_1$ integrin blocking antibody. **(b)** Cell adhesion on mixed ligand surfaces in the presence of an $\alpha_5\beta_1$ integrin blocking antibody. Squares represent cells seeded on increasing densities of FNII7-10 in the absence of GFOGER peptide to verify the action of the $\alpha_5\beta_1$ function-blocking antibody.

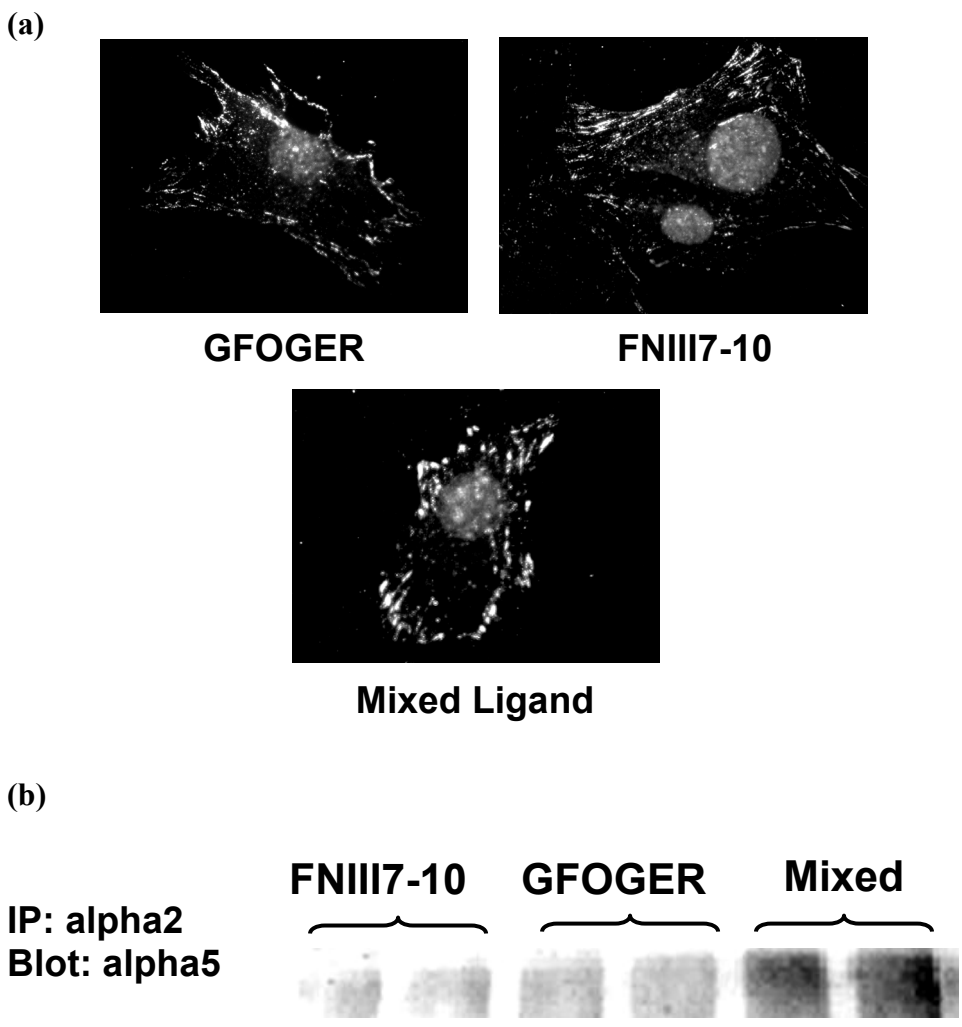

Figure 6.5. **(a)** Immunofluorescent staining for vinculin in focal adhesions on GFOGER, FNIII7-10, and mixed ligand surfaces. **(b)** Immunoprecipitation for alpha 2 and blotting for alpha 5 to identify co-localization of the two integrins in focal adhesions.

Focal Adhesions on the Mixed Ligand Surfaces

HT1080 cells were seeded onto mixed ligand surfaces for 6 hours in 10% serum to promote the formation of focal adhesions, which are characterized by clustered integrin components and intracellular structural and signaling proteins attached to the actin cytoskeleton. The cells were then extracted, fixed, and stained for vinculin, an intracellular structural protein that localizes to focal adhesion plaques. Immunofluorescent staining for vinculin (**Fig. 6.5.a**) reveals that both the single ligand and the mixed ligand surfaces promote the formation of these focal adhesion structures. The two single ligand surfaces are characterized by several relatively small, punctate structures diffusely distributed around the periphery of the cell. In contrast, the mixed ligand surfaces consistently promote the formation of larger, distinct adhesion plaques localized right at the cell edges.

To get a better understanding of these adhesion structures, we have also immunoprecipitated the α_2 integrin under mild lysis conditions and then blotted the IP fraction for the presence of the α_5 integrin. Heightened staining suggests that the two integrins physically co-localize to membrane complexes on the mixed surfaces to a much greater extent than on either of the single component surfaces (**Fig 6.5.b**).

Since focal adhesions represent junctions of integrin-mediated intracellular signaling, these images suggest a possible advantage of the mixed ligand presentation in triggering post-adhesion signaling events.

Synergistic Focal Adhesion Kinase Activation

To analyze the effect of the mixed ligand presentations in triggering post-adhesion signaling events, we examined the extent to which these mixed ligand surfaces

(a)

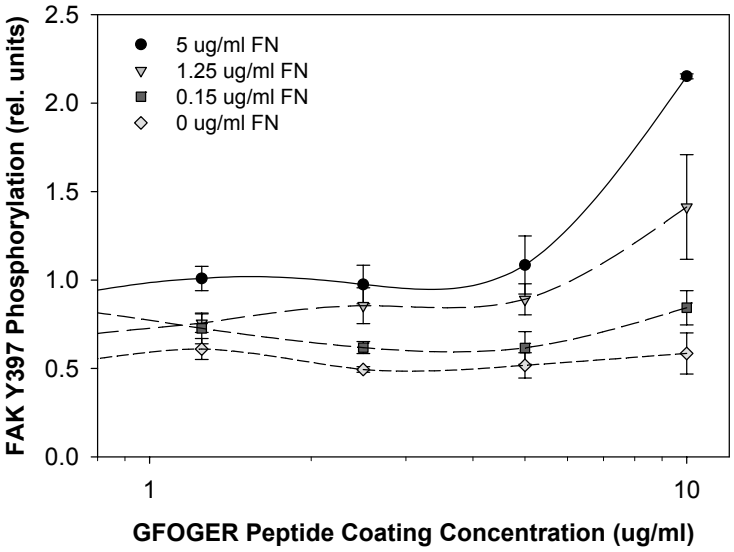

(b)

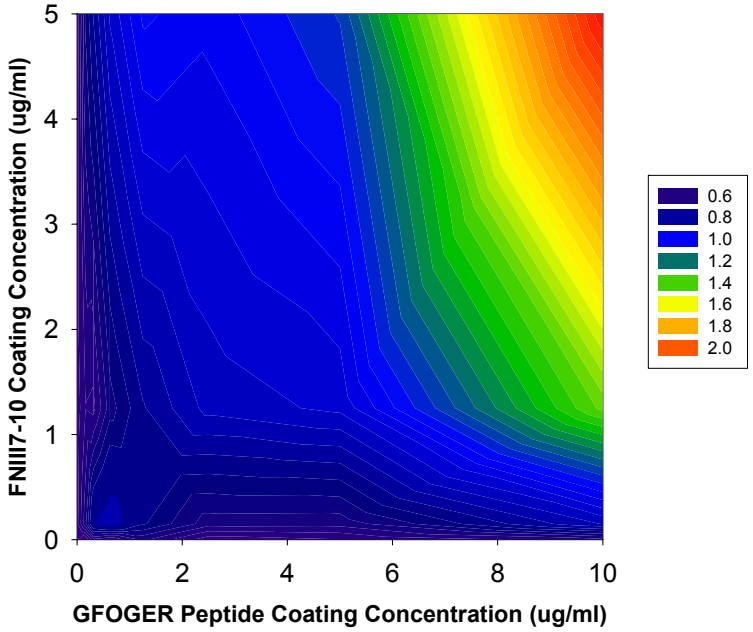

Figure 6.6. Synergistic activation of focal adhesion kinase (FAK) on mixed ligand surfaces. **(a)** Quantification of spot blotting for phosphorylated tyrosine 397 on FAK (2 hour cell adhesion). **(b)** Contour plot of FAK activation on mixed ligand surfaces.

trigger the activation of focal adhesion kinase (FAK), an intracellular signaling molecule implicated in integrin-mediated signal transduction and downstream differntiation pathways. Using standard spot blotting techniques, we probed the phosphorylation of tyrosine 397, which is the autophosphorylation site of FAK and also binds SH2 and PI3-K. The results (**Fig. 6.6**) clearly demonstrate a synergistic activation of FAK on these mixed surfaces. While FAK phosphorylation does increase with both increasing peptide and increasing FN fragment, we observe at least a three-fold increase in FAK activity at high levels of both ligands. At saturating levels of FN fragment alone or GFOGER peptide alone, the FAK activity levels reach ~0.5 (rel. units); at saturating levels of both ligands, FAK activity is around 2.1 (rel. units). This data underscores the advantage of specifically targeting more than one integrin implicated in a particular signaling pathway and downstream cellular effect.

To demonstrate the integrin specificity of this synergistic effect, this assay was repeated using the integrin blocking antibodies (**Fig. 6.7**). The leftmost data set in **Fig. 6.7** shows FAK activation in the absence of any function-blocking antibodies, which recapitulates the same synergistic effect of the mixed ligand presentation demonstrated in **Fig. 6.6**. Antibody blocking of the α_2 integrin reduces FAK activation on the GFOGER surfaces to background levels (**Fig 6.7, middle**). It also eliminates the synergistic enhancement in signaling on the mixed ligand surfaces. Instead the signaling is statistically equivalent to that of the single ligand, FN fragment surface. A similar effect is observed upon blocking the α_5 integrin (**Fig 6.7, right**). Activation levels on the FN fragment surface fall to background levels and the mixed ligand surface is now equivalent to the single component GFOGER surface. This data verifies that the specific

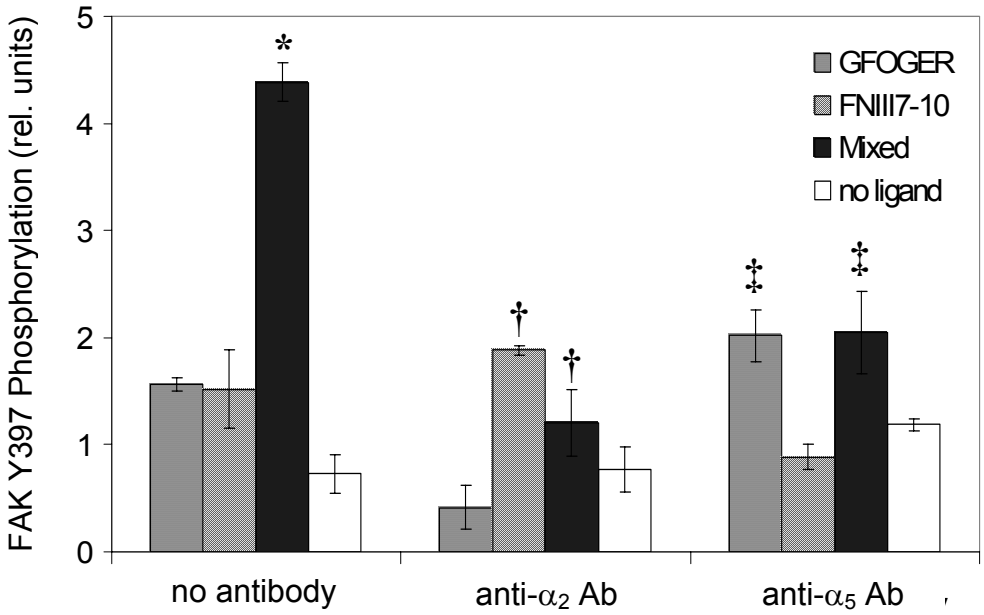

Figure 6.7. Integrin specificity of synergistic FAK activation on mixed ligand surfaces. Data shows tyrosine phosphorylation levels on the biomimetic surfaces in the absence and presence of integrin blocking antibodies. * indicates greater than mixed with anti-α_2 or anti-α_5. † indicates greater than no ligand with anti-α_2. ‡ indicates greater than no ligand with anti-α_5.

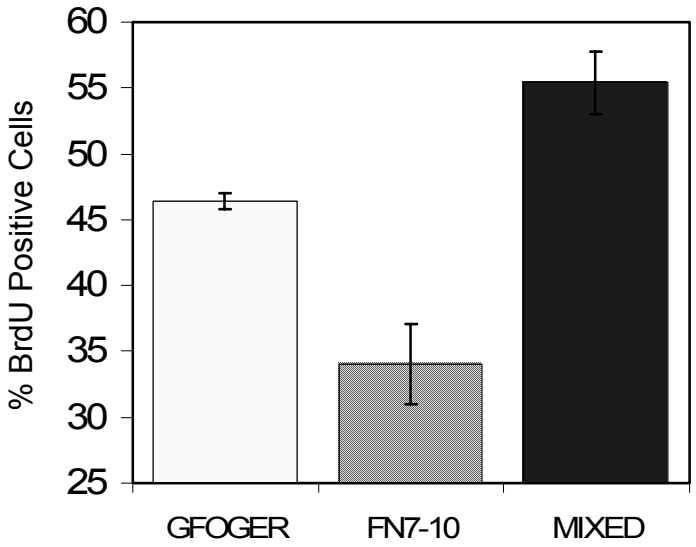

Figure 6.8. Flow cytometry quantification of HT1080 cell proliferation using BrdU incorporation (BrdU added 24 hrs after cell seeding, incorporated for 12 hrs; * indicates different from GFOGER or FN7-10, $p<0.05$).

binding of these two separate integrins on the mixed ligand surface is responsible for the synergistic enhancement of this downstream intracellular signal.

Proliferation on Mixed Ligand Surfaces

To determine whether this synergy in intracellular signaling translates to a downstream cellular response, we examined proliferation on mixed and single ligand functionalized surfaces using BrdU incorporation. **Fig. 6.8** demonstrates enhanced proliferation rate on the mixed surfaces, paralleling both the cell adhesion and the FAK activation data.

Conclusion

The wide range of controlled mixed ligand densities generated by this process demonstrates the feasibility of generating integrin-specific hybrid surfaces. We have shown that these mixed ligand surface formulations result in greater cell adhesion and focal adhesion assembly. The mixed surfaces also trigger a synergistic activation of focal adhesion kinase, when compared with single ligand surfaces. Proliferation results confirm that the enhanced signaling effects of mixed ligand surfaces translate to downstream cellular responses.

In conclusion, we have demonstrated that the presentation of multiple integrin-binding ligands synergize to enhance intracellular signaling and proliferation. This study suggests that, instead of focusing on a single integrin-ligand interaction, in some cases it may be advantageous to consider the interplay of multiple integrins implicated in a desired cell response and their combined effect on downstream cellular signals. This may allow the rational engineering of optimal biospecific surfaces for implant coatings and

tissue engineering scaffolds that exploit that complexity of the extracellular matrix and its signaling characteristics.

CHAPTER 7

COLLAGEN-MIMETIC, FIBRONECTIN-MIMETIC, AND MIXED PEPTIDE SURFACE COATINGS FOR OSSEOINTEGRATION OF ORTHOPAEDIC IMPLANTS

Summary

Extracellular matrix proteins are attractive biomimetic targets for functionalizing orthopaedic implant surfaces in order to promote healing, bone formation, and implant fixation. Extensive studies have focused on functionalizing surfaces with single integrin ligands, such as RGD, FN, or COL, in order to control both cell adhesion and differentiation. However, these strategies are limited by lack of integrin specificity, lack of control over cellular and tissue responses, and lack of complexity inherent in multiple integrin signaling cascades.

We target two specific integrins essential to differentiation in osteoblast cells – the type I collagen (COL-I) receptor $\alpha_2\beta_1$ and the fibronectin (FN) receptor $\alpha_5\beta_1$ – using the GFOGER triple helical peptide and the recombinant FNIII7-10 fibronectin fragment. This study compares the osseointegrative potential of these single-component integrin-specific peptides to a mixed surface treatment presenting both peptides. We also examine the efficacy of the biomimetic integrin-targeted peptides compared to their native matrix proteins as implant coating treatments.

The *in vivo* results indicate that either of the integrin-targeted peptide treatments is sufficient to improve bone formation and implant mechanical integration compared to

unmodified titanium. These biomimetic peptides also show improved osseointegration over the native matrix proteins, fibronectin and type I collagen. However, the combination treatment of both biomimetic peptides did not confer any osseointegrative advantage over the single-component coatings. The *in vitro* bone marrow stromal cell differentiation assays corroborate the *in vivo* results.

Introduction

Implant osseointegration, defined as close bone apposition and functional fixation, is a prerequisite for clinical success in orthopaedic and dental applications, many of which are restricted by implant loosening (Pilliar, 2005;Anderson, 2001). Extracellular matrices (ECMs) play critical roles in tissue morphogenesis and repair by providing structural and signaling scaffolds that organize, coordinate, and regulate cellular activities at an implantation site (De Arcangelis and Georges-Labouesse, 2000b;Reichardt, 1999). Therefore, extracellular matrix proteins are attractive biomimetic targets for functionalizing orthopaedic implant surfaces in order to promote healing, bone formation, and implant fixation (Hubbell, 2004a). Extensive studies have focused on functionalizing surfaces with single integrin ligands, such as RGD, FN, or COL, in order to control both cell adhesion and differentiation. However, these biomimetic strategies are limited by lack of specificity for particular integrins and downstream signaling events and thus allow minimal control over cell and tissue responses. In addition, native ECM proteins often have binding sites for other ligands, such as fibronectin or von Willebrand factor. Such ligands trigger separate signaling cascades that may ultimately confound phenotypic responses and interfere with controlled cell function. Finally, these single-component biomimetic strategies ignore the

complexity of the extracellular matrix and the involvement of more than one integrin signaling pathway in a particular downstream cellular response.

Our strategy to improve osseointegration of titanium implants focuses on mimicking multiple integrin-ECM interactions and conferring integrin specificity using peptides with appropriate binding sites and conformations. We target two specific integrins essential to differentiation in osteoblast cells – the type I collagen (COL-I) receptor $\alpha_2\beta_1$ and the fibronectin (FN) receptor $\alpha_5\beta_1$ – using the GFOGER triple helical peptide and the recombinant FNIII7-10 fibronectin fragment. This study compares the osseointegrative potential of these single-component integrin-specific peptides to a mixed surface treatment presenting both peptides. We also examine the efficacy of the biomimetic integrin-targeted peptides compared to their native matrix proteins as implant coating treatments.

The ligand-modified titanium surfaces are evaluated for osteoblastic differentiation in bone marrow stromal cells *in vitro*, including bone-specific gene expression, alkaline phosphatase activity, and mineral production. They are also examined for their ability to improve peri-implant bone regeneration and mechanical osseointegration in a rat tibia cortical bone implant model. This study establishes integrin-specific peptide implant coatings that enhance bone repair and implant integration for clinical orthopaedic and dental applications.

Materials and Methods

Cell isolation and culture

Primary bone marrow stromal cells were harvested from the femora of young adult male Wistar rats in accordance with an IACUC-approved protocol.(Maniatopoulos,

Sodek, and Melcher, 1988) After excision, hindleg femora and tibiae were cleared of soft tissue and processed through three consecutive 15 min rinses in growth medium (α-minimal essential medium supplemented with 10% fetal bovine serum, 1% penicillin–streptomycin, and 0.3 μg/ml amphotericin B). The ends of the long bones were then removed and the marrow space was flushed with culture medium (3-5 ml), using a syringe with an 18-gauge needle. Marrow isolates were pooled, centrifuged, resuspended in growth medium, and seeded for adhesion-dependent selection on tissue culture polystyrene dishes. Non-adherent hematopoietic cells were removed during subsequent medium exchanges, which occurred every other day. Cells were subcultured every two days according to standard techniques. For *in vitro* osteogenic assays, cells were seeded at 10,000 cells/cm^2 in growth medium. After 24 h, cultures were maintained in osteogenic medium consisting of growth medium supplemented with 50 μg/ml L-ascorbic acid and 3 mM sodium β-glycerophosphate.

In vitro biomimetic surface preparation

For the *in vitro assays*, tissue culture-treated polystyrene dishes were coated with 300 Å of pure titanium using an electron beam evaporator at a chamber base pressure between 1-2 x 10^{-6} torr with a deposition rate of 1.5 Å/second. The GFOGER peptide and FNIII7-10 fragment were diluted to 20 μg/ml in Dulbecco's phosphate-buffered saline (PBS) and incubated on the titanium surfaces for 1 h at 22ºC in preparation for all assays. For mixed surfaces, the FN fragment was incubated first for 1 h, the surface was washed three times with PBS, ad the GFOGER peptide was incubated next for an additional 1 h.

Osteoblast-specific gene expression

Gene expression was analyzed by qRT-PCR.(Byers et al., 2002e) Total RNA was isolated at 7 days after initial cell seeding using the Qiagen RNeasy RNA isolation kit. During RNA isolation and purification, samples were treated with DNaseI (27 Kunitz units/sample) for 15 min at room temperature to eliminate any genomic DNA contamination. The concentration of purified RNA was quantified using a NanoDrop (NanoDrop Technologies) and 1 μg of total RNA was used to synthesize cDNA templates by oligo(dT) priming using the Superscript First-Strand cDNA Synthesis System.

qRT-PCR was performed with the ABI Prism 7700 Sequence Detection System (Applied Biosystems; 40 cycles; melting for 15 s at 95ºC; annealing and extending for 60 s at 60ºC) using SYBR Green DNA intercalating dye. Gene transcript concentration in the sample cDNA template solutions was quantified by preparing a functional range of dilutions from an absolute standard for each gene. Linear standard curves were then generated by plotting the log of the known concentration versus the C_T value (the cycle number at which the fluorescence reached a threshold level). Oligonucleotide primers (**Table 7.1**) were designed using Primer Express software (Applied Biosystems).

Table 7.1. Real-Time PCR Oligonucleotides for Rat Genes

Gene/Gen Bank Accession Number	*Forward Primer*	*Reverse Primer*
OCN / X04141	5'-ACGAGCTAGCGGACCACATT-3'	5'-CCCTAAACGGTGGTGCCATA-3'
BSP / J04215	5'-TGACGCTGGAAAGTTGGAGTT-3'	5'-GCCTTGCCCTCTGCATGTC-3'

Alkaline phosphatase biochemical activity and calcium incorporation assays

ALP activity was quantified at 7 days after cell seeding using a modification of the Sodek and Berkman method (Stephansson, Byers, and Garcia, 2002;Sodek and Berkman, 1987). Briefly, cells were rinsed with PBS and scraped in cold 50 mM Tris-HCl. After sonication and centrifugation, the total protein concentration was quantified using a Pierce Micro BCA protein assay kit. Equal amounts of protein (2.5 μg) were added to 60 μg/ml 4-methyl-umbelliferyl-phosphate fluorescent substrate in diethanolamine buffer (pH 9.5). After a 60 min incubation at 37ºC, the fluorescence was read at an excitation of 360 nm and an emission of 465 nm on an HTS 7000 Plus BioAssay Reader (Perkin Elmer). Enzymatic activity was standardized using purified calf intestinal alkaline phosphatase at known dilutions and normalized to the amount of total protein.

Calcium content was determined by dissolving mineralized deposits with 1 N acetic acid overnight. Appropriately diluted sample (25 μl) was added to 300 μl of arsenazo III-containing Calcium Reagent (Diagnostic Services Ltd). The absorbance of the resulting samples was measured at 650 nm and compared to a linear standard curve of $CaCl_2$ in 1 N acetic acid.

Tibial implantation procedure

Commercially pure titanium implants (**Fig. 7.1**) were sonicated in de-ionized water for 20 min to remove surface debris. Implants were then dipped in 4% HF for 30 sec to remove the existing oxide layer and then incubated in 35% HNO_3 for 30 min at 50

ºC to regenerate a new oxide coating. Samples were transferred to 1.8 N NaOH for 1 min to terminate the oxidation reaction. Implants were then rinsed and boiled in de-ionized water for 1 h. To create the bioactive coating, the implants were incubated in 20 μg/ml GFOGER peptide, FNIII7-10, FN, or type I collagen solution for 1 h. Mixed surfaces were generated by sequential adsorption of FNIII7-10 first, followed by GFOGER peptide. Control titanium rods were incubated in PBS.

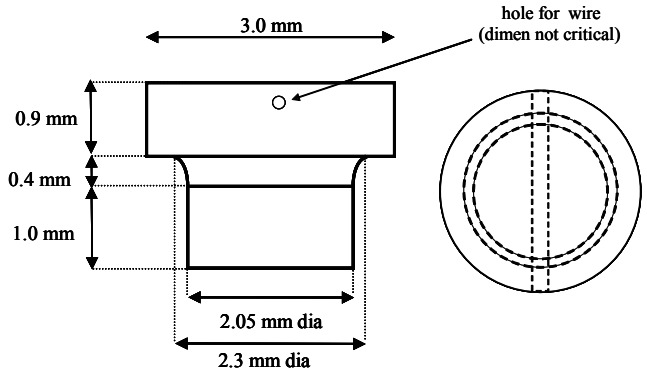

Figure 7.1. Diagram of cylindrical titanium implant rod with tapered stop collar and transverse hole for pull-out mechanical testing. The metal is ASTM F67 Grade 4 commercially pure titanium.

Implantations were conducted in accordance with an IACUC-approved protocol.(Branemark, Ohrnell, Nilsson, and Thomsen, 1997) Both hind legs of anesthetized, mature Sprague-Dawley male rats (250-350 g) were shaved and scrubbed with alcohol. The medial aspect of the proximal tibial metaphysis was exposed through an antero-medial skin incision, leaving the medial collateral ligament intact. Using a saline-cooled drill at ~2 rotations per minute (to avoid thermal trauma), two defects were created in each tibia. Sterile implant rods were press fit into the defects. Periosteum was mobilized and sutured over the implantation site, and the skin was closed with wound clips. Subjects were euthanized after 4 weeks and proximal tibiae were fixed in neutral

buffered formalin for histology or recovered without fixation and maintained in PBS-moistened gauze for immediate mechanical testing.

Based on power calculations and previous reports in the literature,(Branemark, Ohrnell, Nilsson, and Thomsen, 1997) we estimated that a minimum of eight implants per experimental group are required to detect differences of 10% in mechanical testing and a minimum of four implants per experimental group are required for histomorphometry for a total of 11 implants per experimental group. In this model, each animal receives four implants, two per experimental condition. Each tibia contained two implants from the six conditions. The sample conditions were distributed according to a randomized block design, in which the six conditions were randomized according to proximal/distal and left/right tibia placement, but were constrained into blocks containing one each of the six conditions. Within each block, condition placement was randomized. This results in a randomly distributed design that avoids instances where the same condition is implanted twice in a single leg. We used a total of twenty-one animals with 14 implants per condition – four for histology and ten for mechanical testing. Two additional animals with two implants per condition were included as extras in the event of tibia breakage during harvest or during the apparatus set-up for mechanical testing.

Histology and histomorphometry analyses and mechanical testing

Excised tibiae were fixed in 10% neutral buffered formalin for 1 week. Samples were then embedded, ground, and stained by Wasatch Histo Consultants, Inc. Briefly, the formalin-fixed tibiae were dehydrated in a graded series of alcohol incubations and then embedded in poly(methyl methacrylate). Ground sections of 50-80 μm were generated using the Exakt Grinding System. Two longitudinal ground sections were

generated per tibia, each containing two titanium plugs inserted transverse to the tibia's long axis. Sections were then stained with Sanderson's Rapid Bone Stain™ and a van Gieson counter stain. Bone implant contact (BIC) was measured as the percentage of implant's circumference that was in direct contact with bone tissue (Adobe Photoshop CS imaging software).

Implant mechanical fixation to the bone was measured with a pull-out force test using a biomechanical testing apparatus (EnduraTEC Bose ELF 3200). Immediately after explantation, tibiae were cleaned of all soft tissue and prepared for mechanical testing. The ends of each excised tibia were secured in a custom designed holding apparatus with the exposed head of each implant facing in the direction of the pull motion and centered along the axis of motion. A 0.014" diameter piano wire was threaded through the implant head and both wire ends attached firmly to an 11 lb. INTERFACE load cell. Samples were pre-loaded with 2 N to ensure proper and identical wire tautness among implants. Tests were performed at a constant force rate of 0.2 N/sec using WINTEST application software. The direction of the pull was parallel to the long axis of the implant. The pull-out force (N) was the maximum load achieved before failure and was determined from the recorded load vs. displacement data.

Statistics

Data are reported as mean ± standard error. Results were analyzed by one-way ANOVA using SYSTAT 8.0 (SPSS). If treatment level differences were determined to be significant, pair-wise comparisons were performed using a Tukey post-hoc test. A 95% confidence level was considered significant. All of the *in vitro* assays were performed as two separate experiments in triplicate. The quantitative histomorphometry

consisted of a total sample size of seven implants per condition. The mechanical testing consisted of a total sample size of nine implants per condition.

Results

In Vitro Osteoblastic Differentiation on Biomimetic Peptide Coatings

I*n vitro* rat bone marrow stromal cell differentiation assays were performed concurrently with the *in vivo* osseointegration study. To reproduce titanium implant surfaces *in vitro*, polystyrene culture dishes were coated with a 300 Å titanium layer via electron beam evaporation. The biomimetic peptides and matrix proteins were then passively adsorbed onto the titanium at a concentration of 20 μg/ml, creating the integrin-targeted bioactive coating. Mixed ligand surfaces were generated by sequential adsorption of the fibronectin fragment and the GFOGER peptide

To investigate the osteoblastic differentiation potential of these surfaces, we used quantitative RT-PCR (qRT-PCR) to probe osteoblast-specific gene expression in 7 day cultures of bone marrow stromal cells (**Fig. 7.2**). For both bone sialoprotein (BSP) and osteocalcin (OCN), qRT-PCR revealed greater levels of gene expression on the GFOGER-peptide surfaces compared with untreated titanium. These expression levels were equivalent to those observed on surfaces coated with native type I collagen. The FN fragment and mixed ligand surfaces did not enhance BSP and OCN gene expression compared to control titanium.

Osteoblastic differentiation is also characterized by the activation of multiple proteins, including alkaline phosphatase (ALP). The ALP enzyme is often used as a marker for osteoblastic metabolic activity and an early indicator of osteoblastic differentiation.(Aubin and Liu, 1996) An ALP biochemical assay revealed elevated

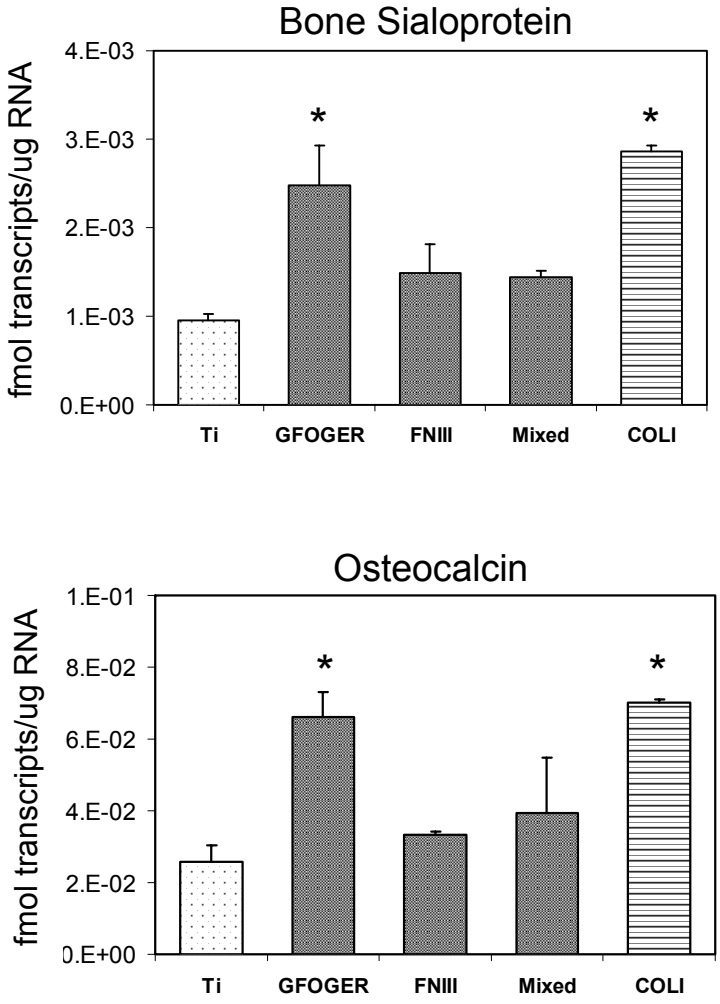

Figure 7.2. GFOGER surfaces enhance the expression of multiple osteoblast-specific genes. Data represent osteoblast-specific gene expression measured by qRT-PCR for osteocalcin (OCN), and bone sialoprotein (BSP) in rat bone marrow stromal cells seeded for 7 days on biomimetic surfaces, native matrix proteins or untreated Ti. BSP ANOVA: $p<0.0007$, *GFOGER, COLI > Ti ($p<0.003$); OCN ANOVA: $p<0.003$, *GFOGER, COLI > Ti ($p<0.008$).

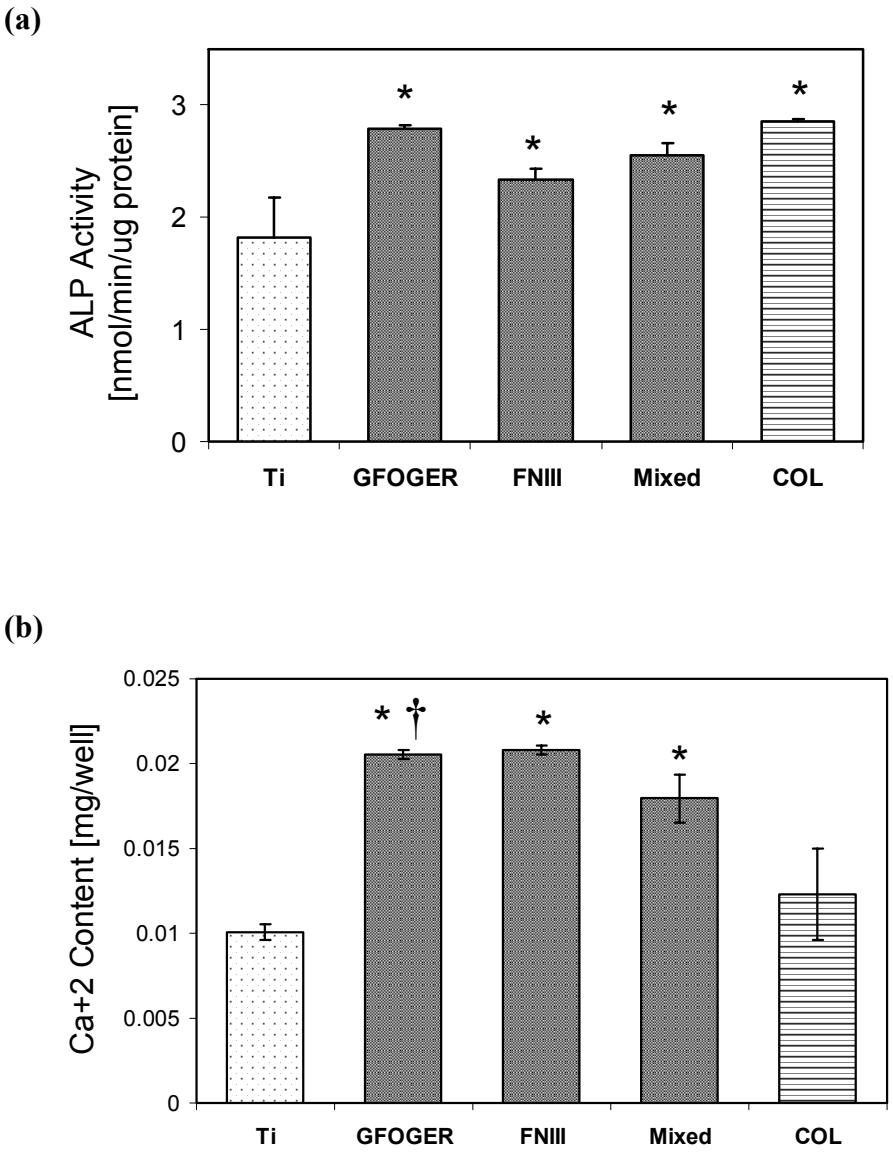

Figure 7.3. Biomimetic surfaces enhance **(a)** alkaline phosphatase (ALP) activity and **(b)** matrix calcification in rat bone marrow stromal cultures compared to untreated titanium (Ti). ALP ANOVA: $p<0.0004$, *GFOGER, FNIII, Mixed > Ti ($p<0.02$); Ca^{+2} ANOVA: $p<0.0007$, *GFOGER, FNIII, Mixed > Ti ($p<0.01$).

levels of activation on the GFOGER-peptide, FN fragment, and mixed ligand coatings compared to untreated titanium (**Fig. 7.3.a**). Because ALP is the enzyme responsible for hydrolyzing phosphate esters and inducing bone mineralization,(Aubin and Liu, 1996) these results suggest that this bioactive surface treatment may also be capable of promoting enhanced bone matrix mineralization.

Mineralization was examined as an *in vitro* end-point indicator of the osteoblastic phenotype in the bone marrow stromal cells. Calcium phosphate mineral deposition was examined after 14 days in culture using calcium content analysis. Cultures on GFOGER-, FN fragment, and mixed ligand-treated surfaces displayed nearly two-fold enhancement in calcium-based mineral deposition compared to untreated titanium (**Fig. 7.3.b**). These results verify the advantageous effects of controlled integrin-binding on cell function, in this case osteoblastic differentiation and matrix mineralization.

Table 7.2. Design for osseointegration study. Samples were implanted using a randomized block design. A total of 21 animals were included in the study.

	Total Number of Samples	
Implant Surface	**Histomorphometry**	**Mechanical Testing**
GFOGER	4	10
FNIII7-10	4	10
Mixed	4	10
Type I Collagen	4	10
Fibronectin	4	10
Ti	4	10

In Vivo Osseointegration of Biomimetic Peptide Coatings

To evaluate the performance of the bioactive treatments *in vivo*, we quantified osseointegration in a rat tibia cortical bone model using quantitative histomorphometry and pull-out mechanical testing.(Branemark, Ohrnell, Nilsson, and Thomsen, 1997) We designed a cylindrical titanium implant rod with a tapered stop collar (**Fig. 7.1**). The

tapered head ensures that all implants are inserted into the bone at the same depth, guaranteeing uniform bone contact among treatments. Using a saline-cooled drill, two defects 2 mm in diameter were created in the medial aspect of the proximal tibial metaphysis. Titanium implant rods were press fit into the cortical defects. **Table 7.2** shows the six coating treatments that were evaluated in this study. After four weeks, the rat tibiae were harvested and evaluated for bone apposition by histological staining and mechanical integration by pull-out testing. Histological sections revealed substantial and contiguous bone mineral along the periphery of GFOGER-treated, FNIII7-10-treated, and mixed ligand-treated titanium implants (**Fig. 7.4.a**), with no apparent increase in bone formation on the mixed ligand condition. Less bone mineral is visible on surfaces treated with the native proteins, FN and type I COL, and the adjacent mineral appears more porous. Significantly less mineral staining was visible on untreated titanium and the mineral deposits appear in isolated patches along the surface of the implants. Image quantification to determine the percentage of the bone-implant apposition (bone implant contact, BIC) demonstrated a nearly forty percent enhancement in bone apposition on the collagen-mimetic, fibronectin-mimetic, and mixed ligand surfaces compared to untreated titanium (**Fig. 7.4.b**). Again, no advantage is evident with the combination treatment. However, the two single component biomimetic peptides induced greater bone formation and apposition than either of native ECM protein coatings, demonstrating the benefit of integrin-target mimetic peptides over whole biomolecules.

Pull-out mechanical testing results reflected the same trends observed in the histology and histomorphometry data. Mechanical testing demonstrated significantly higher mechanical fixation of the peptide-functionalized implants compared to untreated

(a)

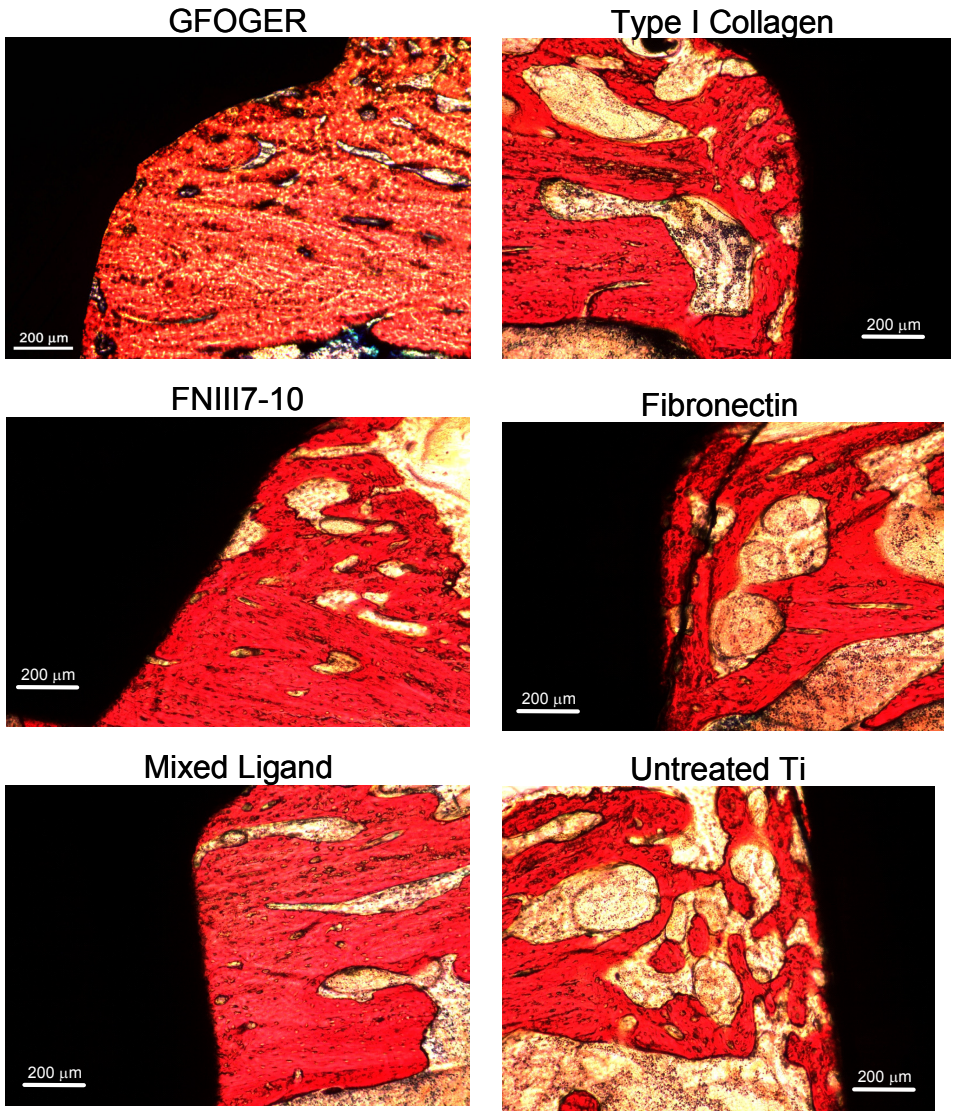
GFOGER
200 μm
Type I Collagen
200 μm
FNIII7-10
200 μm
Fibronectin
200 μm
Mixed Ligand
200 μm
Untreated Ti
200 μm

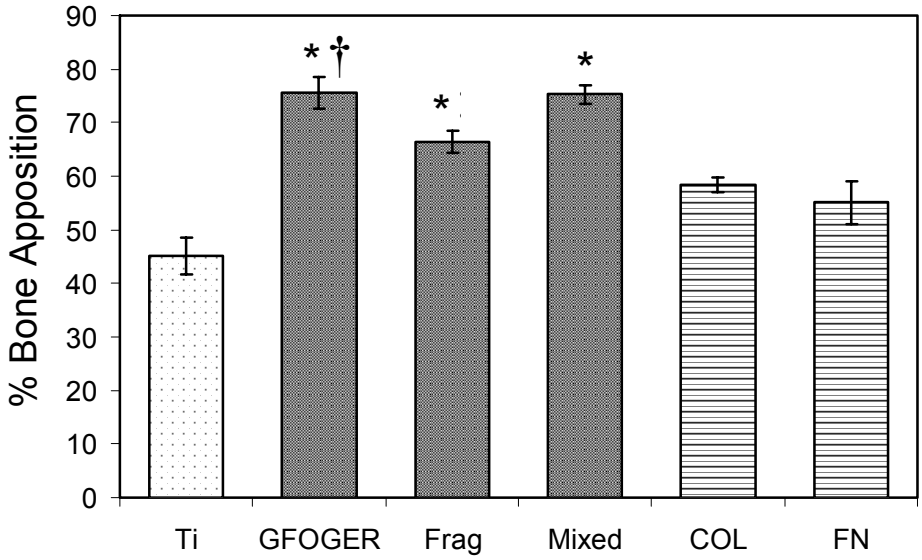

Figure 7.4. Biomimetic surfaces improve peri-implant bone formation and mechanical osseointegration in an *in vivo* rat tibia cortical bone implantation model. **(a)** Representative micrographs show 50-80 μm longitudinal ground sections of rat tibia stained with Sanderson's Rapid Bone Stain™ and van Gieson counterstain. Cells stain dark to light blue, soft tissue elements stain blue-green, and bone matrix stains yellow orange to autumn orange. **(b)** Biomimetic surfaces exhibit greater amounts of newly formed bone at the implant surface compared with untreated Ti or native ECM proteins. Bone apposition is measured as the percentage of implant's circumference that is in direct contact with bone mineral in the histological sections. ANOVA: $p<4E-6$, *GFOGER, Frag, Mixed > Ti ($p<0.002$), †GFOGER > COL ($p<0.01$), ‡Frag > FN ($p<0.004$).

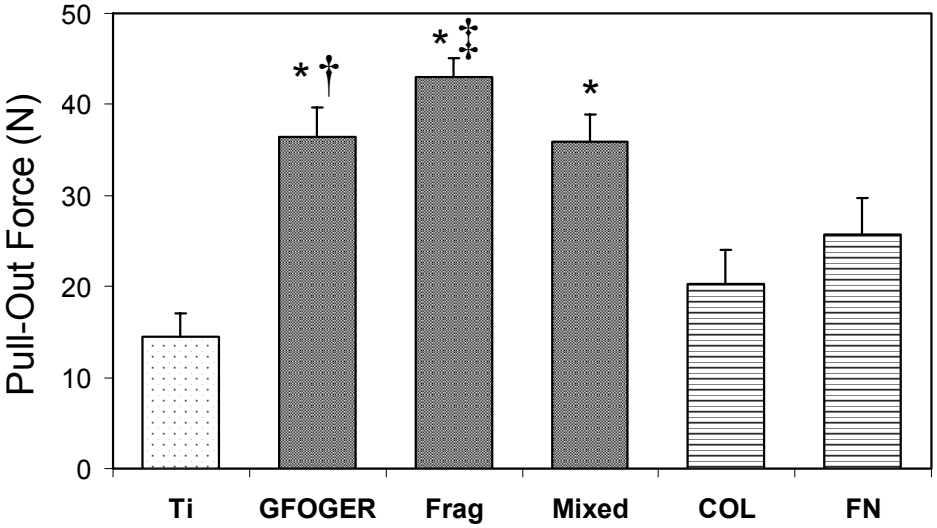

Figure 7.5. Biomimetic surfaces demonstrate greater mechanical integration with the surrounding tissue compared with untreated Ti or native ECM proteins. Osseointegration is measured as the maximum force [N] necessary to dislodge the implant in a pull-out test. ANOVA: $p<9E-7$, *GFOGER, Frag, Mixed > Ti ($p<0.0009$), †GFOGER > COL ($p<0.01$), ‡Frag > FN ($p<0.004$).

titanium (**Fig. 7.5**). No additional mechanical benefit was conferred by the mixed ligand treatment, confirming the results from the bone apposition analysis. Once more, the two biomimetic peptide coatings outperformed both of the native protein coatings.

These results demonstrate a greater quantity and continuity of peri-implant bone mineral on the integrin-targeted peptide surfaces *in vivo* as well as enhanced mechanical integrity and osseointegration when compared with either untreated titanium or titanium treated with native fibronectin or type I collagen. However, the two single biomimetic peptide treatments were sufficient to enhance bone mineral formation and mechanical osseointegration, and there was no additional advantage demonstrated by the mixed ligand presentation.

Discussion

This work evaluates the ability of two peptide coatings to improve bone regeneration and osseointegration, alone and in combination, by exploiting their specificy for integrins that are critical to osteoblast differentiation – the collagen-binding $\alpha_2\beta_1$ and fibronectin-binding $\alpha_5\beta_1$. In particular, type I collagen modulates intracellular signal transduction by binding to the $\alpha_2\beta_1$ integrin, which enhances the expression of the osteoblastic phenotype (Suzawa, Tamura, Fukumoto, Miyazono, Fujita, Kato, and Takeuchi, 2002;Mizuno and Kuboki, 2001;Mizuno, Fujisawa, and Kuboki, 2000;Jikko, Harris, Chen, Mendrick, and Damsky, 1999;Xiao, Wang, Benson, Karsenty, and Franceschi, 1998;Takeuchi, Suzawa, Kikuchi, Nishida, Fujita, and Matsumoto, 1997a). It also exhibits low immunogenicity and high conformational stability, making it extremely suitable for implantation. Osteoblasts and osteoprogenitor cells also express $\alpha_5\beta_1$, the principal FN receptor (Gronthos, Stewart, Graves, Hay, and Simmons, 1997). Adhesive

interactions involving $\alpha_5\beta_1$ and FN have also been identified as central to osteoblastic functions.

However, designing surface treatments using whole matrix molecules, such as type I collagen or FN, is often limited by a lack of specificity for particular integrins and thus exhibit minimal control over cellular responses. In addition, native matrix proteins often have binding sites for other ligands, such as fibronectin or von Willebrand factor. Such ligands may trigger separate signaling cascades that may ultimately confound phenotypic responses and interfere with desired cell function.

The advantage of the short biomimetic peptides over the native ECM proteins was evident in the *in vivo* osseointegration study. The cortical bone implantation studies revealed greater bone tissue formation on the surface of GFOGER-treated and FNIII7-10-treated titanium implants, in terms of both quantity and connectivity, compared to control titanium. The bone formation on the biomimetic peptides was also significantly greater than that observed on the surfaces treated with the native collagen and fibronectin molecules.

Most significantly, we have shown that the GFOGER peptide and the FN fragment improved the titanium implant's mechanical fixation and functional osseointegration as determined by a quantitative pull-out test. Again, mechanical pull-out load was greater on the peptide coatings compared to the full matrix biomolecules. Faster integration of these biomimetic peptide-coated implants would result in sooner and more reliable loading in a clinical setting, improving device function and patient outcomes.

However, is interesting to note that the combination treatment of both GFOGER-peptide and FN fragment did not confer any additional advantage over the single peptide coatings with respect to bone formation, apposition, or mechanical fixation. It is possible that either one of the integrin-targeted peptides saturates the osteogenic potential of the $\alpha_2\beta_1$ and $\alpha_5\beta_1$ signaling pathways. For example, the presence of an $\alpha_2\beta_1$-binding peptide on the implant surface many induce cells at the interface to produce the corresponding $\alpha_5\beta_1$-binding protein and vice versa, thus maximizing the integrin-based osteogenic signaling environment. In this case, a mixed ligand presentation has no additional benefit.

The data also demonstrates that GFOGER-peptide improves bone formation and osseointegration *in vivo* to a much greater extent than native type I collagen. However, *in vitro*, these two treatments are equivalent. This is most likely due to the heterogeneous cell population encountered *in vivo*. In that environment, the full collagen molecule may have multiple effects on a variety of non-osteoblastic cell types. These effects may modulate or confound collagen's enhancement of osteoblastic signaling. Because of GFOGER-peptides' short, integrin-targeted design, many of these effects are eliminated, thus enhancing its specificity for osteoblastic cells. This specificity allows the peptide to encourage an osteogenic cell population at the surface of the implant.

Not only do these bioactive coatings enhance bone formation and implant integration, but they also created using a single-step procedure conducted under physiological conditions, thus eliminating the cytotoxicity and biocompatibility concerns associated with covalent immobilization methods. As such, these peptide surface

treatments represent a simple, clinically relevant approach to improving orthopaedic and dental titanium implant integration.

CHAPTER 8

SUMMARY OF CONCLUSIONS

Bioactive surfaces that provide specific signals to cells through well-characterized integrin-ligand interactions may lead to controlled cellular responses and improved tissue formation in tissue engineering and wound healing applications. The first goal of this study was to engineer stable bioadhesive surfaces that specifically target the $\alpha_2\beta_1$ integrin, allowing us to directly control intracellular signaling and, ultimately, cell function. We designed a stable triple-helical, collagen-mimetic peptide that contains the GFOGER adhesion motif from type I collagen. The peptide has the following primary sequence: GGYGGGPC$(GPP)_5$GFOGER$(GPP)_5$GPC. The GPP triplets on either side of the GFOGER recognition site provide cooperative clusters that promote the formation of a stable right-handed triple helical structure at room temperature (Knight, Morton, Peachey, Tuckwell, Farndale, and Barnes, 2000;Nagarajan, Kamitori, and Okuyama, 1998;Fields and Prockop, 1996). This triple-helical conformation is essential for integrin recognition and $\alpha_2\beta_1$-mediated cell adhesion (Messent, Tuckwell, Knauper, Humphries, Murphy, and Gavrilovic, 1998;Morton, Peachey, Knight, Farndale, and Barnes, 1997;Morton, Peachey, Zijenah, Goodall, Humphries, and Barnes, 1994).

We demonstrate that the GFOGER peptide specifically targets the $\alpha_2\beta_1$ integrin receptor, and its cell adhesion activity is comparable to that of type I collagen. We have also verified its activity using several surface modification techniques, including passive adsorption, specific noncovalent surface interaction, and covalent immobilization, demonstrating that this triple helical peptide represents a robust and versatile approach to

the design of bioadhesive surfaces that specifically target the $\alpha_2\beta_1$ integrin. Surface immobilization remains the most promising method for incorporating the GFOGER peptide into applications that benefit from enhanced control over cell function due to higher adhesion activity and greater surface stability.

In terms of a viable surface modification scheme, these studies reveal that this adhesion-promoting synthetic peptide of minimal recognition sequence and specific tertiary conformation can be covalently grafted to a stable, non-adhesive substrate to produce biologically active, chemically well-defined surfaces that support $\alpha_2\beta_1$-specific cell adhesion. Controlling integrin binding through covalent surface modification in turn allows us to optimize cell function for applications such as biomaterials processing and tissue engineering scaffold design. In addition, these surfaces may be useful in the study of fundamental $\alpha_2\beta_1$-mediated adhesion events in various cell models and biotechnological applications.

The $\alpha_2\beta_1$ integrin interaction with type I collagen is a crucial signal for the induction of osteoblastic differentiation and matrix mineralization. The integrin-specificity of the GFOGER-peptide makes it a very attractive candidate for engineering surfaces to promote osteoblastic differentiation and bone formation. Next, we explored whether this integrin-specific peptide is capable of promoting similar signaling events and differentiation responses as native type I collagen in the osteoblast cell model. We demonstrate that this $\alpha_2\beta_1$ integrin-specific GFOGER-peptide triggers the activation of FAK and alkaline phosphatase in MC3T3-E1 murine immature osteoblast-like cells. These surfaces also support the expression of multiple osteoblast-specific genes and the mineralization of the ECM in a manner similar to type I collagen, suggesting that this

triple-helical peptide represents a robust approach to the design of collagen-mimetic bioadhesive surfaces that specifically target the $\alpha_2\beta_1$ integrin. Controlling specific integrin binding through this biomolecular surface modification strategy may allow the optimization of cell function, in particular osteoblastic differentiation, for applications such as orthopedic biomaterials and bone tissue engineering scaffold design.

Implant osseointegration, defined as close bone apposition and functional fixation, is a prerequisite for clinical success in orthopaedic and dental applications, many of which are restricted by implant loosening (Pilliar, 2005)·(Anderson, 2001). Surface modification approaches have had limited success in promoting integration. Our strategy to improve osseointegration of titanium implants focused on presenting the GFOGER collagen-mimetic peptide that triggers $\alpha_2\beta_1$ cellular integrin receptor binding, which is crucial for bone mineral deposition. We have demonstrated that titanium surfaces presenting integrin-specific GFOGER peptide trigger osteoblastic differentiation in bone marrow stromal cells, including bone-specific gene expression, alkaline phosphatase activity, and mineral deposition, leading enhanced osteoblastic function compared to unmodified orthopaedic-grade titanium.

To evaluate the performance of the bioactive GFOGER peptide treatment *in vivo*, we quantified osseointegration in a rat tibia cortical bone model using quantitative histomorphometry and pull-out mechanical testing (Branemark, Ohrnell, Nilsson, and Thomsen, 1997). Our studies revealed greater bone tissue formation on the surface of GFOGER-treated titanium implants, in terms of both quantity and connectivity. Most significantly, we have shown that the GFOGER peptide coating improved the implant's mechanical fixation and functional osseointegration as determined by a quantitative pull-

out test. Faster integration of these GFOGER coated implants would result in sooner and more reliable loading in a clinical setting, improving device function and patient outcomes.

Not only does this bioactive coating enhance bone formation and implant integration, but it is also created using a single-step procedure conducted under physiological conditions, thus eliminating the cytotoxicity and biocompatibility concerns associated with covalent immobilization methods. As such, this GFOGER peptide surface treatment represents a simple, clinically relevant approach to improving orthopaedic and dental titanium implant integration.

Cell adhesion to the extracellular matrix (ECM) through cell-surface integrin receptors is essential to development, wound healing, and tissue remodeling, and therefore represents a central theme in the design of bioactive surfaces that successfully interface with the body. Extensive studies have focused on functionalizing surfaces with single integrin ligands, such as RGD, FN, or COL, in order to control both cell adhesion and differentiation. However, the native cellular environment is characterized by a variety of matrix proteins that target multiple integrins implicated in a downstream cellular response. Conversely, many biomimetic strategies are limited by low activity of the oligopeptides compared to the native ligand due to the absence of complementary or modulatory domains (Garcia, Schwarzbauer, and Boettiger, 2002).

As an alternative strategy, we have focused on engineering high molecular weight ligands that recapitulate the primary, secondary, and tertiary structure of the native matrix protein in order to reconstitute full biological activity as well as integrin binding specificity. The recombinant fragment of FN encompasses both the PHSRN sequence in

the 9th type III repeat and RGD motif in the 10th type III repeat of FN in their native structural orientations and is therefore specific for the $\alpha_5\beta_1$ integrin. The GFOGER peptide mimics the triple-helical structure of native type I collagen and targets the $\alpha_2\beta_1$ integrin.

The objective of our next study was to engineer bioactive hybrid surfaces that control cell function by mimicking two separate integrin interactions, $\alpha_5\beta_1$ and $\alpha_2\beta_1$, using the FN- and collagen-mimetic ligands to mimic signals from native ECM. Both of these integrin-ligand interactions have been implicated in several differentiation pathways, including osteoblastic differentiation. Our strategy used mixed biotinylated ligands on avidin substrates, providing a simple and easily controlled approach to efficiently screen a large number of mixed surface compositions using short term assays.

The wide range of controlled mixed ligand densities generated by this process demonstrates the feasibility of generating integrin-specific hybrid surfaces. We have shown that these mixed ligand surface formulations result in greater cell adhesion and focal adhesion assembly. The mixed surfaces also trigger a synergistic activation of focal adhesion kinase, when compared with single ligand surfaces. Proliferation results confirmed that the enhanced signaling effects of mixed ligand surfaces translate to downstream cellular responses.

We have demonstrated that the presentation of multiple integrin-binding ligands synergize to enhance intracellular signaling and proliferation. This study suggests that, instead of focusing on a single integrin-ligand interaction, in some cases it may be advantageous to consider the interplay of multiple integrins implicated in a desired cell response and their combined effect on downstream cellular signals. This may allow the

rational engineering of optimal biospecific surfaces for implant coatings and tissue engineering scaffolds that exploit that complexity of the extracellular matrix and its signaling characteristics.

Extracellular matrix proteins are attractive biomimetic targets for functionalizing orthopaedic implant surfaces in order to promote healing, bone formation, and implant fixation. We target two specific integrins essential to differentiation in osteoblast cells – the type I collagen (COL-I) receptor $\alpha_2\beta_1$ and the fibronectin (FN) receptor $\alpha_5\beta_1$ – using the GFOGER triple helical peptide and the recombinant FNIII7-10 fibronectin fragment. Our final study compared the osseointegrative potential of these single-component integrin-specific peptides to a mixed surface treatment presenting both peptides. We also examine the efficacy of the biomimetic integrin-targeted peptides compared to their native matrix proteins as implant coating treatments.

The advantage of the short biomimetic peptides over the native ECM proteins was evident in the *in vivo* osseointegration study. The cortical bone implantation studies revealed greater bone tissue formation on the surface of GFOGER-treated and FNIII7-10-treated titanium implants, in terms of both quantity and connectivity, compared to control titanium. The bone formation on the biomimetic peptides was also significantly greater than that observed on the surfaces treated with the native collagen and fibronectin molecules.

Most significantly, we have shown that the GFOGER peptide and the FN fragment improved the titanium implant's mechanical fixation and functional osseointegration as determined by a quantitative pull-out test. Again, mechanical pull-out load was greater on the peptide coatings compared to the full matrix biomolecules.

Faster integration of these biomimetic peptide-coated implants would result in sooner and more reliable loading in a clinical setting, improving device function and patient outcomes.

However, is interesting to note that the combination treatment of both GFOGER-peptide and FN fragment did not confer any additional advantage over the single peptide coatings with respect to bone formation, apposition, or mechanical fixation. It is possible that either one of the integrin-targeted peptides saturates the osteogenic potential of the $\alpha_2\beta_1$ and $\alpha_5\beta_1$ signaling pathways. For example, the presence of an $\alpha_2\beta_1$-binding peptide on the implant surface many induce cells at the interface to produce the corresponding $\alpha_5\beta_1$-binding protein and vice versa, thus maximizing the integrin-based osteogenic signaling environment. In this case, a mixed ligand presentation has no additional benefit.

In conclusion, this thesis proposes a specific biomolecular strategy to engineer implant surfaces that enhance bone formation and osseointegration. By achieving the three specific aims previously outlined, we achieved the following outcomes. First, we designed and evaluated a collagen mimetic peptide as an $\alpha_2\beta_1$ integrin-specific surface modification agent for biomaterials, implant surface treatments, and tissue engineering scaffolds. This peptide was verified in the osteoblast cell model, but may be applied to several other cell systems that express $\alpha_2\beta_1$, including platelets, epithelial cells, fibroblasts, chondrocytes, endothelial cells, and lymphocytes. We also established the extent to which the presentation of multiple integrin-binding ligands synergize to enhance intracellular signaling. This allows for the rational engineering of optimal biospecific surfaces for implant coatings and tissue engineering scaffolds. Finally, by analyzing the

osseointegrative properties of these bioinspired materials, we have established the potential of this biomimetic ligand approach as a beneficial surface treatment for orthopaedic implants. As a whole, this project has established a targeted biomolecular surface engineering strategy for designing and optimizing biologically active implant coatings and grafting substrates that enhance implant bone repair.

CHAPTER 9

FUTURE CONSIDERATIONS

We heave demonstrated that GFOGER-peptide passively adsorbed to titanium implant surfaces enhances peri-implant bone formation, apposition, and mechanical integration. The main advantage of this approach is the simplicity of the single-step surface coating, compared to covalent modifications schemes. However, future work might focus on determining whether covalent tethering would provide additional benefits in an osseointegration model. While the processing steps for covalent surface modification are more complex, tethering allows prolonged and controlled exposure to the biomimetic ligand. Optimal surface densities for osteoblastic differentiation can be determined *in vitro* and applied to the implant surfaces.

A surface tethering approach would also allow control over the background surface. With our passive adsorption study, the background titanium was left unblocked and thus able to non-specifically adsorb proteins from implant site. With a covalent crosslinking scheme, the anchoring groups can be engineered to present a non-adhesive, non-fouling background surface, allowing precise control over the ligands presented to the cells at the implant interface.

One potential system for peptide tethering is mixed self-assembled monolayers (SAMs) of alkanethiols on gold, which represent a robust, controlled, and stable system for long term assays. Mixed SAMs of an EG_3-terminated thiol [$HS(CH_2)_{11}(OCH_2CH_2)_3OH$] and an EG_6COOH-terminated thiol [$HS(CH_2)_{11}(OCH_2CH_2)_6OCH_2CO_2H$] can be used to generate various surface

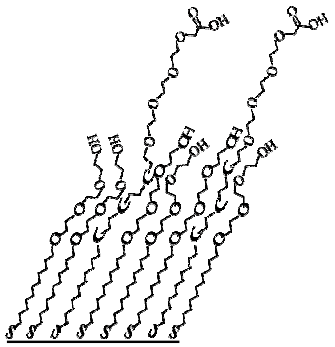

Figure 9.1. Mixed EG_6COOH/EG_3 SAM

compositions (EG = ethylene glycol) (**Fig. 9.1**). The EG_3 moiety provides a non-fouling, protein-resistant background while the COOH group provides a versatile functionality for tethering the GFOGER-peptide, fibronectin-mimetic ligand, or other bio-inspired molecules using conventional EDC/NHS bioconjugation chemistry. This system has been validated for the immobilization of several peptides and proteins by Whitesides and colleagues.(Lahiri et al., 1999) Other possible non-fouling covalent tethering systems include PEG brushes grown on titanium and titanium coated with PEG-based polymer networks.

Future studies might also focus on combining the GFOGER-peptide with other implant surface technologies to enhance osseointegration, such as physicochemical or morphological surface treatments. In particular, several *in vivo* and *in vitro* studies have focused on generating surfaces with rough microtopographies to improve osteoblast differentiation and bone formation (Lossdorfer, Schwartz, Wang, Lohmann, Turner, Wieland, Cochran, and Boyan, 2004;Boyan, Lossdorfer, Wang, Zhao, Lohmann, Cochran, and Schwartz, 2003;Li, Ferguson, Beutler, Cochran, Sittig, Hirt, and Buser, 2002;Martin, Schwartz, Hummert, Schraub, Simpson, Lankford, Jr., Dean, Cochran, and

Boyan, 1995;Groessner-Schreiber and Tuan, 1992;Buser, Schenk, Steinemann, Fiorellini, Fox, and Stich, 1991;Roberts, Smith, Zilberman, Mozsary, and Smith, 1984). *In vivo* studies have demonstrated that rougher surfaces promote higher levels of bone formation and apposition compared to smoother surfaces (Buser, Schenk, Steinemann, Fiorellini, Fox, and Stich, 1991) and exhibit increased removal torque (Li, Ferguson, Beutler, Cochran, Sittig, Hirt, and Buser, 2002). *In vitro* studies reveal that microrough implant surface topographies improve the phenotypic expression of osteoblast-like cells (Martin, Schwartz, Hummert, Schraub, Simpson, Lankford, Jr., Dean, Cochran, and Boyan, 1995;Groessner-Schreiber and Tuan, 1992), promote the formation of an osteogenic microenvironment (Boyan, Lossdorfer, Wang, Zhao, Lohmann, Cochran, and Schwartz, 2003), and reduce osteoclast formation and activity (Lossdorfer, Schwartz, Wang, Lohmann, Turner, Wieland, Cochran, and Boyan, 2004). These results have lead to the development of several methods to produce rougher implant surfaces, including plasma-spraying, acid etching, and sandblasting as well as sintered-bead and metal fiber surfaces. These surface roughness approaches not only improve mechanical interlocking and stability and enhance surface area for greater binding of attachment proteins and growth facts, but they also alter phenotypic expression in osteoblast (Schwartz and Boyan, 1994). However, while these approaches are generally successful, they can be restricted by slow rates of osseointegration and poor mechanical anchorage in challenging clinical cases, such as those associated with large bone loss and poor bone quality (Bauer and Schils, 1999a). These limitations might be alleviated by a combination of microrough implant surfaces with bioactive peptide surface coatings to improve osseointegration at all time points of implant healing.

Our results from the *in vitro* mixed ligands studies were very promising. We demonstrated synergistic enhancement of intracellular signaling with the combined presentation of GFOGER-peptide and FNIII7-10. Proliferation results confirmed that the enhanced signaling effects of mixed ligand surfaces translate to downstream cellular responses. While the mixed ligand presentation did not offer any additional advantage over the single ligands in an osseointegration model, mixed integrin-targeted approaches may be able to enhance cellular response in other applications. This strategy can be examined in other systems, such as chondrocyte differentiation or angiogenesis.

Finally, we have demonstrated the ability of the GFOGER-peptide to improve bone formation in an implant osseointegration application. This collagen-mimetic peptide might also be applied to other orthopaedic applications, such as bone tissue engineering. We have already presented schemes for covalently tethering the peptide to carboxyl groups on a surface. This is a very versatile bioconjugation technique that can easily be applied to polymeric scaffolds to enhance cell adhesion and bone in-growth.

The biomolecular approach validated in this thesis provides a versatile and robust strategy for developing bioactive surfaces that support osteoblastic differentiation and enhance bone repair. Due to the fundamental character of the receptor-ligand principles addressed in this research project, these general engineering strategies can also be applied to a variety of other cell systems in the body and may well contribute to the genesis of research projects that address medical concerns in areas other than orthopedic bioengineering.

APPENDIX A

A CENTRIFUGATION CELL ADHESION ASSAY FOR HIGH-THROUGHPUT SCREENING OF BIOMATERIAL SURFACES*

SUMMARY

A quantitative analysis of cell adhesion is essential in understanding physiological phenomena and designing biomaterials, implant surfaces, and tissue engineering scaffolds. The most common cell adhesion assays used to evaluate biomaterial surfaces lack sensitivity and reproducibility and/or require specialized equipment and skill-intensive operation. We describe a modified centrifugation cell adhesion assay that employs simple and convenient techniques using standard laboratory equipment and provides reliable, quantitative measurements of cell adhesion. This centrifugation assay applies controlled and uniform detachment forces to a large population of adherent cells, providing robust statistics for quantifying cell adhesion. The applicability of this system to the design and characterization of biomaterial surfaces is demonstrated by evaluating cell adhesion on substrates using different coating proteins, cell types, seeding times, and relative centrifugal forces (RCF). Results verify that this centrifugation cell adhesion assay represents a simple, convenient, and standard method for high-throughput characterization of a variety of biomaterial surfaces and conditions.

*Modified from Reyes,C.D. & Garcia,A.J. A centrifugation cell adhesion assay for high-throughput screening of biomaterial surfaces. *J. Biomed. Mater. Res. A* **67**, 328-333 (2003).

INTRODUCTION

Cell adhesion to extracellular matrix proteins influences cellular morphology and migration and provides signals that direct cell proliferation, migration, and differentiation (Hynes, 2002;Hynes, 1992). Soluble adhesion proteins, such as vitronectin and fibronectin, present in blood plasma, peritoneal exudates, and tissue culture solutions adsorb onto biomaterial surfaces (Horbett, 1996). Since cells respond specifically to these proteins, subsequent cell adhesion to this interfacial protein film ultimately directs physiological responses to implanted surfaces. Therefore, a quantitative analysis of cell adhesion is essential in understanding physiological phenomena and designing biomaterials, implant surfaces, and tissue engineering scaffolds.

Cell attachment to surfaces may be influenced by a diverse range of factors, including cellular properties, the physical and chemical properties of the underlying biomaterial, interfacial chemical conditions, and protein adsorption. Methods for examining cell adhesion on various surfaces generally focus on measuring the relative ability of adherent cells to remain attached when exposed to a detachment force(Weiss, 1961). The simplest and most common adhesion assay consists of seeding cells onto substrates of interest, washing off "non-adherent" cells with a physiological buffer, and counting the remaining cells. Although these wash assays provide qualitative observations of cell attachment, they are limited by a lack of sensitivity and reproducibility due to the application of uneven, unknown detachment forces. These limitations often mask important differences among treatments and generally provide inconclusive or contradictory information.

In order to obtain reproducible and reliable measurements of cell adhesion, several quantitative adhesion assays have been developed (Bundy et al., 2001;Nauman et al., 1999;Chesla et al., 1998;Garcia et al., 1997;Nugiel et al., 1996;Usami et al., 1993;Evans et al., 1991;Truskey and Pirone, 1990;Lotz et al., 1989;Horbett et al., 1988;Lawrence et al., 1987;Hertl et al., 1984;McClay et al., 1981;Doroszewski et al., 1977;Mohandas et al., 1974). These assays are generally classified according to the nature of the force used in the detachment process and often fall into the categories of micromanipulation, hydrodynamic shear, and centrifugation. While these assays provide quantitative measurements of cell adhesion, most configurations require specialized equipment and/or time- and skill-intensive operation. In contrast, centrifugation assays employ simple and convenient techniques using standard laboratory equipment and provide reliable, quantitative measurements of cell adhesion. In this configuration, a substrate containing adherent cells is spun at a particular speed to apply a controlled detachment force perpendicular to the cell-substrate contact area (Giacomello et al., 1999;Lotz, Burdsal, Erickson, and McClay, 1989;Hertl, Ramsey, and Nowlan, 1984;McClay, Wessel, and Marchase, 1981). The applied detachment force can be varied over a range of speeds and may be applied for selected intervals of time. However, only a single force can be applied per experiment and, in some cases, the cellular attachment strength may exceed the forces developed in the centrifuge system. We describe a modified centrifugation cell adhesion assay that applies controlled and uniform detachment forces to a large population of adherent cells, providing robust statistics for quantifying cell adhesion. The applicability of this system in biomaterials design/characterization is demonstrated by evaluating cell adhesion on substrates using

different adsorbed protein layers, cell types, seeding times, and relative centrifugal forces (RCF). This assay represents a simple, convenient, and standard method for high-throughput characterization of a variety of biomaterial surfaces and conditions.

Materials and Methods

Cells and Reagents

HT1080 human fibrosarcoma cells (CCL-121, American Type Culture Collection, Manassas, VA) were grown in Dulbecco's Modified Eagle medium containing 10% fetal bovine serum and 1% penicillin-streptomycin. MC3T3-E1 murine immature osteoblast-like cells (RIKEN Cell Bank, Tokyo, Japan) were cultured in α-Modified Eagle Medium supplemented with 10% fetal bovine serum and 1% penicillin-streptomycin. Murine NIH3T3 fibroblasts (CRL-1658, American Type Culture Collection) were grown in Dulbecco's Modified Eagle medium containing 10% newborn calf serum and 1% penicillin streptomycin. All cell types were subcultured every two days using standard techniques.

Calcein-AM was obtained from Molecular Probes (Eugene, OR). Bovine serum albumin (BSA) was purchased from Sigma (St. Louis, MO). Bovine type I collagen (Vitrogen-100) was from Cohesion (Palo Alto, CA). Fetal bovine and newborn calf sera were purchased from Hyclone (Logan, UT). Human plasma fibronectin, Dulbecco's phosphate-buffered saline (DPBS) and additional cell culture reagents were obtained from Invitrogen Life Technologies (Carlsbad, CA).

Cell Adhesion Assay

Cell adhesion to protein-coated surfaces was measured using a centrifugation assay that applies controlled detachment forces. Tissue culture polystyrene 96-well plates (Corning 3595) were coated with fibronectin in Dulbecco's phosphate-buffered saline (DPBS) or type I collagen in deionized H_2O for 1 hour at room temperature. The protein coating concentrations started at 10 μg/ml in the top row and followed 1:2 serial dilutions vertically down the plate with the bottom row serving as negative controls with no adsorbed protein. Conditions were replicated in three separate columns on the same microplate. All wells were then blocked in 1% heat-denatured BSA for 1 hour to prevent non-specific cell adhesion.

Near-confluent HT1080, MC3T3-E1, or NIH3T3 cells growing on 100 mm tissue culture plates were rinsed in PBS and incubated in 5 ml of 2 μg/ml calcein-AM, a membrane-permeable fluorescent label, in PBS + 2 mM dextrose for 20 minutes at 37ºC. Cells were then detached in 0.5% trypsin and 0.53 mM EDTA for 3 minutes and resuspended in serum-containing media. After washing and resuspending in PBS-dextrose, cells were seeded onto protein-coated substrates (10,000 cells/well) and allowed to attach for selected time intervals at 22ºC. Each well was then carefully aspirated to remove floating cells and refilled with fresh PBS-dextrose for an initial fluorescence reading to determine the density of cells prior to detachment. The lid was removed and the plate was covered with sealing tape (Nalge Nunc) and centrifuged upside-down at a specified speed for 5 minutes on a Beckman Allegra 6 centrifuge (GH 6.8 rotor) to detach the cells. The wells were carefully aspirated with a Finnpipette electronic multi-channel pipettor set to the slowest flow rate and refilled with fresh PBS-dextrose for a post-spin fluorescence reading to determine the density of remaining adherent cells. Fluorescence

data was obtained from a Perkin Elmer HTS 7000 Plus Bio Assay microwell plate reader (485 nm excitation, 535 nm emission). The post-spin fluorescence data were normalized by the pre-spin data to obtain adherent fractions (f) which were plotted against protein coating concentration (c) or surface density (measured independently with radiolabeled proteins) to determine adhesion profiles. Adhesion profiles were fitted to the following 4-parameter sigmoidal curve to obtain estimates for the protein concentration for half-maximal adhesion (C_{50}) using SigmaPlot (SPSS Science, Chicago, IL):

$$f = f_o + \frac{f_{sat}}{1 + e^{-\left(\frac{c - c_{50}}{b}\right)}} \tag{1}$$

The parameters f_{sat} and b represent the maximum adhesive fraction and the slope of the curve at the inflection point, respectively. The parameter f_o represents background cell adhesion on the negative control surfaces coated with heat-denatured BSA. The parameter C_{50} represents an effective inverse adhesive affinity for the surface and was used as a measure of adhesion strength to compare different surfaces. All experiments were performed in triplicate in three separate runs.

Determining the Relative Centrifugal Force Across the Plate

The shape of the 96-well plate prevents all wells from being completely in line with the plane of rotation. Therefore the relative centrifugal force imposed on the cells varies laterally across the plate according to the following equation:

$$F_C = (\rho_{cell} - \rho_{medium}) \cdot V_{cell} \cdot \omega^2 \sqrt{r_o^2 + x^2} \tag{2}$$

in which F_c is the relative centrifugal force, ρ_{cell} is the specific density of the cell (~1.07 g/cm^3); ρ_{medium} is the specific density of the medium (~ 1 g/cm^3); V_{cell} is the cell volume (~1700 μm^3), r_o is the radius of rotation (determined by the dimensions of the rotor), and

x is the lateral distance from the center of the plate (determined by the column location). The maximum percentage of variation in centrifugal force for a given system can then be calculated according to the equation:

$$\max \%\ change\ in\ F_c = \frac{\sqrt{r_o^2 + x_{\max}{}^2} - r_o}{r_o} \times 100 \qquad (3)$$

in which x_{max} is the maximum lateral distance from the center of the plate (for columns 1 and 12). The centrifuge rotor used in these experiments had a rotation radius, r_o, of 163 mm. The 96-well plate had a maximum lateral distance, x_{max}, of 5 cm. Therefore, according to Eq. 3, the maximum percentage of variation in centrifugal force in these experiments is ~4.3%, which was considered within the experimental error of the assay. However, to avoid biasing the adhesion data, the column numbers were randomized for each replicate and each separate run. As shown in Eq. 3, the rotation radius of the centrifuge rotor used in these experiments determines the variation in relative centrifugal force across the plate. If a rotor with a shorter rotation radius, r_o, was used for this assay, the force variation across the plate might be too large to ignore. In this case, Eq. 2 should be used to calculate the actual centrifugal force imposed on the cells for each column on the 96-well plate. To ensure a relatively uniform force on all cells, the furthermost columns can also be eliminated based on the results from Eq. 2.

Statistics

C_{50} values were analyzed by one-way ANOVA using SYSTAT 8.0 (SPSS). If treatment level differences were determined to be significant, pair-wise comparisons were performed using a Tukey post-hoc test. A 95% confidence level was considered significant.

Results

Cell Adhesion for Multiple Detachment Forces

To verify that this adhesion assay can distinguish differences in the fraction of remaining cells at different detachment forces, HT1080 cells were seeded onto two separate fibronectin-coated plates as described in Materials and Methods. The plates were then centrifuged at two different centrifugation speeds for 5 minutes to detach cells: 500 rpm, and 1000 rpm, which correspond to 45g, and 182g, respectively. The detachment force imposed on the adherent cell layer is proportional to these relative centrifugal forces (*RCF*) according to the following equation:

$$F_D = (\rho_{cell} - \rho_{medium}) \cdot V_{cell} \cdot RCF \qquad (4)$$

in which F_D is the detachment force per cell; ρ_{cell} is the specific density of the cell (1.07 g/cm^3); ρ_{medium} is the specific density of the medium (1.00 g/cm^3); and V_{cell} is the cell volume (~1700 μm^3). **Fig. A.1.a** shows characteristic adhesion profiles depicting sigmoidal increases in the adherent cell fraction as a function of fibronectin surface density. The sigmoid curve follows the expected relationship for a cell population with a normally distributed adhesive capacity. This profile was curve fit to a sigmoid curve in which C_{50} represents the mean inverse cell adhesion affinity and can be used as a measure of adhesion strength. As shown in **Fig. A.1.a**, increases in the applied detachment force result in rightward shifts in the adhesion profile indicating that higher protein concentrations are required for equivalent adhesion levels. In addition, for a given concentration of fibronectin, the fraction of adherent cells decreases with increasing centrifugation force, verifying that this centrifugation assay provides well-

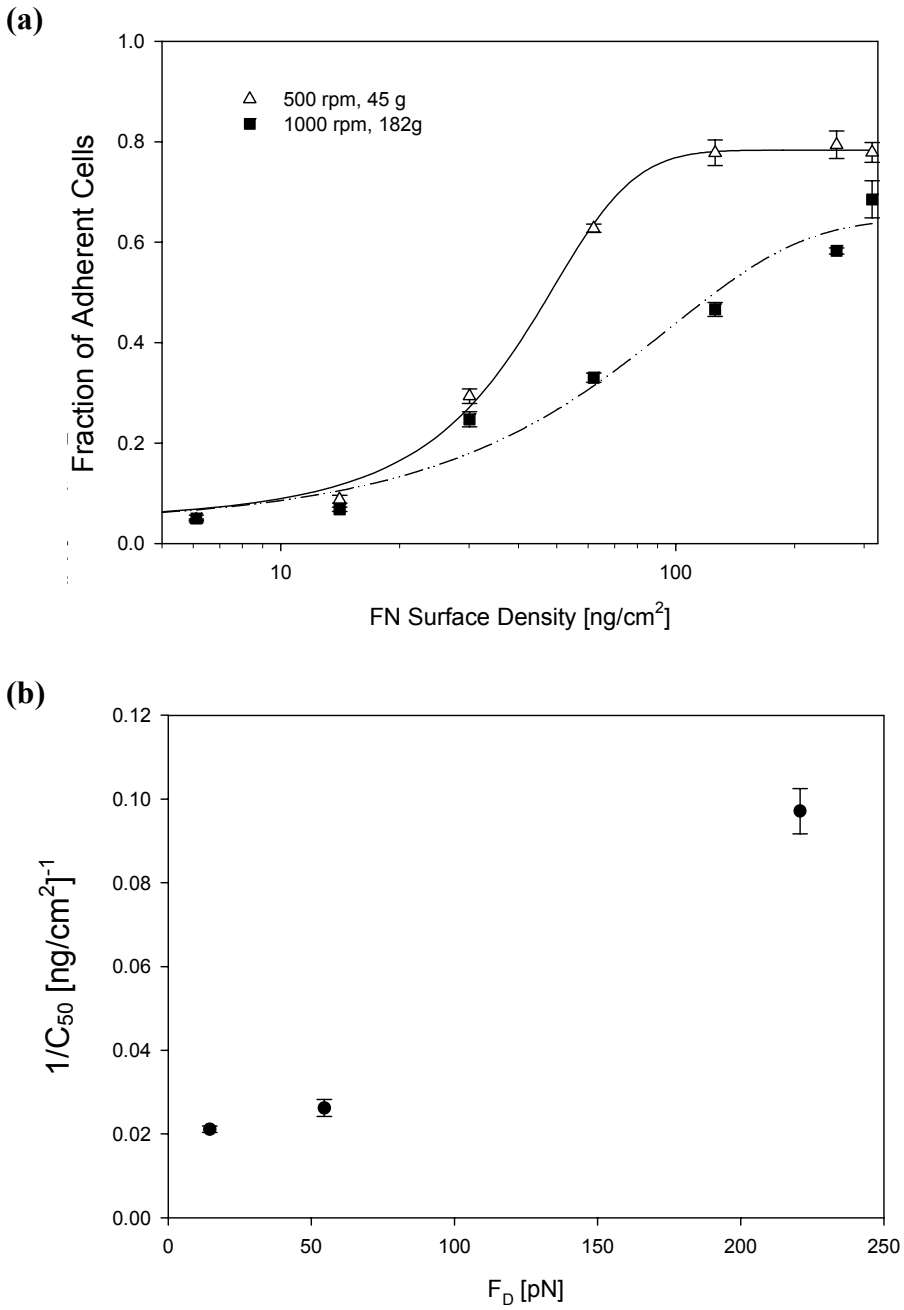

Figure A.1. **(a)** HT1080 cell adhesion to adsorbed fibronectin at two levels of detachment force: 45g and 182g (1 hour cell adhesion, centrifugation for 5 min.). **(b)** Curvefit parameter C_{50} as a function of detachment force (mean ± standard error; three separate experiments in triplicate)

controlled detachment forces that modulate the density of cells remaining on the surface after centrifugation.

A common method of analyzing cell adhesion strength in a centrifugation assay involves generating a plot of the adherent cell fraction as a function of detachment force (Giacomello, Neumayer, Colombatti, and Perris, 1999;Lotz, Burdsal, Erickson, and McClay, 1989;McClay, Wessel, and Marchase, 1981). This method requires a large number of experiments, each performed with a separate plate spun at different centrifugation speeds to generate reasonable curve fit parameters for comparison. The central advantage of the centrifugation assay and analysis presented here lies in its ability to generate reliable measurements of cell adhesion strength in one experiment with a single detachment force, using the cell adhesion parameter, C_{50}. As indicated above, this parameter is related to cell adhesion strength. **Fig. A.1.b** shows decreasing C_{50} values with increasing detachment forces, validating the use of the C_{50} value as a measure of the mean inverse cell adhesion affinity and a reliable indicator of cell adhesion strength. Blocking with antibodies against either fibronectin or fibronectin-specific integrin receptors completely eliminated all adhesion above background (data not shown), demonstrating that this technique specifically evaluates surface-mediated cell adhesion.

Cell Adhesion at Multiple Cell Seeding Times

To demonstrate that this adhesion assay can detect the adhesion strengthening phenomenon that occurs with increased adhesion time(Gallant et al., 2002), HT1080 cells were seeded onto three fibronectin-coated plates and incubated separately for 30 minutes, 1 hour, and 2 hours. At the appropriate seeding time, the plate was centrifuged at 250 rpm (12g) for 5 minutes to detach the cells. **Fig. A.2** shows leftward shifts in the

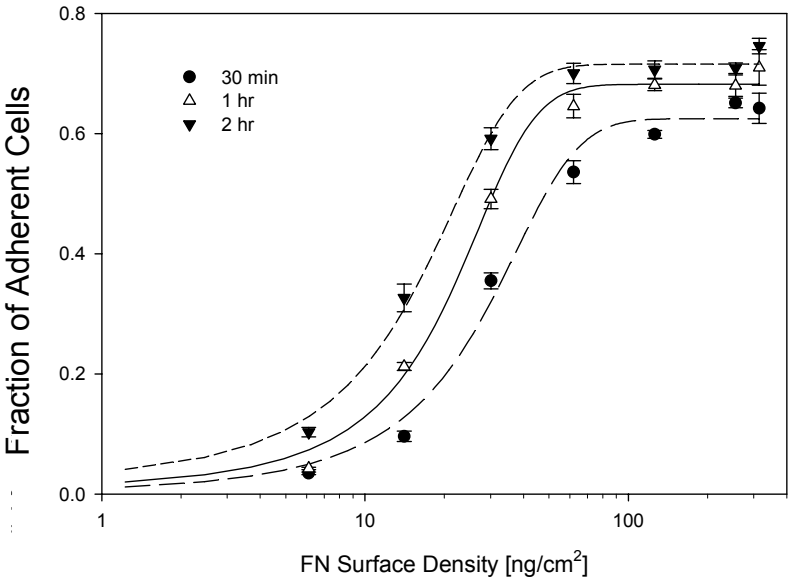

Figure A.2. HT1080 cell adhesion to adsorbed fibronectin at three cell seeding times: 30 minutes, 1 hour, and 2 hours (12g centrifugation for 5 min.). (mean ± standard error; three separate experiments in triplicate)

		Tukey Pairwise Comparison	
	C_{50} (ng/cm^2)	1 hour adhesion	2 hour adhesion
30 min. adhesion	25.1 ± 0.2	$p < 0.002$	$p < 0.0002$
1 hour adhesion	19.6 ± 0.1	-	$p < 0.001$
2 hour adhesion	13.7 ± 0.2	-	-

Table A.1. C_{50} values for HT1080 cell adhesion to adsorbed fibronectin for 3 minutes, 1 hour, and 2 hours (12g centrifugation for 5 min.). (mean ± standard error; three separate experiments in triplicate)

adhesion profiles with increasing adhesion time, resulting in decreasing C_{50} values with increased adhesion time. These leftward shifts indicate higher adhesion at lower fibronectin densities, demonstrating increasing cell adhesion strength with increasing adhesion time. Statistical analyses revealed significant differences in adhesion strength, as determined by C_{50} values, between the different cell seeding times (**Table A.1**). In addition, at any given fibronectin concentration, an increase in the fraction of adherent cells is evident with increasing cell adhesion time, verifying that this adhesion assay can resolve differences in cell adhesion strength as a result of time-dependent adhesion strengthening.

Cell Adhesion to Different Proteins

To confirm that this centrifugation assay can screen different adhesion substrates in a single experiment, three columns of a 96-well plate were coated with fibronectin and three columns were coated with type I collagen. HT1080 cells were seeded simultaneously on both protein layers and incubated for 1 hour. The plate was then centrifuged at 250 rpm (12g) for 5 minutes to detach the cells. **Fig. A.3** shows the adhesion profiles for these cells on the two protein-coated surfaces, revealing differences in adhesion based on the different receptor-ligand interactions characteristic of these two systems. These results verify that this adhesion assay can resolve differences in cell adhesion on multiple adhesion substrates.

Adhesion of Various Cell Models

All previous experiments were performed using HT1080 human fibrosarcoma cells. To demonstrate the versatility of this assay, adhesion experiments were also performed using two other cell models: NIH3T3 fibroblasts and MC3T3-E1 immature

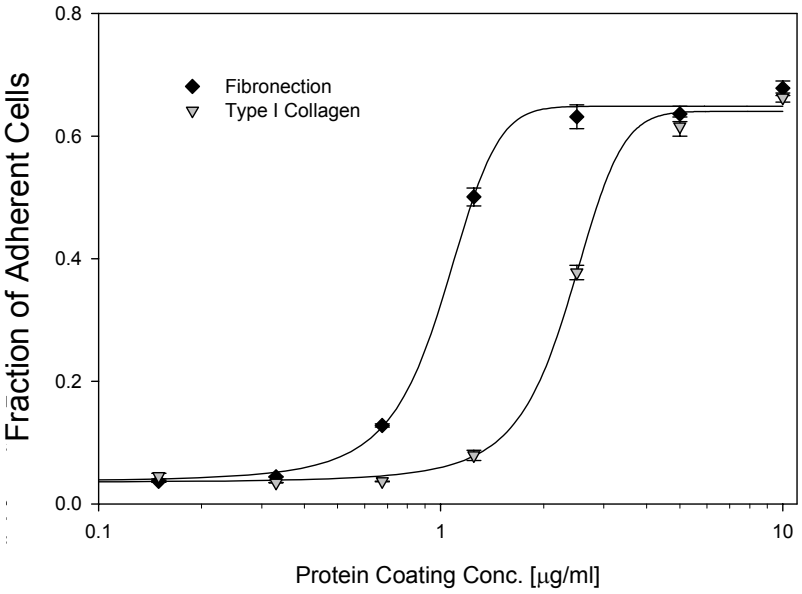

Figure A.3. HT1080 cell adhesion to adsorbed fibronectin and adsorbed type I collagen (1 hour cell adhesion, 12g centrifugation for 5 min.). (mean ± standard error; three separate experiments in triplicate)

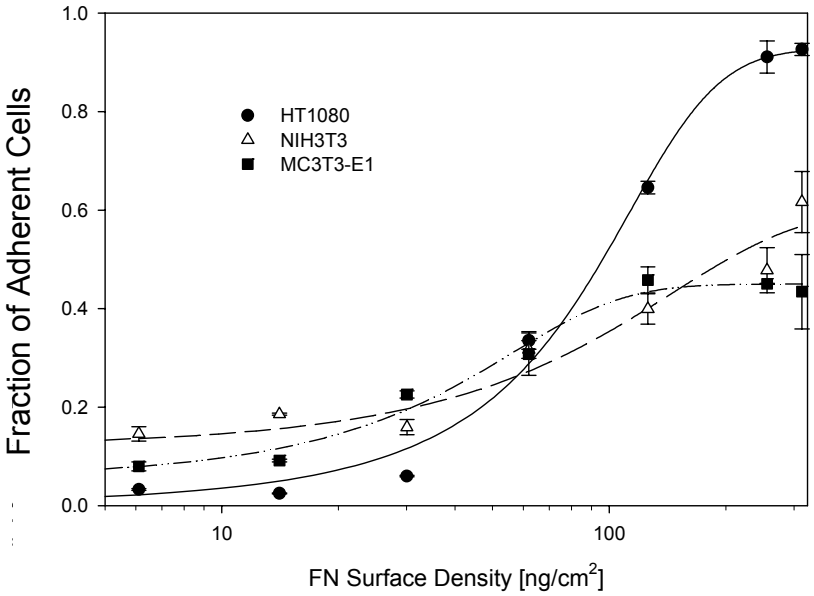

Figure A.4. HT1080, NIH3T3, and MC3T3-E1 cell adhesion to adsorbed fibronectin (1 hour cell adhesion, 12g centrifugation for 5 min.). (mean ± standard error; three separate experiments in triplicate)

osteoblast-like cells. All three cell types were seeded onto a single plate coated with fibronectin. The plate was then centrifuged at 250 rpm (12g) for 5 minutes to detach the cells. **Fig. A.4** demonstrates unique adhesion profiles for the three cell models, verifying that this adhesion assay can screen multiple cell types in one experiment.

Discussion

This paper describes a simple protocol for a centrifugation cell adhesion assay that applies controlled and steady detachment forces normal to the growth surface and quantifies cell density before and after the force application. The ease and convenience of this assay underscores its relevance to the initial design, evaluation, and comparison of a variety of surfaces for biomaterials and tissue engineering applications. It requires neither the construction nor characterization of a specific hydrodynamic environment, as would be the case with any flow assay, yet provides sensitive and reproducible measurements, unlike the commonly used yet uncontrolled wash assay. Following centrifugation, the fraction of adherent cells is plotted as a function of ligand concentration to obtain the adhesion profile characteristic of a given cell model and test surface. As demonstrated in the present analysis, curve fitting to a sigmoidal profile (adherent fraction vs. ligand density) provides robust measurements of adhesion strength that allow for direct comparisons among treatments. The curve-fit parameter C_{50} (see Eq. 1), the concentration of protein required for 50% maximal adhesion, represents a reliable measurement of cell adhesion. This value is less sensitive to variations among separate experimental runs than the absolute fluorescence levels and thus is most appropriate for statistical comparisons across experiments.

We have verified that this centrifugation assay can apply various detachment forces for *in vitro* studies of adhesion. For analytical purposes, a cell adhesion assay must also provide a simple system in which the environment, the cell model, and the substratum surface may be varied in a well-defined manner. Experiments with different adsorbed protein layers and different cell models demonstrate that this centrifugation assay is capable of evaluating multiple cell-surface combinations on a single 96-well plate. We have recently used this assay to analyze cell adhesion to biomimetic surfaces (Reyes and Garcia, 2002) and substrates of varying surface chemistry (Keselowsky et al., 2002). Therefore this assay can distinguish differences in adhesion among different types of cells and surfaces under various conditions of growth and chemical environment, allowing high-throughput screening of various biomaterials surfaces and coatings as well as engineered protein and peptide surface layers. In addition to cell type and surface conditions, the time-dependent adhesion strengthening may also be of interest in evaluating cell-surface interactions. Several morphological and biochemical changes, including cell spreading, focal adhesion formation, and stress fiber assembly, occur over time as cells adhere to the underlying substratum (Burridge and Chrzanowska-Wodnicka, 1996;Lotz, Burdsal, Erickson, and McClay, 1989). Adhesion experiments with multiple cell seeding times demonstrate that this centrifugation assay can resolve differences in adhesion profiles due to time-dependent adhesion strengthening. However, subsequent experiments suggest that the assay loses sensitivity for longer adhesion times (>2 hrs). This limitation most likely results from the centrifuge's inability to generate a high enough detachment force to isolate an accurate adhesion profile for cells that have been seeded for extended periods of time.

In summary, this centrifugation adhesion assay proves a flexible tool for quantitatively examining the adhesive properties of cells seeded on various substrates under controlled detachment conditions. The adhesion profiles generated from this assay allow the efficient comparison of multiple biomaterial surface treatments and protein coatings relevant to cell culture applications as well as biomaterial surface modifications and tissue engineering scaffold design.

Reference List

Agrawal,C.M., Pennick,A., Wang,X., and Schenck,R.C. 1997. Porous-coated titanium implant impregnated with a biodegradable protein delivery system. *J Biomed. Mater. Res.* 36:516-521.

Akiyama,S.K., Aota,S., and Yamada,K.M. 1995. Function and receptor specificity of a minimal 20 kilodalton cell adhesive fragment of fibronectin. *Cell Adhes. Commun.* 3:13-25.

Alsberg,E., Anderson,K.W., Albeiruti,A., Rowley,J.A., and Mooney,D.J. 2002a. Engineering growing tissues. *Proc. Natl. Acad. Sci. U. S. A* 99:12025-12030.

Alsberg,E., Anderson,K.W., Albeiruti,A., Rowley,J.A., and Mooney,D.J. 2002b. Engineering growing tissues. *Proc. Natl. Acad. Sci. U. S. A* 99:12025-12030.

American Academy of Orthopaedic Surgeons. Arthoplasty and Total Joint Replacement Procedures.

Anderson,J.M. 2001. Biological responses to materials. *Annu. Rev. Mater. Res.* 31:81-110.

Anderson,R.C., Cook,S.D., Weinstein,A.M., and Haddad,R.J., Jr. 1984. An evaluation of skeletal attachment to LTI pyrolytic carbon, porous titanium, and carbon-coated porous titanium implants. *Clin. Orthop. Relat Res.* 242-257.

Aota,S., Nomizu,M., and Yamada,K.M. 1994a. The short amino acid sequence Pro-His-Ser-Arg-Asn in human fibronectin enhances cell-adhesive function. *J. Biol. Chem.* 269:24756-24761.

Aota,S., Nomizu,M., and Yamada,K.M. 1994b. The short amino acid sequence Pro-His-Ser-Arg-Asn in human fibronectin enhances cell-adhesive function. *J. Biol. Chem.* 269:24756-24761.

Arthritis Foundation, and CDC. 1999. National Arthritis Action Plan: A Public Health Strategy.

Athanasou,N.A. 1996. Cellular biology of bone-resorbing cells. *J. Bone Joint Surg.* 78-A:1096-1112.

Aubin,J.E., and Liu,F. 1996. The osteoblast lineage. *In* Principles of Bone Biology. J.P.Bilezikian, L.G.Raisz, and G.A.Rodan, editors. Academic Press, New York. 51-67.

Banerjee,C., Javed,A., Choi,J.Y., Green,J., Rosen,V., van Wijnen,A.J., Stein,J.L., Lian,J.B., and Stein,G.S. 2001a. Differential regulation of the two principal Runx2/Cbfa1 n-terminal isoforms in response to bone morphogenetic protein-2 during development of the osteoblast phenotype. *Endocrinology* 142:4026-4039.

Bauer,T.W., and Schils,J. 1999a. The pathology of total joint arthroplasty. I. Mechanisms of implant fixation. *Skeletal Radiol.* 28:423-432.

Becker,D., Geissler,U., Hempel,U., Bierbaum,S., Scharnweber,D., Worch,H., and Wenzel,K.W. 2002. Proliferation and differentiation of rat calvarial osteoblasts on type I collagen-coated titanium alloy. *J. Biomed. Mater. Res.* 59:516-527.

Benson,M.D., Aubin,J.E., Xiao,G., Thomas,P.E., and Franceschi,R.T. 1999. Cloning of a 2.5 kb murine bone sialoprotein promoter fragment and functional analysis of putative Osf2 binding sites. *J. Bone Miner. Res.* 14:396-405.

Bernhardt,R., van den,D.J., Bierbaum,S., Beutner,R., Scharnweber,D., Jansen,J., Beckmann,F., and Worch,H. 2005. Osteoconductive modifications of Ti-implants in a goat defect model: characterization of bone growth with SR muCT and histology. *Biomaterials* 26:3009-3019.

Bobyn,J.D., Pilliar,R.M., Cameron,H.U., Weatherly,G.C., and Kent,G.M. 1980. The effect of porous surface configuration on the tensile strength of fixation of implants by bone ingrowth. *Clin. Orthop. Relat Res.* 291-298.

Boone,P.S., Zimmerman,M.C., Gutteling,E., Lee,C.K., Parsons,J.R., and Langrana,N. 1989. Bone attachment to hydroxyapatite coated polymers. *J Biomed. Mater. Res.* 23:183-199.

Boyan,B.D., Hummert,T.W., Dean,D.D., and Schwartz,Z. 1996. Role of material surfaces in regulating bone and cartilage cell response. *Biomaterials* 17:137-146.

Boyan,B.D., Lossdorfer,S., Wang,L., Zhao,G., Lohmann,C.H., Cochran,D.L., and Schwartz,Z. 2003. Osteoblasts generate an osteogenic microenvironment when grown on surfaces with rough microtopographies. *Eur. Cell Mater.* 6:22-27.

Branemark,R. 1996. A biomechanical study of osseointegration: In-vivo measurements in rat, rabbit, dog, and man. Goteborg University, 1-89.

Branemark,R., Ohrnell,L.O., Nilsson,P., and Thomsen,P. 1997. Biomechanical characterization of osseointegration during healing: an experimental in vivo study in the rat. *Biomaterials* 18:969-978.

Branemark,R., Ohrnell,L.O., Skalak,R., Carlsson,L., and Branemark,P.I. 1998. Biomechanical characterization of osseointegration: an experimental in vivo investigation in the beagle dog. *J Orthop. Res.* 16:61-69.

Broberg,A., Nissinen,L., Potila,M., and Heino,J. 2001. Three-dimensional collagen regulates collagen gene expression by a mechanism that requires serine/threonine kinases and is independent of mechanical contraction. *Biochem. Biophys. Res. Commun.* 280:328-333.

Buckwalter,J.A., Glimcher,M.H., Cooper,R.R., and Recker,R. 1995a. Bone biology. Part I: Structure, blood supply, cells, matrix and mineralization. *J Bone Joint Surg.* 77-A:1256-1275.

Buckwalter,J.A., Glimcher,M.H., Cooper,R.R., and Recker,R. 1995b. Bone biology. Part II: Formation, form, modeling, remodeling, and regulation of cell function. *J Bone Joint Surg.* 77-A:1276-1289.

Bundy,K.J., Harris,L.G., Rahn,B.A., and Richards,R.G. 2001. Measurement of fibroblast and bacterial detachment from biomaterials using jet impingement. *Cell Biol. Int.* 25:289-307.

Burridge,K., and Chrzanowska-Wodnicka,M. 1996. Focal adhesions, contractility, and signaling. *Annu. Rev. Cell Dev. Biol.* 12:463-518.

Buser,D., Schenk,R.K., Steinemann,S., Fiorellini,J.P., Fox,C.H., and Stich,H. 1991. Influence of surface characteristics on bone integration of titanium implants. A histomorphometric study in miniature pigs. *J Biomed. Mater. Res.* 25:889-902.

Byers,B.A., Pavlath,G.K., Murphy,T.J., Karsenty,G., and Garcia,A.J. 2002a. Cell-type-dependent up-regulation of in vitro mineralization after overexpression of the osteoblast-specific transcription factor Runx2/Cbfal. *J. Bone Miner. Res.* 17:1931-1944.

Calalb,M.B., Zhang,X., Polte,T.R., and Hanks,S.K. 1996. Focal adhesion kinase tyrosine-861 is a major site of phosphorylation by Src. *Biochem. Biophys. Res. Commun.* 228:662-668.

Cardarelli,P.M., Yamagata,S., Taguchi,I., Gorcsan,F., Chiang,S.L., and Lobl,T. 1992. The collagen receptor alpha 2 beta 1, from MG-63 and HT1080 cells, interacts with a cyclic RGD peptide. *J. Biol. Chem.* 267:23159-23164.

Cheng,S.L., Lai,C.F., Blystone,S.D., and Avioli,L.V. 2001. Bone mineralization and osteoblast differentiation are negatively modulated by integrin alpha(v)beta3. *J Bone Miner Res* 16:277-288.

Chesla,S.E., Selvaraj,P., and Zhu,C. 1998. Measuring two-dimensional receptor-ligand binding kinetics by micropipette. *Biophys. J.* 75:1553-1572.

Choi,J.Y., Lee,B.H., Song,K.B., Park,R.W., Kim,I.S., Sohn,K.Y., Jo,J.S., and Ryoo,H.M. 1996. Expression patterns of bone-related proteins during osteoblastic differentiation in MC3T3-E1 cells. *J. Cell Biochem.* 61:609-618.

Clark,E.A., and Brugge,J.S. 1995. Integrins and signal transduction pathways: the road taken. *Science* 268:233-239.

Clemow,A.J., Weinstein,A.M., Klawitter,J.J., Koeneman,J., and Anderson,J. 1981. Interface mechanics of porous titanium implants. *J Biomed. Mater. Res.* 15:73-82.

Cook,S.D., Walsh,K.A., and Haddad,R.J., Jr. 1985. Interface mechanics and bone growth into porous Co-Cr-Mo alloy implants. *Clin. Orthop. Relat Res.* 271-280.

Danen,E.H., Aota,S., van Kraats,A.A., Yamada,K.M., Ruiter,D.J., and van Muijen,G.N. 1995. Requirement for the synergy site for cell adhesion to fibronectin depends on the activation state of integrin alpha 5 beta 1. *J. Biol. Chem.* 270:21612-21618.

De Arcangelis,A., and Georges-Labouesse,E. 2000a. Integrin and ECM functions: roles in vertebrate development. *Trends Genet* 16:389-395.

de,G.K., Geesink,R., Klein,C.P., and Serekian,P. 1987. Plasma sprayed coatings of hydroxylapatite. *J Biomed. Mater. Res.* 21:1375-1381.

Dee,K.C., Andersen,T.T., and Bizios,R. 1998. Design and function of novel osteoblast-adhesive peptides for chemical modification of biomaterials. *J. Biomed. Mater. Res.* 40:371-377.

Dee,K.C., Rueger,D.C., Andersen,T.T., and Bizios,R. 1996. Conditions which promote mineralization at the bone-implant interface: a model in vitro study. *Biomaterials* 17:209-215.

Dhert,W.J., Klein,C.P., Wolke,J.G., van,d., V, de,G.K., and Rozing,P.M. 1991. A mechanical investigation of fluorapatite, magnesiumwhitlockite, and hydroxylapatite plasma-sprayed coatings in goats. *J Biomed. Mater. Res.* 25:1183-1200.

Dhert,W.J., Verheyen,C.C., Braak,L.H., de,W., Jr., Klein,C.P., de,G.K., and Rozing,P.M. 1992. A finite element analysis of the push-out test: influence of test conditions. *J Biomed. Mater. Res.* 26:119-130.

Di Lullo,G.A., Sweeney,S.M., Korkko,J., Ala-Kokko,L., and San Antonio,J.D. 2002. Mapping the ligand-binding sites and disease-associated mutations on the most abundant protein in the human, type I collagen. *J. Biol. Chem.* 277:4223-4231.

Disegi,J.A. 2000. Titanium alloys for fracture fixation implants. *Injury* 31 Suppl 4:14-17.

Disegi,J.A., and Eschbach,L. 2000. Stainless steel in bone surgery. *Injury* 31 Suppl 4:2-6.

Doroszewski,J., Skierski,J., and Przadka,L. 1977. Interaction of neoplastic cells with glass surface under flow conditions. *Exp. Cell Res.* 104:335-343.

Ducheyne,P., and Cuckler,J.M. 1992. Bioactive ceramic prosthetic coatings. *Clin. Orthop.* 276:102-114.

Ducheyne,P., De,M.P., and Aernoudt,E. 1977. Influence of a functional dynamic loading on bone ingrowth into surface pores of orthopedic implants. *J Biomed. Mater. Res.* 11:811-838.

Ducheyne,P., and Qiu,Q. 1999. Bioactive ceramics: the effect of surface reactivity on bone formation and bone cell function. *Biomaterials* 20:2287-2303.

Ducy,P., and Karsenty,G. 1995. Two distinct osteoblast-specific cis-acting elements control expression of a mouse osteocalcin gene. *Mol. Cell Biol.* 15:1858-1869.

Eid,K., Chen,E., Griffith,L., and Glowacki,J. 2001. Effect of RGD coating on osteocompatibility of PLGA-polymer disks in a rat tibial wound. *J Biomed Mater Res* 57:224-231.

Elmengaard,B., Bechtold,J.E., and Soballe,K. 2005b. In vivo effects of RGD-coated titanium implants inserted in two bone-gap models. *J. Biomed. Mater. Res. A* 75:249-255.

Elmengaard,B., Bechtold,J.E., and Soballe,K. 2005a. In vivo study of the effect of RGD treatment on bone ongrowth on press-fit titanium alloy implants. *Biomaterials* 26:3521-3526.

Emsley,J., Knight,C.G., Farndale,R.W., Barnes,M.J., and Liddington,R.C. 2000. Structural basis of collagen recognition by integrin alpha2beta1. *Cell* 101:47-56.

Evans,E., Berk,D., and Leung,A. 1991. Detachment of agglutinin-bonded red blood cells. I. Forces to rupture molecular-point attachments. *Biophys. J.* 59:838-848.

Feighan,J.E., Goldberg,V.M., Davy,D., Parr,J.A., and Stevenson,S. 1995. The influence of surface-blasting on the incorporation of titanium-alloy implants in a rabbit intramedullary model. *J Bone Joint Surg. Am.* 77:1380-1395.

Ferris,D.M., Moodie,G.D., Dimond,P.M., Gioranni,C.W., Ehrlich,M.G., and Valentini,R.F. 1999a. RGD-coated titanium implants stimulate increased bone formation in vivo. *Biomaterials* 20:2323-2331.

Fields,G.B., and Prockop,D.J. 1996. Perspectives on the synthesis and application of triple-helical, collagen-model peptides. *Biopolymers* 40:345-357.

Galante,J.O., and Jacobs,J. 1992. Clinical performances of ingrowth surfaces. *Clin. Orthop. Relat Res.* 41-49.

Gallant,N.D., Capadona,J.R., Frazier,A.B., Collard,D.M., and Garcia,A.G. 2002. Micropatterned surfaces to engineer focal adhesions for analysis of cell adhesion strengthening. *Langmuir* 18:5579-5584.

Garcia,A.J., and Boettiger,D. 1999. Integrin-fibronectin interactions at the cell-material interface: initial integrin binding and signaling. *Biomaterials* 20:2427-2433.

Garcia,A.J., Ducheyne,P., and Boettiger,D. 1997. Quantification of cell adhesion using a spinning disc device and application to surface-reactive materials. *Biomaterials* 18:1091-1098.

Garcia,A.J., Schwarzbauer,J.E., and Boettiger,D. 2002. Distinct activation states of alpha5beta1 integrin show differential binding to RGD and synergy domains of fibronectin. *Biochemistry* 41:9063-9069.

Geissler,U., Hempel,U., Wolf,C., Scharnweber,D., Worch,H., and Wenzel,K. 2000. Collagen type I-coating of Ti6Al4V promotes adhesion of osteoblasts. *J Biomed. Mater. Res.* 51:752-760.

Giacomello,E., Neumayer,J., Colombatti,A., and Perris,R. 1999. Centrifugal assay for fluorescence-based cell adhesion adapted to the analysis of ex vivo cells and capable of determining relative binding strengths. *Biotechniques* 26:758-6.

Globus,R.K., Doty,S.B., Lull,J.C., Holmuhamedov,E., Humphries,M.J., and Damsky,C.H. 1998. Fibronectin is a survival factor for differentiated osteoblasts. *J. Cell Sci.* 111 (Pt 10):1385-1393.

Goodman,M., Bhumralkar, Jefferson,E.A., Kwak,J., and Locardi,E. 1998. Collagen mimetics. *Biopolymers* 47:127-142.

Gotfredsen,K., Nimb,L., Hjorting-Hansen,E., Jensen,J.S., and Holmen,A. 1992. Histomorphometric and removal torque analysis for TiO2-blasted titanium implants. An experimental study on dogs. *Clin. Oral Implants. Res.* 3:77-84.

Grabarek,Z., and Gergely,J. 1990. Zero-length crosslinking procedure with the use of active esters. *Anal. Biochem.* 185:131-135.

Grenz,H., Carbonetto,S., and Goodman,S.L. 1993. Alpha 3 beta 1 integrin is moved into focal contacts in kidney mesangial cells. *J. Cell Sci.* 105 (Pt 3):739-751.

Groessner-Schreiber,B., and Tuan,R.S. 1992. Enhanced extracellular matrix production and mineralization by osteoblasts cultured on titanium surfaces in vitro. *J Cell Sci.* 101 (Pt 1):209-217.

Gronthos,S., Stewart,K., Graves,S.E., Hay,S., and Simmons,P.J. 1997. Integrin expression and function on human osteoblast-like cells. *J. Bone Miner. Res.* 12:1189-1197.

Guan,J.L. 1997. Role of focal adhesion kinase in integrin signaling. *Int. J. Biochem. Cell Biol.* 29:1085-1096.

Hahn,H., and Palich,W. 1970. Preliminary evaluation of porous metal surfaced titanium for orthopedic implants. *J Biomed. Mater. Res.* 4:571-577.

Harrigan,T.P., Kareh,J., and Harris,W.H. 1990. The influence of support conditions in the loading fixture on failure mechanisms in the push-out test: a finite element study. *J Orthop. Res.* 8:678-684.

Heck,D.A., Nakajima,I., Kelly,P.J., and Chao,E.Y. 1986. The effect of load alteration on the biological and biomechanical performance of a titanium fiber-metal segmental prosthesis. *J Bone Joint Surg. Am.* 68:118-126.

Heino,J. 2000. The collagen receptor integrins have distinct ligand recognition and signaling functions. *Matrix Biol.* 19:319-323.

Hersel,U., Dahmen,C., and Kessler,H. 2003. RGD modified polymers: biomaterials for stimulated cell adhesion and beyond. *Biomaterials* 24:4385-4415.

Hertl,W., Ramsey,W.S., and Nowlan,E.D. 1984. Assessment of cell-substrate adhesion by a centrifugal method. *In Vitro* 20:796-801.

Horbett,T.A. 1996. Proteins: Structure, Properties, and Adsorption to Surfaces. *In* Biomaterials Science: An Introduction to Materials in Medicine. B.D.Ratner, A.S.Hoffman, F.J.Shoen, and J.E.Lemons, editors. Academic Press, San Diego. 133-141.

Horbett,T.A., and Brash,J.L. 1987. Proteins at interfaces: current issues and future prospects. *In* Proteins at interfaces: physiochemical and biochemical studies. J.L.Brash, and T.A.Horbett, editors. American Chemical Society, Washington, D.C. 1-80.

Horbett,T.A., Waldburger,J.J., Ratner,B.D., and Hoffman,A.S. 1988. Cell adhesion to a series of hydrophilic-hydrophobic copolymers studied with a spinning disc apparatus. *J. Biomed. Mater. Res.* 22:383-404.

Hubbell,J.A. 2004a. Biomaterials science and high-throughput screening. *Nat. Biotechnol* 22:828-829.

Hubbell,J.A. 1999. Bioactive biomaterials. *Curr. Opin. Biotechnol.* 10:123-129.

Hunter,G.K., Hauschka,P.V., Poole,A.R., Rosenberg,L.C., and Goldberg,H.A. 1996. Nucleation and inhibition of hydroxyapatite formation by mineralized tissue proteins. *Biochem. J.* 317:59-64.

Hynes,R.O. 1992. Integrins: versatility, modulation, and signaling in cell adhesion. *Cell* 69:11-25.

Hynes,R.O. 2002. Integrins: bidirectional, allosteric signaling machines. *Cell* 110:673-687.

Ikeuchi,M., Dohi,Y., Horiuchi,K., Ohgushi,H., Noshi,T., Yoshikawa,T., Yamamoto,K., and Sugimura,M. 2002. Recombinant human bone morphogenetic protein-2 promotes osteogenesis within atelopeptide type I collagen solution by combination with rat cultured marrow cells. *J. Biomed. Mater. Res.* 60:61-69.

Ivanoff,C.J., Sennerby,L., and Lekholm,U. 1996. Influence of mono- and bicortical anchorage on the integration of titanium implants. A study in the rabbit tibia. *Int. J Oral Maxillofac. Surg.* 25:229-235.

Jikko,A., Harris,S.E., Chen,D., Mendrick,D.L., and Damsky,C.H. 1999. Collagen integrin receptors regulate early osteoblast differentiation induced by BMP-2. *J. Bone Miner. Res.* 14:1075-1083.

Joos,U., Wiesmann,H.P., Szuwart,T., and Meyer,U. 2006. Mineralization at the interface of implants. *Int. J Oral Maxillofac. Surg.*

Kapyla,J., Ivaska,J., Riikonen,R., Nykvist,P., Pentikainen,O., Johnson,M., and Heino,J. 2000. Integrin alpha(2)I domain recognizes type I and type IV collagens by different mechanisms. *J. Biol. Chem.* 275:3348-3354.

Keselowsky,B.G., Collard,D.M., and Garcia,A.J. 2005a. Integrin binding specificity regulates biomaterial surface chemistry effects on cell differentiation. *Proc. Natl. Acad. Sci. U. S. A* 102:5953-5957.

Kieswetter,K., Schwartz,Z., Dean,D.D., and Boyan,B.D. 1996. The role of implant surface characteristics in the healing of bone. *Crit. Rev. Oral Biol. Med.* 7:329-345.

Klein,C.P., Patka,P., van der Lubbe,H.B., Wolke,J.G., and de,G.K. 1991. Plasma-sprayed coatings of tetracalciumphosphate, hydroxyl-apatite, and alpha-TCP on titanium alloy: an interface study. *J Biomed. Mater. Res.* 25:53-65.

Knight,C.G., Morton,L.F., Onley,D.J., Peachey,A.R., Messent,A.J., Smethurst,P.A., Tuckwell,D.S., Farndale,R.W., and Barnes,M.J. 1998. Identification in collagen type I of an integrin alpha2 beta1-binding site containing an essential GER sequence. *J. Biol. Chem.* 273:33287-33294.

Knight,C.G., Morton,L.F., Peachey,A.R., Tuckwell,D.S., Farndale,R.W., and Barnes,M.J. 2000. The collagen-binding A-domains of integrins alpha(1)beta(1) and alpha(2)beta(1) recognize the same specific amino acid sequence, GFOGER, in native (triple-helical) collagens. *J. Biol. Chem.* 275:35-40.

Lahiri,J., Isaacs,L., Tien,J., and Whitesides,G.M. 1999. A strategy for the generation of surfaces presenting ligands for studies of binding based on an active ester as a common reactive intermediate: a surface plasmon resonance study. *Anal. Chem.* 71:777-790.

Lai,C.F., Chaudhary,L., Fausto,A., Halstead,L.R., Ory,D.S., Avioli,L.V., and Cheng,S.L. 2001. Erk is essential for growth, differentiation, integrin expression, and cell function in human osteoblastic cells. *J. Biol. Chem.* 276:14443-14450.

Lawrence,M.B., McIntire,L.V., and Eskin,S.G. 1987. Effect of flow on polymorphonuclear leukocyte/endothelial cell adhesion. *Blood* 70:1284-1290.

Lee,T.M., Wang,B.C., Yang,Y.C., Chang,E., and Yang,C.Y. 2001. Comparison of plasma-sprayed hydroxyapatite coatings and hydroxyapatite/tricalcium phosphate composite coatings: in vivo study. *J Biomed. Mater. Res.* 55:360-367.

Lee,T.M., Yang,C.Y., Chang,E., and Tsai,R.S. 2004. Comparison of plasma-sprayed hydroxyapatite coatings and zirconia-reinforced hydroxyapatite composite coatings: in vivo study. *J Biomed. Mater. Res. A* 71:652-660.

Lehninger,A.L., Nelson,D.L., and Cox,M.M. 1993. Principles of Biochemistry. Worth Publishers, New York, NY.

Leng,J., Klemke,R.L., Reddy,A.C., and Cheresh,D.A. 1999. Potentiation of cell migration by adhesion-dependent cooperative signals from the GTPase Rac and Raf kinase. *J. Biol. Chem.* 274:37855-37861.

Li,D., Ferguson,S.J., Beutler,T., Cochran,D.L., Sittig,C., Hirt,H.P., and Buser,D. 2002. Biomechanical comparison of the sandblasted and acid-etched and the machined and acid-etched titanium surface for dental implants. *J Biomed. Mater. Res.* 60:325-332.

Li,F., Carlsson,D., Lohmann,C., Suuronen,E., Vascotto,S., Kobuch,K., Sheardown,H., Munger,R., Nakamura,M., and Griffith,M. 2003. Cellular and nerve regeneration within a biosynthetic extracellular matrix for corneal transplantation. *Proc. Natl. Acad. Sci. U. S. A* 100:15346-15351.

Lossdorfer,S., Schwartz,Z., Wang,L., Lohmann,C.H., Turner,J.D., Wieland,M., Cochran,D.L., and Boyan,B.D. 2004. Microrough implant surface topographies increase osteogenesis by reducing osteoclast formation and activity. *J Biomed. Mater. Res. A* 70:361-369.

Lotz,M.M., Burdsal,C.A., Erickson,H.P., and McClay,D.R. 1989. Cell adhesion to fibronectin and tenascin: quantitative measurements of initial binding and subsequent strengthening response. *J. Cell Biol.* 109:1795-1805.

Lutolf,M.P., and Hubbell,J.A. 2005. Synthetic biomaterials as instructive extracellular microenvironments for morphogenesis in tissue engineering. *Nat. Biotechnol.* 23:47-55.

Lynch,M.P., Stein,J.L., Stein,G.S., and Lian,J.B. 1995. The influence of type I collagen on the development and maintenance of the osteoblast phenotype in primary and passaged rat calvarial osteoblasts: modification of expression of genes supporting

cell growth, adhesion, and extracellular matrix mineralization. *Exp. Cell Res.* 216:35-45.

Maniatopoulos,C., Sodek,J., and Melcher,A.H. 1988. Bone formation in vitro by stromal cells obtained from bone marrow of young adult rats. *Cell Tissue Res.* 254:317-330.

Marks,Jr.S.C., and Hermey,D.C. 1996. The Structure and Development of Bone. *In* Principles of Bone Biology. J.P.Bilezikian, L.G.Raisz, and G.A.Rodan, editors. Academic Press, New York. 3-14.

Marti,A. 2000. Cobalt-base alloys used in bone surgery. *Injury* 31 Suppl 4:18-21.

Martin,J.Y., Schwartz,Z., Hummert,T.W., Schraub,D.M., Simpson,J., Lankford,J., Jr., Dean,D.D., Cochran,D.L., and Boyan,B.D. 1995. Effect of titanium surface roughness on proliferation, differentiation, and protein synthesis of human osteoblast-like cells (MG63). *J Biomed. Mater. Res.* 29:389-401.

McCarthy,J.B., Vachhani,B., and Iida,J. 1996. Cell adhesion to collagenous matrices. *Biopolymers* 40:371-381.

McClay,D.R., Wessel,G.M., and Marchase,R.B. 1981. Intercellular recognition: quantitation of initial binding events. *Proc. Natl. Acad. Sci. U. S. A* 78:4975-4979.

Messent,A.J., Tuckwell,D.S., Knauper,V., Humphries,M.J., Murphy,G., and Gavrilovic,J. 1998. Effects of collagenase-cleavage of type I collagen on alpha2beta1 integrin-mediated cell adhesion. *J. Cell Sci.* 111 (Pt 8):1127-1135.

Mizuno,M., Fujisawa,R., and Kuboki,Y. 2000. Type I collagen-induced osteoblastic differentiation of bone-marrow cells mediated by collagen-alpha2beta1 integrin interaction. *J. Cell Physiol* 184:207-213.

Mizuno,M., and Kuboki,Y. 2001. Osteoblast-related gene expression of bone marrow cells during the osteoblastic differentiation induced by type I collagen. *J. Biochem. (Tokyo)* 129:133-138.

Mohandas,N., Hochmuth,R.M., and Spaeth,E.E. 1974. Adhesion of red cells to foreign surfaces in the presence of flow. *J. Biomed. Mater. Res.* 8:119-136.

Morra,M., and Cassinelli,C. 1997. Organic surface chemistry on titanium surfaces via thin film deposition. *J Biomed. Mater. Res.* 37:198-206.

Morton,L.F., Hargreaves,P.G., Farndale,R.W., Young,R.D., and Barnes,M.J. 1995. Integrin alpha 2 beta 1-independent activation of platelets by simple collagen-like peptides: collagen tertiary (triple-helical) and quaternary (polymeric) structures are sufficient alone for alpha 2 beta 1-independent platelet reactivity. *Biochem. J.* 306 (Pt 2):337-344.

Morton,L.F., Peachey,A.R., Knight,C.G., Farndale,R.W., and Barnes,M.J. 1997. The platelet reactivity of synthetic peptides based on the collagen III fragment alpha1(III)CB4. Evidence for an integrin alpha2beta1 recognition site involving residues 522-528 of the alpha1(III) collagen chain. *J. Biol. Chem.* 272:11044-11048.

Morton,L.F., Peachey,A.R., Zijenah,L.S., Goodall,A.H., Humphries,M.J., and Barnes,M.J. 1994. Conformation-dependent platelet adhesion to collagen involving integrin alpha 2 beta 1-mediated and other mechanisms: multiple alpha 2 beta 1- recognition sites in collagen type I. *Biochem. J.* 299 (Pt 3):791-797.

Moursi,A.M., Damsky,C.H., Lull,J., Zimmerman,D., Doty,S.B., Aota,S., and Globus,R.K. 1996. Fibronectin regulates calvarial osteoblast differentiation. *J. Cell Sci.* 109 (Pt 6):1369-1380.

Moursi,A.M., Globus,R.K., and Damsky,C.H. 1997a. Interactions between integrin receptors and fibronectin are required for calvarial osteoblast differentiation in vitro. *J. Cell Sci.* 110 (Pt 18):2187-2196.

Mrksich,M., Chen,C.S., Xia,Y., Dike,L.E., Ingber,D.E., and Whitesides,G.M. 1996. Controlling cell attachment on contoured surfaces with self-assembled monolayers of alkanethiolates on gold. *Proc. Natl. Acad. Sci. U. S. A* 93:10775-10778.

Muller,M., Hennig,F.F., Hothorn,T., and Stangl,R. 2005a. Bone-implant interface shear modulus and ultimate stress in a transcortical rabbit model of open-pore Ti6Al4V implants. *J Biomech.*

Muller,R., Abke,J., Schnell,E., Macionczyk,F., Gbureck,U., Mehrl,R., Ruszczak,Z., Kujat,R., Englert,C., Nerlich,M., and Angele,P. 2005b. Surface engineering of stainless steel materials by covalent collagen immobilization to improve implant biocompatibility. *Biomaterials* 26:6962-6972.

Murai,K., Takeshita,F., Ayukawa,Y., Kiyoshima,T., Suetsugu,T., and Tanaka,T. 1996. Light and electron microscopic studies of bone-titanium interface in the tibiae of young and mature rats. *J Biomed. Mater. Res.* 30:523-533.

Nagarajan,V., Kamitori,S., and Okuyama,K. 1998. Crystal structure analysis of collagen model peptide (Pro-pro-Gly)10. *J. Biochem. (Tokyo)* 124:1117-1123.

Nanci,A., Wuest,J.D., Peru,L., Brunet,P., Sharma,V., Zalzal,S., and McKee,M.D. 1998. Chemical modification of titanium surfaces for covalent attachment of biological molecules. *J Biomed. Mater. Res.* 40:324-335.

Nauman,E.A., Risic,K.J., Keaveny,T.M., and Satcher,R.L. 1999. Quantitative assessment of steady and pulsatile flow fields in a parallel plate flow chamber. *Ann. Biomed. Eng* 27:194-199.

Nobes,C.D., and Hall,A. 1999. Rho GTPases control polarity, protrusion, and adhesion during cell movement. *J. Cell Biol.* 144:1235-1244.

Nugiel,D.J., Wood,D.J., and Paul Sung,K.-L. 1996. Quantification of adhesiveness of osetoblasts to titanium surfaces in vitro by the micropipette aspiration technique. *Tissue Eng* 2:127-140.

Nykvist,P., Tu,H., Ivaska,J., Kapyla,J., Pihlajaniemi,T., and Heino,J. 2000. Distinct recognition of collagen subtypes by alpha(1)beta(1) and alpha(2)beta(1) integrins. Alpha(1)beta(1) mediates cell adhesion to type XIII collagen. *J. Biol. Chem.* 275:8255-8261.

O'Toole,G.C., Salih,E., Gallagher,C., FitzPatrick,D., O'Higgins,N., and O'Rourke,S.K. 2004. Bone sialoprotein-coated femoral implants are osteoinductive but mechanically compromised. *J Orthop. Res.* 22:641-646.

Onley,D.J., Knight,C.G., Tuckwell,D.S., Barnes,M.J., and Farndale,R.W. 2000. Micromolar Ca2+ concentrations are essential for Mg2+-dependent binding of collagen by the integrin alpha 2beta 1 in human platelets. *J. Biol. Chem.* 275:24560-24564.

Oonishi,H., Yamamoto,M., Ishimaru,H., Tsuji,E., Kushitani,S., Aono,M., and Ukon,Y. 1989. The effect of hydroxyapatite coating on bone growth into porous titanium alloy implants. *J Bone Joint Surg. Br.* 71:213-216.

Piattelli,A., Scarano,A., Corigliano,M., and Piattelli,M. 1996. Effects of alkaline phosphatase on bone healing around plasma-sprayed titanium implants: a pilot study in rabbits. *Biomaterials* 17:1443-1449.

Pilliar,R.M. 2005. Cementless implant fixation - toward improved reliability. *Orthop. Clin. North. Am.* 36:113-119.

Pohler,O.E. 2000. Unalloyed titanium for implants in bone surgery. *Injury* 31 Suppl 4:7-13.

Prockop,D.J., and Kivirikko,K.I. 1995. Collagens: molecular biology, diseases, and potentials for therapy. *Annu. Rev. Biochem.* 64:403-434.

Puleo,D.A. 1999. Release and retention of biomolecules in collagen deposited on orthopedic biomaterials. *Artif. Cells Blood Substit. Immobil. Biotechnol.* 27:65-75.

Puleo,D.A. 1997. Retention of enzymatic activity immobilized on silanized Co-Cr-Mo and Ti-6Al-4V. *J Biomed. Mater. Res.* 37:222-228.

Puleo,D.A. 1995. Activity of enzyme immobilized on silanized Co-Cr-Mo. *J Biomed. Mater. Res.* 29:951-957.

Puleo,D.A., and Nanci,A. 1999. Understanding and controlling the bone-implant interface. *Biomaterials* 20:2311-2321.

Redick,S.D., Settles,D.L., Briscoe,G., and Erickson,H.P. 2000. Defining fibronectin's cell adhesion synergy site by site-directed mutagenesis. *J Cell Biol* 149:521-527.

Regazzoni,C., Winterhalter,K.H., and Rohrer,L. 2001. Type I collagen induces expression of bone morphogenetic protein receptor type II. *Biochem. Biophys. Res. Commun.* 283:316-322.

Reichardt,L.F. 1999. Introduction: Extracellular matrix molecules. *In* Guidebook to the Extracellular Matrix, Anchor, and Adhesion Proteins. T.Kreis, and R.Vale, editors. Oxford University Press, New York, NY. 335-344.

Reust,P.J., Roy,S., Ergang,S., Mernaugh,R.L., and Hanks,S.K. 2000. Phosphospecific antibodies reveal focal adhesion kinase activation loop phosphorylation in nascent and mature focal adhesions and requirement for the autophosphorylation site. *Cell Growth Differ.* 11:41-48.

Reyes,C.D., and Garcia,A.J. 2003b. Engineering integrin-specific surfaces with a triple-helical collagen- mimetic peptide. *J. Biomed. Mater. Res.* 65A:511-523.

Reyes,C.D., and Garcia,A.J. 2003a. A centrifugation cell adhesion assay for high-throughput screening of biomaterial surfaces. *J. Biomed. Mater. Res. A* 67:328-333.

Reyes,C.D., and Garcia,A.J. 2004. Alpha2beta1 integrin-specific collagen-mimetic surfaces supporting osteoblastic differentiation. *J. Biomed. Mater. Res. A* 69:591-600.

Rezania,A., and Healy,K.E. 1999. Biomimetic peptide surfaces that regulate adhesion, spreading, cytoskeletal organization, and mineralization of the matrix deposited by osteoblast-like cells. *Biotechnol. Prog.* 15:19-32.

Rezania,A., Thomas,C.H., Branger,A.B., Waters,C.M., and Healy,K.E. 1997. The detachment strength and morphology of bone cells contacting materials modified with a peptide sequence found within bone sialoprotein. *J Biomed. Mater. Res.* 37:9-19.

Rivero,D.P., Fox,J., Skipor,A.K., Urban,R.M., and Galante,J.O. 1988. Calcium phosphate-coated porous titanium implants for enhanced skeletal fixation. *J Biomed. Mater. Res.* 22:191-201.

Roberts,W.E., Smith,R.K., Zilberman,Y., Mozsary,P.G., and Smith,R.S. 1984. Osseous adaptation to continuous loading of rigid endosseous implants. *Am. J Orthod.* 86:95-111.

Roskelley,C.D., Desprez,P.Y., and Bissell,M.J. 1994. Extracellular matrix-dependent tissue-specific gene expression in mammary epithelial cells requires both physical and biochemical signal transduction. *Proc. Natl. Acad. Sci. U. S. A* 91:12378-12382.

Ruggiero,F., Comte,J., Cabanas,C., and Garrone,R. 1996. Structural requirements for alpha 1 beta 1 and alpha 2 beta 1 integrin mediated cell adhesion to collagen V. *J. Cell Sci.* 109 (Pt 7):1865-1874.

Ruoslahti,E. 1996. RGD and other recognition sequences for integrins. *Annu. Rev. Cell Dev. Biol.* 12:697-715.

Rutherford,R.B., Sampath,T.K., Rueger,D.C., and Taylor,T.D. 1992. Use of bovine osteogenic protein to promote rapid osseointegration of endosseous dental implants. *Int. J Oral Maxillofac. Implants.* 7:297-301.

Schense,J.C., Bloch,J., Aebischer,P., and Hubbell,J.A. 2000. Enzymatic incorporation of bioactive peptides into fibrin matrices enhances neurite extension. *Nat. Biotechnol* 18:415-419.

Schliephake,H., Scharnweber,D., Dard,M., Rossler,S., Sewing,A., Meyer,J., and Hoogestraat,D. 2002. Effect of RGD peptide coating of titanium implants on periimplant bone formation in the alveolar crest. An experimental pilot study in dogs. *Clin. Oral Implants. Res.* 13:312-319.

Schwartz,Z., and Boyan,B.D. 1994. Underlying mechanisms at the bone-biomaterial interface. *J Cell Biochem.* 56:340-347.

Sechler,J.L., and Schwarzbauer,J.E. 1998. Control of cell cycle progression by fibronectin matrix architecture. *J. Biol. Chem.* 273:25533-25536.

Sennerby,L., Thomsen,P., and Ericson,L.E. 1993. Early tissue response to titanium implants inserted in rabbit cortical bone, Part I: Light microscopic observations. *J Mater. Sci. Mater. Med.* 4:240-250.

Shirazi-Adl,A., Dammak,M., and Zukor,D.J. 1994. Fixation pull-out response measurement of bone screws and porous-surfaced posts. *J Biomech.* 27:1249-1258.

Sodek,J., and Berkman,F.A. 1987. Bone cell cultures. *Methods Enzymol.* 145:303-324.

Staros,J.V., Wright,R.W., and Swingle,D.M. 1986. Enhancement by N-hydroxysulfosuccinimide of water-soluble carbodiimide- mediated coupling reactions. *Anal. Biochem.* 156:220-222.

Stein,G.S., Lian,J.B., Stein,J.L., van Wijnen,A.J., Frenkel,B., and Montecino,M. 1996. Mechanisms regulating osteoblast proliferation and differentiation. *In* Principles

of Bone Biology. J.P.Bilezikian, L.G.Raisz, and G.A.Rodan, editors. Academic Press, New York. 69-86.

Stephansson,S.N., Byers,B.A., and Garcia,A.J. 2002. Enhanced expression of the osteoblastic phenotype on substrates that modulate fibronectin conformation and integrin receptor binding. *Biomaterials* 23:2527-2534.

Stewart,J. 1997. Clinical Anatomy and Pathophysiology for the Health Professional. MedMaster, Inc., Miami. 30-45 pp.

Sudo,H., Kodama,H.A., Amagai,Y., Yamamoto,S., and Kasai,S. 1983. In vitro differentiation and calcification in a new clonal osteogenic cell line derived from newborn mouse calvaria. *J. Cell Biol.* 96:191-198.

Sumner,D.R., Turner,T.M., Purchio,A.F., Gombotz,W.R., Urban,R.M., and Galante,J.O. 1995. Enhancement of bone ingrowth by transforming growth factor-beta. *J Bone Joint Surg. Am.* 77:1135-1147.

Suzawa,M., Tamura,Y., Fukumoto,S., Miyazono,K., Fujita,T., Kato,S., and Takeuchi,Y. 2002. Stimulation of Smad1 transcriptional activity by Ras-extracellular signal-regulated kinase pathway: a possible mechanism for collagen- dependent osteoblastic differentiation. *J. Bone Miner. Res.* 17:240-248.

Takeuchi,Y., Suzawa,M., Kikuchi,T., Nishida,E., Fujita,T., and Matsumoto,T. 1997a. Differentiation and transforming growth factor-beta receptor down- regulation by collagen-alpha2beta1 integrin interaction is mediated by focal adhesion kinase and its downstream signals in murine osteoblastic cells. *J. Biol. Chem.* 272:29309-29316.

Tamura,Y., Takeuchi,Y., Suzawa,M., Fukumoto,S., Kato,M., Miyazono,K., and Fujita,T. 2001a. Focal adhesion kinase activity is required for bone morphogenetic protein--Smad1 signaling and osteoblastic differentiation in murine MC3T3-E1 cells. *J. Bone Miner. Res.* 16:1772-1779.

Tanahashi,M., and Matsuda,T. 1997. Surface functional group dependence on apatite formation on self-assembled monolayers in a simulated body fluid. *J Biomed. Mater. Res.* 34:305-315.

Thomas,K.A., Cook,S.D., Renz,E.A., Anderson,R.C., Haddad,R.J., Jr., Haubold,A.D., and Yapp,R. 1985. The effect of surface treatments on the interface mechanics of LTI pyrolytic carbon implants. *J Biomed. Mater. Res.* 19:145-159.

Truskey,G.A., and Pirone,J.S. 1990. The effect of fluid shear stress upon cell adhesion to fibronectin- treated surfaces. *J. Biomed. Mater. Res.* 24:1333-1353.

Tuckwell,D., Calderwood,D.A., Green,L.J., and Humphries,M.J. 1995. Integrin alpha 2 I-domain is a binding site for collagens. *J. Cell Sci.* 108 (Pt 4):1629-1637.

Tulla,M., Pentikainen,O.T., Viitasalo,T., Kapyla,J., Impola,U., Nykvist,P., Nissinen,L., Johnson,M.S., and Heino,J. 2001. Selective binding of collagen subtypes by integrin alpha 1I, alpha 2I, and alpha 10I domains. *J. Biol. Chem.* 276:48206-48212.

Usami,S., Chen,H.H., Zhao,Y., Chien,S., and Skalak,R. 1993. Design and construction of a linear shear stress flow chamber. *Ann. Biomed. Eng* 21:77-83.

Vasu,R., Carter,D.R., Schurman,D.J., and Beaupre,G.S. 1986. Epiphyseal-based designs for tibial plateau components I - Stress analysis in the frontal plane. *J. Biomech.* 19:647-662.

Walsh,W.R., Kim,H.D., Jong,Y.S., and Valentini,R.F. 1995. Controlled release of platelet-derived growth factor using ethylene vinyl acetate copolymer (EVAc) coated on stainless-steel wires. *Biomaterials* 16:1319-1325.

Wang,X., Subramanian,A., Dhanda,R., and Agrawal,C.M. 1996. Testing of bone-biomaterial interfacial bonding strength: a comparison of different techniques. *J Biomed. Mater. Res.* 33:133-138.

Weinreb,M., Shinar,D., and Rodan,G.A. 1990. Different patterns of alkaline phosphatase, osteopontin, and osteocalcin expression in developing rat bone visualized by in situ hybridization. *J. Bone Miner. Res.* 5:831-842.

Weiss,L. 1961. The measurement of cell adhesion. 141-153.

Weston,S.A., Hulmes,D.J., Mould,A.P., Watson,R.B., and Humphries,M.J. 1994. Identification of integrin alpha 2 beta 1 as cell surface receptor for the carboxyl-terminal propeptide of type I procollagen. *J. Biol. Chem.* 269:20982-20986.

Wong,M., Eulenberger,J., Schenk,R., and Hunziker,E. 1995. Effect of surface topology on the osseointegration of implant materials in trabecular bone. *J Biomed. Mater. Res.* 29:1567-1575.

Xiao,G., Gopalakrishnan,R., Jiang,D., Reith,E., Benson,M.D., and Franceschi,R.T. 2002. Bone morphogenetic proteins, extracellular matrix, and mitogen- activated protein kinase signaling pathways are required for osteoblast- specific gene expression and differentiation in MC3T3-E1 cells. *J. Bone Miner. Res.* 17:101-110.

Xiao,G., Jiang,D., Thomas,P., Benson,M.D., Guan,K., Karsenty,G., and Franceschi,R.T. 2000a. MAPK pathways activate and phosphorylate the osteoblast-specific transcription factor, Cbfa1. *J. Biol. Chem.* 275:4453-4459.

Xiao,G., Wang,D., Benson,M.D., Karsenty,G., and Franceschi,R.T. 1998. Role of the alpha2-integrin in osteoblast-specific gene expression and activation of the Osf2 transcription factor. *J. Biol. Chem.* 273:32988-32994.

Yaszemski,M.J., Payne,R.G., Hayes,W.C., Langer,R., and Mikos,A.G. 1996a. Evolution of bone transplantation: molecular, cellular and tissue strategies to engineer human bone. *Biomaterials* 17:175-185.

Yu,X., and Bellamkonda,R.V. 2003. Tissue-engineered scaffolds are effective alternatives to autografts for bridging peripheral nerve gaps. *Tissue Eng* 9:421-430.

Zhao,G., Schwartz,Z., Wieland,M., Rupp,F., Geis-Gerstorfer,J., Cochran,D.L., and Boyan,B.D. 2005. High surface energy enhances cell response to titanium substrate microstructure. *J Biomed. Mater. Res. A* 74:49-58.

Zhu,X., Ohtsubo,M., Bohmer,R.M., Roberts,J.M., and Assoian,R.K. 1996. Adhesion-dependent cell cycle progression linked to the expression of cyclin D1, activation of cyclin E-cdk2, and phosphorylation of the retinoblastoma protein. *J. Cell Biol.* 133:391-403.

VITA

CATHERINE DIANE REYES

Catherine was born in Washington D.C. on July 28, 1978, to William and Ursula Reyes. Three months later, Catherine's family moved to Frankfurt, Germany, where she attended preschool and kindergarten. While learning how to count, fingerpaint, and eat liverwurst, Catherine aspired to become a fireman (because of the red hats) or a radio host (because she loved hearing herself on tape). The arrival of a baby brother was only a brief obstacle in her round-the-clock red hat/microphone training.

Her career aspirations shifted, however, when the family relocated to Bangkok, Thailand, where she attended the International School of Bangkok. Selected to participate in a program inexplicably called Reading Radish, which involved surprisingly little reading and much coloring, drawing, and painting, she discovered her calling as an artist. She produced many significant works during this period, including "The Wonderful World of OZ" and "Still Life with Pumpkins."

However, the winds of fate would once again shift with another move, this time to sunny Miami, Florida, just in time for Catherine to start the fourth grade at Holy Rosary Catholic School. Her wildly creative artistic spirit was soundly squashed by the inexorable presence of green plaid and nothing but green plaid, as far as the eye could see. Surrounded by what were surely living fossils dressed up as nuns, Catherine became obsessed with paleontology. Dinosaurs were her passion. She would become a paleontologist and travel to exotic lands in search of the next –asaurus and possibly find treasure and fame and Indiana Jones along the way.

In the fifth grade, she had a brief bite from the drama bug when she was chosen to portray the pivotal role of Girl #3 in a play about a witch with a blue nose. While her practiced elocution was admittedly pitch-perfect, her aversion to general attention doomed her acting career early on.

Her introduction to the public school system began in the seventh grade, when she transferred to Southwood Middle School. In a desperate effort to avoid any sort of physical education class, Catherine signed up for Creative Writing. In a rather transparent attempt to increase the extremely unpopular class's enrollment the next year, Ms. Levin proclaimed Catherine the next great American writer, the likes of (and I'm not kidding here, she actually said this) Leo Tolstoy or Michael Crichton. It worked. Catherine took Creative Writing all three years of Middle School (successfully avoiding P.E.). She would be a writer, a great American one, the likes of… well, you know.

With a growing body of sappy poetry and eerie yet brilliant short stories, Catherine began the tenth grade at Miami Palmetto Senior High School, secure in her intentions to join the upper ranks of the literati. However, Palmetto High offered no writing class whatsoever. It did, however, mandate the dreaded physical education. Catherine confronted P.E. head-on, running the mile in a respectable fourteen minutes and fifty-nine seconds (although, she is quite sure she skipped the final lap), coming in second to last in her class. Clearly, athletics were not for her.

She did, however, demonstrate an aptitude for physics (even though she was never really sure what "physics" meant) and later chemistry (which involve lots of letters and arrows… fun!). Teachers were impressed. Especially since it seemed that scientific

aptitude usually resided on the Y chromosome, explaining their propensity to add the incredulous phrase “and she’s a girl” to every bit of praise.

She moved to Boston in 1996, in what was, climatically speaking, the worst decision she has ever made, to attend the Massachusetts Institute of Technology. Freshman year was rocky. Luckily, due to an odd pass/fail system, freshman year no longer exists. So we’ll move to the sophomore year, when she discovered a passion for anthropology, became one of four people to frequent the literature department, and resigned herself to an engineering major. Catherine graduated in 2000 with an S.B. in Materials Science and Engineering, otherwise know as the science of “stuff.”

Fate called that Spring and, oddly, Fate had a Puerto Rican accent. Catherine began graduate school at Georgia Tech, made lots of cool friends, learned all kinds of fascinating things, met and married a cute, amazing, sweet, wonderful boy, adopted a stripey gray cat with an attitude and an addiction to cuddlies and a blonde, silly, pink-nosed, crazy puppy with a cowlick, visisted many incredible places, had tons of adventures, and lived happily ever after.